ABIOTIC STRESS SIGNALLING IN THE *FUCUS* EMBRYO

BY

SUSANA COELHO

A thesis submitted to the University of Plymouth in partial fulfilment for the degree of

DOCTOR OF PHILOSOPHY

SEPTEMBER 2002

ABIOTIC STRESS SIGNALLING IN THE *FUCUS* EMBRYO

By

SUSANA COELHO

A thesis submitted to the University of Plymouth in partial fulfilment for the degree of

DOCTOR OF PHILOSOPHY

Department of Biological Sciences, Faculty of Sciences

University of Plymouth

In collaboration with

Marine Biological Association of the UK

SEPTEMBER 2002

ABSTRACT

Fucoid algae live in the intertidal region where they experience daily fluctuations in light and external osmotic environment. High light, especially in combination with ultraviolet (UV) radiation and hyper-osmotic stress affected the cellular physiology of *Fucus* embryos. Two photoinhibition responses were recognised. Firstly, a rapid decline of the photosystem II (PSII) efficiency, linked with the operation of the xanthophyl cycle, followed by a slower decline correlated with reactive oxygen species (ROS) production. As a result of enhanced ROS production, a slower repair of the PSII efficiency was observed, particularly with increased UV-B doses. Development of the embryos was transiently affected by UV-B. The cellular signal transduction pathway during hyper-osmotic stress was investigated. ROS production in response to hyper-osmotic stress comprised two distinct components. The first ROS component coincided closely with the origin of a Ca^{2+} wave in the peripheral cytosol at the growing cell apex, had an extracellular origin, and was necessary for the Ca^{2+} wave. Patch clamp experiments showed that a non-selective cation channel was stimulated by H_2O_2, and may underlie the initial cytosolic Ca^{2+} elevation. The spatio-temporal pattern of the Ca^{2+} wave was thus determined by peripheral ROS production. The second, later ROS component localised to the mitochondria and was a direct consequence of the Ca^{2+} wave. The first, but not the second component was required for short-term adaptation to osmotic stress, probably through the activity of cell wall bromoperoxidases. Mitogen-activated protein kinases may be involved in the hyper-osmotic stress response downstream or independently of the mitochondrial ROS production.

LIST OF CONTENTS

Coelho S., Taylor, A., Ryan, K., Brown M.T., Sousa-Pinto I. and Brownlee C. (2002). Spatio-temporal pattern of reactive oxygen production and Ca^{2+} wave propagation in *Fucus* rhizoid cells. Plant Cell 14: 2369-2381

Coelho S., Rijstenbil J.W., Sousa-Pinto I. and Brown M.T. (2001) Cellular responses of *Fucus* embryos to elevated light levels. Plant, Cell and Environment 24(8): 801-810

Coelho S., Brown M.T. and Rijstenbil J.W. (2000) Impacts of anthropogenic stress on the early stages of development of seaweeds. J. Aquat. Ecosystem Stress and Recovery, 7: 317-333

Rijstenbil J., Coelho S. and Eijsackers M (2000) A method for the assessment of light-induced oxidative stress in embryos of fucoid algae via confocal laserscan microscopy. Marine Biology 137: 763-774.

LIST OF ABBREVIATIONS

ASW: artificial seawater

Br_2BAPTA: dibromo-1-2-bis(o-aminophenoxy)ethane-N,N,N',N'-tetraacetic acid.

BSA: bovine serum albumin

Ca^{2+}_{cyt}: cytoplasmatic free calcium

CDPK: calcium-dependent protein kinase

CG-1: Calcium green-1 (Ca^{2+} sensitive dye)

CLSM: confocal laserscan microscope

CM-DCFH_2-DA: chloromethyl dichlorofluorescein diacetate;

DAB: 3,3'-diaminobenzidine

DCF: dichlorofluorescein

DMSO: dimethyl sulphoxide

DTT: dithiotriol

EGTA: ethylene glycol bis (β-aminoethyl ether)-N,N,N',N'-tetracetic acid

ER: endoplasmatic reticulum

ERM: elicitor responsive MAP kinase

F-actin: filamentous actin

FCCP: carbonyl cyanide p-(trifluoro-methoxy) phenyl-hydrazone

GPX: glutathione peroxidase

HEDTA: N-(2-hydroxyethyl)ethylenediamine-N,N'N'-tricetic acid

HEPES: N-(2-hydroxyethyl)piperazine-N-(2-ethanesulfonic acid)

HOSAK: high osmotic stress-activated protein kinase

HPAR: high PAR

HR: hypersensitive response

Ins(1,4,5)P_3: inositol tris(1,4,5)phosphate

Ins(1,4,5)P_3R: Ca^{2+} receptor protein that binds Ins(1,4,5)P_3

K_d: dissociation constant

kD: kilo (x10^3) Daltons

LPAR: low PAR

MAPK: mitogen activated protein kinase

MAPK: mitogen-activated protein kinase

MOPS: 3-(N-morpholino) propanesulfonic acid

mRNA: messenger ribonucleic acid

NBT: nitroblue tetrazolium

NTA: nitriloaceptic acid

OGA: oligogalacturonide

PA: PAR+UVA;

PA: phosphatidic acid

PAB: PAR+UVA+UVB

PAL: phenylalanine ammonia-lyase (defence gene)

PAM: pulse-amplitude modulation

PAR (μM photons.m^{-2}.s^{-1}): photosynthetic active radiation

PLC: phospholipase C

PM: plasma membrane

PPFD: photosynthetically active photon flux density

PR protein: pathogenesis-related protein

PSI/II: photosystem I/II

Pto: resistance gene product

qN: non-photochemical quenching

qP: photochemical quenching

ROS: reactive oxygen species

SA: salicylic acid

SAR: systemic acquired resistance

SBTI: soybean trypsin inhibitor

SIMK: salt stress inducible MAP kinase

SIPK: salicylate-induced protein kinase

SW: seawater

TAPS: N-tris(hydroxymethyl)methyl-3-aminopropane sulfonic acid

UV: ultraviolet

V: violoxanthin

WIPK: wound-induced protein kinase

Z: zeaxanthin

$\Delta F/F'_m$: effective quantum yield of PSII

ACKNOWLEDGEMENTS

To my friends in the MBA (in particular to the Brownlee's lab) who, for the last 3 years, helped entertaining me - Hanne Nielsen, Pedro and Susana Lima, Lydia Mategher, Toby Collins, Lorraine Berry, Amanda Humble, Maria Ganderton, John Bothwell (extra thanks for the help with my "portuglish"), Laure Noel, Paco Arenas and so many more. A special thank you to Matthew Sanders and Agnès Marahdur for patiently listening to my "theories" about *Fucus* outside in the "smoker's corner" and also to Nick Manison, for introducing me to the Brownlee's lab and for his enthusiastic advises on how to patch clamp *Fucus*.

I have to thank Isabel Sousa Pinto for introducing me to the Algae and also to Murray Brown, my supervisor at the University of Plymouth.

Most of the work has been carried out at the MBA, and the very special thank you has to go to Colin Brownlee, who warmly (and with infinite patience) received me in his Colin's basement and guided me into the *Fucus* cell biology. His dedication, positivism and perseverance were for me a model to follow.

To Florence Corellou and François-Yves Bouget, for their friendship, excellent criticism and for provoking ideas, and to Dr. Alison Taylor who taught me the magic skills of laser microsurgery and patch clamping.

A big thanks to everyone in the Station Biologique de Roscoff, in particular to Stephane, Frank, Gaytan and Lionel (the patch clampers) and to Bernard Kloareg's team (especially Florence Corellou, François-Yves Bouget and Ludovic Delage). I am also grateful to everyone in the NIOO laboratory (Holland) where I worked during the first year of the thesis.

Thank you to my friends in Portugal for their many e-mails and phone calls. To my grand parents (who are now experts in *Fucus* cell biology), for the good luck candles lighted during difficult experiments. A very very special thank you to my parents and Cristiano, who encouraged me through long phone calls to Portugal. Finally, I am grateful to Sébastien, for his unique support, encouragement and understanding, especially in the last stages of this thesis.

AUTHOR'S DECLARATION

At no time during the registration for the degree of Doctor of Philosophy has the author been registered for any other University award.

This study was financed with the aid of a grant from the Fundação para a Ciência e Tecnologia (Portugal) and mainly carried out in the Marine Biological Association of the UK. The first year of this thesis was undertaken in Netherland's Institute of Ecology (Holland) and some experiments were performed in the Station Biologique de Roscoff, France.

Relevant scientific seminars and conferences were regularly attended at which work was always presented in the form of posters or oral communications. External institutions were visited for consultation purposes and several papers prepared for publication.

Workshops

May 2002 – "Apoptosis across kingdoms" – EMBO workshop, Roscoff, France.

July 1999 – "Apoptosis and reactive oxygen species" – Institute for Molecular and Cell Biology, University of Porto, Portugal.

Communications

May 2002 – "Unravelling the signalling pathway during hyper-osmotic stress in *Fucus* embryos – towards apoptosis?" **S. Coelho**, A. Taylor and C. Brownlee – Conference Jacques Monod/EMBO workshop – "Apoptosis across kingdoms" Roscoff, France.

May 2002 – "Signalling pathways during environmental stress in *Fucus* sp. embryos" **S. Coelho**, M. T. Brown and C. Brownlee – "Asia-Pacific Conference on Marine Science and Technology", Malasia (best poster paper award).

August 2001 – "Role of H_2O_2 in patterning Ca^{2+} signals" **S. Coelho**, MT Brown and C. Brownlee. "Plant Membrane Biology" – Madison, Wisconsin, EUA.

July 2000 – "Ca^{2+} and oxidative stress: signal or response?" **S. Coelho**, MT Brown, I. Sousa-Pinto and C. Brownlee - "Plant Biology 2000" San Diego, EUA.

June 2000 – "Ca^{2+} and H_2O_2 during hyper-osmotic stress response in *Fucus* embryos" **S. Coelho** and C. Brownlee "Conference Calcium 2000", Warwick, UK.

January 2000 – "Effects of light, desiccation and copper on active oxygen production and photosynthesis of *Fucus* sp. embryos". **S. Coelho**, MT Brown, I Sousa-Pinto and C. Brownlee "British Phycological Society Annual Meeting", Birmingham, U.K.

Publications

Coelho S., Taylor, A., Ryan, K., Brown M.T., Sousa-Pinto I. and Brownlee C. (2002). Spatio-temporal pattern of reactive oxygen production and Ca^{2+} wave propagation in *Fucus* rhizoid cells. Plant Cell 14: 2369-2381

Coelho S., Rijstenbil J.W., Sousa-Pinto I. and Brown M.T. (2001) Cellular responses of *Fucus* embryos to elevated light levels. Plant, Cell and Environment 24(8): 801-810

Coelho S., Brown M.T. and Rijstenbil J.W. (2000) Impacts of anthropogenic stress on the early stages of development of seaweeds. J. Aquat. Ecosystem Stress and Recovery, 7: 317-333

Rijstenbil J, **Coelho S.** and Eijsackers M (2000). A method for the assessment of light-induced oxidative stress in embryos of fucoid algae via confocal laserscan microscopy. Marine Biology 137: 763-774.

S Coelho 27/04/03

"... as for certain truth, no man has known it,
Nor shall he know it, neither of the gods
Nor yet of all the things of which I speak,
For even if by chance he were to utter
The final truth, he would himself not know it:
For all is but a woven web of guesses."

Xenophanes, 6th century BC

CHAPTER 1

GENERAL INTRODUCTION

1.1. ENVIRONMENTAL STRESS IN INTERTIDAL ALGAE

Destined to reside in their habitats of germination, plants are frequently exposed to unfavourable external conditions such as extreme temperatures, drought, pollution, high light, etc. In order to survive, plants have developed complex signal-response networks that sense and protect them from an ever-changing environment. In this context, algae living on the upper littoral zone of rocky shores are particularly subject to marked environmental variations during each tidal cycle. Therefore, mechanisms of accommodation to these changes are an essential feature for the survival of these individuals.

Most of the investigations on how environmental factors affect intertidal organisms have focused almost exclusively on the responses of adult stages to natural and anthropogenic stresses. However, the impact of stress factors on algal embryonic stages or during the first days after settlement may be particularly severe. It is well documented that early developmental stages are far more sensitive to environmental stress than adult stages, and are, thus, a potential weak link in any life cycle. Various researchers have recognized the importance of young stages in the structure and dynamics of intertidal rocky-shore communities (Underwood and Fairweather, 1989; Reed, 1990; Bellgrove et al., 1997). The survival of early stages of intertidal organisms is believed to be critical to the successful establishment of benthic populations (Vadas et al., 1992), and, therefore, of great importance to the management of marine habitats. With intertidal algae, attention has been progressively given to the ecology and physiology of early life history phases, including dispersal, settlement, dislodgement,

intra- and inter-specific competition, stress tolerance and photosynthesis of zygotes and germlings (Norton 1983; Reed, 1992; Wright and Reed, 1990; Brawley and Johnson, 1991; Vadas et al., 1990, 1992; Amsler and Neushul, 1991; Fletcher and Callow, 1992; Kendrick and Walker, 1994; Beach et al., 1995; Creed et al., 1997; Andersson et al., 1994). Davison et al. (1993) suggested that sub-lethal stress might play an important role in the recruitment success of individual plants and the development of seaweed communities on rocky intertidal seashores. Reductions in growth rate arising from a decrease in photosynthetic capacity due to sublethal stresses may influence the competitive ability and resistance to grazing.

Fucales comprise an order of brown algae that colonize extensively the rocky intertidal zone of temperate regions. They are important as the basis of a very rich animal and algal community, providing shelter for a number of organisms. With every turn of the tide, Fucales are markedly affected by osmotic and temperature changes, light intensity and quality changes, and mechanical stress. Therefore, they can potentially provide a valuable model system for the study of plant stress responses and adaptation.

1.2. *FUCUS* AS A MODEL SYSTEM FOR STRESS INVESTIGATIONS

1.2.1. Life cycle

1.2.1.1. Introduction

Fucales (comprising the genera *Fucus* and *Pelvetia*) are brown macrobenthic algae that live in the intertidal zone of rocky shores in temperate regions. The fact that both fertilisation and development are external, without the protection of a mother tissue, makes gametes and zygotes very tractable for manipulation in the laboratory. Gametes of the dioecious species (*Fucus vesiculosus*, *Fucus serratus*) can be obtained separately, allowing good temporal control of fertilisation. On the other hand, in monoecious species (*Fucus spiralis*, *Fucus distichus*, *Pelvetia compressa*, *Pelvetia canaliculata*) the release of antherozoids and oospheres allows high rates of viable zygotes and homogeneous populations. The reproductive season is usually during the winter, although some variation can occur with species and region. *Fucus serratus* and *Fucus spiralis* have a relatively long reproductive season and gametes can be obtained throughout the year, so they were chosen as the model system in this investigation.

The reproductive structures in the adult *Fucus* are small sacs called receptacles, situated at the extremities of the fronds (Figure 1.1). At the surface of the receptacles, the conceptacles (where the gametes develop) open to the exterior through an ostiole. At the internal surface, the oogonia contain 2-8 oospheres. The antherozoids, contained inside antheridia, have one chloroplast with an eyespot that gives them an orange colour. Gametes are released preferentially during day-time low tides (Pearson

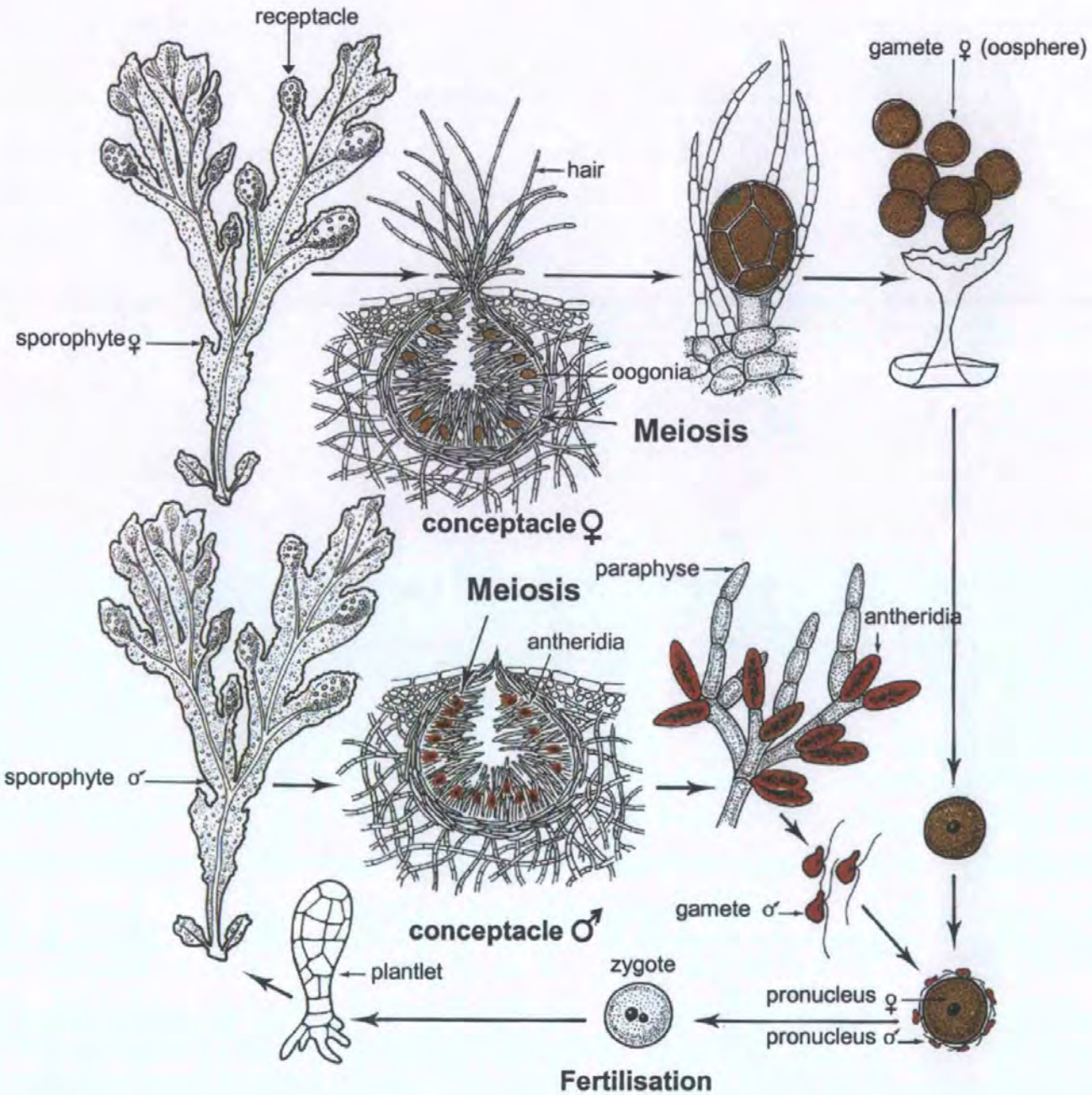

Figure 1.1. Life cycle of a dioecious *Fucus* species.

Adapted from Gayral, 1975

and Brawley, 1996), and antherozoids (negatively phototactic and positively chemotactic) are attracted to the sinking eggs by fucoserratine (Muller and Gassman, 1978).

1.2.1.2. Fertilisation

In the laboratory, successful release of gametes is achieved after some days of keeping the receptacles in the dark at 4°C. The receptacles are submitted to a quick osmotic and light shock (briefly rinsed with tap water, then illuminated after immersion in seawater), which induces gamete release and fertilisation in the case of monoecious species. In dioecious species, male and female gamete solutions are mixed at approximately 300 sperm: 1 oosphere. The contact of the gametes induces a fertilisation potential initiated by the opening of Na^+ channels (Brawley, 1991; Roberts et al., 1993; Taylor and Brownlee, 1993; Roberts and Brownlee, 1995). The depolarisation of the membrane from -60 mV to -20 mV constitutes an immediate electrochemical barrier to polyspermy (Brawley, 1991), reinforced by cell wall formation a few minutes after fertilisation. The metabolic activation of the oosphere is marked by an increase in the respiration (Levring, 1952) and synthesis of messenger RNA (mRNA) and proteins (Koehler and Linskens, 1967).

1.2.1.3. From zygote to adult stage

Zygotes settle and adhere to the substrate by 1 h after fertilisation (AF). Zygotes are initially non-polar and polarise in response to vectorial cues such as unidirectional light. The morphological expression of this polarity is a protuberance emerging from the pole opposite the incident light (germination, Figure 1.2). This becomes the rhizoid.

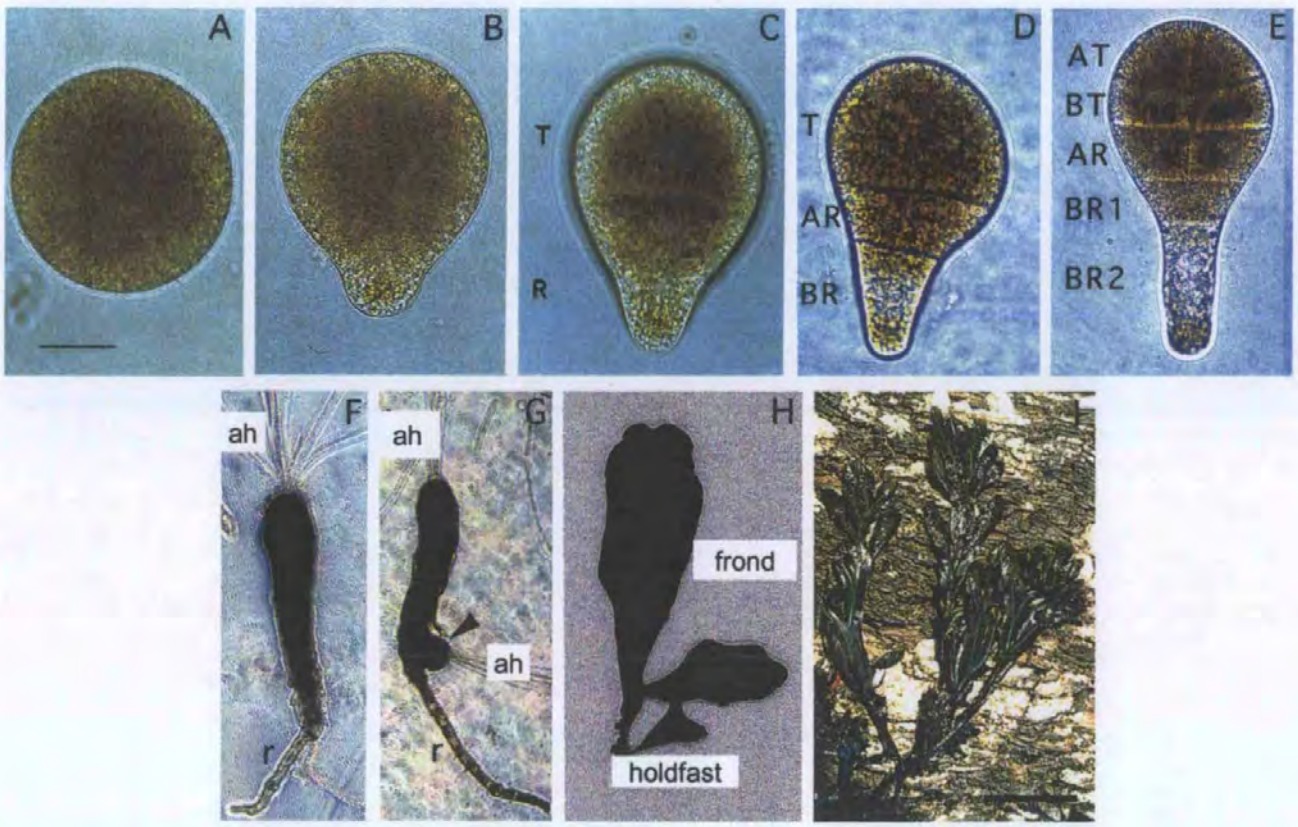

Figure 1.2. Early embryogenesis in *Fucus spiralis*. **A)** Zygotes are spherical during the polarisation process (14-15 h AF). **B)** Morphological expression of polarity by rhizoid emergence in the pole opposite to the light source (18-20 h AF). **C)** First asymmetric division, perpendicular to the axis of polarity, separates thallus cell (T) and rhizoid cell (R) (24 h AF). **(D)** Rhizoid cell divides and forms apical rhizoid (AR) and basal rhizoid (BR). **E)** At the rhizoid cell, the second and further divisions take place transversely (32 h AF). In the thallus cell, the divisions are alternatively paralell and prependicular to the polarity axis. **AT**, thallus apical cells; **BT**, thallus basal cells; **AR**, rhizoid apical cells, **BR1** and **BR2**, rhizoid basal cells. **F)** After two to three weeks, a meristematic region is localised at the apex of thallus and preceeds the emergence of apical hairs (**ah**). **G)** In some cases, there is development of adventitious embryos from the rhizoid part of the algae. After two months, the young algae is developed (**H**) and grows into the adult plant (**I**). Bar represents in **A-D** 30 μm, in **E** 40 μm, in **F** and **G** 100 μm, in **H** 400 μm and in **I** 20 cm.

After Bouget et al., 1998

The first asymmetric division takes place perpendicular to the axis of polarity and separates the zygote into rhizoid and thallus cells. The smaller rhizoid cell elongates by apical growth and is the precursor of the holdfast; the larger thallus cell gives rise to the stipe and fronds of the mature alga. In the culture conditions used in the present study (continuous light 15°C) germination and the first cleavage take place approximately 14-16 h AF and 22-24 h AF respectively. The rhizoid elongates and repeatedly divides transverse to the growth axis, whereas the thallus cell undergoes a well-defined sequence of transverse and longitudinal divisions (Figure 1.2). Developing embryos of many higher plants, including *Arabidopsis*, undergo a similar pattern of cell divisions (Kropf, 1997).

The 2-3 week old embryo measures approximately 1 mm and possesses several rhizoids. At the apical pole a depression is observed from which apical hairs appear. At the base of the hairs is the meristematic zone (Oltmanns, 1922). The pattern of divisions in this zone determines to the dichotomous branching of the mature frond.

1.2.2. Polarisation and early *Fucus* development

1.2.2.1. Photopolarisation

Polarisation of *Fucus* zygotes in response to environmental gradients results in the formation of two poles with distinct morphology and cytology: the rhizoid pole and the thallus pole. The zygote possesses different temporal windows of sensitivity to external vectors (reviewed by Quatrano et al., 1974). Responses to light have been the most studied. The zygote is sensitive to light from 4-6 h AF to 10 h AF. If placed in darkness after a light stimulus, however, it will germinate along an axis determined by

the previous light direction. During this period, the polar axis can be re-oriented by changing the light direction. The period during which the orientation of the polar axis can be changed is called "axis formation". This is followed by a pre-germination phase (10-14 h AF), during which the zygote will no longer respond to changes in the light orientation ("axis fixation").

1.2.2.2. Axis formation

In *Fucus* and *Pelvetia*, karyogamy takes place at 2-4 h AF. At this time, no cytological asymmetry can be detected (Brawley et al., 1976). The female pronucleus is kept in a central position by a cytoskeleton of microfilaments and microtubules (Figure 1.3). If the zygotes are kept in a homogeneous medium in darkness they will germinate in a random orientation. At the beginning of the last century, studies performed with *Cystoseira barbata* suggested that the entry point of the sperm determined the polarity. Yamanouchi (1909) observed the presence of fibrous material at the sperm entry point, just after fertilisation. This fibrous material was later been found to be a transient actin localisation (Alessa and Kropf, 1999). Further support for the idea of polarity being determined by sperm entry comes from the tight connection between polyspermy rates and presence of double rhizoids at opposite poles (Hable and Kropf, 2000). Thus, antherozoid entry may induce an initial asymmetry due to transient actin localisation, which will be sufficient to induce polarisation in the absence of other stimuli.

The period during which no asymmetry is detected, and thus the cell is able to respond to the various external triggers, lasts for approximately 6 h in *Fucus*. The cell wall components (cellulose, alginates, fucans, polyphenols) are localised uniformly

during this period and allow the zygote to adhere to the substrate (Vreeland et al., 1993). Simultaneously, mRNA and proteins necessary for polarisation are synthesised.

The first asymmetries are difficult to detect because they are very faint. These asymmetries are observed in response to a light vector and can be repositioned by changing the orientation of this vector (Figure 1.3; 1.4). The early-detected asymmetries are amplified during the period of axis fixation and in summary are:

- Transcellular ionic currents (Nuccitelli and Jaffe, 1976);
- Localisation of actin microfilaments at the presumptive rhizoid pole (Alessa and Kropf, 1999; Pu et al., 2000);
- Elevated Ca^{2+} at the rhizoid pole (Pu and Robinson, 1997);
- Localised secretion at the rhizoid pole (Quatrano and Shaw, 1997);
- Localisation of dihydropyridine receptors at the presumptive rhizoid pole, suggesting a redistribution of Ca^{2+} channels (Shaw and Quatrano, 1996a).

1.2.2.3. Ca^{2+} currents in the developing zygote

Studies with an external self-referencing "vibrating probe" electrode showed that positive current enters the presumptive rhizoid pole (Nuccitelle and Jaffe, 1976). The study of these ionic currents in *Fucus* zygotes with different media of different ionic compositions suggests that these currents can be, at least in part, attributed to Ca^{2+} ions (Nuccitelli, 1978). Ca^{2+} entry at the presumptive rhizoid pole is 6 times greater than that found in other regions of the zygote surface (Nuccitelli and Jaffe, 1976). The use of $^{45}Ca^{2+}$ showed a significant Ca^{2+} influx at the rhizoid pole 2h after stimulation of *Pelvetia* zygotes by light (6 h AF) (Robinson and Jaffe, 1975). At this stage of development, Ca^{2+} is mainly responsible for the transcellular ionic current. The role of

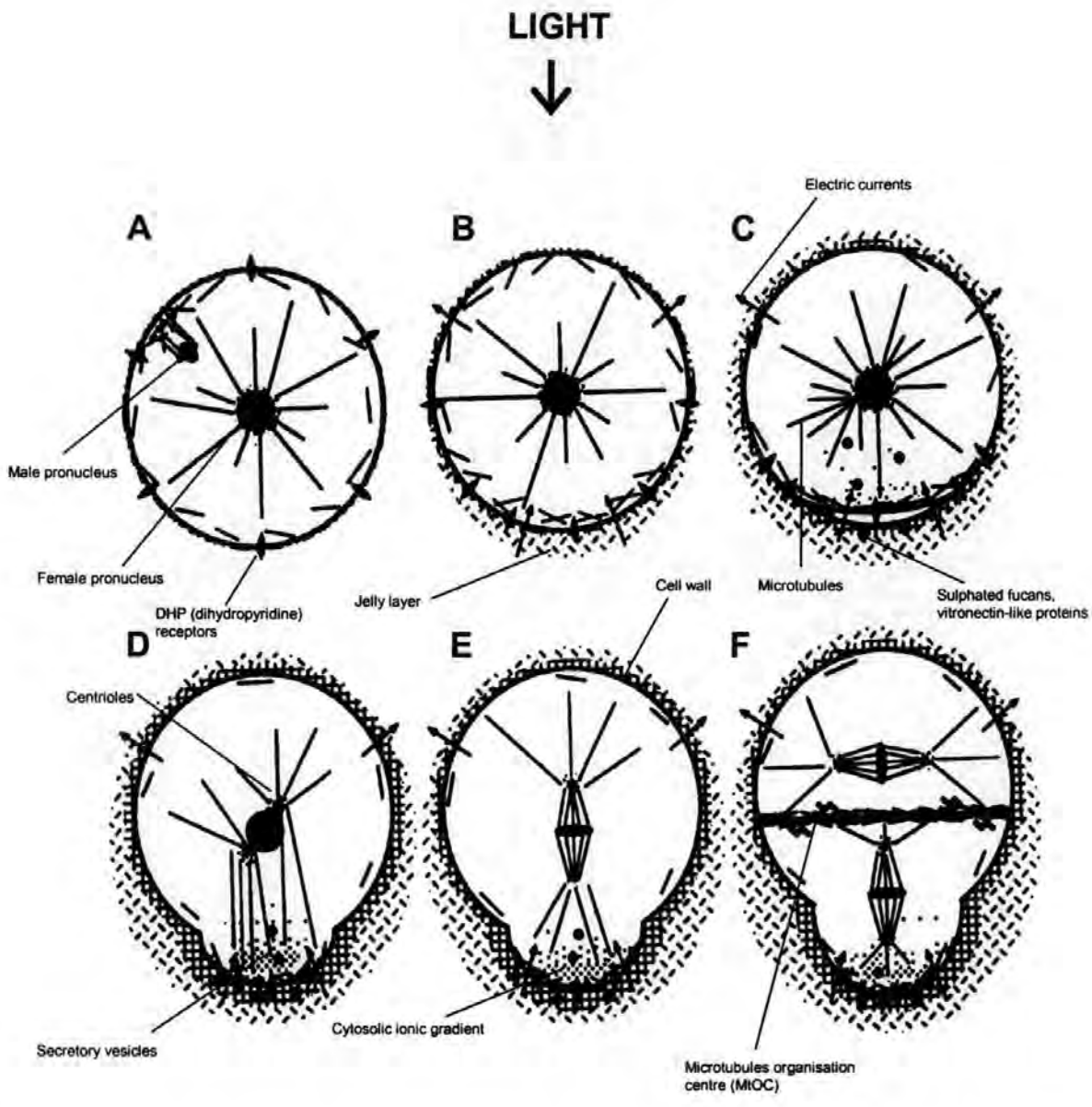

Figure 1.3. Fertilisation and light-induced polarisation in *Fucus*. **A)** 1 h AF - Male pronucleus migrates towards female pronucleus. Zygote does not show structural asymmetry. **B)** Axis formation (4-6 h to 8-10 h AF) - Transcellular currents are established, DHP receptors and cortical actin redistributed at the future rhizoid site, centrosomes start separating. **C)** Axis fixation (8-10 h to 14-16 h AF) - Amplification of polarisation events. A Ca^{2+} gradient is detectable and polarised secretion takes place. Sulphated fucans are localised at the rhizoid pole cell wall. **D)** Germination (16-18 h AF) - Polarised secretion increases, and from the rhizoid pole a protuberance emerges. Microtubules elongate towards rhizoid pole and allow nuclear rotation. **E)** Mitosis (16-20 h AF) - Achievement of nuclear rotation, alignment of centrosomes with the polarity axis. Segregation of chromosomes. **F)** Cytokinesis (20-24 h AF) - Formation of membrane and cell wall transverse to the polarity axis. Actin and actin mRNA are localised at the division plane.

After Kropf, 1997

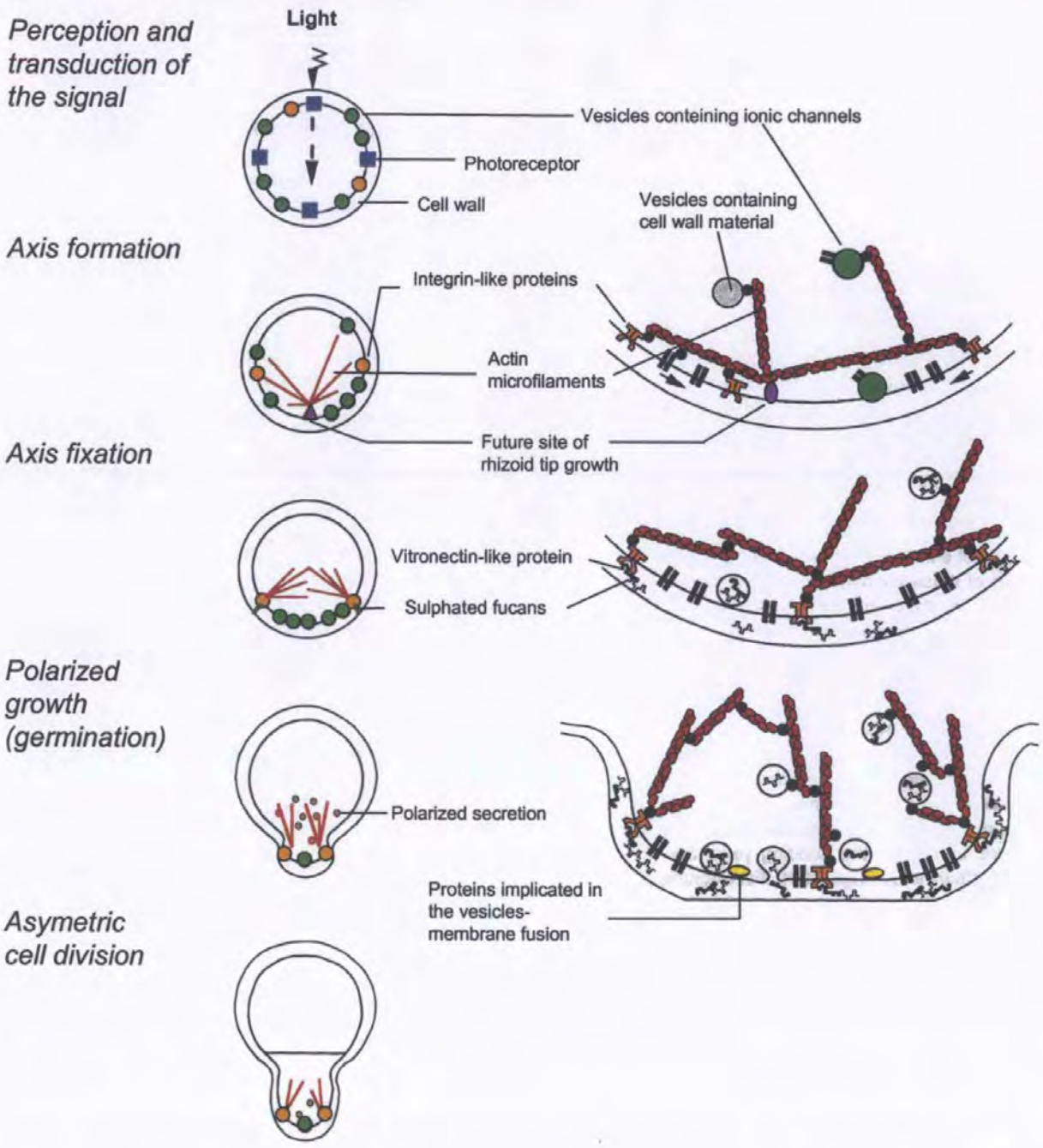

Figure 1.4. Schematic model of polarity establishment and polarised growth in *Fucus*. Figure ilustrates the global polarisation process. Right half of the scheme shows details of the molecular events proposed to take place at the rhizoid pole. During axis formation, the future site of rhizoid growth is selected. Polarisation of the actin cytoskeleton at this site allows the polarised transport of vesicles containing ionic channels, responsible for the Ca^{2+} gradient. Ca^{2+} favours actin polymerisation. Other molecules, such as integrins, vitronectin and sulphated fucans have been proposed to be stabilised by exocytosis. They may allow amplification of the polarisation and anchorage of the cytoskeleton at the rhizoid pole.

After Goodner and Quatrano, 1993

Ca^{2+} in rhizoid growth is well established, and one of the earliest detectable gradients during polarisation is a crescent of elevated Ca^{2+} centred at the future rhizoid pole (Berger and Brownlee, 1993; Pu and Robinson, 1997). This, together with a very low Ca^{2+}_{cyt}, allows a well-defined Ca^{2+}_{cyt} gradient to develope at the presumptive rhizoid pole. The Ca^{2+} concentrations vary from 400 nM at the rhizoid pole to 100 nM away from the rhizoid pole. In addition, this Ca^{2+} gradient seems to be essential for polarisation: Robinson (1996) observed that zygotes of *Pelvetia* do not photopolarise in artificial seawater without Ca^{2+}, indicating an important role of extracellular Ca^{2+} for the establishment of polarity. This conclusion has been challenged by other authors who report that *Fucus* zygotes can photopolarise in medium depleted of Ca^{2+} (Kropf and Quatrano, 1987; Love et al., 1997). They state that K^+ alone is enough for polarisation (Hurst and Kropf, 1991). However, Love et al. demonstrated that different putative Ca^{2+} channel blockers and Ca^{2+} antagonists (nifidipine, TMB 8, bepridil, verapamil) inhibit photopolarisation, reinforcing the data of Robinson obtained with the Ca^{2+} antagonists D600 and Gd^{3+} (Robinson, 1996) and propose that free intracellular Ca^{2+} has a major role in the photopolarisation process (Love et al., 1997). The differences observed in the dependence of external Ca^{2+} for photopolarisation could be due to variations in the capacity of model systems to chelate external Ca^{2+}. In fact, brown algae cell wall contains polymers of guluronic acid, a Ca^{2+} chelator, and this probably constitutes a significant Ca^{2+} store (Kloareg and Quatrano, 1988).

The Ca^{2+} gradient at the presumptive rhizoid pole may result from an asymmetrical distribution of Ca^{2+} channels. It has been postulated that polarisation involves the migration of Ca^{2+} channels in the plasma membrane to the rhizoid pole (Brawley and

Robinson, 1985). In response to light, a fluorescent derivative of the Ca^{2+} channel blocker, dihydropyridine (DHP), is localised asymmetrically at the rhizoid pole. This localisation coincides spatially and temporally with locally elevated Ca^{2+} monitored with the fluorescent indicator Calcium Green (Shaw and Quatrano, 1996). This pattern of distribution could be changed if the direction of the photopolarising stimulus was reoriented before axis fixation (Shaw and Quatrano, 1996). This phenomenon of reversibility and the localisation, time and actin dependence suggests that DHP receptors may correspond to ion channels that are transported to the future rhizoid site to create the changes in Ca^{2+}_{cyt} that are required for polarisation (Shaw and Quatrano, 1996). However, the specificity of fluorescent DHP for Ca^{2+} channels at the rhizoid pole remains to be demonstrated.

1.2.2.4. Axis fixation

Axis fixation was initially defined as the pre-germination period during which the zygote no longer responds to changes in the orientation of the light vector and through which the processes initiated during axis formation (ionic currents, Ca^{2+} gradient, polarised secretion) are amplified (Figure 1.4).

The actin cytoskeleton has been shown to be an important component in axis fixation. F-actin localisation at the rhizoid pole is associated with the Ca^{2+} gradient during axis fixation and rhizoid germination (Kropf et al., 1989; Pu et al., 2000). F-actin localisation, visualised by fluorescently labelling F-actin with rhodamine-conjugated phalloidin, occurs at the future rhizoid germination site by a cytochalasin-sensitive process and was not localised in the zygote until the time of axis fixation (Brawley and

Robinson, 1985). Pu et al. (2000) imaged fluorescent microinjected phalloidin in *Pelvetia* zygotes and did not observe any actin localisation until rhizoid germination. In contrast, Hable and Kropf (2000), using rhodamine conjugated phalloidin, showed that a patch of cortical actin could be observed at the site of sperm entry within minutes of fertilisation. This actin localisation could also be observed in response to a polarising light vector (Alessa and Kropf, 1999). This latter experiment showed that an actin localisation could be observed within 3 h of fertilisation corresponding to early stages of photopolarisation and before axis fixation. Methodological differences have been suggested to explain these contrasting results. Despite the differences in these results, the general consensus is that there is an absolute requirement for actin in photopolarisation.

The enzymatic digestion of the cell wall of young *Fucus* zygotes specifically inhibits axis fixation. The resulting protoplasts are capable of recognising a light stimulus and can photopolarise only once the cell wall is regenerated (Kropf et al., 1988). Spheroplasts of rhizoid or thallus cell can be obtained through laser microsurgery, from the two-cell embryo (Berger and Brownleee, 1995). These loose their polarity and can be induced to develop into new photopolarisible zygotes, which shows the essential role of the cell wall for the maintenance of the polarity, essential to cellular differentiation (Berger and Brownlee, 1995).

The molecules implicated in the interaction of the plasma membrane and cell wall, and their roles, have been subjected to extensive investigation that led to the elaboration of a working model (Figure 1.4).

In *Fucus* zygotes, sulphated fucans are incorporated into the rhizoid cell wall during axis fixation (about 2 h before germination). These molecules were considered to be good candidates for wall-associated components of the axis fixation complexes proposed by Goodner and Quatrano (1993). Zygotes cultivated in seawater without sulphate do not have wall-associated sulphated fucans, and thus remain spherical although they are able to divide.

Shaw and Quatrano (1996b) showed that the inhibition of secretion by brefeldin A inhibits the localisation of the sulphated compounds and also inhibits axis fixation. Together, these results led to the hypothesis that sulphated fucans, localised at the rhizoid pole by exocytosis and dependent on actin filaments, are essential for axis fixation (Figure 1.4). In contrast, Crayton et al. (1974) showed that zygotes cultivated in seawater without sulphate but supplemented with methionine did not adhere to the substrate but were capable of photopolarisation although they did not contain sulphated fucans in their walls. Moreover, experiments performed by Corellou and Bouget (unpublished results) showed that zygotes cultivated in seawater without sulphate but which were adhered to a substrate with poly-L-lysine do not germinate but form and fix a polarity axis. The polarisation, although delayed, happens in the absence of localisation of sulphated compounds at the rhizoid pole. Similar results were obtained with inhibitors of polyphenol sulphatation (dichloronitrophenol and pentachlorophenol). In addition, they observed that the cell wall localisation of polyphenols during normal development is identical to that of sulphated compounds. Whatever the nature of the sulphated compounds is, they seem to be involved more in rhizoid germination and growth than in the fixation of polarity. The inhibition of axis

fixation by brefeldin A probably impairs the proper localisation of other key molecules (not yet identified) for the fixation of the axis.

Other attempts have been made to isolate the molecules implicated in the putative actin-cytoskeleton and cell wall complex. Thus, proteins recognised by the antibodies anti-vitronectin, anti-vinculin and anti-β-integrin were found in extracts of two-cell embryos (Quatrano et al., 1991). Anti-vitronectin antibody added to the culture directly had an inhibitory effect on their capacity for adhesion and on the maintenance of polarity but not on the establishment of polarity. However, the role of these proteins in plants and algae is questionable. Though functionally equivalent molecules are likely to exist, the absence of integrins from the genome of *Arabidopsis* and yeast suggests that these functional homologues may not exist in *Fucus*.

1.2.3 Model of *Fucus* zygote polarisation

The initial mechanisms through which asymmetric environmental cues are translated into cytological asymmetries is still not well understood. Nevertheless, actin localisation seems to have a predominant role (Figures 1.3, 1.4, reviewed by Kropf, 1997). The actin cytoskeleton, essential for the polarisation process, orients the polarised secretions. At axis formation, vesicle exocytosis at the rhizoid pole could be responsible for the localisation of Ca^{2+} channels. It is also conceivable that an early activation of Ca^{2+} channels operates at the rhizoid pole and participates in the production of a transcellular ionic current between the rhizoid pole and the thallus pole. Ca^{2+} elevation favours actin polymerisation and exocytosis at the rhizoid pole, providing positive feedback amplification. Adhesive protein exocytosis and sulphated

polyphenols would allow the interaction between cytoskeleton and cell wall. Simultaneously, the localisation of sulphated fucans at the rhizoid pole potentially alters cell wall proprieties associated with rhizoid emergence.

1.2.4. Germination

At the rhizoid apex, actin microfilaments and a Ca^{2+} gradient are detected (Brownlee and Wood, 1986; Kropf and Quatrano, 1987). The Ca^{2+} gradient is closely associated with rhizoid apical growth. The Ca^{2+} concentration can reach 1 μM at the rhizoid pole. Injection of Ca^{2+} chelators such as Br_2BAPTA and reduction of extracellular Ca^{2+} concentration inhibits rhizoid growth (Speksnijder et al., 1989). Similar Ca^{2+} gradients can be observed in many instances of polarised growth, such as pollen tubes (Rathore et al., 1991; Miller et al., 1992). Ca^{2+} stabilises actin microfilament polymerisation and favours exocytosis of vesicles at the cell apex.

Transcellular currents get stronger during germination, reaching up to 100 pA cm^{-2} (Nuccitelli and Jaffe, 1974). They result from the influx of Ca^{2+}, K^+, Na^+ and the efflux of Cl^- at the rhizoid pole and vice-versa at the thallus pole (Robinson and Jaffe, 1974). In the germinated rhizoid, these currents depend on the integrity of the actin cytoskeleton (Brawley and Robinson, 1985). It has been proposed that the increase in transcellular currents result from the localisation of novel channels by exocytosis (Brawley and Robinson, 1985).

Cytological polarisation becomes progressively more pronounced following germination: the rhizoid accumulates an increasing number of mitochondria and a well developed secretory machinery (Golgi) while at the thallus pole there are numerous

chloroplasts (Quatrano, 1972; Brawley et al., 1976). Experiments which artificially alter organelle distribution by centrifugation have shown that the thallus pole develops on the side where the chloroplasts are more concentrated (Whitiker, 1940). However, this treatment is very aggressive and implies perturbation of numerous other processes and so does not allow conclusions to be drawn about the role of organelle distribution in the establishment of polarisation.

1.2.5. Cell division and cell cycle

The rotational alignment of the nucleus 13-16 h after fertilisation, which is necessary for cell division, is helped by microtubules, which are anchored to centrosomes at one end and appear to grow and attach to actin-stabilising complexes at the rhizoid tip (Kropf, 1994; Figure 1.3, 1.4). Treatment with cytochalasin D results in improper rotation (Allen and Kropf, 1992) probably due to disruption of these actin-stabilising complexes. Similar mechanisms are thought to be involved in the orientation of asymmetric divisions in yeast cells (Li et al., 1993). Mitosis begins about 18-22 h after fertilisation and is followed by division into two unequal cells, rhizoid and thallus cell. A partition cross-cell wall forms transverse to the growth axis, probably composed of alginates, cellulose and fucans. Although no plasmodesmata were observed in *Fucus* embryos, cytoplasmatic connections do remain for some time after cell division (Brawley et al., 1976). For example, cells have been shown to exhibit dye coupling (Brownlee and Pulsford, 1988) and electrical coupling (Weisenseel and Jaffe, 1972) until at least the four-cell stage.

The cell cycle in the *Fucus* embryo consists of well-defined G1, S, G2 and M phases and presents the main features of a somatic cell cycle instead of a cell cycle typical of animal embryos. Cyclin-dependent kinases (CDKs) have been shown to tightly control cell cycle progression (Corellou et al., 2001b). Two functional DNA replication and spindle assembly checkpoints block cell cycle progression by altering CDKs activities. CDKs are regulated at both the transcriptional and transductional levels and by phosphorylation. *Fucus* embryos cell cycle exerts a tight control on morphogenesis during early embryogenesis. The photopolarisation period and the G1/S transition were found to be concomitant, providing a link between cell cycle control and establishment of polarity (Corellou et al., 2001a). Inhibiting entry into S phase with purine derivatives prevented the early expression of the morphogenesis, i.e. germination. Other purine derivatives as olomoucine and amino-purvalanol inhibit photopolarisation and germination only when applied before or at the time of sensitivity to light (or entry into S phase) suggesting that inhibition of germination is due to the inhibition of polarisation.

1.2.6. Fucus as a model system

There are a number of difficulties inherent in plant embryogenesis studies. The embryos, of small size, are enclosed in the maternal tissue, making pharmacological and cellular biological approaches extremely difficult. The genetic approach, mainly in *Arabidopsis* offers significant advantages while the study of somatic embryogenesis constitutes an alternative, though the first stages of development do not necessarily reflect the zygotic embryogenesis.

Fucus zygotes develop autonomously, can be harvested in large quantities and an entire population can be induced to establish polar axes synchronously by the application of external vectors such as unidirectional light. Young zygotes attach firmly to the substratum and populations of attached zygotes can be grown synchronously through early development. In addition, their relatively large size (80-100 μm) and the absence of significant vacuoles allows the use of microinjection techniques and image analysis, which are more difficult to achieve in other plants. The abundance of material also makes biochemical and molecular approaches possible during fucoid development. Finally, the first development events take place slowly enough to be studied with precision. Thus, the zygotes of *Fucus* provide a unique cellular system that allows an experimental approach to embryogenesis in its own physiological conditions.

1.3. PHOTOSYNTHESIS AS AN INDICATOR OF STRESS STATUS

1.3.1. Introduction

Because damage to photosystem II (PSII) is often one of the first manifestations of stress (reviewed by Osmond, 1994), photosynthesis is considered to be an important parameter in assessing the health of a photosynthetic organism. Recently, progress has been made in developing alternative methods for non-intrusive assessment of *in vivo* photosynthesis. In particular, chlorophyll fluorescence has evolved as a useful method and informative indicator for photosynthetic electron transport in intact plant leaves, algae and isolated chloroplasts (reviewed by Krause and Weis, 1991). As a result of intensive investigation, highly selective fluorescence meters are now available which can allow quantitative analysis of photosynthetic quantum yields and electron transport rates. Chlorophyll fluorescence is an appropriate indicator of the stress status of a plant, because it can indicate the extent to which photosystem II (PSII) is using the energy absorbed by chlorophyll and to what extent it is being damaged by excess light or other stress factors.

1.3.2. Chlorophyll fluorescence methods

1.3.2.1. The basis of chlorophyll fluorescence measurements

The principle underlying chlorophyll fluorescence analysis is relatively straightforward. Light energy absorbed by chlorophyll molecules can undergo one of three fates: it can be used to drive photosynthesis (photochemistry), excess energy can be dissipated as heat (for example through the xanthophylll cycle pigment pool) or it

can be re-emitted as light (chlorophyll fluorescence). These three processes occur in competition, so any increase in the efficiency of one will result in a decrease in the yield of the other two (quenching). Hence, by measuring the yield of chlorophyll fluorescence, information about changes in the efficiency of photochemistry and heat dissipation can be obtained.

The interrelationship between the three different fates of harvested light energy provides information about the efficiency with which photosynthesis is performed. During photosynthetic electron transport through PSII and acceptance by quinone A (Q_A) of one electron, the PSII is "closed" until the electron is passed on from Q_A to plastoquinone (PQ) (Figure 1.5). As the proportion of closed reaction centres increases, the amount of light energy channelled into photosynthesis decreases, resulting in an increase in chlorophyll fluorescence. This happens upon transfer from dark to light, when a disproportionate number of reaction centres becomes closed, resulting in increased chlorophyll fluorescence. After a few seconds, PSII begins to adapt to the light and chlorophyll fluorescence decreases over several minutes to a steady state level in a process called "chlorophyll quenching".

Measurement of chlorophyll fluorescence is relatively easy; the spectrum of fluorescence is different to that of absorbed light, with the peak of fluorescence emission being of longer wavelength (and thus less energetic) than that of absorption. Therefore, fluorescence yield can be quantified by exposing the material to light of defined wavelengths and measuring the amount of light re-emitted at longer wavelengths.

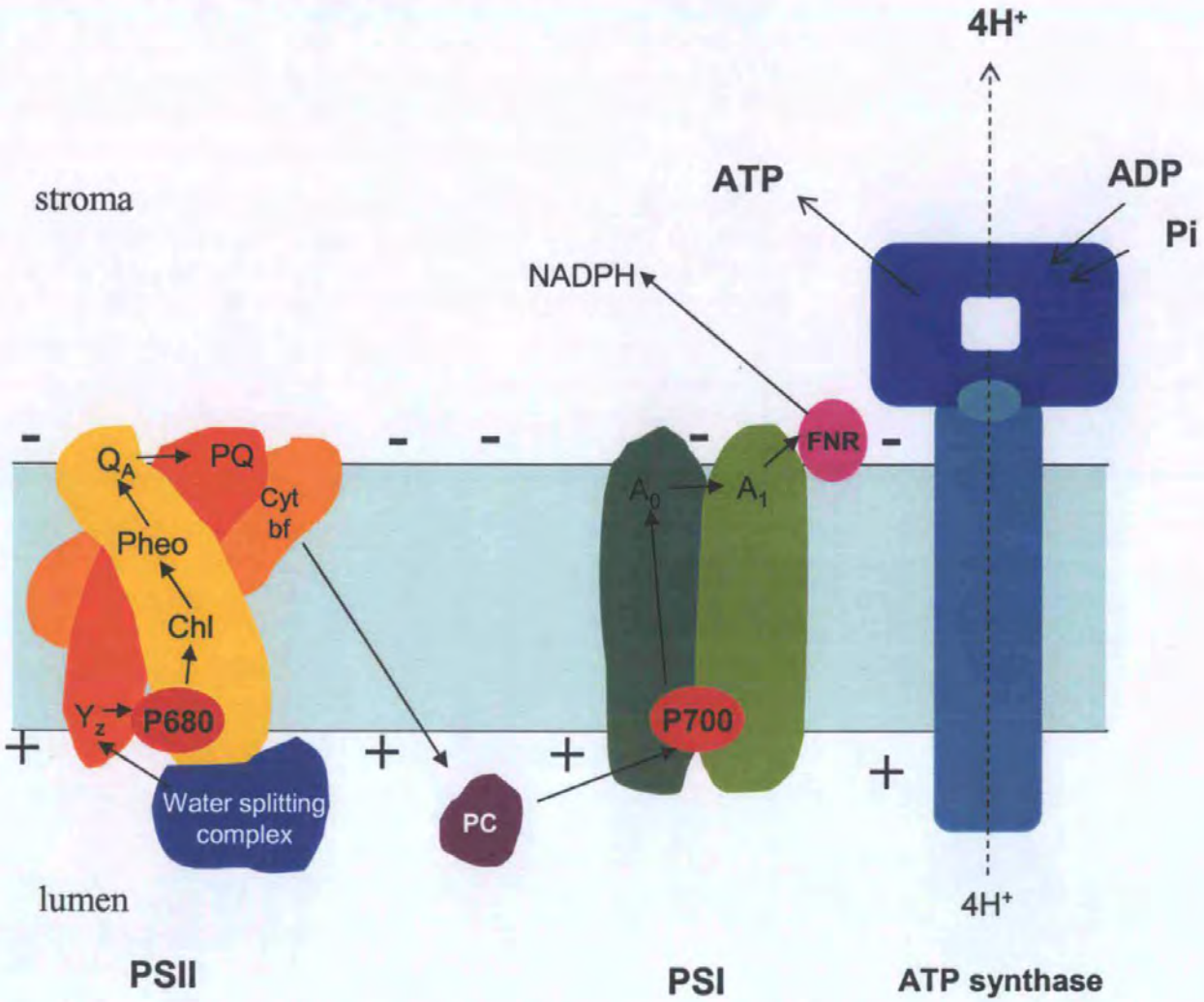

Figure 1.5. Schematic cross-section of a thylakoid membrane. The orientation and some of the major components of the photosynthetic apparatus are shown. Electron transport chain is represented by closed arrows. Electrons extracted from water in PSII are sequentially transferred to the cytochrome bf complex (cytbf) and thence through plastocyanine (PC) to PSI where they are used to reduce NADP to NADPH.

Abbreviations: Qa – bound quinone; PQ – free plastoquinone; P680 and P700 – reaction centres chlorophyll a molecules of PSII and PSI respectively; FNR – ferredoxin/NADP oxireductase; PC – plastocyanin; Pheo - a pheophytin a molecule; Y_z – a tyrosine that is the immediate electron donor to the PSII chlorophyll P680; A_0 – the immediate electron acceptor from P700 (a chlorophyll a molecule); A_1 – phylloquinone; chl – chlorophyll molecule.

After Falkowvki and Raven, 1997

In "modulated" measuring systems, the light source used to measure fluorescence is modulated (i. e., switched on and off at very high frequency) and the detector is tuned to detect only fluorescence excited by measuring light. Therefore, the relative yield of fluorescence can be measured in the presence of background light.

1.3.2.2. Deconvoluting fluorescence signals

To gain more information about photosynthesis using chlorophyll fluorescence, it is necessary to distinguish between photochemical and non-photochemical contributors to quenching. The approach used is to "switch off" one of the two components, namely that due to photochemistry, so that fluorescence yield solely in the presence of the non-photochemical contributors can be estimated. The technique used involves giving the sample a high intensity, short duration flash of light, which transiently closes all the PSII reaction centres reducing photochemical quenching to negligible levels (SL, Figure 1.6). Provided the flash is short enough, no increase in non-photochemical quenching will occur and no long-term effect on the efficiency of photosynthesis is induced. During the flash, the system reaches the maximum fluorescence (F_m), and comparison of this value with the steady-state fluorescence (F_s) and the yield of fluorescence in the absence of an actinic (photosynthetic) light (F_0) gives information about the efficiency of photochemical quenching and performance of PSII.

1.3.2.3. Terminology in quenching analysis

A large number of coefficients have been used to quantify photochemical and non-photochemical quenching. The terminology used here is summarised in Table 1.1. See also Figure 1.6.

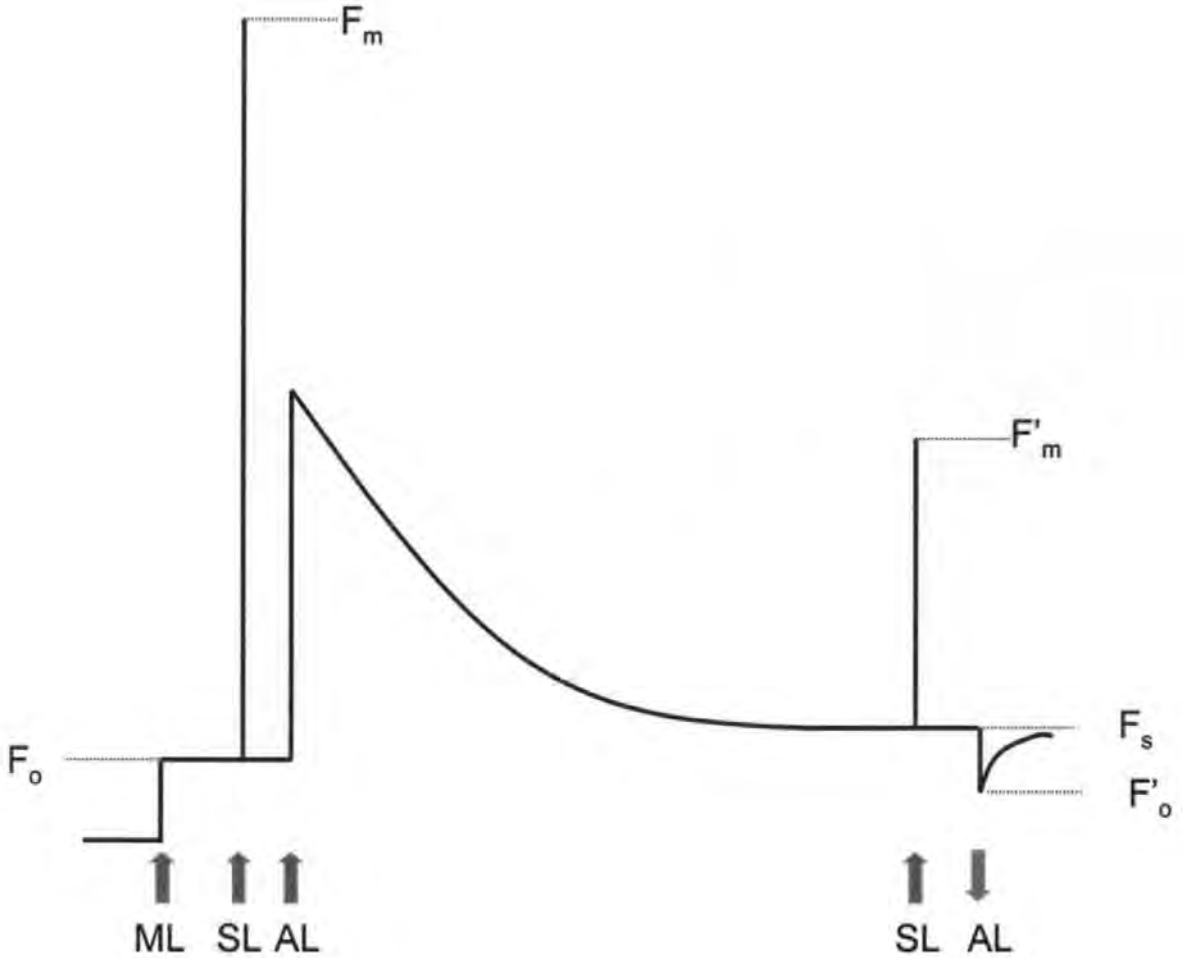

Figure 1.6. Sequence of a typical fluorescence trace. A measuring light is switched on (↑ML) and the zero fluorescence level is measured (F_0). Application of a saturating light flash (↑SL) allows measurement of the maximum fluorescence level F_m. A light to drive photosynthesis (↑AL) is then applied. After a period of time, another saturating light flash (↑SL) allows the maximum fluorescence in the light, F'_m to be measured. The level of fluorescence immediately before the saturating pulse is termed F_s. Turning off the actinic light (AL↓) allows measurement of zero fluorescence in the light, F'_0.

After Maxwell and Johnson, 2000

Table 1.1. *Nomenclature used for chlorophyll fluorescence methods and respective definitions.*

Parameter	Definition	Equation
Φ_{PSII}	Effective quantum yield	$\Delta F/F'_m=(F'_m - F_s)/F'_m$
F_v/F_m	Optimal (maximum) quantum yield	$(F_m - F_0)/F_m$
F_s	Steady-state fluorescence, light adapted	
F_m	Maximum fluorescence yield, dark adapted	
F'_m	Maximum fluorescence yield, light adapted	
F_0	Minimal fluorescence yield, dark adapted	
F'_0	Minimal fluorescence yield, light adapted	
qP	Photochemical quenching (proportion of open reaction centres)	$(F'_m-F_s)/(F'_m-F'_0)$
qN	Non-photochemical quenching	$1 - (F'_m-F'_0)/(F_m-F_0)$
NPQ	Alternative definition of qN	$(F_m-F'_m)/F'_m$
rel. ETR	Relative electron transport rate	PPFD * Φ_{PSII}

Whereas $\Delta F/F'_m$ (Φ_{PSII}) expresses the efficiency of energy conversion at a given light intensity, qN gives an indication of the proportion of PSII reaction centres that are open. F_v/F_m is a measure of the intrinsic (maximal) efficiency of PSII (i.e. the quantum efficiency if all the PSII reaction centres were open) provides information about the general condition of PSII.

1.3.2.4. Photochemical processes

The parameter $\Delta F/F'_m$ measures the efficiency of PSII, i.e. the proportion of light absorbed by chlorophyll in PSII that is used in photochemistry. It gives a measure of the electron transport, and hence an indication of the overall photosynthetic rate. Multiplying $\Delta F/F'_m$ by the light absorbed gives the relative electron transport rate (ETR). In intact plant leaves, it is not practical to measure the light absorbed by the leaf tissue. However, provided similar samples are being compared (i.e. the absorption of light is constant) changes in relETR can simply be calculated by multiplying $\Delta F/F'_m$ by light intensity.

The parameter qP gives an indication of the proportion of reaction centres that are open, i.e., available to transfer electrons to PSII. qP and $\Delta F/F'_m$ can be correlated by a third parameter, F_v/F_m, which is a measure of the intrinsic (optimal) efficiency of PSII. A change in qP is due to closure of reaction centres, resulting from saturation of photosynthesis by light. A change in F_v/F_m is due to a change in the efficiency of non-photochemical quenching. After dark adaptation, F_v/F_m can be calculated, and it gives a good indication of the plant photosynthetic performance. F_v/F_m is generally expected to be around 0.83 and lower values are an indication that PSII is being exposed to stress such as photoinhibition (Maxwell and Johnson, 2000). Calculation of F_0 is achieved by applying far-red light for a few seconds before and immediately after the end of each illumination step.

1.3.2.5. Non-photochemical processes

NPQ and qN measure changes in heat dissipation. Any change in these parameters measures a change in the efficiency of heat dissipation relative to the dark-adapted situation. In general, such an increase can be a result either of processes that protect the tissue from light-induced damage or by the damage itself. Thus both reversible non-photochemical quenching (q_E) and irreversible non-photochemical quenching (q_I) may contribute to NPQ. However, reversible non-photochemical quenching is usually considered more important (Maxwell and Johnson, 2000). q_E is initiated by acidification of the luminar side of the thylakoid membrane during high rates of H^+ transport and by a large ΔpH across the thylakoid membrane, which may occur at photosynthetically saturating irradiances (Ruban and Horton, 1999). Very low luminar pH results in activation of de-epoxidase and consequent de-epoxidation of the carotenoid violaxanthin to zeaxanthin in the xanthophyll cycle, which coincide with thermal dissipation of excess light energy (Demmig-Adams, 1990; Demmig-Adams and Adams, 1992; Ort, 2001). For most purposes, all processes that relax at a time scale of minutes after the cessation of illumination can be regarded as photoprotective processes. Processes that relax after hours are usually referred to as photoinhibition (Maxwell and Johnson, 2000).

1.3.2.6. PSII quantum yield as measure of photosynthesis

Chlorophyll fluorescence can be used, in a simplified manner, to give a measure of the efficiency of PSII photochemistry ($\Delta F/F'_m$). This measure can be converted into a relative rate of electron transport (rel.ETR) by multiplying it by the light intensity. Under laboratory conditions, PSII electron transport and CO_2 fixation are very well

correlated, although some discrepancies are found in field measurements (Genty et al., 1989).

1.3.2.7. Measuring stress status and stress tolerance

One of the advantages of chlorophyll fluorescence measurements lies in their capacity to give insights into the ability of a photosynthetic organism to tolerate environmental stresses and the extent to which those stresses have damaged the photosynthetic apparatus. Such measurements have given information on for example the extent of photoinhibition in response to light, temperature, and other stresses (Bilger et al., 1995) and the occurrence of photoinhibitory damage (Groom and Baker, 1992). Thorough investigations of photochemical efficiency, photosynthesis and the xanthophyll cycle (Demmig-Adams, 1990; Demmig-Adams and Adams, 1992) showed that photosynthetic organs of plants naturally subjected to high light intensities usually have a large xanthophyll cycle pool, with de-epoxidation of violoxanthin to zeaxanthin strongly related to non-photochemical quenching.

1.3.3. The photosynthesis-irradiance curve

The photosynthesis/irradiance (PI) curve can usually be resolved into three distinct regions, namely a light-limited region, a light saturated region and a photoinhibition region (Falkovski and Raven, 1997). At low irradiance levels, photosynthetic rates are proportional to irradiance. In this region of the PI curve, the rate of photon absorption determines the rate of steady-state electron transport from water to CO_2, and thus it is called the light-limited region. The light intensity at which photosynthesis balances respiration is called the compensation light intensity (Ec). The initial slope of the PI

curve (α) is proportional to the maximum quantum yield of photosynthesis (Kok, 1948), and is usually taken as a direct measure of this parameter (Lawlor, 1993).

As irradiance increases, photosynthetic rates become non-linear and rise to a saturation level (P_{max}). At light saturation, the rate of photon absorption exceeds the rate of steady-state electron transport from water to CO_2. Further increases in irradiance beyond light saturation can lead to a reduction in photosynthetic rate from the maximum saturation level. This reduction is called photoinhibition, and results in a reduction in the photochemical efficiency of PSII ($\Delta F/F'_m$; Falkovski et al., 1994).

1.3.4. Photosynthesis under stress situations - production and scavenging of reactive oxygen species

Under natural conditions, plants experience fluctuations in the light environment from which they cannot escape. Furthermore, other photosynthetic environmental factors, such as water supply and carbon dioxide concentration are also variable, and not always favourable when in combination with strong light intensities. Under conditions where the photon intensity is in excess of the photon-utilising capacity, excess photons produce reactive molecules in chloroplasts, and these reactive molecules oxidise target molecules. All these processes can lead to photoinhibition (Asada, 1994). Other environmental conditions, alone or in combination, such as chilling stress (Michaeli et al., 2001), ultraviolet light (Smith et al. 2001), ozone (Manes et al., 2001) and pollution stress (e.g. copper, Patsikka et al., 2002) also lower the photon-utilising capacity and induce photoinhibition.

A strong relationship between photoinhibition and reactive oxygen species (ROS) is emerging. Photosynthesis has a high capacity for production of hydrogen peroxide, although the intracellular levels of this relatively weak oxidant are kept in strict control by the antioxidant system, which comprises a network of enzymatic and non-enzymatic components. An example of the tight connection found between ROS, photoinhibition and antioxidant systems is the study performed by Payton et al. (2001) and Kornyeyev et al. (2001). The authors found enhanced photochemical light utilisation and decreased chilling-induced photoinhibition of photosystem II in cotton leaves over-expressing genes encoding chloroplast-targeted antioxidant enzymes.

Permanent photoinhibition of photosynthesis is caused by oxidative damage of photosynthetic compounds by the photoproduced reactive molecules. The D1 protein in the PSII reaction centre and several Calvin cycle enzymes are the primary targets (Asada, 1993; Nishiyama et al., 2001).

Dissipation of excess energy in the form of heat is the safest method available to photosynthetic organisms, but photon energy transfers to chlorophyll and dioxygen molecules are inevitable, producing triplet-excited chlorophyll and singlet excited oxygen (Santabarbara et al., 2002). Furthermore, the electron transfer to dioxygen in photosystem I (PSI) generates superoxide anion radicals and the disproportionation of superoxide by superoxide dismutase generates hydrogen peroxide (see Figure 1.7; 1.8). In conclusion, several recent studies are emerging showing the tight connection between ROS generated at the photosynthetic machinery level and the process of photoinhibition of thylakoids. Section 1.4 treats in more detail the chemistry of ROS in biological systems.

1.4. Reactive Oxygen Species (ROS) production and function during stress

1.4.1. Chemistry of ROS in biological systems

All animals and plants require oxygen for the efficient production of energy, with the exception of those organisms that are specially adapted to anaerobic conditions. Aerobic conditions, however, can potentially cause oxidative damage due to the tendency of oxygen to form free radicals. The term "free radical" refers to any species capable of independent existence that contains one or more unpaired electrons (Halliwell and Gutteridge, 1999). The presence of impaired electrons causes the species to be very reactive. The oxygen molecule, as it occurs naturally, qualifies as a radical, because it has two unpaired electrons. For the purpose of this work, the term "reactive oxygen species" (ROS) is used to describe the products of the sequential reduction of molecular oxygen: if a single electron is added to the ground state O_2 molecule the product is the superoxide radical $^{\bullet}O_2^-$; the two-electron reduction product of oxygen in biological systems exists as hydrogen peroxide (H_2O_2) and the four electron product is water (Figures 1.7 and 1.8). Hydrogen peroxide mixes readily with water and acts as an oxidising agent. Hydrogen peroxide decomposes easily and its homolytic fission gives rise to the most aggressive ROS, the hydroxyl radical ($^{\bullet}OH$).

The generation of superoxide requires a slight input of energy. In living cells, superoxide exists in equilibrium with its protonated form, the hydroperoxyl radical ($^{\bullet}O_2H$). The latter form is more hydrophobic than superoxide and can more easily penetrate the lipid bilayer of the membranes. However, at physiological pH, superoxide

is not very reactive against the majority of macromolecules of the cell. In aqueous solutions, at neutral or slightly acidic pH, this radical in either form disproportionates to H_2O_2 and O_2 (Figures 1.7, 1.8). This reaction either occurs spontaneously or is catalysed by superoxide dismutase (SOD) found in the cytosol, chloroplasts, mitochondria and extracellularly (reviewed by Alscher et al., 2002). Thus, in any system producing superoxide, substantial amounts of H_2O_2 are also formed.

Hydrogen peroxide is a relatively stable ROS: because it is electrically neutral and not very reactive, it can diffuse across membranes and reach cell locations relatively remote from its site of production. In plant cells, hydrogen peroxide can be disproportionated by catalase (Figure 1.8), used as a substrate by peroxidases or be detoxified by ascorbate peroxidase acting in concert with dehydroascorbate reductase and glutathione reductase in the Halliwell-Asada pathway (Figure 1.8). Under appropriate conditions, however, H_2O_2 can be generated by peroxidases (Halliwell and Gutteridge, 1999, Bolwell et al., 2002).

The hydroxyl radical is the most reactive species among ROS. It can be formed by the direct reaction of H_2O_2 and $^{\bullet}O_2^-$ (Haber-Weiss reaction, Figure 1.8). In plants, however, this reaction is very slow (Bartosz, 1997). Nevertheless, significant amounts of $^{\bullet}OH$ can be formed through the cycle of reactions involving oxidation of transition metals such as Fe^{2+} and Cu^{+} (Fenton reaction, Figure 1.8), and subsequent regeneration of the oxidised ions to their reduced state via reaction with superoxide. Transition metals in this case act as catalysts, so the cellular site of $^{\bullet}OH$ formation depends upon the location and accessibility of transition metals. Hydroxyl radical is

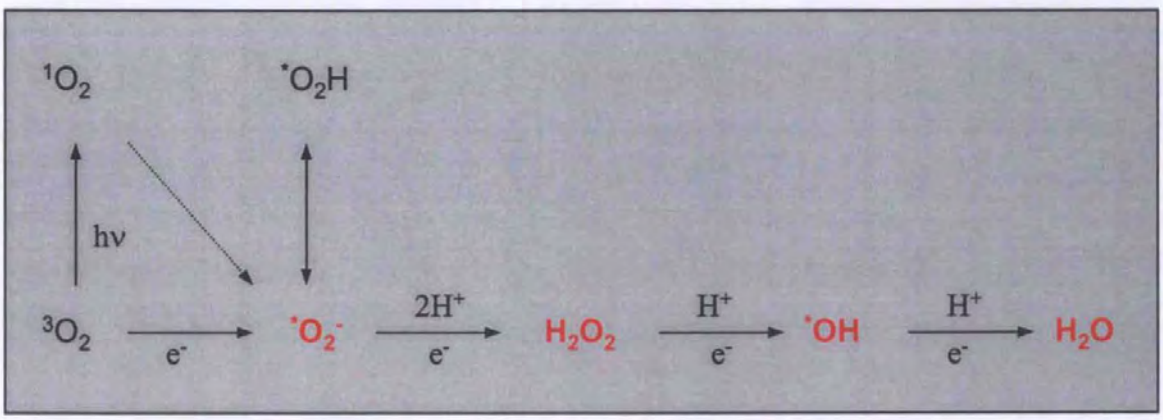

Figure 1.7. Interactions between molecular oxygen and ROS generated in reactions likely to occur in plant cells.

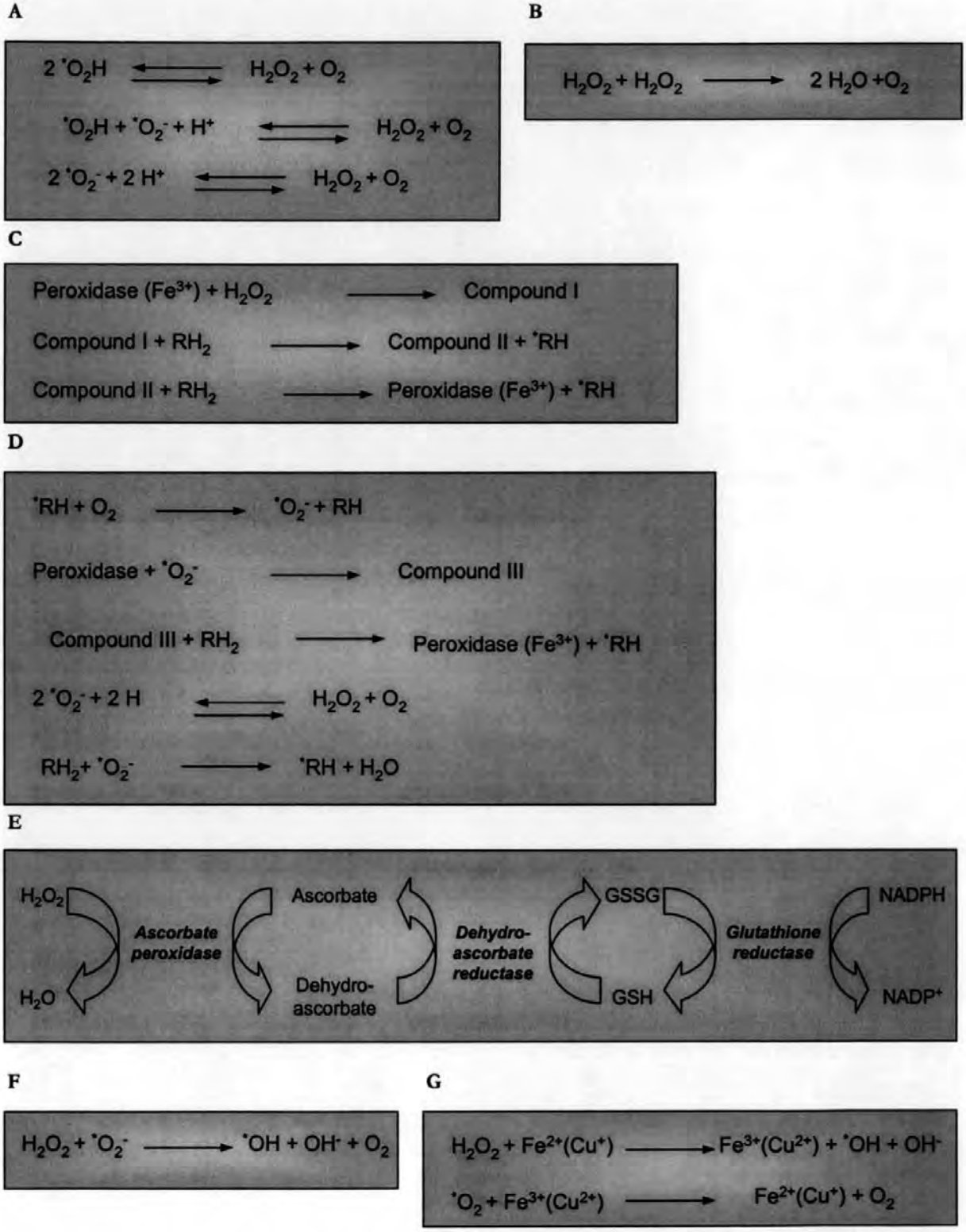

Figure 1.8. Summary of ROS chemical reactions. These major reactions determine the fate and possible inter-conversions of ROS in plants. **A)** Superoxide disproportionation by superoxide dismutase (SOD); **B)** Reaction catalyzed by catalase; **C)** Reactions catalyzed by peroxidase; **D)** Generation of H_2O_2; **E)** Halliwell-Asada pathway; **F)** Haber-Weiss reaction; **G)** Fenton reaction.

After Wojtaszek, 1997

believed to be the major cause of irreversible modification of cellular molecules and damage of organelles (Halliwell and Gutteridge, 1999).

1.4.2. Sources of ROS

1.4.2.1. NADPH oxidase

In neutrophils, the oxidative burst involves the reaction O_2 + NADPH $\Rightarrow$ $^{\bullet}O_2^-$ + NAD^+ + H^+, followed by dismutation of $^{\bullet}O_2^-$ to H_2O_2 (Morel et al., 1991). Superoxide production is catalysed by a multi-component plasma membrane oxidase that accepts NADPH at the cytosolic side of the membrane and donates this to molecular oxygen at the other side of the membrane, either in the outside of the cells or in the phagosome that contains ingested micro-organisms. In animal systems, the NADPH oxidase is composed of a b-type cytochrome with two membrane-bound subunits, p22-phox and gp91-phox which together comprise cytochrome b558, and two cytosolic components called p47-phox and p67-phox (Figure 1.9). Upon cell activation, the latter two proteins are phosphorylated and, together with a third cytosolic p40-phox component, translocate to cytochrome b558 in the plasma membrane to form the active enzyme. G-proteins including Rap1A and rac are also involved in the assembly of the active complex. In plants, less is known about the configuration of NADPH oxidase.

Several biochemical-based studies (mainly pharmacological) indicate that plant NADPH oxidase shares many characteristics with neutrophil NADPH oxidase. An NADPH oxidase-dependent $^{\bullet}O_2^-$ generating system is present in microsomes from potato tubers (Doke and Miura, 1995). Elicitation with an incompatible race of

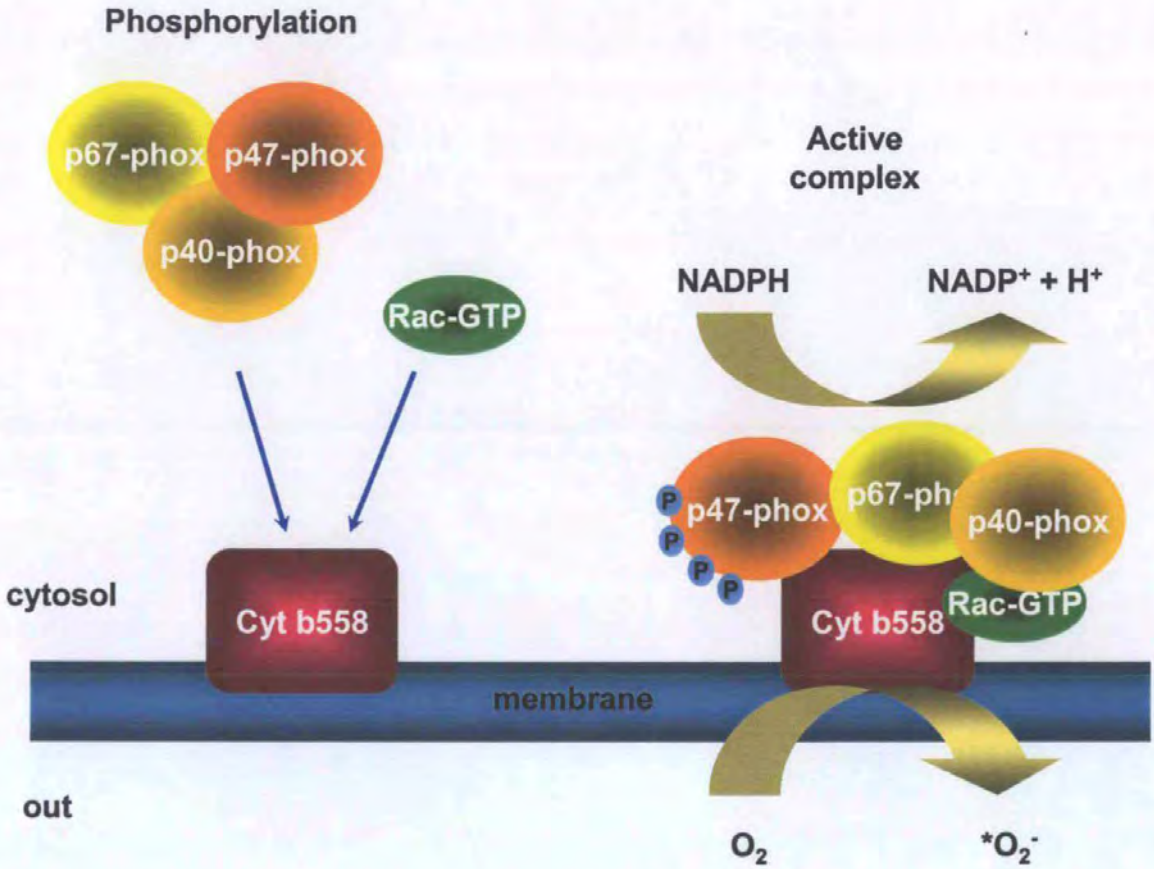

Figure 1.9. Summary of NADPH oxidase components in animal cells. Activation of the phagocyte NADPH oxidase complex requires the assembly of cytosolic components p67, p47-phox, p40-phox and rac1 or rac2, with the membrane bound cytochrome b558 (a heterodimer comprising gp91-phox and p22-phox). Phosphorylation of the cytosolic components is an essential step for initiation of the interaction with the membrane bound oxidase components and thus activation of the enzyme complex. The most studied phosphorlyations are on p47-phox where this is thought to lead to a conformational change allowing interaction with gp91-phox and p22-phox.

Phytophthora infestans or treatment with cell-wall-derived elicitors stimulates NADPH-dependent superoxide production, mainly at the plasma membrane level (Doke and Miura, 1995). Release of superoxide was extracellular, and did not depend on the presence of a cell wall. Superoxide generation at the external surface is followed by a rapid enzyme-catalysed dismutation to hydrogen peroxide.

Several inhibitors of the neutrophil NADPH oxidase, including the suicide substrate inhibitor diphenylene iodonium (DPI) also block the fungal elicitor-stimulated oxidative burst (Levine et al., 1994; Auh and Murphy, 1995; Desikan et al., 1996; Lingterink et al., 1997; Pugin et al., 1997; Sagi and Fluhr, 2001). Moreover, a polyclonal antiserum to a specific peptide of the neutrophil NADPH oxidase reacts with a single polypeptide of the same size in western blots of soybean microsomal membrane preparations (Tenhaken et al., 1995). Antibodies raised against human p22-phox, p47-phox and p67-phox react with plant cytosolic polypeptides of appropriate size (Desikan et al., 1996; Tenhaken et al., 1995; Xing et al., 1997). Molecular cloning of respiratory burst oxidase homolog (Rboh) in *Arabidopsis* (AtrbohA-F) and tomato (Lerboh1) define transcripts that can encode a protein of about 105 kDa in size with a C terminal region that shows pronounced similarity to the 69 kDa apoprotein of the gp91-phox. The AtrbohA and Lerboh1 proteins have a large hydrophilic N-terminal domain that is not present in gp91-phox. This domain contains two Ca^{2+}-binding EF hand motifs and has extended similarity to the human RanGTPase-activating protein (Keller et al., 1998, Torres et al., 1998). A rice expressed sequence tag, RICR1091A, has been identified and shows similarity to a human gene sequence encoding the apoprotein gp91-phox, and the corresponding rice gene rbohA (for respiratory burst oxidase homologue A) has been isolated (Groom et al., 1996). Unlike the mammalian

NADPH oxidase, plant oxidase has been shown to produce superoxide in the absence of additional cytosolic components (Sagi and Fluhr, 2001). Identification of plant gene sequences suggests that there are functional and mechanistic similarities between neutrophil and plant oxidative burst, although regulation of the oxidase activity may be different.

1.4.2.2. Other sources of ROS

Mitochondria and chloroplasts are major producers of reactive oxygen species (Gonzalez-Flecha and Boveris, 1995; Poyton and McEwen, 1996), mainly due to their electron transport chains, which are prone to electron leakage.

In chloroplasts, one main generation site of superoxide radicals is PSI at the level of ferredoxin-$NADP^+$ reductase, but the reduced form of monodehydroascorbate reductase (MDHAR) also produces superoxide (Asada, 1999). Furthermore, the generation of superoxide and hydroxyl radicals by PSII has been reported, and P_{680}, pheophytin and protein Q_A have all been proposed as responsible for superoxide production (Navari-Izzo et al., 1999).

Under conditions of high light, elevated temperatures and low CO_2 availability the Mehler reaction and photorespiration are important producers of ROS (Noctor et al., 2000). In the Mehler reaction, the low potential acceptors in the chloroplast PSI reduce O_2 to superoxide, from which hydrogen peroxide is then produced. Hydrogen peroxide is processed by catalases, which catalyse its disproportionation, and peroxidases that use reductants to convert it into water. In plants, a very important reductant for peroxidase activity is ascorbate, which is oxidised to

monodehydroascorbate radical (MDHA). Ascorbate peroxidase activity can be linked directly to electron transport chains via reduction of MDHA reductase activity or to glutathione redox cycling through the ascorbate-glutathione cycle (see Figure 1.8; reviewed by Noctor et al., 2000).

Peroxisomes also play an important role in ROS production. The main metabolic processes responsible for generation of ROS in these organelles are photorespiration, glycolate oxidase reaction, fatty acid β-oxidation, the enzymatic reaction of flavin oxidases and the disproportionation of superoxide radicals by superoxide dismutase (Corpas et al., 2001).

Mitochondria are one of the most powerful generators of ROS within the cell (Morel and Barouki, 1999; see also Figure 1.10). In this organelle, the electron-deficient dioxygen molecule O_2 is brought close to electron suppliers. Indeed, the respiratory chain involves several successive complexes containing electron carriers (cytochrome c, ubiquinone, etc.) that allow the progressive and controlled reduction of O_2 to water. A dysfunction at one step of this chain may thus result in excessive production of ROS. For example, the inhibition of complex III leads to H_2O_2 release (Garcia-Ruiz et al., 1995), and several stimuli have been shown to induce mitochondrial H_2O_2 release (Quillet-Mary et al., 1997). In animal systems, it is well documented that one of the important sources of ROS during the oxidative burst is the mitochondrial electron transport chain (Coyle and Puttfarcken, 1993; Tan et al., 1998; Quillet-Mary et al., 1997). This oxidative burst is consistently associated with Ca^{2+} influx to mitochondria and with initiation of apoptosis and ageing. In the fungus *Podospora anserina*, for example, mitochondrial oxidative stress is a major contributor to ageing (Osiewacz,

2002). ROS are generated as a result of electron leakage during respiration and lead to damage of components of the electron transport chain in ageing cultures. Damaged proteins cannot be replaced because the mitochondrial genes encoding some of the corresponding subunits gradually become deleted from the mitochondrial DNA due to the oxidative damage. Consequently, these defects result in increased production of ROS and cell death. Thus, when the usually well-organised mitochondrial biochemical pathways are perturbed by biotic or abiotic stress, the mitochondria may suffer damage by oxidative stress. Crawford et al. (1998) found that mitochondrial RNA undergoes specific degradation upon oxidative stress. This results in a dramatic shut-down of mitochondrial protein biosynthesis. Oxidative stress caused by H_2O_2 treatment, catalase knock-out or ageing contributes to mitochondrial dysfunction in the fruit fly *Drosophila melanogaster* (Schwarze et al., 1998). Oxidative stress was shown to reduce the levels of complex IV cytochrome c oxidase RNA. Furthermore, mitochondria have been shown to be central integrators of apoptosis (Susin et al., 1998; Jones, 2000), and ROS are believed to have a central role in this matter.

As in animal cells, the mitochondrial electron transport chain (ETC) is potentially a major source of ROS production in plants. In addition to complexes I to IV, plant mitochondria ETC possess non-proton-pumping NAD(P)H dehydrogenases on each side of the inner membrane - NDex and NDin (see Figure 1.10). These are Ca^{2+}dependent enzymes and they are active only when the cell is stressed (for a review see Moller, 2001). Complex I is the major enzyme oxidising NADH under normal conditions and a major site of ROS production together with complex III. The mitochondria of plants (along with those of some protists, fungi and algae) also possess an alternative respiratory pathway composed of a single terminal oxidase

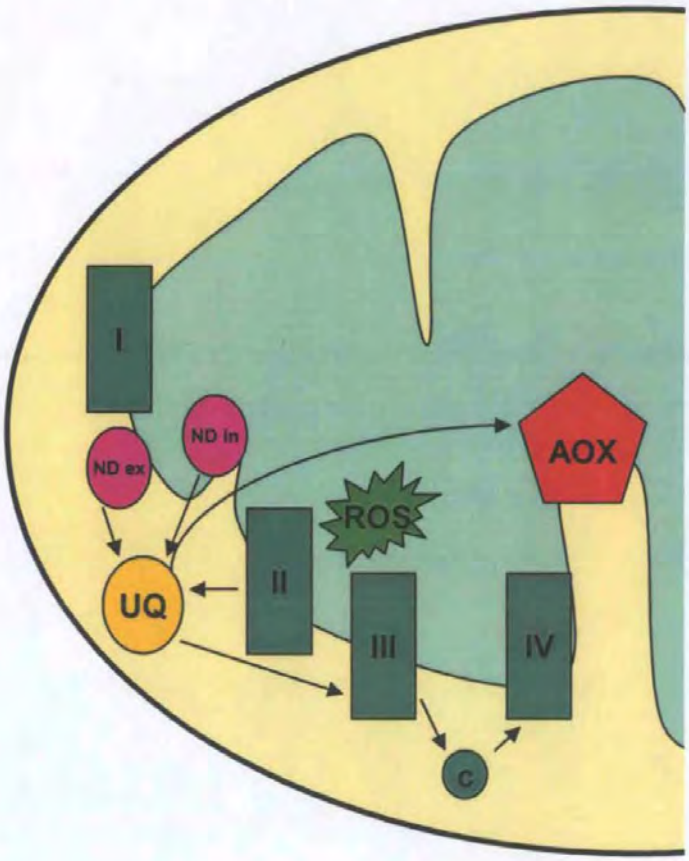

Figure 1.10. Summary of plant mitochondrial electron transport chain. Plant mitochondria contain two terminal oxidases - **complex IV** (cytochrome oxidase) and **alternative oxidase** (AOX). The energy-transducing inner membrane includes **complex I** (NADH-dehydrogenase), several proposed internal (int) and external (ext) NAD(P)H-dehydrogenases; **complex II** (succinate dehydrogenase); **complex III** (the cytochrome bc1 complex) and cytochrome c (C). ROS arise from this electron transport pathway and along with citrate, are known to induce nuclear-encoded alternative oxidase.

After Mackenzie and McIntosh, 1999

(Figure 1.10, reviewed in Mackenzie and McIntosh, 1999). This alternative oxidase (AOX) pathway is up-regulated during stress, including cold, pathogen attack, drought and wounding, and since these stresses also induce ROS formation in the mitochondria, a function as been proposed in plant stress adaptation. Further evidence comes from the observation that addition of external H_2O_2 to cultured plant cells induces alternative pathway respiration (Wagner, 1995) and inhibition of alternative oxidase stimulates H_2O_2 accumulation in soybean and pea (Popov et al., 1997). Recent experiments in transgenic tobacco under- or over-expressing AOX support this hypothesis. Furthermore, addition of antimycin A (an inhibitor of the cytochrome oxidase pathway) dramatically increases H_2O_2 production, and cells over expressing AOX have little H_2O_2 production compared to controls (McIntosh et al., 1998). Interestingly, a role for Ca^{2+} is starting to emerge as a physiological transducer of pathways involved in expression of alternative oxidase (Tsuji et al., 2000).

An estimated 1% of the total O_2 consumption of a plant tissue goes to ROS production (Puntarulo et al., 1988). The relative importance of chloroplasts and mitochondria in plant ROS production in the light is not known.

Although mitochondria and chloroplasts are major producers of ROS, surprisingly few reports have addressed the relative importance of these organelles in ROS production in plants. ROS production by mitochondria is mentioned mainly in reports associated with programmed cell death (reviewed by Jones, 2000), and in relation to mitochondrial Ca^{2+} efflux during hypoxia (Subbaiah et al., 1998). Allan and Fluhr (1997) reported an increase in ROS inside chloroplasts and the nucleus after elicitation with cryptogein in tobacco cells. The atmospheric air pollutant ozone (O_3) induces

ROS production, and the subcellular localisation of O_3-induced H_2O_2 production was studied in *Betula pendula*: O_3 stimulated accumulation of ROS in the plasma membrane and cell wall and then continued to the cytoplasm, mitochondria and peroxisomes but, in contrast with the report from Allan and Fluhr, not in chloroplasts (Pellinen et al., 1999). The timing of the mitochondrial oxidative burst coincided with the first signals of visible damage, and, at the same time, mitochondria showed matrix disintegration. These responses may indicate changes in the oxidative balance within the cells that affect mitochondrial metabolism and whole cell homeostasis, possibly leading to apoptosis.

1.4.3. Methods for determination/localisation of ROS production

Table 1.2 shows a summary of the methods found in the scientific literature for the determination and localisation of ROS production in plants. The extinction of fluorescence of scopoletin during its oxidation by horseradish peroxidase (HPO) provides a sensitive and specific assay for small quantities of free H_2O_2 in solution, and is a widely used method (see Table 1.2). H_2O_2 mediates the oxidation of the fluorescent probe pyranine, leading to decrease of fluorescence (Apostol et al., 1989). Superoxide radical levels can be determined by cytochrome c reduction, which displays a change in absorbance when it accepts an electron from the superoxide anion.

Except in the study from Allan and Fluhr (1997), which uses a live cell approach with a fluorescent probe (dichlorofluorescein), the methods used do not allow great spatial or temporal resolution especially at the cellular level, and the intracellular distribution of ROS production is consequently poorly understood.

Table 1.2 – *Table summarising examples of methods used for determination and localisation of ROS production in plant systems.*

ROS	Localisation	Method	Reference
H_2O_2	------	luminol	Pugin et al., 1997
H_2O_2	------	epiniphrine	Minibayeva et al., 1998
H_2O_2	------	scopeletin	Levine et al., 1994
H_2O_2	Chloroplasts, nucleus, apoplast	dichlorofluorescein	Allen and Fluhr, 1997
H_2O_2	apoplast	Fixed samples	Bestwick et al. 1997, 1998
H_2O_2	------	pyranine	Chandra et al., 1996
H_2O_2	------	pyranine	Yahraus et al., 1995
H_2O_2	------	luminol	Schwacke and Hager, 1992
H_2O_2	------	luminol	Chandra and Low, 1997
H_2O_2	--------	CM-$DCFH_2$-DA	Pei et al., 2000
H_2O_2	-------	luciferin	Kawano et al., 1998
H_2O_2	-------	scopeletin	Cazale et al., 1998,1999
H_2O_2	-------	pyranine	Chandra et al., 1996
H_2O_2	-------	xylenol orange	Marre et al., 1998
H_2O_2	-------	luminol	Glazener et al., 1996
H_2O_2, $^{\bullet}O_2^-$	-------	luminol, lucigenin	Papadakis and Roubelakis-Angelakis, 1999
H_2O_2	-------	pyranine	Apostol et al., 1989
H_2O_2	-------	pyranine	Harding and Roberts, 1998
H_2O_2	cell walls	$CeCl_3$	Grant et al., 2000
H_2O_2	plasma membrane, cytoplasm, mitochondria and peroxisomes	$CeCl_3$	Pellinen et al., 1999
H_2O_2	----------	scopoletin	Shirasu et al. 1997
H_2O_2	----------	titanium tetrachloride precipitation	Wu et al. 1995
H_2O_2	---------	DAB	Ren et al., 2002

H_2O_2	Plasma membrane, apoplast	$CeCl_3$	Blokhina et al., 2001
H_2O_2	Cell wall	$CeCl_3$	Orozco-Cárdenas et al., 2001
H_2O_2	Chloroplasts mainly	$DCFH_2$-DA	Zhang et al., 2001
H_2O_2, $^*O_2^-$, $^*OH$	----------	$DCFH_2$, scopoletin, tetrazolium salts, benzoate hydroxylation and deoxy-rib degradation assay	Schopfer et al., 2001
H_2O_2, $^*O_2^-$	Cell wall	DAB, NBT	Mellersh et al., 2001, 2002

1.4.4. ROS production and stress in plants

A common plant response to different abiotic and biotic stress factors, such as heat, chilling, excessive light, UV, wounding, pathogens and osmotic shock is the accelerated production or/and accumulation of reactive oxygen species, including hydrogen peroxide, superoxide anion and hydroxyl radicals.

During electron transport processes (at the chloroplast and mitochondria level) O_2 is progressively reduced by a controlled supply of four electrons to yield water. However, the incomplete reduction of O_2 is possible and leads to the formation of reactive oxygen species (ROS). It is also known that excess irradiance, cold, heat and drought can trigger increased production of harmful ROS such as hydrogen peroxide (H_2O_2), superoxide radicals ($^*O_2^-$) and hydroxyl radicals ($^*OH$) (Foyer et al., 1994). Intracellular production of deleterious reactive oxygen species occurs in all organisms but is more problematic in phototrophs because they produce these metabolites during photosynthetic metabolism (Halliwell and Gutteridge, 1999). Basal cellular metabolism continuously produces ROS, mainly in the chloroplasts and mitochondria. "Oxidative stress" occurs when redox homeostasis in the cell is altered. Oxidative stress can be

countered by a set of antioxidative enzyme-mediated reactions. The usually well-controlled enzymatic systems that use electron transfer may undergo leakage. In the presence of O_2, any such electron leakage may result in ROS production. This mainly occurs in the mitochondria, but also in other cellular compartments owing to the activities of oxidases (e.g. NADPH oxidase and xanthine oxidase). For example, following physiological signals that are transmitted through membrane receptors, ROS can be produced within the cell via the activation of an NADPH oxidase. Cytochrome P450 mono-oxygenase may also produce ROS due to electron leakage in the ETC (Morel and Barouki, 1999).

If the production of ROS is very high, it can cause necrosis via irreversible degradation of cellular components. ROS can also induce programmed cell death (Jones, 2000). However, when the increase in ROS is transient and moderate, it is not lethal, and ROS may actually function as intra- and inter-cellular signalling molecules, regulate gene expression, interfere with signal pathways and modulate general development (Morel and Barouki, 1999). In animal cells, ROS have been shown to activate several stress-activated protein kinases or phosphatases (Morel and Barouki, 1999). In one case (Ste-20 like protein kinase) H_2O_2 is the exclusive activator (Morel and Barouki, 1999). Taken together, these observations suggest that ROS mediate specific stress signalling pathways within the cell.

Plant literature concerning the effects of external stresses on ROS production is extensive. The pathogen-related oxidative burst has received most attention (e.g. Schwacke and Hager, 1992; Bolwell, 1995; Low and Merida, 1996; Xu and Heath, 1996; Chandra et al., 1996; Ligterink et al., 1997; Keller et al., 1998; Romeis et al., 1999,

2000; Bolwell et al., 2002). There are also reports on the effects of wounding (Minibayeva et al., 1998), chilling (Payton et al., 2001), mechanical stress (Cazale et al., 1998; 1999), oligogalacturonic acid (Yahraus et al., 1995; Chandra et al., 2000) and hypo-osmotic stress (Chandra and Low, 1997; Cazale et al., 1998, 1999) on ROS production. The general concept is that external stresses induce elevated production of ROS in a relatively short period of time after elicitation, and this ROS production is believed to have its origin in a plasma membrane NADPH oxidase.

1.4.5. Functions of ROS

Few biological molecules have a worse reputation than ROS. For many years, they were though to be unwanted and toxic by-products of an aerobic environment. Although the cell had clearly evolved defence mechanisms against ROS, their production was associated with damage and it was widely believed that these molecules had only a harmful role. However, recent evidence suggests that the production of ROS is actually tightly regulated and serves very specific physiological functions.

1.4.5.1. Direct anti-microbial activity

Rapid generation of superoxide and accumulation of hydrogen peroxide is a characteristic feature of the hypersensitive response following perception of pathogen avirulence signals. Hydrogen peroxide inhibits the germination of spores of a number of fungal pathogens (Peng and Kuk, 1992). In mammals, neutrophils, eosinophils and macrophages phagocytose invading bacteria and kill them, through an oxidative burst. The plasma membrane NADPH oxidase was identified as the major contributor for this bactericidal capacity (reviewed in Babior et al., 2002). The superoxide and H_2O_2

generated are thought to be used to directly destroy the phagocytosed bacteria, although the mechanism of killing is still a matter of debate.

1.4.5.2. Induction of defence mechanisms

The oxidative burst appears to play a role in strengthening the plant cell wall in response to pathogen attack. Elicitor treatment of bean and soybean cells has been shown to result in H_2O_2-mediated oxidative cross-linking of specific structural proteins (Bradley et al., 1992). This response was rapid (within 2 min), appeared to depend on *de novo* synthesised H_2O_2 and resulted in an increased wall resistance to the action of fungal wall-degrading enzymes. Other reports show that fungal elicitor treatment increases the resistance of cell walls to digestion by microbial degrading enzymes (Brisson et al., 1994).

Rapid cross-linking in the cell wall may slow pathogen ingress and spread. Fungal elicitors and wounding inhibit expression of genes encoding cell wall proteins with low tyrosine content and stimulate those encoding tyrosine-rich versions (Sauer et al., 1990; Sheng et al., 1991; Kawalleck et al., 1995). This may increase the capacity for subsequent oxidative cross linking, protecting against secondary infections. In conclusion, a number of observations show that the plant oxidative burst has a direct effect at the cell wall level, increasing its strength to protect cells from pathogens. In contrast, a recent study shows that hydroxyl radical can actually decrease cell wall cross linking, suggesting a role for ROS production in the loosening of cell wall components to allow growth (Schopfer et al., 2002).

The possibility that ROS may serve as signal intermediates for phytoalexin biosynthesis has received considerable attention. Doke (1983) observed that superoxide dismutase (SOD) inhibited both superoxide generation and phytoalexin accumulation in aged potato discs infected with a hyper-sensitive response (HR) - inducing fungal pathogen. Similar effects by free radical scavengers and antioxidant enzymes have been reported (Epperlein et al., 1986, Apostol et al., 1989). In contrast, other studies failed to find this inhibitory effect – a variety of antioxidant treatments in white clover cell suspensions treated with bacteria failed to inhibit phytoalexin accumulation (Devlin and Gustin, 1992). A definitive conclusion is difficult as antioxidant molecules might have different access to the cells depending on the model system used, and this could explain the lack of effect observed by Devlin and Gustin. It has been shown that H_2O_2 alone or ROS generating systems can induce phytoalexin accumulation in the absence of elicitor, which reinforces the hypothesis that ROS are involved in phytoalexin synthesis (Apostol et al., 1989). How ROS specifically induce phytoalexin synthesis is not understood. Zhang et al. (1993) have shown that treatment of soybean with H_2O_2 induces accumulation of mRNA encoding enzymes required for phytoalexin synthesis. These data support a role for ROS as signalling molecules in pathways leading to defence-related gene expression, although not excluding other ROS-independent pathways.

H_2O_2 has been shown to stimulate the transcription of genes encoding proteins that protect against oxidative stress (Levine et al., 1994). 2 mM H_2O_2 can induce transcription of glutathione-S-transferase and glutathione peroxidase in cultured soybean cells. Since both enzymes can ameliorate H_2O_2 toxicity through the Halliwell-Asada pathway, (see Figure 1.8) their expression may help a stressed plant to avoid

damaging ROS effects. Moreover, recent work suggested that H_2O_2 is an intermediary-signalling molecule involved in the regulation of the CAT1 antioxidant gene, which encodes for one isoform of the antioxidant enzyme catalase, in response to ABA and osmotic stress (Guan et al., 2000).

Induction of peroxisome biogenesis genes in both plant and animal cells by H_2O_2 has recently been shown (Lopez-Huertas et al., 2000). In addition, a role for H_2O_2 in plant cell cycle control is also emerging - oxidative stress imposed using menadione impaired G1/S transition, slowed DNA replication and delayed the entry of BY-2 tobacco cells into mitosis (Reichheld et al., 1999).

1.4.5.3. Programmed cell death

Programmed cell death (PCD) is the active process of cell death that occurs during development and in response to environmental cues. In plants, PCD is essential for development and survival. In animals, programmed cell death is a way to rid the organism of unwanted cells. When dying cells exhibit certain characteristics such as DNA strand breaks with 3'OH end, condensation and fragmentation of the nucleus, membrane blebbing and cytoplasmatic condensation, PCD is called apoptosis (Kerr et al., 1972). Recent evidence suggests that plant cell death, in some cases, might be mechanistically similar to apoptosis in animals since some dying plant cells exhibit morphological features similar to apoptotic cells in the way that they form apoptotic bodies (Levine et al., 1996; Beers and McDowell, 2001). In addition, some types of plant cell show DNA cleavage characteristic of endonucleotidically processed DNA, a hallmark of apoptosis (Levine et al., 1996). Finally, a homologue of one gene, DAD-1, involved in repressing PCD in animals (Sugimoto et al., 1995) has been found in plants

(Apte et al., 1995) although its function is still not determined. PCD-like processes are commonly observed in plants during xylogenesis, reproduction, senescence, and pathogenesis (reviewed by Greenberg, 1996). The hypersensitive response (HR) of plants to certain pathogens appears to be a form of PCD, and results in the formation of a zone of dead cells around the infected tissue, synthesis of salicylic acid and accumulation of antimicrobial agents such as pathogenesis-related (PR) proteins and phytoalexins (Goodman and Novaky, 1994; Dangl et al., 1996; Hammond-Kosack and Jones, 1996). In plants, PCD is accompanied by an increase in production of ROS and lipid peroxidation (Mehdy, 1994; Hammond-Kosack and Jones, 1996; MacCarrone et al., 2000). Furthermore, hydrogen peroxide and superoxide radicals are thought to be key mediators of plant PCD during the HR (Levine et al., 1994; Shirasu et al., 1997; Mittler et al., 1996, Jabs et al., 1996; Huckelhoven et al., 2001) and may function as part of the signal transduction pathway leading to the induction of PR proteins and systemic resistance (Chen et al., 1993, Green and Fluhr, 1995; Huckelhoven et al., 2001). In addition, Mittler et al. (1998) found that suppression of cytosolic ascorbate peroxidase expression during pathogen induced PCD in tobacco contributes to the reduction of capacity of cells to scavenge H_2O_2 which enables accumulation of H_2O_2 and acceleration of PCD.

1.5. STRESS SIGNALLING PATHWAYS IN PLANTS

Stress signal transduction networks are essential to plant growth and development, allowing cells and tissues to perceive and respond to continuous changes in their environment. Multiple stress signalling pathways exist in plant cells, controlling important processes such as hormone and light perception, pathogen defence, and wounding, osmotic and extreme temperature responses.

1.5.1. Ca^{2+} and ROS

Cytosolic Ca^{2+} (Ca^{2+}_{cyt}) is a key messenger that regulates various important cellular functions. Many studies have addressed the importance of Ca^{2+} in the oxidative stress response of plant cells to pathogen attack (Schwack and Hager, 1992; Xu and Heath, 1998; Harding and Roberts, 1998; Blume et al., 2000). During severe oxidative stress, disruption of the cytosolic Ca^{2+} homeostasis is probably a critical step in the injury of cells leading to the activation of several Ca^{2+}-dependent degrading enzymes (Price et al., 1994). Price et al. (1994) showed that treatment of seedlings of tobacco with exogenous hydrogen peroxide (10 mM) resulted in a transient Ca^{2+} elevation. The Ca^{2+}_{cyt} increase was apparently regulated by the redox status of the cell, i.e., the cellular pro-oxidant/antioxidant ratio. This suggests a role for Ca^{2+} in plant responses to oxidative stress (Price et al., 1994; Murata et al., 2001). Additionally, Chandra and Low (1997) using aequorin-transformed tobacco cells showed that Ca^{2+} pulses were associated with the transduction of the oxidative burst signal. The oxidative burst in challenged plant cells resembles that exhibited by human neutrophils, producing H_2O_2 that originates from superoxide generated by a plasma membrane associated NADPH

oxidase. The major component of the plant NADPH oxidase complex has been cloned and experiments have showed that its activation involves a protein kinase cascade that can be blocked by Ser/Thr kinase inhibitor K252a (Rajasekhar et al., 1999). Ion fluxes, Ca^{2+} uptake, G-proteins and kinase cascades have been implicated as signal transduction components in the induction of oxidative burst (see references in Table 1.3). Experiments with transgenic tobacco expressing a foreign calmodulin gene indicate that calmodulin is a target of Ca^{2+} fluxes in response to environmental stress, and plant NAD kinase may be a downstream target which potentiates ROS production by altering NAD(H)/NADP(H) homeostasis (Harding et al., 1997). Calmodulin has been shown to bind to and activate plant catalases in the presence of Ca^{2+}. Ca^{2+} /calmodulin can thus down regulate H_2O_2 levels in plants by stimulating the catalytic activity of plant catalase (Yang and Poovaiah, 2002). Table 1.3 provides a summary of investigations that indicate that Ca^{2+} and ROS are tightly linked in the stress response of a variety of systems.

Table 1.3. *Examples of stress signalling pathways involving Ca^{2+} and ROS.*

General pathway	Reference
H_2O_2 (0.05-10 mM) =>transient increase in Ca^{2+}	Price et al., 1994
Pathogen elicitor =>Ca^{2+} increase (2 phases), Ca^{2+} influx =>ROS	Blume et al., 2000
Elicitor (pathogen) =>Pto gene =>kinases =>oxidase complex (PM) =>Ca^{2+}	Chandra et al., 1996
OGA =>receptor =>G-proteins =>Ca^{2+} influx =>PLC =>kinases => oxidase complex (PM) =>H_2O_2	Low and Merida, 1996
OGA =>MAPKKK =>47 kD MAPK =>Ca^{2+} increase =>44 kD MAPK => oxidase complex (PM) =>H_2O_2	Low (pers. comm.)
Hypo-osmotic and mechanical stress =>Ca^{2+} increase/ion channels =>MAPK activation =>oxidative burst	Cazalé et al., 1999
Hypo-osmotic and mechanical stress =>Ca^{2+} and phosphorylation events => oxidative burst (from NADPH oxidase)	Cazalé et al., 1998
Elicitor (pathogen) and wounding =>Ca^{2+} =>CDPK change from non-elicited to elicited form (phosphorilation-dependent) =>oxidative burst	Romeis et al., 1999; 2000
H_2O_2 =>Ca^{2+} influx	Levine et al., 1996
Pathogen =>Ca^{2+} increase =>oxidative burst	Xu and Heath, 1998
H_2O_2 (>0.5 mM) =>Ca^{2+} influx	Pei et al., 2000
SA =>reacts with catalase =>H_2O_2 increase =>using H_2O_2, the extracellular GPX forms superoxide (extracellular) =>Ca^{2+} elevation in 90 s (superoxide scavengers sensitive but DPI insensitive)	Kawano et al., 1998
Elicitor =>receptor on cell surface =>activation of ion channels => alkalinisation of extracellular medium =>activation of pH dependent peroxidases => H_2O_2	Bolwell, 1995
Elicitor (fungal) =>Ca^{2+} =>kinases =>H_2O_2 (NADPH oxidase)	Schwacke and Hager, 1992
OGA , MAS-7, hypo-osmotic stress, harpin =>Ca^{2+} =>oxidative burst	Chandra and Low, 1997
Elicitor =>Ca^{2+} =>protein phosphorylation/G-proteins =>NADPH oxidase =>oxidative burst	Keller et al., 1998
Cryptogein =>Ca^{2+} elevation, NADPH oxidation =>NADPH oxidase activation =>oxidative burst, cytosol acidification, extracellular alkalinisation	Pugin et al., 1997

Wounding =>increase permeability for K^+, membrane depolarization => NADPH oxidase activation (Ca^{2+} dependent)	Minibayeva et al., 1998
Cryptogein =>2 sources of H_2O_2 (chloroplasts and apoplastic)	Allen and Fluhr, 1997
Pathogen =>H_2O_2 (within secondary walls)	Bestwick et al., 1997
Pathogen =>Ca^{2+} influx =>membrane depolarization =>NADPH oxidase activation =>ROS =>electrolyte leakage	Marrè et al., 1998
Cryptogein =>protein phosphorylation =>Ca^{2+}, K^+ influx and Cl^- efflux => membrane depolarisation =>NADPH oxidase =>ROS and cytosol acidification => MAPK, activation of PP pathway	Lebrun-Garcia et al., 1999
Cellulase =>superoxide and H_2O_2	Papadakis and Roubelakis-Angelakis, 1999
Pathogen =>activation of ion channels and phosphorylation =>G-proteins coupled to receptors =>oxidative burst	Rajasekhar et al., 1999
Pathogen =>Ca^{2+} =>calmodulin dependent NAD kinase	Harding and Roberts, 1998
Pathogen =>Ca^{2+} elevation =>oxidative burst (NADPH oxidase)	Grant et al., 2000
Ca^{2+} (from internal stores, through protein kinases and anion channels) => oxidative burst	Cessna and Low, 2001

1.5.2. MAPK cascades and oxidative stress

An increasing body of evidence suggests that a subset of plant responses is shared by both biotic and abiotic stresses. These include generation of ROS, induction of defence genes and activation of mitogen-activated protein kinases (MAPK; Zhang and Klessig, 2001). It is well documented that ROS are implicated in the activation of adaptive responses of plants to biotic and abiotic stresses including wounding, ozone exposure, UV radiation and osmotic stress. All these stresses also activate MAPK with kinetics that either precede (e.g. Lingterink et al., 1997) or are downstream (e.g. Kovtun et al., 2000) of ROS production. Most of the evidence about the relationship between ROS and MAPK comes from the use of inhibitors. The broad-spectrum kinase inhibitors K-252a and staurosporine were found to block the oxidative burst in response to several stimuli in a concentration dependent manner (Lamb et al., 1997; Yoshioka et al., 2001). However, a role for MAPK in the oxidative burst pathway should be interpreted with caution due to the non-specific action of these inhibitors. In contrast, PD98059, a specific inhibitor of MAPK, had no effect on the onset of H_2O_2 production, suggesting that MAPK are not necessary for ROS production (Romeis et al., 1999), or belong to an independent stress pathway. Results from Cazalé et al. (1999) and Kovtun et al. (2000) also support the downstream positioning of MAPK in the stress response order of events, showing that ROS induce MAPK cascades. Therefore, the role of ROS and MAPK and their relative positions in the stress signal pathway are still not clear. One possibility (Zhang and Klessig, 2001) is that the pathways leading to the H_2O_2 burst and MAPK activation separate early after stimulation of cells, and that ROS generation can feed into the MAPK pathway, forming a positive feedback loop.

1.6. GENERAL OBJECTIVES

The present work focuses on the cellular responses of early developmental stages of *Fucus* to environmental stress factors, in particular light and hyper-osmotic stress. *Fucus* embryos are subjected to marked changes in light and osmotic environments with every change of the tide, from which they cannot escape. An appropriate cellular response system must have evolved to deal with these changes and adapt the growing embryo to further stresses. Of particular interest is the role of ROS in the response of *Fucus* embryos to external light and osmotic changes, as they are ubiquitous components of the stress response in animals, plants, fungi and algae.

The role of Ca^{2+} as a second messenger is also an important feature in a variety of stress responses. Moreover, the interaction between Ca^{2+} and ROS at the cellular level needs to be elucidated in order to determine how the stress signal is converted into a response. Ca^{2+} has already been shown to be involved in polarisation and rhizoid germination in the *Fucus* zygote, which suggests it has a role in signal transduction during early development. Furthermore, Ca^{2+} has also been related to osmoregulation in *Fucus* (Taylor et al., 1996; Goddard et al., 2000).

Therefore, the major objectives of this present study are:

I. To evaluate how physiological processes of *Fucus* embryos are affected by light and hyper-osmotic stress, integrating chlorophyll fluorescence with reactive oxygen species production (Chapter II);

II. To determine the sequence of events that culminates in the cellular oxidative burst response to hyper-osmotic stress, in particular the positioning of key

signalling molecules H_2O_2 and Ca^{2+}, and to characterise the spatio-temporal cellular patterns of ROS production and Ca^{2+} elevation during hyper-osmotic stress(Chapter III);

III. To determine the downstream effects of hyper-osmotic stress-induced ROS elevation, in particular to ascertain the specific function of the different ROS components (Chapter IV);

IV. To study the implication of protein kinases in the hyper-osmotic stress signaling pathway (Chapter IV).

CHAPTER 2

PHYSIOLOGICAL RESPONSES OF *FUCUS* EMBRYOS TO LIGHT AND HYPER-OSMOTIC STRESS

2.1. INTRODUCTION

2.1.1. Abiotic stress in early life history phases of algae

Fucoid algae (Phaeophyceae) are important members of marine intertidal communities in the North Atlantic. Variability in the recruitment and regeneration of the *Fucus* canopy are major influences on the rate of succession and on the abundance of other species (McCook and Chapman, 1997). Despite the importance of stress tolerance in intertidal seaweeds, the underlying mechanisms that confer such tolerance are still poorly understood (Davison and Pearson, 1996). To date, most studies have focused on adult stages but the mechanisms by which *Fucus* embryos withstand the prevailing physical forces in the intertidal zone (light, tidal movement, waves) are key determinants of their ability to survive and establish a population. The impact of stress on embryonic stages in the first days after settlement may be particularly severe. It has become apparent that the response of early life history stages to the environmental conditions cannot necessarily be predicted from knowledge of the adult canopy (Davison et al., 1993). Although fucoid embryos are easily manipulated in laboratory culture and their early development has been well characterised (Kropf and Quatrano, 1987; Kropf, 1997) little is known about their stress physiology.

Fucus embryos develop under low light conditions, typically in rock crevices and under the protection of the adult canopy, so exposure to an elevated light climate, especially during emersion, is likely to result in photoinhibition. With every turn of the tide, intertidal seaweeds must be able to cope with hyper-osmotic stress and increased irradiance. The ability to tolerate one stress is often correlated with the ability to

tolerate others (Bowler and Fluhr, 2000), however, very little is known of tolerance/sensitivity interactions involving light, hyper-osmotic and ultraviolet B (UV-B) stress, other than the UV-B/light relationship. One of the most conspicuous consequences of dehydration in plants is a limitation in photosynthesis (Kirst, 1989). This limitation might have serious consequences, as the exposure of the plant to excess energy if not safely dissipated, results in over-reduction of the PSII reaction centres (Demmig-Adams and Adams, 1992) and increased production of ROS in the chloroplasts (Smirnoff, 1993). This harmful ROS production, resulting from excess light energy or from other factors, stimulates photodamage of PSII by inhibiting the synthesis of the D1 protein, a component of the reaction centre of PSII (Nishiyama et al., 2001). Because the targets of both light and hyper-osmotic stress are comparable, the combination of these two factors may have severe cumulative effects on the cell physiology of *Fucus* embryos.

2.1.2. Photoinhibition during abiotic stress

Variable chlorophyll fluorescence techniques are suitable tools for studying photosynthetic performance and inhibition, as activity of the PSII reaction centre is measured. The pulse amplitude modulation (PAM) method is based on the principle that under *in vivo* conditions, fluorescence changes originate almost exclusively from chlorophyll a and the associated antenna pigments in PSII (see Genty et al., 1989; Schofield et al., 1998).

The potential inhibition of photosynthesis due to light stress can be minimised through several physiological mechanisms (Schofield et al., 1998), including the

involvement of the xanthophyll cycle pigment pool in dissipating excess energy from the reaction centres (Kroon, 1994). It is also known that excess light, cold, heat and osmotic changes can trigger increased production of harmful ROS. Intracellular production of ROS occurs in all organisms but may be more problematic in phototrophs because of the photosynthetic metabolism (Halliwell and Gutteridge, 1999).

2.1.3. Objectives

The aim of this study was therefore to assess the impact of a combination of potential stress factors (high light, ultraviolet A and B, hyper-osmotic treatment) on the physiology of developing *Fucus* embryos during the first 4 days after fertilisation. This was achieved by investigating: (1) photosynthetic performance and protection under stress conditions, using chlorophyll fluorescence techniques; (2) intracellular production of ROS, using the fluorescent label CM-DCFH$_2$-DA, confocal laser scanning microscopy (CLSM) and quantitative image analysis; (3) the ability of embryos to recover from oxidative stress and (4) the impacts of light/hyper-osmotic treatment on the development of the embryos.

2.2. Material and Methods

2.2.1. Plant material and growth conditions

Receptacles of mature *Fucus spiralis* were collected from the compact intertidal seaweed belt growing on concrete substrata along the shoreline of the Oosterschelde basin (2.9% salinity) near Yerseke (SW-Netherlands), from September 1998 to April

1999. 2.9% was considered to be the normal salinity seawater. Receptacles were stored at 4°C in the dark until used (within one week). To achieve synchronous release of gametes, receptacles were incubated in filtered seawater (0.45 µm) under strong white light at 15°C. The gamete solution was then filtered through a 120 µm nylon mesh to discard debris and oogonia. Time of fertilisation was considered to be 30 min after gamete release. Fertilised eggs were then pipetted onto the surface of coverslips for CLSM and placed inside small Petri dishes containing 8 mL filtered seawater, where they attached and grew. For the analysis of chlorophyll fluorescence and xanthophyll cycle pigments the embryos were grown onto cellulose nitrate filters in small Petri dishes. Attached zygotes were incubated at 15°C under 15 µmol m^{-2} s^{-1} photosynthetic photon flux densities (PPFD) (4π-sensor QSL-100 Biospherical Instruments) on a 12:12 h light:dark cycle. Replicate cultures (n=3-5) were maintained for each treatment.

2.2.2. Light and hyper-osmotic treatments

In SW Netherlands, the reproductive season for *F. spiralis* is Autumn/Winter. The control/low photosynthetic photon flux density (PPFD, 15 µmol m^{-2} s^{-1}) was selected on the basis of *in situ* measurements taken during a cloudy day at 10 am and 4 pm in February, when the adult canopy almost completely covers the embryos. These were considered to be the standard growth conditions for the first days after fertilisation. The elevated PPFD (300 µmol $m^{-2}s^{-1}$) was chosen based on *in situ* measurements at noon on a sunny day in February, when the adult canopy was partially removed and the embryos were exposed to higher light levels. In nature, fertilisation occurs during

daytime low tide (Pearson and Brawley, 1996), so the first potential exposure to high light is ~24 h after fertilisation, at the next daytime low tide.

Experiments were conducted under 4 different light regimes:

- 15 μmol m^{-2} s^{-1} - control/low photosynthetic active radiation (*LPAR*); Philips TLD18W33 fluorescent lamps,
- 300 μmol m^{-2} s^{-} - high PAR (*HPAR*),
- HPAR + UV-A (*PA*),
- HPAR + UV-A + UV-B (*PAB*).

A zabu UV-D clear acrylate sheet (Wientjes BV, Roden) was used to filter out UVC radiation (below 285 nm) under all light conditions, a Mylar filter was used to cut off UV-B radiation (below 320 nm) and a plexiglass filter was used to remove UV-A radiation (below 380 nm). A PPFD spectrum (250-700 nm) was scanned with a spectroradiometer equipped with a 2π cosine-corrected sensor (MACAM Photometrics SR-9910-PC). The biologically effective dose of Jones and Kok (1966) was 2.1 (PAB), 0.6 (PA), 0.1 (HPAR) and 0 (LPAR) $W.m^{-2}$ and was calculated using a weighting factor $WF_\lambda = 1000 \times e^{-0.023*\lambda}$ ($R^2 = 1$) derived from the plot in Forster and Lüning (1996) which sets $WF_{300} = 1$. For the calculation of this effective dose λ = 280-400 nm are considered, using the formula: $BED_{J/K} = {}^{\lambda=280\text{-}400}\Sigma\ (WF_\lambda \times Q_\lambda)$, in which Q_λ is the PPFD ($W.m^{-2}$) at wavelength λ (nm).

Hyper-osmotic treatment consisted of increasing the salinity of normal seawater (normal seawater is 3.2% salinity). Measurements of PSII yield using a pulse-amplitude

modulation apparatus (PAM 2000, Walz, Germany) during combined light and hyper-osmotic stress and recovery, were recorded at 20% salinity.

2.2.3. Fluorescence measurements

In vivo light-modulated chlorophyll fluorescence was monitored in 1 d, 2 d and 4 d old embryos with a PAM 2000, based on the principles described by Schreiber et al. (1986, see Chapter I). The saturating pulse method provides information on processes related to the quantum yield of PSII in response to light stress. Yield is usually determined under steady state illumination in which the effective quantum yield of PSII is close to the overall quantum yield of photosynthesis. The effective quantum yield was determined according to the equation $\Delta F/F'_m = (F'_m - F_s)/F'_m$ (Genty et al., 1989), where ΔF is the difference between the respective maximal fluorescence F'_m of light adapted algae and the ambient fluorescence level (current steady state fluorescence, Fs). $\Delta F/F'_m$ was used a parameter since it is correlated with oxygen production (Hanelt et al., 1994; 1995). Changes in photochemical quenching of chlorophyll fluorescence were calculated according to the expression: $qP = (F'_m - F_s)/(F'_m - F'_o)$ and in non-photochemical quenching as $qN = 1 - (F'_m - F'_o) / (F_m - F_o)$. Zygotes were well dispersed over the cellulose nitrate filter to ensure that all embryos were submitted to similar light conditions. The PAM fibre was placed carefully over the attached population of embryos and the fluorescence yield was measured at a minimum of 5 different positions on the filter (i.e. 5 measurements for each data point which correspond to independent embryos in the dish population). The measurements were performed at short intervals (ca. 5 min) during 60 min exposure under each light

condition. The change in yield during a 60-180 min recovery period, under LPAR and 2.9% salinity seawater , was also assessed.

Chlorophyll fluorescence was also used to analyse the light response curves (photosynthesis versus PPFD curves) of *F. spiralis* embryos during their early development stages, from 3 hours after fertilisation to 10 days. Zygotes were obtained as described before, and the growing embryos were incubated in LPAR, 15°C and a 12 h photoperiod. Samples were exposed to increasing PPFDs of actinic red light (650 nm); PPFDs ranged from 10 to 504 μmol m^{-2} s^{-1} with, in total, 20 PPFD values. The material was dark adapted before the beginning of the measurements. The light response curves were fitted by the model equations given by Platt et al. (1980). Relative electron transport rates (rel.ETR) were calculated by multiplying quantum yield by PPFD (rel.ETR $=\Delta F/F'_m$ x PPFD) and plotted against PPFD. Alpha (α) (initial slope under light limited conditions), and P_{max} (gross photosynthesis under saturating light) were also determined.

2.2.4. Pigment analysis

For pigment (violaxanthin, zeaxanthin, β-carotene, chlorophyll-a) analysis of embryos exposed to PAB, samples were obtained at short intervals during the 60-min period of exposure to elevated light, and also during recovery under dim light. Frozen samples (-80°C) of *F. spiralis* embryos, grown onto cellulose nitrate filters, were extracted in 90% methanol in 0.5 M ammonium acetate, the pigments separated and concentrations determined by HPLC following the procedures of Wright et al. (1991) and Kraay et al. (1992). Methanol extracts were injected into a PC-controlled

(Milennium 2.15 software) HPLC system (Waters) equipped with a reversed-phase column (Nova-pak C18, 4 μm, 15 cm; Waters Wat086344). Gradient-mixing HPLC pumps delivered three mobile-phase solvents: ammonium acetate / methanol, 90% acetonitril and 100% ethyl acetate. A photodiode array detector was used (Waters 1996) in which the absorption characteristics of the eluted pigments are matched with those described in Jeffrey et al. (1997). Antheraxanthin, the xanthophyll intermediate of violaxanthin and zeaxanthin, could not be detected. Commercially available standards of the pigments were used (VKI Hørsholm, Denmark). Pigment concentrations of β-carotene, violaxanthin and zeaxanthin were normalised to the chlorophyll a peak area. The relative pool of xanthophyll cycle pigments was estimated as Z/(Z+V), where Z and V are the concentrations of zeaxanthin and violaxanthin respectively. Values of Z/(Z+V) were plotted against non-photochemical quenching (qN) to characterise the relationship between the de-epoxidized xanthophyll cycle pigments and non-photosynthetic energy dissipation (Schofield et al., 1998).

2.2.5. Quantitative detection of ROS

The formation of DCF from DCFH-DA is currently used for the assessment of oxidative stress in microalgae and seaweeds (Malanga and Puntarulo, 1995; Lesser, 1996; Collén and Davison, 1997). DCFH-DA is a non-polar non-fluorescent compound that diffuses across membranes. Within the cell, acetate is cleaved-off by esterases to give 2',7'-dichlorohydrofluorescein (DCFH), a polar compound that is retained in the cell. Oxidation of DCFH by reactive oxygen species (Royall and Ischiropoulos, 1993) yields a fluorescent compound 2'-7'-dichlorofluorescein (DCF). The oxidising agent is either $^{\bullet}OH$, which may be formed from H_2O_2 and Fe^{2+} in the

Fenton reaction, or H_2O_2, which may react with DCFH via peroxidases (Zhu et al., 1994). Here, intracellular ROS was studied by measuring the oxidation of the label 5-(and-6-)-chloromethyl-2′,7′dichlorodihydrofluorescein diacetate (CM-DCFH_2-DA; Molecular Probes, Eugene, Oregon), a chloromethyl derivate of DCFH-DA; use of this minimises the risk of DCFH leakage from living cells as its thiol-reactive chloromethyl group links CM-DCF with intracellular thiols (e.g. glutathione). Subsequent DCFH oxidation yields DCF that is trapped inside the cell. *Fucus* embryos grown under low light, on coverslips (~50 per coverslip), were loaded with a 100 µM CM-DCFH_2-DA. Loading of the label (30 min; 15°C) was terminated by rinsing the sample with filtered seawater (0.2 µm). Embryos were then submitted to each condition, defined earlier, for 30 min. Following exposure, the coverslips with the attached embryos were mounted in a sample chamber (Attofluor, Molecular Probes, Eugene, Oregon). 0.01 mL ascorbate solution (1 mg mL^{-1}; pH 8) was added. This compound is both an anti-fading reagent preventing bleaching of DCF fluorescence and an antioxidant stopping further oxidation of DCFH in cells (Pawley, 1995). Stock solutions of CM-DCFH_2-DA, filtered seawater and ascorbate were prepared fresh daily.

2.2.6. Confocal laser scanning microscopy and image analysis

Dye fluorescence was imaged with a Leica TCS NT confocal scanning laser on an inverted microscope (Leica-IRB). The 488-nm excitation line was chosen. A 25x 0.75NA/oil objective (Leica UV-PLFLUO) was used and the emission pinhole set at 90 µm matching 1 Airy Disc Unit (Pawley, 1995). In these analyses the intersection (z)

intervals were set at 1.5 µm to minimise loss of digital information. Green and red fluorescence from the focal plane were separated using emission filters BP530/30 and LP590, respectively. Both fluorescence emitted at 530 nm by DCF and autofluorescence were measured using photomultiplier detectors. Simultaneously, three digital images were collected: (1) fluorescence emission of DCF; (2) fluorescence emission from chloroplasts; (3) transmitted-light image. A daily calibration procedure was introduced using standardised fluorescent spheres (Focal Check; 15 µm; Molecular Probes, Eugene, Oregon). For conversion of the relative fluorescent units to real concentrations of DCF, standard solutions of DCF (Sigma) were used to build a calibration curve ($R^2 = 0.997$). Using the image analysis programme QWIN (Leica), an automated scanning procedure was written in QUIPS language. This routine controls the CLSM scanning software, the xy-stage and the z-focus of the objective. Thirty to 40 independent embryos were used for each experimental condition. In the figures, DCF concentrations (µM) are presented (±S.D.) and values of ROS represent a production rate, µM DCF $(30\ min)^{-1}$.

2.2.7. Growth experiments

Fucus embryos were grown on small plastic Petri dishes in filtered SW and 12 h photoperiod as described earlier, until 24 h after fertilisation. They were then submitted to each of the light treatments in combination or not with hyper-osmotic treatment for 30 min. Growth of the embryos was measured daily using an inverted Nikon Diaphot microscope (Nikon, Tokyo Japan) equipped with a graduated ocular

lenses. Average length of 3 replicates (25-30 embryos per replicate) ± standard deviation is shown. Results are representative of 4 independent experiments.

2.2.8. Statistical analysis

Data were analysed using the statistical programme STATISTICA® version 6.0, by two or three-way analysis of variance (ANOVA), with multiple comparisons determined using the Sheffé test. Since measurements taken at days 1, 2 and 4 were performed on different batches of embryos, the factor 'time', when included in the analysis is treated as an independent variable. Differences were considered to be significant at a probability of 5% ($P \leq 0.05$). Correlation coefficients were determined according to Sokal and Rohlf (1995).

2.3. RESULTS

2.3.1. Effects of high irradiance on photosynthetic efficiency

The impact of 1 h exposure to 300 μmol m^{-2} s^{-1} on the effective quantum yield of PSII, $\Delta F/F'_m$, was dramatic (Figure 2.1). Values decreased within 3 min of embryos being transferred from dim (LPAR) to any of the three elevated light conditions (HPAR/PA/PAB). The steepest decline was observed in 1 d old embryos. After a 10-min exposure period, $\Delta F/F'_m$ decreased, on average, to 20% and 55% of the initial value, in the youngest and oldest embryos, respectively; 2 d old embryos had intermediate values (Table 2.1). Initial reduction in $\Delta F/F'_m$ was consistently more pronounced in the presence of UV-B, where a decrease to 17%, 24% and 43% of the

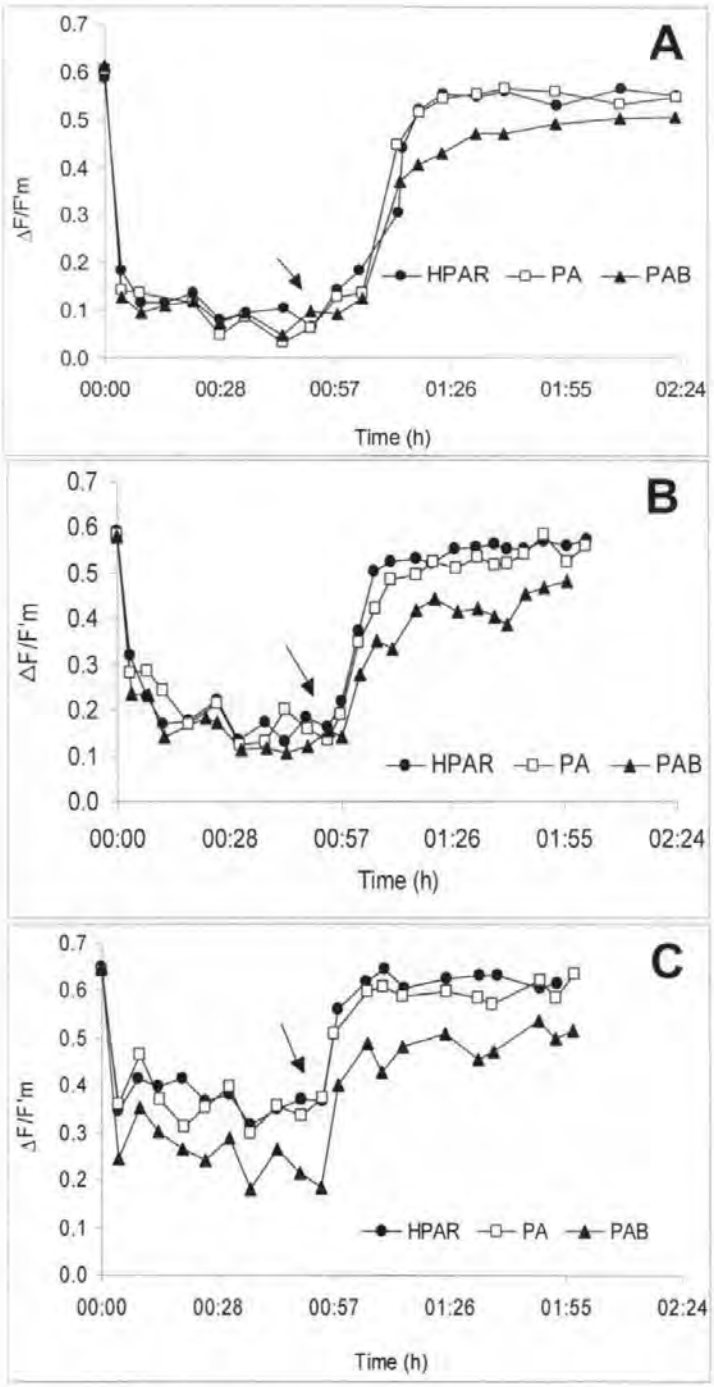

Figure 2.1. Photosynthetic efficiency of *Fucus* embryos at different stages of development exposed to different experimental conditions. HPAR (300 $\mu mol.m^{-2}.s^{-1}$); PA (HPAR + UVA); PAB (HPAR + UVA + UVB). Significant differences ($P<0.05$) were found between the response of 4 d old relative to 1 d and 2 d old embryos. Arrows indicate the start of the recovery period. Time zero corresponds to the beggining of the stress stimulus. **A)** 1d old; **B)** 2 d old; **C)** 4 d old.

initial values in 1 d, 2 d and 4 d old embryos, respectively, was found. The initial decrease in $\Delta F/F'_m$ (0-8 min) was followed by a second, slower decline (ca. 8-45 min). At the end of 1 h exposure to PAB, 1 d old embryos had 8% of their initial value of $\Delta F/F'_m$, 2 d old, 24% and 4 d old, 26%.

Table 2.1. *Changes in* $\Delta F/F'_m$ *in* Fucus *embryos during different light treatments. Recovery in LPAR is also shown (rec).*

Time after stress	24 h AF (% control)			2 d AF (% control)			4 d AF (% control)		
	HPAR	PA	PAB	HPAR	PA	PAB	HPAR	PA	PAB
0'	100	100	100	100	100	100	100	100	100
10'	20	23	17	29	41	24	61	58	43
30'	17	12	14	22	22	19	59	61	42
1h	11	16	8	27	32	24	56	58	26
10' rec	52	69	21	88	83	56	100	94	61
30' rec	93	95	72	93	86	71	98	94	68
1h rec	97	95	88	98	95	90	98	98	84

A rapid recovery in $\Delta F/F'_m$ occurred on transfer from HPAR and PA to LPAR, reaching pre-exposure values within 1 h. After exposure to UV-B, recovery was significantly slower ($P < 0.01$). Complete (100%) recovery was achieved only after 3 h (not shown).

The photoinhibition observed under elevated PPFD was further evaluated by examining changes in photochemical (qP) and non-photochemical quenching (qN) of chlorophyll fluorescence. The quantitative indication of the fraction of active PSII centres that are closed by the background light at the moment of the F'_m measurement

can be defined as (1-qP). The ratio (1-qP)/qN provides a more appropriate measure of the capacity of photoprotection to excess light than analysing the parameters qN and (1-qP) separately (Jiménez et al., 1998). The ratio (1-qP)/qN increased with time of exposure and decreased slowly as the embryos recovered under more favourable conditions. 1 d old embryos, despite having a lower initial value of (1-qP)/qN, displayed the largest increase in this ratio (Figure 2.2), while 4 d old embryos increased the least ($P < 0.05$).

2.3.2. Effects of elevated light in combination with hyper-osmotic treatment on photosynthetic efficiency

The combination of light and hyper-osmotic treatment (20% salinity seawater) induced the same pattern of $\Delta F/F'_m$ response as elevated light treatment alone, i.e., a steep initial decrease in $\Delta F/F'_m$ that was more evident in younger embryos (Figure 2.3). After incubation for 1 h under high light plus hyper-osmotic stress, the younger embryos had only 9% of the initial effective quantum yield, while older embryos (4 d old) had 18% (Table 2.2). 4 d old embryos appear to be able to adapt to the imposed stress - under LPAR they recovered $\Delta F/F'_m$ even in presence of hyper-osmotic treatment (Figure 2.3.C). Hyper-osmotic treatment combined with high irradiance plus UV-A and UV-B induced the highest inhibition of $\Delta F/F'_m$. Compared to the situation where irradiance was the only stress factor (Figure 2.1), recovery of $\Delta F/F'_m$ was slower and less complete when high light was combined with hyper-osmotic stress (Table 2.2 and Figure 2.3) and $\Delta F/F'_m$ increased slowly during the recovery period. This pattern was more evident in embryos submitted to PAB and hyper-osmotic treatment: no

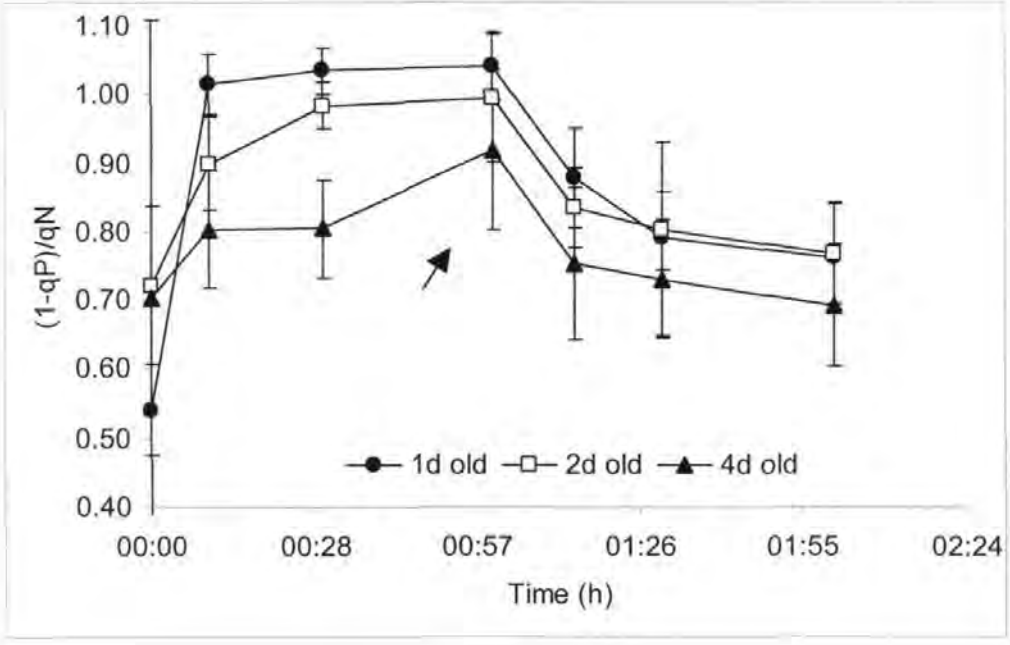

Figure 2.2. (1-qP)/qN in *Fucus* embryos during incubation under PAB (HPAR + UVA + UVB) and during a 1 h recovery period. Arrow indicates the start of the recovery period under low light. Values represent means of at least 5 measurements. Significant differences ($P<0.05$) were found between the response of 4 d old relative to 1 d and 2 d old embryos.

recovery occurred during the next 120 min and a 24 h period was needed to achieve initial $\Delta F/F'_m$ values (result not shown). The slow recovery was more evident in younger embryos (Figure 2.3).

Table 2.2. *Changes in $\Delta F/F'_m$ in* Fucus *embryos during different light treatments in presence of hyper-osmotic stress (20% salinity SW). Recovery in LPAR and 2.9% salinity seawater (rec.) is also shown.*

Time after stress	24 h AF (% control)				2 d AF (% control)				4 d AF (% control)			
	LPAR	HPAR	PA	PAB	LPAR	HPAR	PA	PAB	LPAR	HPAR	PA	PAB
0'	100	100	100	100	100	100	100	100	100	100	100	100
10'	11	28	30	21	26	30	31	27	29	33	25	30
30'	7	9	19	16	28	23	25	21	42	24	14	16
1h	7	9	11	9	28	20	20	19	43	21	17	15
10' rec	93	54	33	23	28	22	23	17	99	67	70	42
30' rec	96	59	48	27	98	63	48	37	96	89	87	67
1h rec	100	89	70	61	102	82	73	62	99	93	94	73

2.3.3. Xanthophyll cycle pigments

The change in xanthophyll cycle pigments during stress treatment was only analysed for light-stressed embryos. After exposure to PAB for 1 h, both photoinhibition and changes in the xanthophyll cycle pigment ratios were observed. Figure 2.4 shows the Z/(V+Z) values plotted against non-photochemical quenching (qN). The correlation between these parameters improved with the age of the embryos. Average β-carotene concentration (normalised by chlorophyll a content) was found to be 0.027 ± 0.008 (1

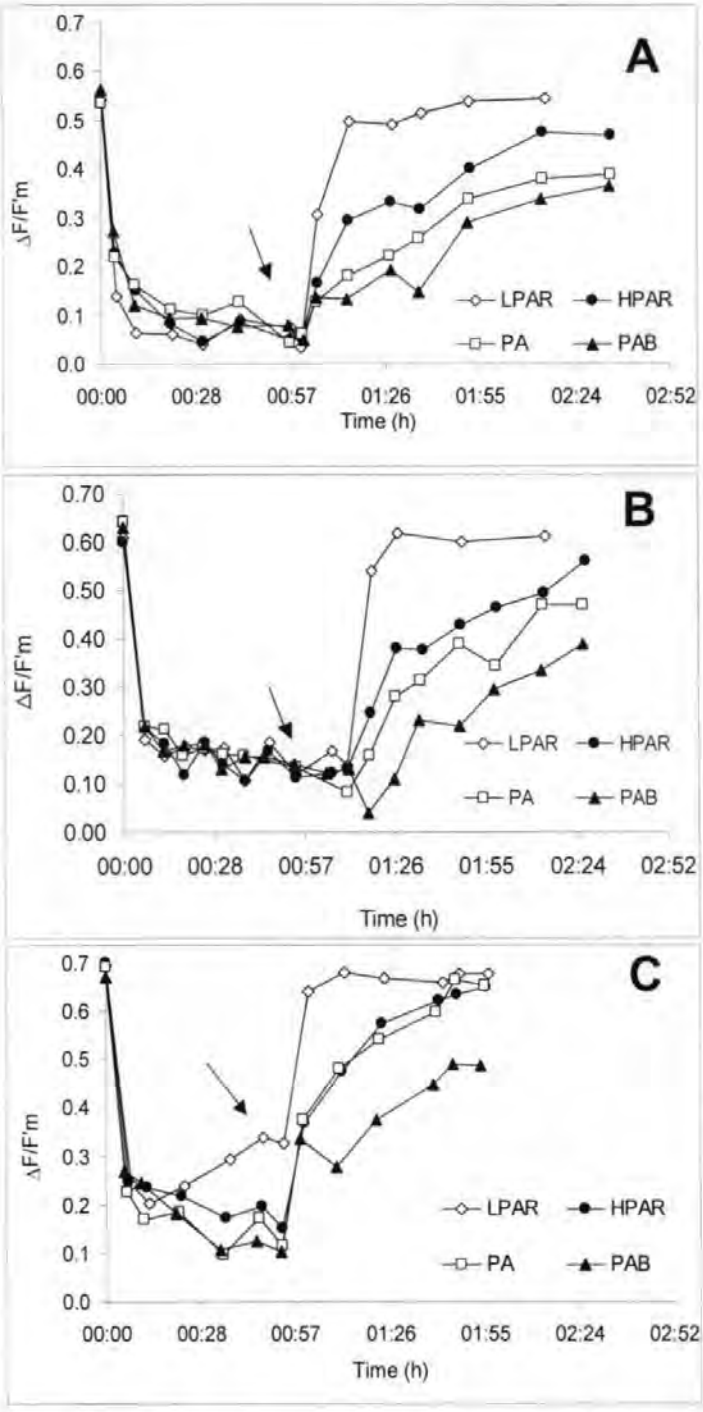

Figure 2.3. Photosynthetic efficiency in hyper-osmotically treated embryos in different stages of development and exposed to distinct light conditions. The embryos were treated with 20% salinity seawater. $\Delta F/F'_m$ was measured during 60 min stress and during subsequent 60-120 min recovery (arrows) under low light in 2.9% salinity filtered seawater. Values represent means of at least 5 measurements. Significant differences ($P<0.05$) were found between the response of 4 d old relative to 1 d and 2 d old embryos. **A)** 1 d old; **B)** 2 d old; **C)** 4 d old embryos.

d old), 0.019 ± 0.009 (2 d old), 0.015 ± 0.002 (4 d old), and did not change during treatments.

2.3.4. Electron transport during different stages of development

Although exposure to elevated light caused a steep decline in $\Delta F/F'_m$, considerable electron transport was still possible. Figure 2.5 shows the light response curves of the different developmental stages, from 3 h after fertilisation to 10 d old. As embryos developed, there was an increase in the initial slope under limiting light (α) and also in light-saturated photosynthetic rate (P_{max}). From these observations it is estimated that saturation PPFD ranged from 150 to 300 μmol m^{-2} s^{-1} at the respective ages investigated here.

2.3.5. Effects of high light on ROS production

The production of ROS, as measured by formation of DCF, increased with PPFD (Figure 2.6). Older embryos produced more ROS than younger ones. In accord with the ETR increase observed in Figure 2.5, this may be attributable to the progressive development of the photosynthetic apparatus in the growing embryo cells. When embryos were transferred from LPAR to higher PPFD there was a significant increase in ROS formation with more ($P < 0.001$) produced under PAB than either HPAR or PA (Figure 2.7).

The response of the embryos depended upon their stage of development ($P < 0.001$). ROS formation was higher in older (4 d) embryos (Figure 2.7). On transfer back to LPAR, production of ROS continued for some time, in some situations even after 60

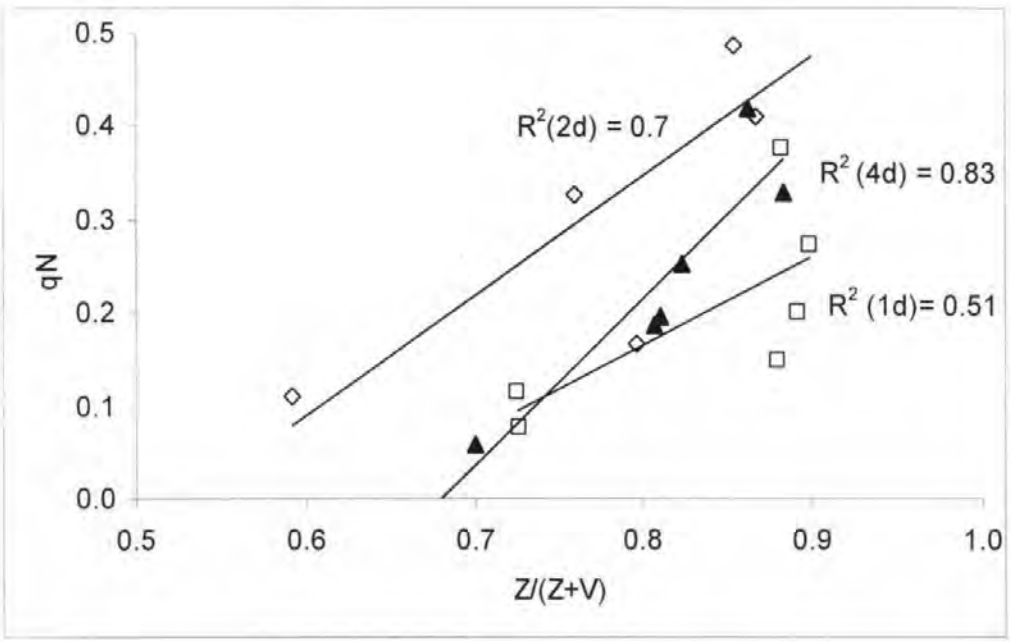

Figure 2.4. Photoinhibition in *Fucus* embryos. Correlation between qN (non-photochemical quenching) and the ratio zeaxanthin/violoxanthin+zeaxanthin of embryos sampled at different times during PAB treatment. Each data point represents average of 5-7 replicates. Open squares = 1 day old embryos; triangles = 4 days old embryos; diamonds = 2 days old embryos.

min; this is most evident in 1 d and 2 d old embryos previously exposed to UV-B (Figure 2.7). ROS production in all embryos, no matter what their stage of development (1-4 d) or treatment, returned to control values after 90 min under LPAR conditions.

An increase in both ROS production and electron transport rate (rel.ETR= PPFD * $\Delta F/F'_m$) with the stage of development of the embryos were observed. A correlation was found ($n=15$; $R^2=0.75$; $P<0.001$) between ROS production rates and relative ETR. Thus, ROS production seems to be proportional to the electrons transported by PSII, regardless of the age of the embryo.

2.3.6. Effects of combination of light and hyper-osmotic treatment on ROS production

Experiments to compare ROS production in control and hyper-osmotically treated embryos were designed under three conditions of hyper-osmotic stress (6%, 12% and 20% salinity seawater) and at the four light conditions: LPAR (no light treatment) and the high-light stress conditions HPAR, PA and PAB. Hyper-osmotic treatment alone or in combination with high light conditions induced an increase in ROS production (Figures 2.8; 2.9). There was a significant difference in ROS production ($P<0.05$) between different ages. As the degree of hyper-osmotic stress increased, there was a slight general increase in ROS production (Figure 2.8).

The highest ROS production was obtained when high irradiance was supplemented with UV-B and 20% salinity. The results show a highly significant correlation between

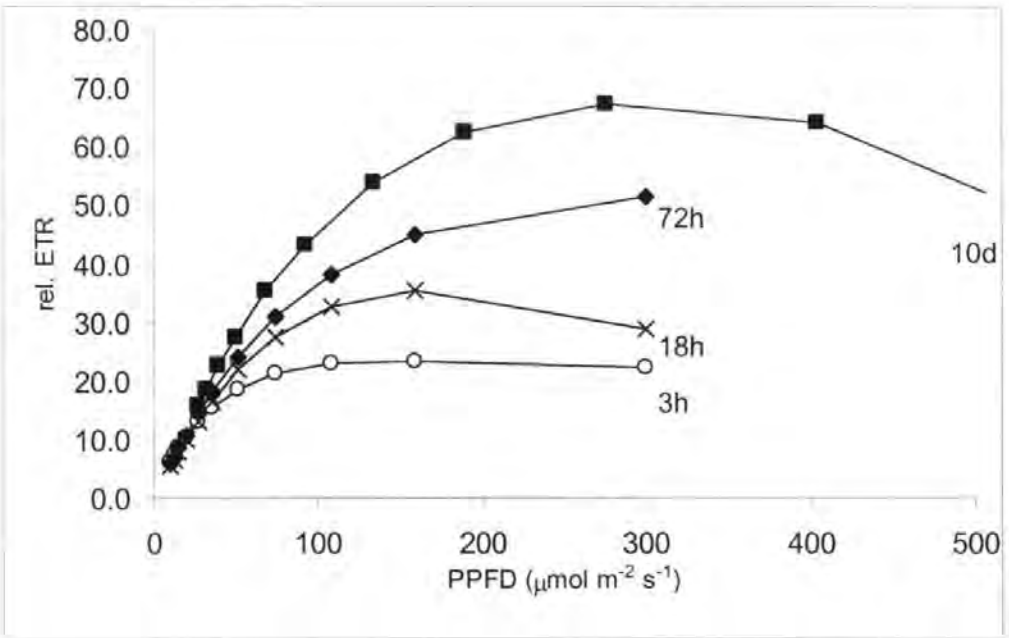

Figure 2.5. Photosynthetic light response curves of *Fucus* embryos at different stages of development. Curves were fitted using the equations of Platt et al. (1980). P_{max} varies between 23.3 (3 h old) and 67.4 (10 d old). α varies between 0.68 (3 h old) and 1.75 (10 d old). Each data point represents the average of 7 replicates.

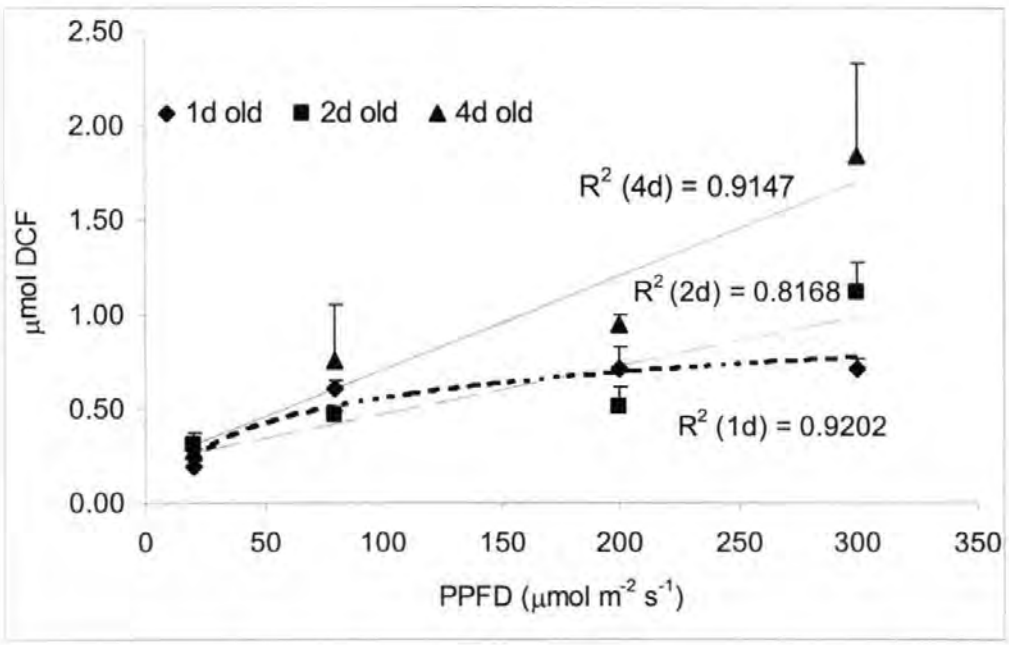

Figure 2.6. ROS production by *Fucus* embryos in response to increasing light levels measured 30 min after stress. Values represent mean ± S.D. (n=30-40).

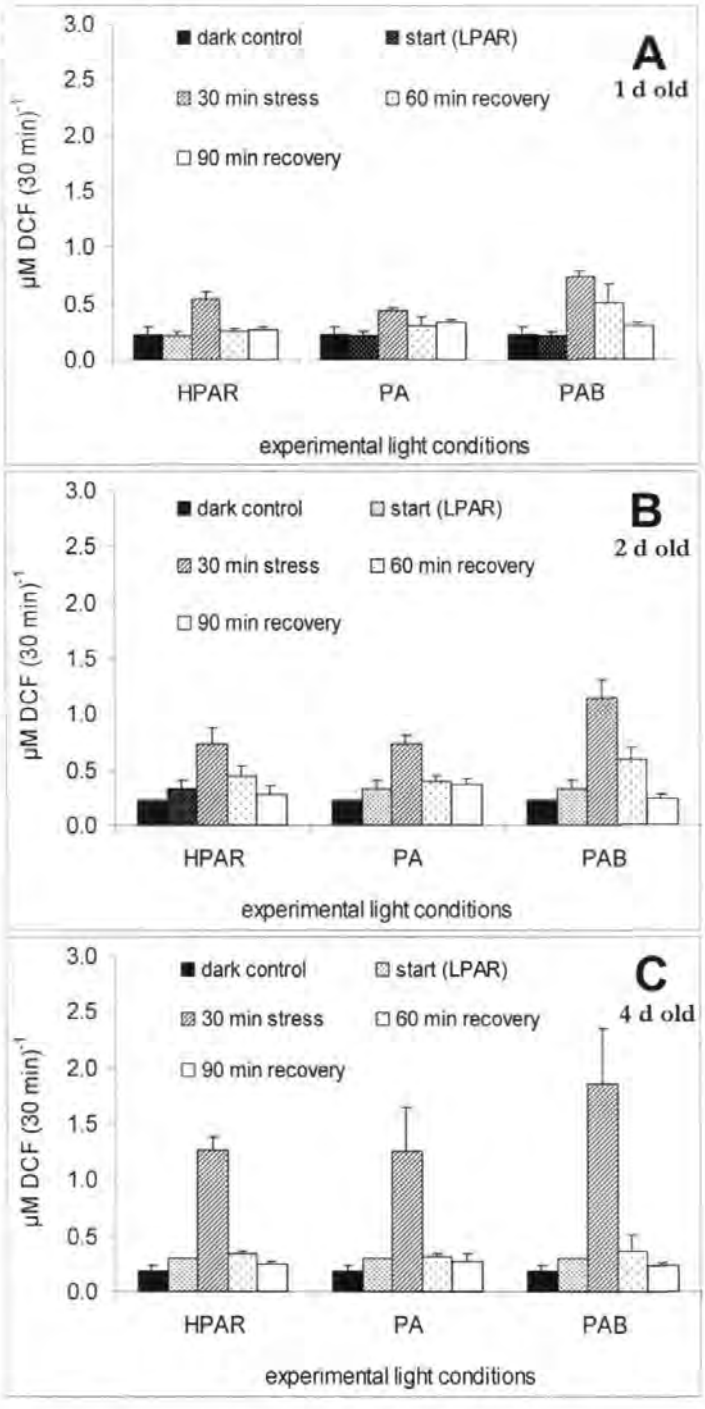

Figure 2.7. ROS production in *Fucus* embryos in different light conditions. Experimental conditions were: dark control, low light (start, LPAR), exposed for 30 min to high light (HPAR, PA, PAB) and after different recovery periods (60 min and 90 min) under LPAR. Values represent mean ± S.D. (n=30-40). **A)** 1 d old; **B)** 2 d old; **C)** 4 d old.

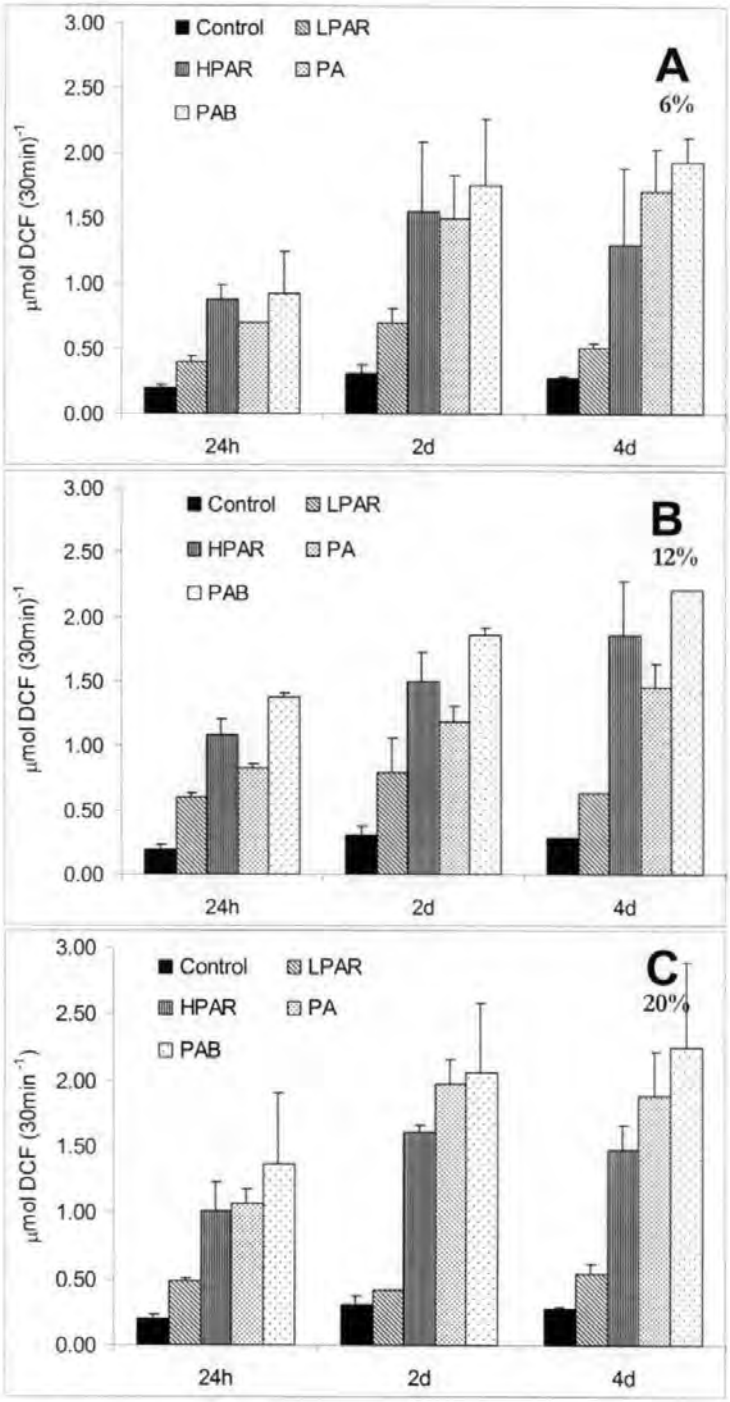

Figure 2.8. ROS production of desiccated *Fucus* embryos in different developmental stages exposed to several light conditions. A) 6 % salinity seawater **B)** 12% salinity seawater and **C)** 20% salinity seawater. Control represents samples in LPAR and normal seawater. Values represent mean ± S.D. (n=30-40).

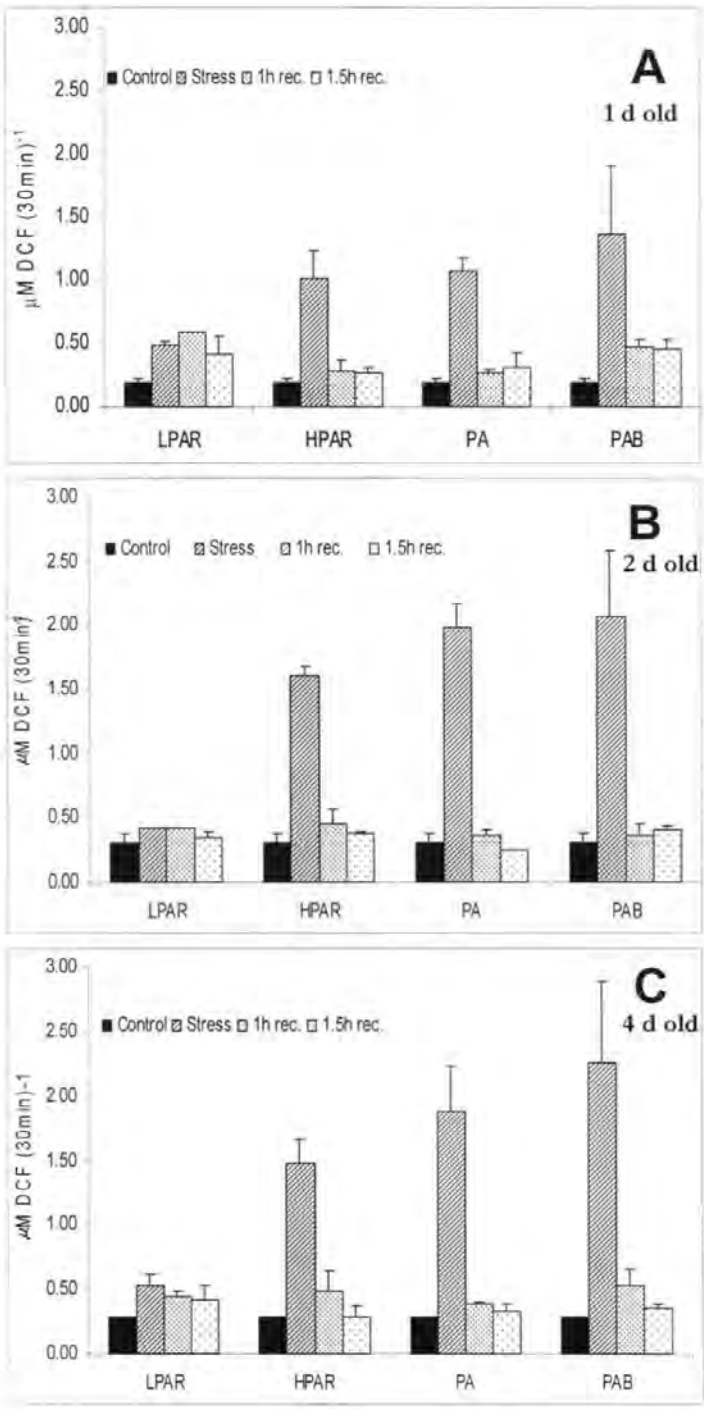

Figure 2.9. ROS production in hyper-osmotically stressed *Fucus* embryos (20% salinity seawater) exposed to different light conditions and after 60 min and 90 min recovery under LPAR and normal seawater (2.9% salinity). Controls represent embryos under LPAR and normal salinity seawater. Values represent mean ±S.D. (n=30-40). **A)** 1 d old; **B)** 2 d old; **C)** 4 d old.

hyper-osmotic and light treatment ($P < 0.001$), suggesting that these two variables act in an additive fashion to increase ROS production.

2.3.7. Growth of *Fucus* embryos after light and/or hyper-osmotic stress

Fucus embryos were subjected to light and/or hyper-osmotic stress for 1 h and their growth during the next 3 days was followed. Measurements of embryo length (Figure 2.10) show that growth of *Fucus* is only transiently affected by the different treatments. The most noticeable effect on growth was in response to PAB in combination with hyper-osmotic stress, where a significant decrease in growth rate during the following 2 days was observed ($P < 0.05$). PAB alone also affected significantly the development of the embryos during the following 24 h ($P < 0.05$). Nevertheless, embryos show a high capacity to recover, and 3 days after the treatment they show no significant difference compared to control embryos ($P = 0.32$).

2.4. Discussion

2.4.1. Photoinhibitory effects of light and hyper-osmotic stress

Treatment with 300 μmol m^{-2} s^{-1} light (with/without UV radiation) induced measurable physiological responses in *Fucus* embryos. Embryos subjected to high light (with or without UV radiation) showed a rapid reduction in effective quantum yield and this was maintained at a low value during incubation under high light conditions. Changes in $\Delta F/F'_m$ have been closely related to photoinhibition effects in other plant systems (Schofield et al., 1998). Photoinhibition can result from two different mechanisms (Demmig et al., 1987). The first is dynamic photoinhibition, which implies

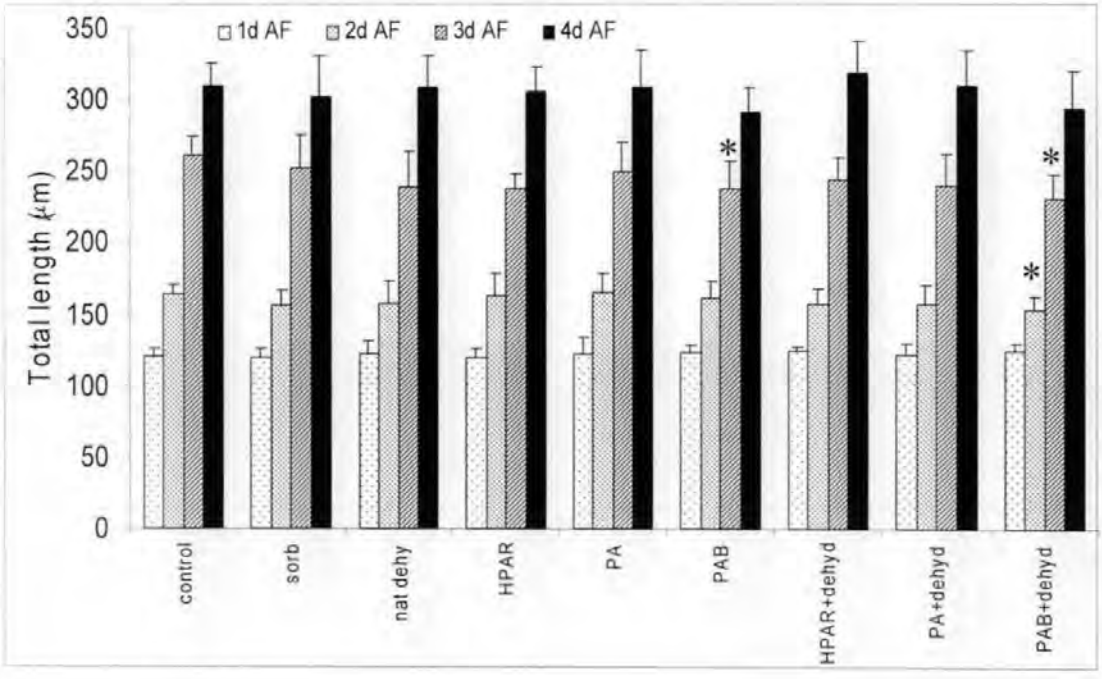

Figure 2.10. Development of *Fucus* embryos in response to different treatments. 1 d old embryos were subjected to each of the treatments for 30 min and then returned to LPAR and normal salinity seawater. Growth was measured as further changes in embryo length. Average of 3 replicates + S.D. is represented. * indicates significant difference ($P<0.05$) compared to control embryos.

photoprotection. The second type of photoinhibition is more permanent and is known to cause photodamage to PSII reaction centres (Bilger and Björkman, 1990). The results presented here suggest that dynamic photoinhibition was dominant in *Fucus* embryos challenged with high light. Reductions in $\Delta F/F'_m$ were readily reversible after transfer to more favourable conditions (low light), indicating that the reduction in the photosynthetic effective quantum yield upon high light levels represents a photoprotective mechanism rather than a long term inhibitory effect. In contrast, when high light treatment, in particular high light plus UV-B, was combined with hyper-osmotic stress, the effective quantum yield of PSII recovered more slowly. Under such conditions, initial $\Delta F/F'_m$ levels were not regained within 2 hours, and recovery was only partial (between 2 h and 48 h) which indicates that more permanent PSII damage might be occurring (Dring and Brown, 1982; Pearson and Davison, 1994).

2.4.2. Photoprotection during light stress

The results presented here indicate that *Fucus* embryos, in particular 2 d and 4 d old, have the capacity to use the violaxanthin-zeaxanthin pathway for the dissipation of excess energy, being, thus, able to partially protect themselves against excessive electrons. 1 d old embryos have a less clear correlation between non-photochemical quenching and dissipation of energy through the xanthophyll cycle. This lower capacity for dissipation of energy through V-Z cycle could potentially explain the slower recovery of photosynthetic efficiency and ROS production levels that are observed in younger embryos. The non-destructive dissipation of excitation energy into heat via pathways other than photochemistry is recognised as an efficient protective mechanism. The site of energy-dependent dissipation during dynamic photoinhibition

is generally believed to be the light harvesting complex antennae of PSII and is associated with the reversible de-epoxidation of violaxanthin to zeaxanthin in the xanthophyll cycle (Demmig-Adams and Adams, 1992; Havaux et al., 2000, Harvaux et al., 2001). Carotenoids, which are present in the membranes of all photosynthetic organisms, help protect against light-dependent oxidative damage (Havaux et al. 2000; Harvaux et al., 2001). In plants, the xanthophyll cycle is known to have a key photoprotective role. For example, *Arabidopsis* overexpression of the CHYB gene that encodes beta-carotene hydroxylase (an enzyme in the zeaxanthin biosynthetic pathway) causes a stress protection probably due to the function of zeaxanthin in preventing oxidative damage of membranes (Davison et al., 2002).

In the present study there is no evidence for variation in β-carotene concentration that would suggest any role in protection against light stress. The role of β-carotene as a biologically significant antioxidant in plants is highly controversial. Results of certain studies suggest that β-carotene plays a significant role *in vivo* by protecting the PSII reaction centre against photooxidative damage by scavenging superoxide in higher plants (Siefermann-Harms, 1987). However, other studies (e.g. Day et al., 1998) have concluded that β-carotene was ineffective in exerting protection and had no antioxidant effect. Uhrmacher et al. (1995) similarly found no change in β-carotene concentration during 2 h exposure of the algae *Dictyota dichotoma* to high irradiance.

2.4.3. Relationship between photoinhibition and ROS production

A slower, second phase, decline in $\Delta F/F'_m$ occurred from 8 min to about 45 min, under all high light and/or hyper-osmotic treatments. A positive correlation was found

between the slopes of the $\Delta F/F'_m$ curves and relative ROS production in *Fucus* embryos. Because H_2O_2 is known to inhibit directly the photosynthetic electron transport chain (Samuilov et al., 2001; He and Hader, 2002a) leading to photoinhibition, the results presented here suggest that the further reduction in $\Delta F/F'_m$ could be related to ROS production.

Similar increases in ROS production in response to UV radiation have been reported in other algal systems, such as *Chlorella vulgaris* (Malanga and Puntarulo, 1995). Transient inhibition of photosynthesis may be a result of both increased light and UV damage. UV radiation, in particular UV-B, reacts photochemically with oxygen to form ROS in cells and in the aquatic environment (Zhou and Mopper, 1990; Palenik, 1991; Scully et al., 1996; He and Hader, 2002b). ROS generating reactions also occur as a result of the photochemical interaction between UV-B and organic molecules (Gille and Sigler, 1995; Malanga, 1997; Cockell, 1998). In cells, toxic hydroxyl radicals ($^{\bullet}OH$), formed from hydrogen peroxide and superoxide radicals in the Haber-Weiss reaction, react with photosynthetic apparatus components (Strid et al., 1994; Ishida et al. 1998; Sgherri et al., 1999). Hideg and colleagues (1994) observed that in light-stressed thylakoid isolates, $^{\bullet}OH$ radicals at PSII induced photoinhibition. These ROS are potentially damaging to thylakoid membrane structure, most pigments (carotenoids, chlorophyll), and the D1 protein in the PSII core (Hideg and Vass, 1996; Nishiyama et al., 2001). Other proteins (such as enzymes involved in dark reactions), DNA and membrane lipids can also be damaged by ROS production (Foyer et al., 1994). Enhanced $^{\bullet}OH$ formation can lower the photosynthetic efficiency of algae at elevated light, as well as under UV-B (Tschiersch and Ohmann, 1993; Hirayama et al., 1995).

In the present work, the effect of PAB on ROS production was exacerbated by simultaneous treatment with hyper-osmotic stress. Increased ROS production due to osmotic treatments has been measured in a variety of plant systems (for example Cazalé et al., 1998, 1999). Thus, the additive effect on global cellular ROS production between light and osmotic treatment found here is not surprising. However, the exact mechanism whereby light and osmotic stress interact is not known. From the data presented it is not possible to assess if ROS are being produced in the same cellular compartments (presumably chloroplasts and peroxisomes for the light stress) or if osmotic stress has effects on other cellular components. Drought is known to induce ROS production at the chloroplast level (Smirnoff, 1993) and to reduce $\Delta F/F'_m$ (Loggini et al., 1999; Lu and Vonshak, 2002), so it could be intensifying the light stress effect at the photosynthetic apparatus level. Alternatively, osmotic stress could be inducing ROS production in other cellular compartments, such as mitochondria (Coelho et al., 2002). On the other hand, the activity of NADPH oxidase that could counter the excess reductants (NADPH) arising from the chloroplast electron transport chain under high light, would also lead to further ROS production. High resolution imaging of ROS production during the light/hyper-osmotic stress would allow a definitive conclusion to be drown about the origin of the oxidative burst.

An increase in the ratio (1-pP)/qN indicates that high light had a relatively greater impact on photosynthetic electron transport by the closure of reaction centres, than it had on the increase of the non-photochemical quenching, which is due mainly to protective energy dissipation. Consequently, a higher (1-qP)/qN value would also indicate a greater susceptibility to light stress (Jimenéz et al., 1998). Thus, according to

the present results, older embryos showed a higher capacity for photoprotection than younger ones. This dissipation of excess energy might have been achieved through the xanthophyll cycle, as older embryos present a higher correlation between non-photochemical quenching and violaxanthin conversion to zeaxanthin (section 2.4.2.).

Embryos were found to produce ROS in total darkness, although to a lesser extent, indicating that processes other than photosynthesis were involved in ROS production. Collén and Davison (1997) have also observed this in adult *Fucus*. 1 d old embryos had the highest and 4 d old ones the lowest production of ROS in darkness. Dark production of ROS can be explained by respiration of storage products, as the mitochondrial electron transport chain is an important source of basal ROS production (Halliwell and Guteridge, 1999).

2.4.4. ROS production in different developmental stages

ROS production increased significantly with the age of the embryos under all conditions tested. In relation to the light stress response, this is most likely due to older embryos having a more developed photosynthetic machinery and greater pigment synthesis (McLachlan, 1974; McLachlan and Bidwell, 1978; Davison et al., 1993; Lamote et al., 1998). This is supported by the light response curves which show an increase in α and P_{max} with age. More electron transport means a greater likelihood of electron leakage from the transport chain, and thus more potential ROS production at the chloroplast level.

2.4.5. Effects of light and hyper-osmotic stress on *Fucus* growth

Growth of embryos was found to be transiently affected by high light and/or hyper-osmotic stress, in particular when PAB in combination with hyper-osmotic stress was present. The growth rate reduction found in the hyper-osmotically-stressed embryos could be due to increased cell wall cross-linking due to H_2O_2 production (Bradley et al., 1996), thus decreased elongation capacity. Another possibility is the temporary reduction in photosynthesis that could perturb embryo growth. However, *Fucus* embryos are able to grow even in total darkness, using mannitol as a storage compound. It is likely that energy is directed to the production of protection-related substances, such as osmotically compatible compounds that could be used to compensate turgor changes, antioxidant molecules and cell wall strengthening-related compounds. This potential energy re-allocation would lead to the observed transient growth rate decrease.

2.4.6. Conclusion

In conclusion, the data presented here indicate that a single, ecologically relevant, dose of high light, especially with UV-A or UV-B, in combination or not with hyper-osmotic stress can affect the cellular physiology of *Fucus* embryos. Two photoinhibition responses were recognised. Firstly a rapid decline of the PSII yield ($\Delta F/F'_m$) which is probably related to the violaxanthin-zeaxanthin cycle (photoprotection), followed by slower second-phase decline which is most likely correlated with ROS production. In the developing photosynthetic apparatus, electron transport rates increased with the age of the embryo and were correlated with ROS

production rates. The capacity for photoprotection was found to increase with age. As a result of enhanced ROS production, a slow repair of the photosynthetic efficiency was observed, particularly with increased UV doses. In the absence of UV-B, embryos were generally able to recover quickly from the imposed high light/hyper-osmotic stress. Development of the embryos was found to be transiently affected by UV-B with or without hyper-osmotic treatment. Overall, the data presented here suggest that, under natural conditions, embryos of *Fucus* are susceptible to high light, especially in combination with dehydration, and that solar UV-B radiation is an important additional stress factor.

CHAPTER 3

INTERACTIONS BETWEEN REACTIVE OXYGEN PRODUCTION AND Ca^{2+} SIGNALLING

3.1. INTRODUCTION

3.1.1. ROS production during stress

The formation of reactive oxygen species (ROS) such as hydrogen peroxide, superoxide and possibly nitric oxide is ubiquitous in plant systems. They are often formed as by-products of normal metabolism as a result of leaky electron transport systems, but it has also become apparent that there is a rapid and deliberate production of these ROS in plant defence responses. ROS are produced by plant and animal cells in response to a range of stimuli, from osmotic stress to chilling, wounding and pathogen response (see Table 1.3 and Bac et al., 1997; Minibayeva et al. 1998; Tan et al. 1998; Grant and Loake, 2000). Such oxidative bursts can underlie anti-microbial activity or downstream responses such as modulation of gene expression and cell cycle control (Finkel, 1998; Reichheld et al., 1999; Shackelford et al., 2000; Bowie and O'Neill, 2000; Desikan et al., 2000).

There is still a considerable debate about the identity of the oxidative burst generator(s). Several sources are known to exist for the generation of ROS. These include plasma-membrane associated NADPH and NADH oxidases, amine oxidases and oxalate oxidases and protoplastic sources from mitochondria, chloroplasts and peroxisomes (Halliwell and Gutteridge, 1999). Of these systems, the neutrophil-like NADPH oxidase system has received most attention, especially in plant-pathogen interactions (Table 1.3 and reviewed by Morel and Barouki, 1999; McDowell and Dangl, 2000). Superoxide generation by NADPH oxidase at the external surface of the cells is followed by a rapid dismutation to hydrogen peroxide, which readily crosses

membranes. Inhibitors of the animal NADPH oxidase, including the suicide substrate inhibitor diphenyleneiodonium (DPI) also block the elicitor-stimulated oxidative burst in plant cells (Levine et al., 1994; Desikan et al., 1996; Pugin et al., 1997). Analogues of the mammalian gp91phox have been cloned from rice (Groom et al., 1996) and *Arabidopsis* (Keller et al., 1998; Torres et al., 1998). Plant equivalents of the mammalian cytosolic components p22-phox, p47-phox and p67-phox have been demonstrated by cross-reactivity with antibodies to the subunits of the mammalian complex but have not been cloned (Murphy et al., 1998). An equivalent of the fourth cytosolic component, p21 rac, however, has been cloned and is potentially involved in H_2O_2 production in differentiating xylem (Potikha et al., 1999). In general, molecular and physiological data seem to indicate functional and mechanistic similarities between animal and plant NADPH oxidase related-oxidative burst, but interpretations and generalisations should be careful as more detailed functional molecular data is still lacking.

In addition to plasma membrane NADPH oxidase, mitochondria, peroxisomes and chloroplasts are potentially powerful intracellular generators of ROS (e.g. Pastori and del Rio, 1997; Morel and Barouki, 1999). Plant mitochondria can produce high amounts of ROS when the activity of the enzyme alternative oxidase is suppressed (Maxwell et al., 1999). Allan and Fluhr (1997) studied ROS generation using the fluorescent dye dichlorofluorescein and showed an accumulation of oxidised dye in the chloroplasts and nucleus in intact tobacco epidermal cells, which suggests production of ROS in these compartments. However, little information is available on the sub-cellular spatio-temporal dynamics of ROS production in response to specific stimuli.

3.1.2. Signalling involved in the generation of ROS

A number of cellular events have been correlated with ROS production during plant stress responses. These include hormone signalling, ion-fluxes, protein kinases, phospholipases, etc. (reviewed by Vranova et al. 2002). For example, gp91-phox has been considered a target for kinase action linked to Ca^{2+} fluxes (Blumwald et al., 1998). Plant NADPH oxidase has also been found to include a large hydrophilic N-terminal domain that contains two Ca^{2+} -binding EF hand motifs (Torres et al., 1998). It has been postulated that the mammalian NADPH oxidase is activated by a protein kinase C (PKC) mediated phosphorylation of p47-phox and p67-phox. In tomato cells, race-specific elicitors are also thought to promote translocation of cytosolic p47-phox and p67-phox to the plasma membrane of tomato cells. In contrast to mammals, this process is not dependent on protein kinase C (Xing et al., 1997). The assembly process was found to involve a Ca^{2+}-dependent protein kinase that catalyses the phosphorylation of p47-phox and p67-phox, facilitating their translocation to the plasma membrane. MAPK have been implicated both up- and downstream of the oxidative burst (see Table 4.1). Proton fluxes are also ubiquitous in higher plant elicitor systems and extracellular alkalinisation has been found to be present during the apoplastic oxidative burst in tomato plants (Schaller and Oecking, 1999). Abscisic acid (ABA) has been shown to elevate ROS in guard cells (Pei et al, 2000) and ROS was reported to be an intermediary in the pathway leading to ABA-induced antioxidant (CAT1) gene expression (Guan et al., 2000).

3.1.3. Ca^{2+} signalling

Ca^{2+} is a ubiquitous plant second messenger responsible for the regulation of a variety of cellular processes (Sanders et al., 1999, 2002). Ca^{2+} concentration in the cytoplasm of plant cells is highly regulated and kept at a low level (100 to 200 nM, Roberts et al., 1993). Ca^{2+} signals are generated through the opening of ion channels that allow the flux of Ca^{2+} from a compartment where it is present at relatively high electrochemical potential (outside the cell or from an intracellular store) to one where Ca^{2+} is at a lower potential. Such channels are referred as Ca^{2+}-permeable channels and this term reflect the importance of non-selective cation channels in generating plant Ca^{2+} signals (Sanders et al., 2002).

Small fluxes of Ca^{2+} into the cytosol lead to large changes in concentration due to Ca^{2+} release from internal stores such as ER and vacuole. Ca^{2+} binds reversibly and rapidly to many proteins and enzymes and small increases in pump activity can rapidly remove elevated Ca^{2+}. These characteristics enable Ca^{2+} to be used as an efficient second messenger (Sanders et al., 1999; 2002). Cytosolic Ca^{2+} concentration is maintained low by binding to proteins (Thomas, 1982), and by the activity of membrane-bound ATP-driven Ca^{2+} extrusion pumps (Bush, 1993) on the ER (Bonza et al., 2000) vacuole (Yuasa and Maeshima, 2001) Golgi (Surroca and Wolff, 2000) and plasma membranes (Bonza et al., 2000).

3.1.3.1. Ca^{2+}-permeable channels at the plasma membrane

Electrophysiological studies have revealed the presence of Ca^{2+}-permeable channels in higher plant plasma membranes that are activated by membrane depolarisation

(reviewed by White, 2000). Perception of a stimulus results in membrane depolarisation and downstream opening of Ca^{2+}-permeable channels that results in elevation of cytosolic Ca^{2+}. In addition, the presence of hyper-polarisation-activated Ca^{2+}-permeable channels (HACC) is becoming evident (Hamilton et al., 2000, Very and Davies, 2000). HACCs in the plasma membrane of guard cells are opened by ABA (Hamilton et al., 2000) and they are probably responsible for the generation of tip-to-base Ca^{2+} gradient in root hairs of *Arabidopsis* essential to maintain polarised growth (Very and Davies, 2000).

In *Arabidopsis* guard cells, ABA-induced stomatal closure involves the production of ROS and HACCs play an important role in this effect (Pei et al., 2000, Zhang et al., 2001). H_2O_2 was found to stimulate HACCs and thereby an increase in cytosolic Ca^{2+}.

3.1.3.2. Ca^{2+}-permeable channels in endomembranes

The vacuole of plant cells is the principal intracellular Ca^{2+} store (reviewed by Sanders et al., 1999) and a number of Ca^{2+} release channels have been reported at the vacuolar membrane level. Two of these channels are ligand-gated by $Ins(1,4,5)P_3$ and cyclic ADP-ribose. Two others are gated by voltage, one by hyper-polarisation and a second by membrane depolarisation (slowly-activating vacuolar - SV - channel) (reviewed by Sanders et al., 2002) in reference to its voltage-activation kinetics. The SV channel is activated at physiological cytoplasmatic Ca^{2+} concentrations and may have the capacity to catalyse Ca^{2+}-induced Ca^{2+} release (CICR; Bewell et al., 1999). Although the presence of Ca^{2+} alone would not allow CICR *in vivo*, the presence of Mg^{2+} ions at physiological concentrations potentiates the Ca^{2+} response thereby suggesting a role in CICR (Pei et al., 1999; Carpaneto et al., 2001).

Recent studies have highlighted the importance of other intracellular stores, in particular the endoplasmatic reticulum (ER). Voltage-dependent Ca^{2+}-selective channels have been identified in this compartment (Klusener et al., 1999) and demonstration of $Ins(1,4,5)P_3$ binding sites suggesting the presence of $Ins(1,4,5)P_3$-gated Ca^{2+}-release channels has been demonstrated (Martinec et al., 2000). The presence of cADPR-mobilizable Ca^{2+} has also been demonstrated in ER vesicles (Navazio et al., 2001). A Ca^{2+} release pathway induced by NAADP (nicotinic acid adenine dinucleotide phosphate) has been also identified (Navazio et al., 2000).

Several roles have been suggested for the different ligands. $Ins(1,4,5)P_3$ is thought to have a function in transduction of salt and hyper-osmotic stress (Drobak and Watkins, 2000; DeWald et al., 2001) and gravitropism (Perera et al., 1999). cADPR is probably involved in activation of plant defence genes (Durner et al., 1998) and ABA signalling pathways (McAinsh and Hetherington, 1998).

Cytoplasmatic Ca^{2+} elevations can be created in *Fucus* rhizoid cells by photorelease of caged $Ins(1,4,5)P_3$ (Goddard et al., 2000). Other possible intracellular Ca^{2+} stores in plants include mitochondria (Subbaiah et al., 1998), chloroplasts (Ettinger et al., 1999), plastids (Bednarska and Butowt, 1995) and vesicles (Ladyzhenskaya et al., 1991).

3.1.4. Ca^{2+} during osmotic stress

The spectrum of stimuli that evoke changes in cytoplasmatic Ca^{2+} have been listed in recent reviews (Sanders et al., 1999, Knight and Knight, 2001). Abiotic stimuli include light (with different qualities acting via different pathways; Baum et al., 1999, Frohnmeyer et al., 1999) cold shock (Knight et al., 1991; 1996), gravity (Gehring et al.,

1990), light (Gehring et al., 1990), salinity or drought (Knight et al., 1991; 1997), touch (Knight et al., 1991; 1992) hypo-osmotic treatment (Taylor et al., 1996; Goddard et al., 2000), and wind (Knight et al., 1992). Biotic stimuli include hormones such as ABA (McAinsh et al., 1990; 1992) and giberellin, fungal elicitors and Nod factors (reviewed in Sanders et al., 2002). In particular, Ca^{2+} is a well-established second messenger during osmotic signalling in animal, yeast, algal and higher plant cells (Okazaki et al., 1987; Rothstein and Mack, 1990; Oike et al., 1994; Tazawa et al., 1995; Batiza et al., 1996; Takahashi et al., 1997; Altamirano et al., 1998). Goddard et al. (2000) and Taylor et al. (1996) have shown that osmotically-induced Ca^{2+} signals are necessary for osmotic volume regulation in the *Fucus* zygote. The Ca^{2+} transient produced by hypo-osmotic shock is restrited to the rhizoid cell of the two-celled embryo and propagates as a wave of elevated Ca^{2+} in response to large hypo-osmotic shcoks (Taylor et al. 1996). The size and duration of the hypo-osmotic Ca^{2+} transient in *Fucus* is graded according to the severity of the shock. The pattern of propagation of tthis hypo-osmotically-induced Ca^{2+} wave was found to depend on the strengh of the stimulus (Goddard et al., 2000). Mild or severe shocks generate separate apical Ca^{2+} elevations and/or bi-directionally-propagating Ca^{2+} waves that initiate in the rhizoid peri-nuclear region (Goddard et al., 2000).

3.1.5. Objectives

A close relationship between stress-induced Ca^{2+} signals and ROS production is becoming increasingly clear from studies in both plant and animal cells. Both a Ca^{2+}-dependence of H_2O_2 production (Grant and Loake, 2000) and a modulation of plasma membrane Ca^{2+} channels and cytosolic Ca^{2+} by H_2O_2 (Pei et al., 2000) have been

demonstrated. However, essential spatio-temporal data that would allow mechanistic interpretations of the inter-dependence of Ca^{2+} and ROS signals is lacking. Therefore, the specific objectives of this chapter were the following:

I. To determine the spatio-temporal patterns of Ca^{2+} and ROS elevation in *Fucus* rhizoid cells in response to hyper-osmotic stress.

II. To determine the inter-dependence of Ca^{2+} and ROS signals.

III. To determine the sequence of events involving ROS and Ca^{2+} during hyper-osmotic stress.

3.2. METHODS

3.2.1. Embryo culture

Fucus serratus embryos were cultured on glass coverslips fitted to the base of culture dishes in filtered seawater for 24 h in unidirectional light at 16°C as described previously (Goddard et al., 2000). All experiments were performed using two-cell embryos. Dishes were perfused during experiments on the stage of a Nikon Diaphot 300 inverted microscope with a gravity perfusion system that allowed rapid solution changeover.

3.2.2. Ca^{2+}_{cyt} measurements

3.2.2.1. Ca^{2+} indicators

The visible light-excitable Ca^{2+} indicators used were Calcium Green-1-dextran (CG-1) and Texas Red-dextran (TR). CG-1 exhibits an increase in fluorescence emission intensity when bound to Ca^{2+}, whereas TR does not change fluorescence intensity. This property allows ratiometric measurements of cellular Ca^{2+} changes during a stress stimulus. These fluorescent dyes are attached to a dextran molecule (10 kD). Dextrans are thought to have low toxicity and be biologically inert due to their poly-(α-D-1,6-glucose) linkages which render them resistant to cleavage by most endogenous enzymes. Dextran attachments prevent dye leakage across the plasma membrane and compartmentalisation into organelles following microinjection into the cytosol (Berger and Brownlee, 1993).

$[Ca^{2+}]_{cyt}$ was measured in rhizoid cells using Calcium Green-dextran (10 kDa) ratioed against Texas Red-dextran (10 kDa, Molecular Probes, Oregon, USA) (Goddard et al., 2000). Images were acquired using a BioRad (Hemel Hampstead, UK) 1024 confocal microscope equipped with a krypton/argon laser (see section 3.2.3.). Calcium Green and Texas Red were excited simultaneously at 488 nm (523 nm emission) and 567 nm (605 emission) respectively.

3.2.2.2. Pressure microinjection

Dyes and buffers were dissolved to a final concentration of 1 mM in an artificial intracellular solution (200 mM KCl, 10 mM HEPES, 550 mM mannitol, pH 7.0) and

pressure microinjected (Taylor et al., 1996; Goddard et al., 2000) using pipettes fabricated from 1.2 mm filamented borosilicate glass and dry bevelled (Taylor et al., 1996) before back filling. The micropipette was connected to a pressure microinjection unit (Picoinjector PL1-100; Medical System Corp., Greenville, NY). Back pressure of +20 kPa was applied to the pipette at all times to prevent any back filling by the extracellular solution (0.1-0.2 M sorbitol in artificial seawater). Embryos were incubated in 0.1-0.2 M sorbitol to reduce internal turgor pressure during microinjection and recovered in SW for >1h before measurements were taken. Zygotes were impaled at 20 μm from the tip of the germinating rhizoid. After impalement, dye was introduced with up to 4 pulses of 90 s in duration at increasing pressure from 30 kPa to 150 kPa. In some cells, the Ca^{2+} chelator Br_2BAPTA (intracellular final concentration 4 mM) was microinjected along with the Ca^{2+} dyes to buffer Ca^{2+}_{cyt} changes. Ca^{2+} dyes were injected to a final intracellular concentration of 10-50 μM. Final concentration of dyes was estimated by comparing the fluorescence of microinjected Texas Red with that of solutions containing known concentrations of TR. It has been estimated that the microinjection procedure injected 1-5% of total cell volume (Taylor et al. 1996).

Pressure microinjection of Ca^{2+} indicators has some potential difficulties such as temporary Ca^{2+} elevation with needle impalement and damage to the cell (Cobbold and Rink, 1987) and the limited number of cells that can be microinjected. However, this process allows controlled injection of dyes to specific regions of the cell and the use of Ca^{2+} dyes attached to dextran molecules. The microinjection protocol used in the

present study has been shown to have minimal disruption to the rhizoid growth (Berger and Brownlee, 1993, Taylor et al., 1996, Goddard, 2001).

3.2.2.3. Ca^{2+} dye calibration

Simultaneous fluorescence images were obtained from embryos microinjected with CG-1 and the Ca^{2+} insensitive dye TR-dextran (10 kDa). Assuming that both dyes distributed equally inside the cell, changes in the ration of CG-1 to TR fluorescence values reflected changes in cytoplasmatic Ca^{2+} concentration and are independent of factors such as dye distribution, cell thickness and photobleaching.

➢ *In vitro* calibration. *In vitro* calibrations were obtained from different Ca^{2+} buffer solutions containing mixtures of 50 μM CG-1 and TR-dextrans. A calibration graph (Figure 3.1) gave values for cytoplasmatic Ca^{2+} levels.

Table 3.1. *Composition of buffered Ca^{2+} solutions.* Each contained 550 mM mannitol. KOH was used to adjust pH (Tsien and Rink, 1980).

pCa	[$CaCl_2$] (mM)	Ca^{2+} ligand	[KCl] (mM)	pH buffer (10mM)	pH
5	5	NTA	90	TAPS	8.42
6	5	HEDTA	90	HEPES	7.70
7	5	EGTA	90	MOPS	7.29
8	5	EGTA	100	HEPES	7.80

➢ *In vivo* calibration. The "R_{min}/R_{max}" method (Grynkiewicz et al., 1985) was used for *in vivo* calibrations (Figure 3.1). Embryos microinjected with CG-1 and TR-dextrans (1 mM) were perfused with altering Ca^{2+} free artificial seawater (ASW, 0.1 mM EGTA) and 50 mM Ca^{2+}-ASW to obtain R_{min}/R_{max}. All solutions contained 100 mM

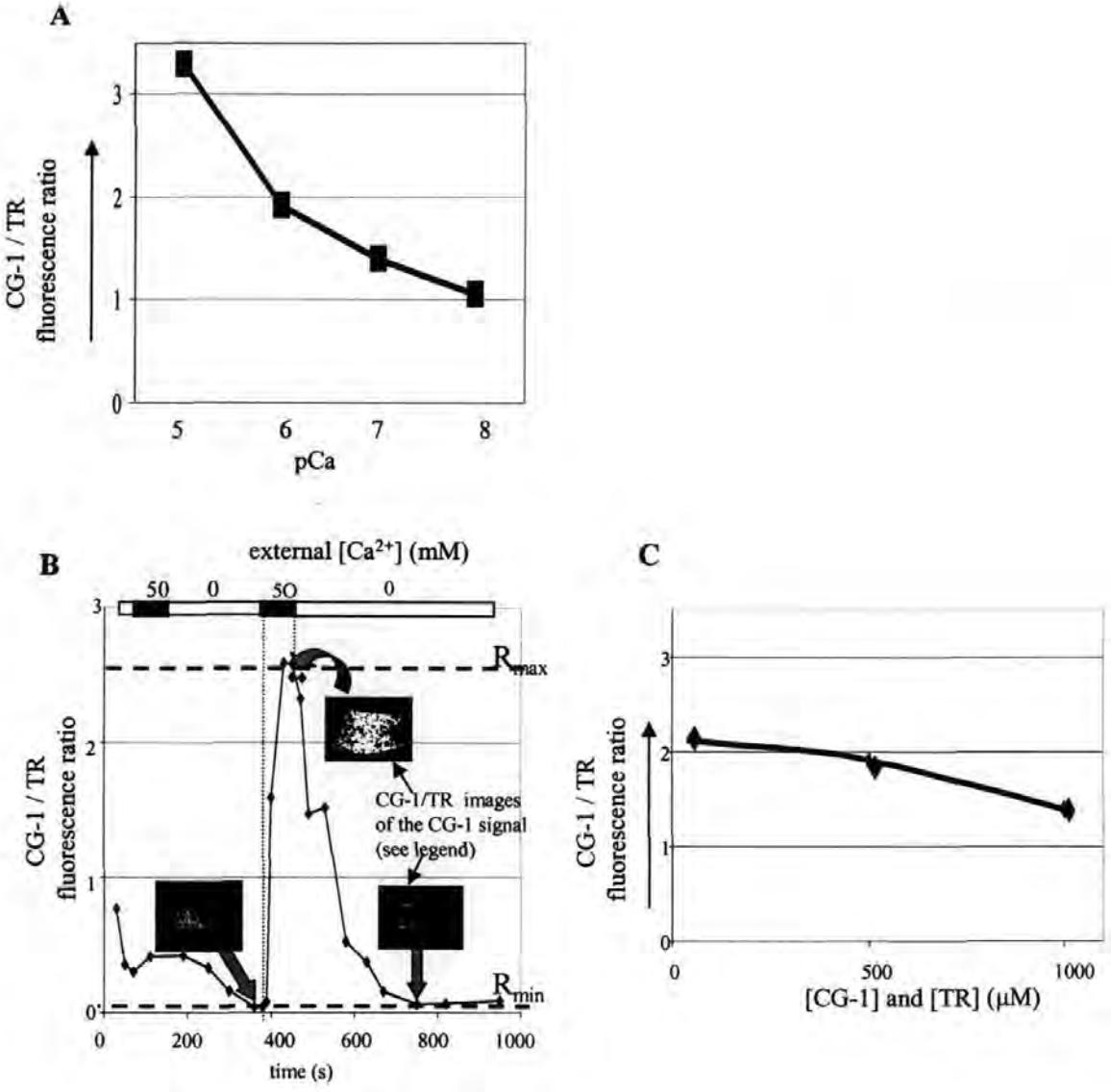

Figure 3.1. Ca^{2+} dye calibration. A) *In vitro* calibration of CG-1-dextran (1 mM). **B)** *In vivo* calibration of CG-1-dextran was obtained using 'R_{min} R_{max}' method. CG-1 fluorescence was visibly much brighter in the rhizoid cell at R_{max}. Resting Ca^{2+} concentration ($[Ca^{2+}]$) in seawater was approximately 100 nM **C)** CG-1 and TR -dextrans at concentrations of 100, 500 and 1000 μM were added to Ca^{2+} buffer solutions (pCa 6) settings. The concentration of the dye affected the CG-1 / TR fluorescence ratio as a result of isometric resonance fluorescence (Goddard, 2001).

ionomycin (Calbiochem, Nottingham, UK). For ratio values of a Ca^{2+}-dependent signal against a Ca^{2+}-independent signal calibrations were calculated as follows (Grynkiewicz et al., 1985).

$$[Ca^{2+}] = K_d \cdot (R - R_{min}) / (R_{max} - R)$$

where R is the fluorescence ration, K_d of CG-1 is 190 nM; R_{min} = CG/TR fluorescence ration of Ca^{2+} free dye; R_{max} = CG/TR fluorescence ratio of Ca^{2+}-bound dye.

➢Isometric resonance fluorescence. Different concentrations of CG-1-dextran and TR-dextran were added to a set of Ca^{2+}-buffer solution and imaged as before. The dye concentration used affected the CG-1 to TR fluorescence ratios (Figure 3.1). This phenomena is called isometric resonance fluorescence and has implications for the estimates of cytoplasmatic Ca^{2+} concentrations using calibration curves based on different concentrations of dye.

3.2.3. Imaging with CLSM

3.2.3.1. The CLSM unit

In CLSM a laser beam is passed through a x-y deflection mechanism, which turns the static beam into a scanning beam. This is focused to a small spot onto a fluorescent specimen by an objective lens (Figure 3.2). Reflected light and emitted fluorescence light is captured by the same objective and (after conversion into a static beam by the x-y scanner device) fluorescent light is focused onto a photomultiplier tube (PMT) via a dichroic mirror (beam splitter). A confocal pinhole aperture is placed in the front of

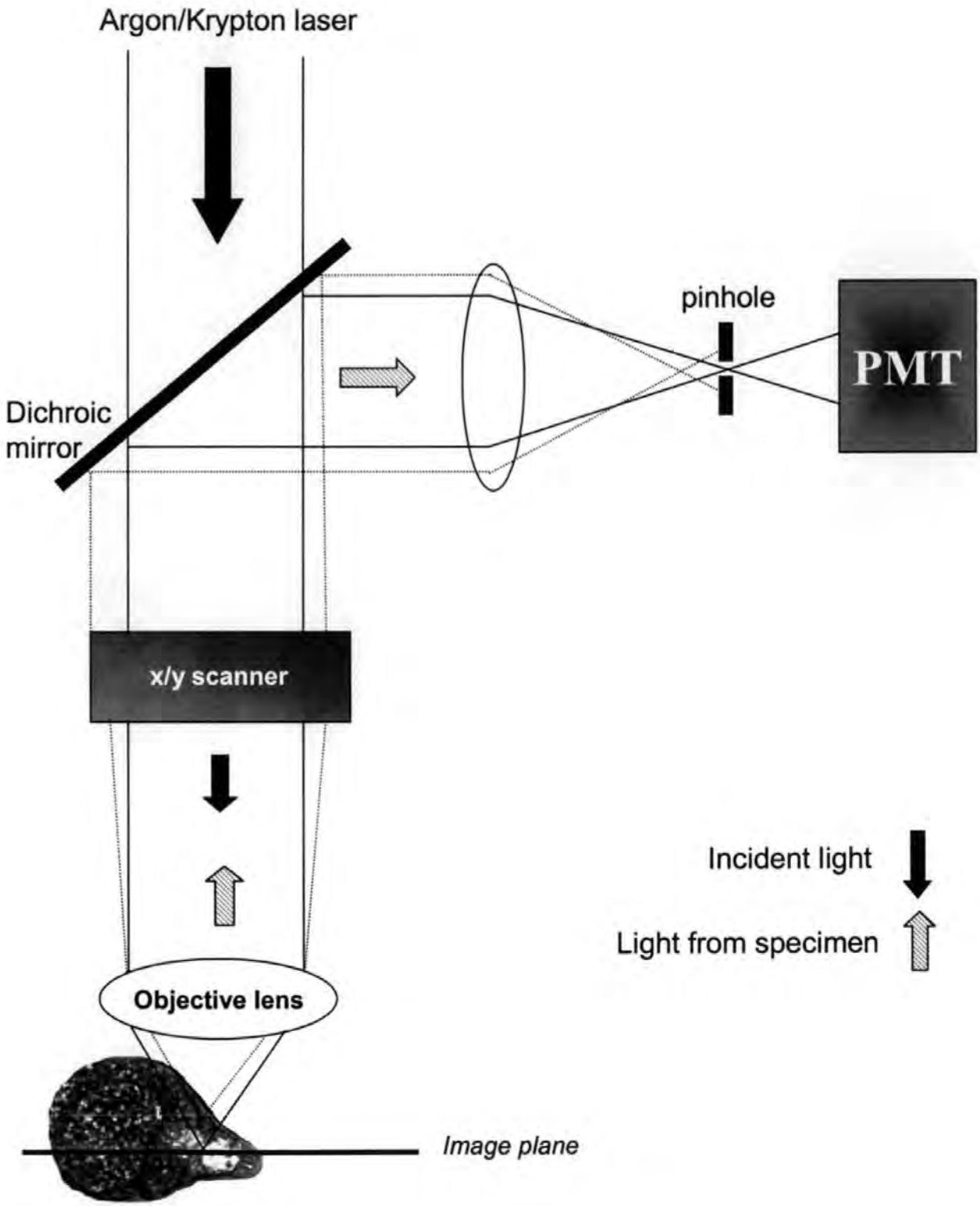

Figure 3.2. Diagram of a CLSM system.

the PMT in order that light coming from out of focus planes is largely blocked (Figure 3.2). This effect is also known as optical sectioning since it permits the imaging of separate axial slices within the specimen. The size of the pinhole determines how much reduction of the out-of-focus information can be realised. As the laser scans the specimen, the analogue light signal, detected by the PMT is converted into a digital signal contributing to a pixel-based image displayed on a computer monitor. The plane of focus is selected by a computer-controlled fine-stepping motor that moves the objective up and down. A non-confocal transmitted light image can also be obtained which is completely in register with the confocal fluorescence image.

3.2.3.2. Image analysis

Images were acquired using TIMECOURSE software (BioRad) and CG-1 and TR signals were ratioed using TIMECOURSE (BioRad). KALCIUM ANALYSE (Kinetic Imaging, Liverpool, UK) software was used to quantify fluorescence in determined areas of the zygote (apical, subapical, perinuclear). Cell volume changes were analysed using transmitted light images obtained simultaneously with CG-1/TR fluorescent images using the KONTRON 300 Image Analysis Package (Zeiss, Germany). Representative images/graphs for each of the experiments are shown.

3.2.4. Intracellular ROS measurements

ROS production was monitored as oxidation of 5-(and-6-)-chloromethyl-2′,7′dichlorodihydrofluorescein diacetate (CM-DCFH$_2$-DA, Molecular Probes). Different dye loading protocols were used to visualize preferentially either early peripheral cytosolic ROS production or longer-term mitochondrial production. For

visualisation of early ROS increases in both the cytosol and mitochondria, embryos were incubated in 100 μM CM-$DCFH_2$-DA in 1% ethanol for 20 min. Dye was retained in the experimental solution throughout the experiment. For preferential visualization of mitochondrial ROS production, cells were washed in seawater for 20 min prior to experiments. This removed dye from the cytosol, but not from the mitochondrial compartment. Confocal images were obtained following excitation at 488 nm and emission monitored at 522 nm. Because CM-$DCFH_2$-DA is a non-ratiometric dye, changes in fluorescence due to decrease in cell volume during hyper-osmotic shock were accounted for by simultaneously monitoring the fluorescence of microinjected Texas Red dextran (see above). One representative image/graph for each experiment is shown.

To estimate intracellular ROS production in non-stressed cells and during hyper-osmotic shock, an *in vivo* calibration protocol was used. First, an *in vitro* calibration curve of fluorescence of droplets of CM-$DCFH_2$ (chemically hydrolyzed from CM-$DCFH_2$-DA as indicated by the manufacturer) mixed with known concentrations of H_2O_2 (calibration curve A, not shown) was constructed together with an *in vitro* calibration curve of fluorescence of droplets of various known concentrations of Texas Red (calibration curve B, not shown). Rhizoid cells were injected with equal proportions of Texas Red-dextran and CM-$DCFH_2$-DA. The average cellular fluorescence of each dye was monitored before and after hyper-osmotic shock treatment. The concentration of Texas Red, and thus concentration of DCFH was determined from calibration curve B. Using calibration curve A, the intracellular total ROS production that gave rise to the observed fluorescence was calculated.

3.2.5. Mitochondria localisation

Mitochondria were localised following incubation with 0.1 μM MitoTracker Red for 30 min or 0.2 μM MitoTracker Green for 1 h 30 min. Mitochondrial membrane potential was monitored using the lipophilic cationic probe tetramethylrhodamine ester (TMRE, 0.1 μM for 5 min, Molecular Probes). Each dye was dissolved in 0.1% DMSO in filtered seawater.

TMRE enters mitochondria in a membrane potential ($\Delta\Psi_m$)-dependent manner. Mitochondrial accumulation of TMRE has been shown to cause quenching of fluorescence, whereas mitochondrial depolarisation induces TMRE release from mitochondria and a consequent increase in average cellular fluorescence (Boitier et al., 1999; Zimmermann, 2000; Duchen, 2000). Changes in TMRE fluorescence have thus been used to monitor mitochondrial membrane potential changes in animal systems (Zimmerman, 2000; Duchen 2000), and changes in mitochondrial membrane potential are thought to reflect Ca^{2+} movements across the membrane of the organelle (Duchen et al., 1998). TMRE fluorescence was monitored with the confocal microscope at 568 nm excitation and 605 nm emission. Cells loaded simultaneously with CM-DCFH$_2$-DA and MitoTracker Red or with X-rhod-FF (see below) and MitoTracker Green were scanned at 488/568 nm (excitation wavelengths) and 522/605 nm (emission wavelengths).

3.2.6. Inhibitors

The mitochondrial uncoupler carbonylcyanide p-trifluoromethoxyphenyl-hydrazone (FCCP, Sigma, Poole, UK) was dissolved in 0.1% DMSO and filtered seawater (final

concentration 1 μM). The NADPH oxidase inhibitor diphenyleneiodonium (DPI, Sigma) was dissolved in 0.1% DMSO to a final concentration of 10 μM in filtered seawater. Cells were exposed to inhibitors for 1 h before the beginning of the experiment, and inhibitors were also included in the perfusing solutions. The PLC inhibitor U73122 or its inactive analogue U73343 were dissolved in 0.1% DMSO and filtered seawater (final concentration 10 μM), and cells were pre-incubated for 2 h. Catalase (Sigma) was used at a concentration of 450 units/ml.

3.2.7. Mitochondrial Ca^{2+}

X-rhod-FF (Molecular Probes) was used to monitor mitochondrial Ca^{2+} changes. X-Rhod-FF is a lower-affinity Ca^{2+} indicator fluorinated analogue of Rhod-2. Its Ca^{2+} dissociation constant (Kd) is 17 μM compared with 0.60 μM for rhod-2. Mitochondria have high capacity for Ca^{2+} uptake (Rizutto et al., 2000) and therefore require low affinity Ca^{2+} indicators to accurately measure Ca^{2+} changes. A cell-permeant AM ester form was used. X-rhod-FF has a net positive charge, which facilitates its sequestration inside mitochondria due to potential-driven uptake. Cells were loaded with 2 μM X-rhod-FF AM (0.1% DMSO) for 1.5 h. The residual extracellular and cytosolic dye was eliminated by washing in seawater for 2 h. The mitochondrial localization of the dye was checked by co-loading the cells with MitoTracker Green. Channel cross-contamination was also accounted for. Confocal images of X-rhod-FF fluorescence were obtained at 568 nm (excitation) and 605 nm emission.

3.2.8. Ins(1,4,5)P_3 photorelease

Flash photolysis of photoactivable or "caged" compounds provides a means of controlling the release - both spatially and temporally - of biologically active products or other reagents of interest. Rhizoid cells were microinjected with caged Ins(1,4,5)P_3 (Calbiochem, Nottingham, UK), final intracellular concentration 10-50 μM, and a mixture of Calcium Green and Texas Red dextran as described above. To monitor ROS production, cells were injected with Ins(1,4,5)P_3 and Texas Red dextran (final intracellular concentration 10-50 μM), and then incubated with CM-DCFH_2-DA as described above. Photorelease was achieved with a pulsed nitrogen UV laser (10 ns pulses, 20 Hz for 1 s; VSL337, Laser Science, Cambridge, USA) delivered via the microscope objective and focused to an adjustable spot via a beam expander and adjustable focusing lens (Goddard et al., 2000). Laser intensity was adjusted with a diaphragm in the delivery optics to a level that caused photorelease of Ins(1,4,5)P_3 but did not by itself induce an oxidative burst. Control cells were microinjected only with Texas Red-dextran, loaded with CM-DCFH_2-DA and exposed to identical laser excitation.

3.2.9. Patch clamping

3.2.9.1. Laser microsurgery

In *Fucus*, removal of the cell wall to obtain access to the plasma membrane can be obtained by enzyme digestion (Kloareg and Quatrano, 1987). However, this is potentially damaging and polarity is lost. To overcome these problems, a technique has been developed whereby a small section of the cell wall is removed using a fine-

focused pulsed nitrogen laser (Taylor and Brownlee, 1992). The laser is focused to a small spot by the objective. Small plasma membrane-bound sub-protoplasts can be obtained by gentle mechanical pressure on the thallus cell (Figure 3.3, 3.4), and GΩ seals for patch clamp experiments can be obtained on the freshly released protoplast. Laser derived protoplasts (spheroplasts) from the *Fucus* rhizoid have previously been shown to be amenable to the patch clamp technique allowing the characterisation of ion channels in the rhizoid plasma membrane (Taylor and Brownlee, 1992; Taylor et al., 1996).

Zygotes were plasmolysed with artificial SW + 0.5-1 M sorbitol until the plasma membrane could be seen visibly shrinking from the cell wall at the rhizoid apex. Only zygotes firmly attached to the coverslip base of the laser chamber were chosen for laser microsurgery.

A pulsed nitrogen UV laser (VSL 337 Laser Science Inc., Cambridge, MA, USA) was coupled to an inverted Nikon Diaphot microscope (Nikon, Tokyo, Japan) via the epifluorescence port with beam expanding optics (Spindler and Hoyer, Gottingen, Germany); Figure 3.3). The laser beam was introduced into the microscope via a dichroic mirror (No. 400DCLPO2, Omega Optical, Brattleboro, VT, USA) in the microscope filter cassette so that the beam filled the back focal plane of a x40 microscope objective (Nikon UV-fluor x40 numerial aperture 1.3). The UV beam was focused to a spot <1 μm in adjusting the distance between the plano-concave and the plano-convex lenses of the beam expander. When pulsed, the laser could be seen etching the upper surface of the glass coverslip. Cells were viewed with a CCD camera (TK-1280E, JVC, Japan) attached to the microscope. The location of the fixed laser

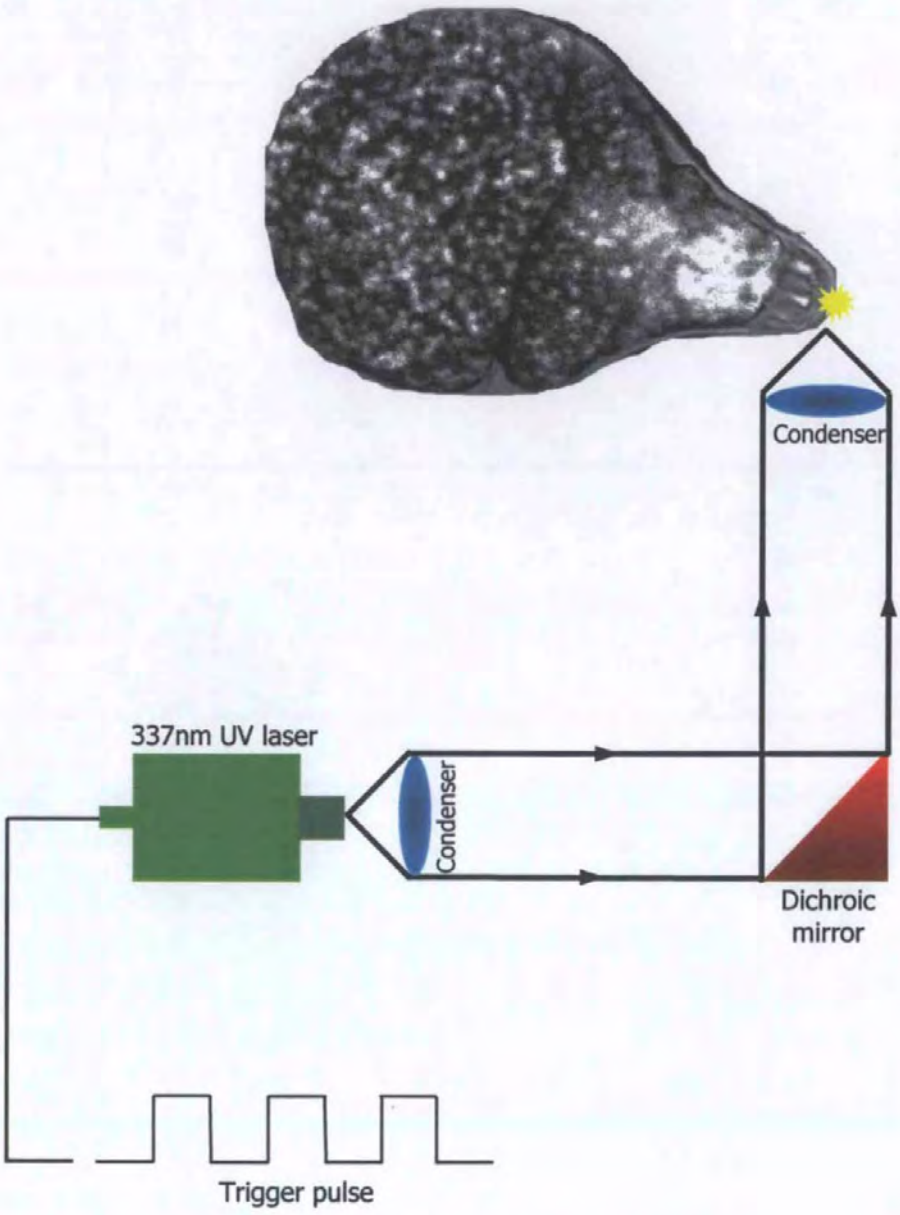

Figure 3.3. Diagram of laser microsurgery equipment. 2-cell *Fucus* zygotes are plasmolysed with 0.5-1 M sorbitol in seawater. The cell wall is cut using a finely focused 377 nm UV laser beam.

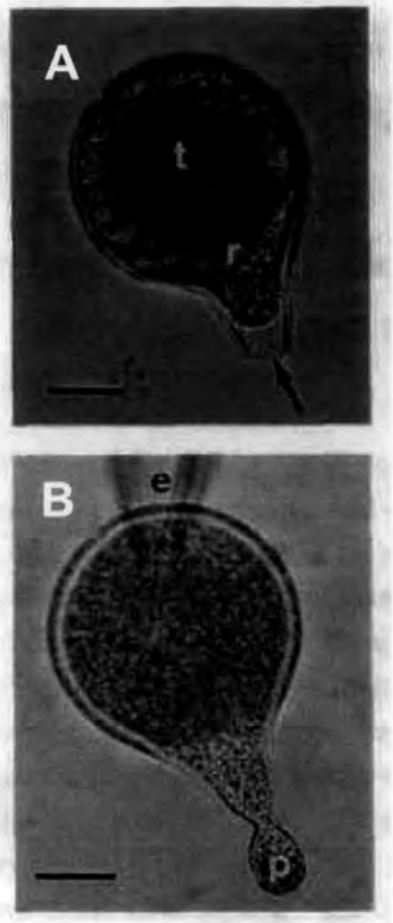

Figure 3.4. Laser ablation of *Fucus* cell wall. A - 24h-old *Fucus* zygote with thallus (t) and rhizoid (r) cells after plasmolysis in ASW plus 0.5 M sorbitol. **B** - After cell wall ablation with the UV laser beam, application of gentle mechanical pressure to the thallus cell causes a small plasma membrane bound protoplast to emerge from the hole, where patch clamp experiments can be performed. p = protoplast; e = electrode.

beam was determined by etching a hole in the upper surface of the glass coverslip and marking the position on the TV monitor (VM-14PSN(G), JVC, Japan). The plasmolysed *Fucus* zygote was then moved into the fixed laser beam by manipulation of the microscope stage. The laser was triggered remotely by a 12 V stimulator at a frequency of 20 Hz. Typical pulse energy = 200 μJ with a pulse duration of 10 ns. Cell wall perforation on average took 2-4 min. Once a clear hole could be visualised on the cell wall, mechanical pressure with a patch pipette on the thallus cell was used to control the extrusion of the protoplast (Figure 3.4). Protoplasts that did not show smooth plasma membrane-bound cytoplasm were discarded.

3.2.9.2. Patch clamping

Cell-attached recordings were obtained from apical protoplasts by using conventional patch clamp techniques (Taylor et al., 1996). The reference electrode consisted of an Ag/AgCl pellet in a holder containing seawater and was connected to the bath via a 3% agar bridge made up with artificial seawater. Patch pipettes were fabricated from borosilicate glass (GC150TF, Clark, Pangbourne, UK) with a Narishige pipette puller (P-833; Narishige, Tokyo, Japan). Electrodes were briefly dipped in 0.001% poly-lysine solution (Sigma) before back filling with ultra-filtered pipette solution (30 mM $CaCl_2$ 30 mM KCl 10 mM Hepes pH 7.8). This simple treatment enhanced seal formation. Patch pipettes were connected via a pipette holder to the head stage of a patch clamp amplifier (Axopatch 1D, Axon Instruments Foster City, CA, USA). Slight positive pressure was applied to the pipette via a water-filled manometer until the pipette was observed to touch the protoplast. Occasionally, gentle suction (<0.5 kPa) was applied to promote seal formation. Seal formation was

monitored by applying a 30 ms 2mV square pulse at low headstage gain. After a high resistance seal (0.8 GΩ in average) was formed, the headstage gain was increased to resolve single channel currents. Bath solutions were exchanged (from filtered seawater to 1 mM H_2O_2 in filtered seawater and back to filtered seawater) through a gravity fed inflow and suction outflow using a peristaltic system. Single channel recordings were filtered at 2 kHz, digitised using a pulse code modulator (Medical Instruments) and stored on video tape. Analysis of data was conducted off-line by sampling at 6 kHz with an analogue-to-digital converter (Labmaster, Axon Instruments) driven by a personal computer and analysed with PCLAMP software (Axon Instruments). The probability of opening (P_{open}) at any voltage was determined using all points histogram (Bertl and Slayman, 1990) according to the formula

$$P_{open} = A_1 + 2A_2 \ldots + nA_n/n(A_0 + A_1 + \ldots A_n),$$

Where A_0 represents the area under baseline or the closed peak representing the total time that all channels are closed, and A_1, A_2 to A_n are the areas under the peaks for each open level.

All points histograms were constructed from representative segments of single channel data. All points histograms were filtered by Gaussian functions with the mean of each Gaussian peak representing the closed and subsequent open state.

Data presented are representative of 22 replicate experiments. Cell attached patches were used to construct I/V curves in order to calculate the channel conductance of the presumptive channel. Data were corrected for liquid junction potentials (LJP, Barry and Lynch, 1991) which were calculated using Pclamp8 LJP

calculation programme based on Barry and Lynch, 1991. LJP was found to be 10 mV for the present cell attached conditions, and was added to the membrane potential as Vm = Vcell - Vpipette + LJP.

3.2.10. Electron microscopy

To confirm the mitochondrial localization of Mitotracker, embryos labelled with Mitotracker Red or Mitotracker Green were fixed, embedded and sectioned for TEM as described previously (Brownlee and Pulsford, 1988), but without osmium post-fixation. Confocal fluorescence images of sections mounted on 3x1 mm slot grids (0.1-0.5 μm) were acquired and sections were subsequently exposed to osmium vapor from a drop of osmium tetroxide in a closed Petri dish. They were then stained in 4% methyl acetate and lead citrate and viewed with a Jeol 200 CX electron microscope. This allowed direct identification of fluorescent cellular structures.

3.3. RESULTS

3.3.1. Hyper-osmotic stress and ROS production at the rhizoid apex

The fluorescent probe CM-$DCFH_2$-DA was used to measure intracellular ROS production by *Fucus* embryos. Oxidation of $DCFH_2$ by reactive oxygen species yields the fluorescent DCF. Although the oxidizing agent is believed to be either $^{\bullet}OH$ or H_2O_2 (Zhu et al., 1994), it is assumed that the main ROS reported is H_2O_2 (Pei et al., 2000). In cells that were loaded with CM-$DCFH_2$-DA to visualise both early cytosolic and mitochondrial ROS production (see Material and Methods), hyper-osmotic treatment (transfer from seawater to seawater + 2 M sorbitol) induced a fast (within a

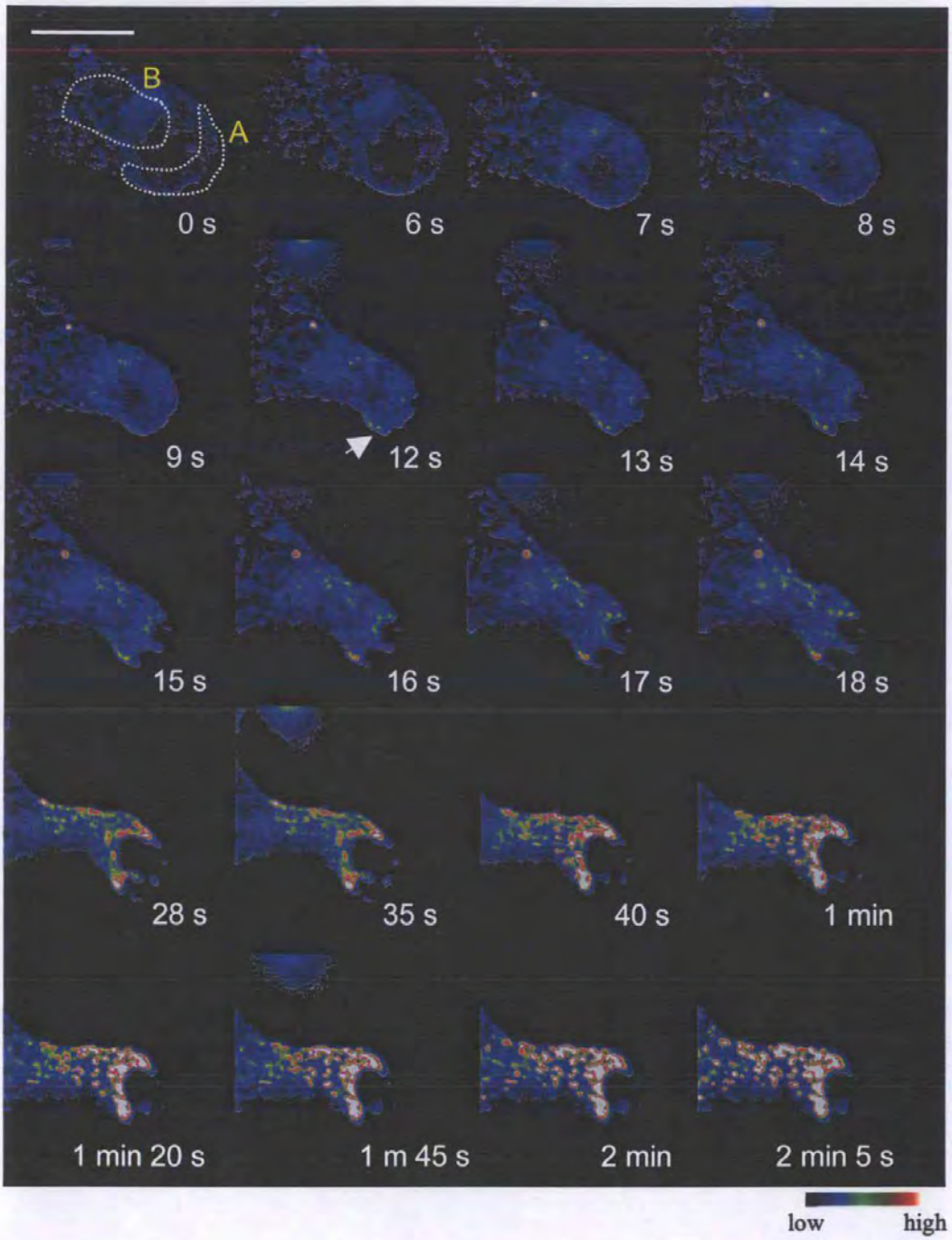

Figure 3.5. Time course of intracellular ROS production during hyper-osmotic treatment. Early peripheral ROS production is obvious at the rhizoid apex during hyper-osmotic shock (transfer from SW to SW + 2 M sorbitol). ROS production initiates at plasma membrane-wall adhesion sites (arrow). Cells were incubated for 20 min in 100 µM CM-DCFH$_2$-DA, immediately followed by hyper-osmotic treatment. Bar = 20 µm. *A* = peripheral region; *B* = sub-apical region. Bar = 30 µm.

few seconds) peripheral production of ROS at the rhizoid cell apex, particularly noticeable at sites of membrane-cell wall adhesions (Figure 3.5, n=10). After approx. 40 s ROS production was also detectable in more discrete areas in sub-apical cellular regions, becoming more evident after 120 s. The time course of the ROS production clearly showed an earlier onset in the peripheral region compared with the sub-apical region (Figure 3.6).

3.3.2. Hyper-osmotic stress and transient Ca^{2+}_{cyt} elevation

Hyper-osmotic treatment induced a transient cytosolic Ca^{2+} (Ca^{2+}_{cyt}) elevation in rhizoid cells within 10-12 s, coincident with a reduction in cell volume (Figure 3.7, 3.8; n=10). This Ca^{2+}_{cyt} transient reached peak average cellular levels of 483 $\pm$ 45.2 nM within 10 s of the onset of the Ca^{2+} elevation before returning to resting levels over the following 24-40 s. Confocal ratio images revealed that the hyper-osmotically-induced Ca^{2+} transient initiated at a discrete location in the rhizoid apex, where the plasma membrane remained attached to the cell wall during cytoplasmatic shrinkage, and propagated through the cell as a unidirectional wave with an estimated velocity of 15 $\mu m.s^{-1}$, reaching peak levels of at least 1 μM (Figure 3.7). Smaller excursions in resting Ca^{2+} were also occasionally observed, occurring either spontaneously or in response to return to seawater following hyper-osmotic treatment. In Figure 3.8 these are apparent as a small decrease from 100 nM to 50 nM Ca^{2+}_{cyt} at the beginning of the trace and small transient increases following return to seawater. These small changes in resting Ca^{2+} were probably related to growth or turgor regulation (Taylor et al., 1996).

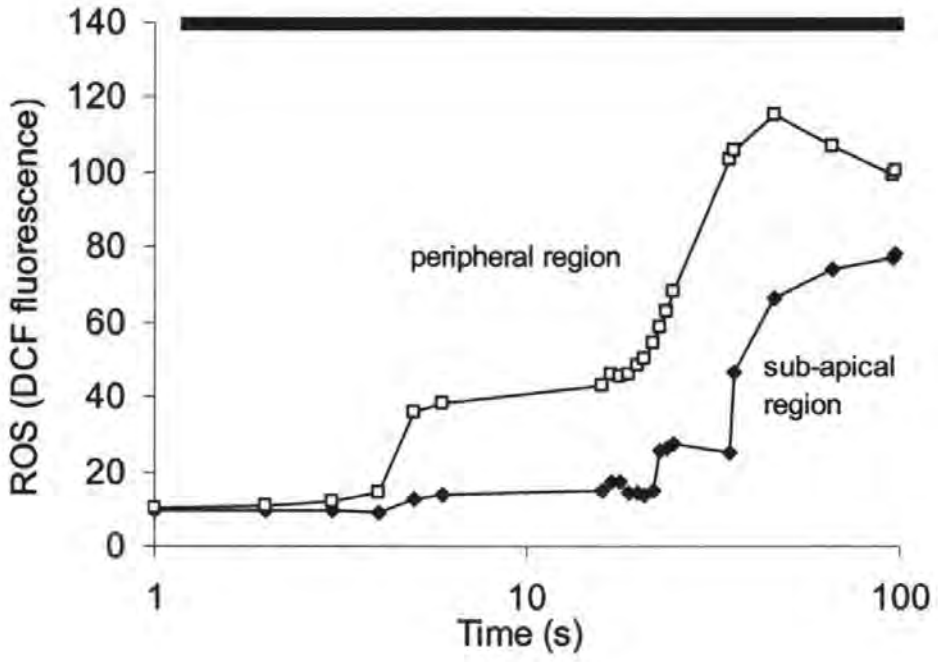

Figure 3.6. Time course of DCF fluorescence in peripheral and sub-apical regions following hyper-osmotic shock. This graph is representative of the cell shown in Figure 3.5, showing clear temporal separation of the onset of ROS production in each region. Peripheral and subapical region correspond to A and B, respectively, in Figure 3.5. Black bar represents hyper-osmotic treatment.

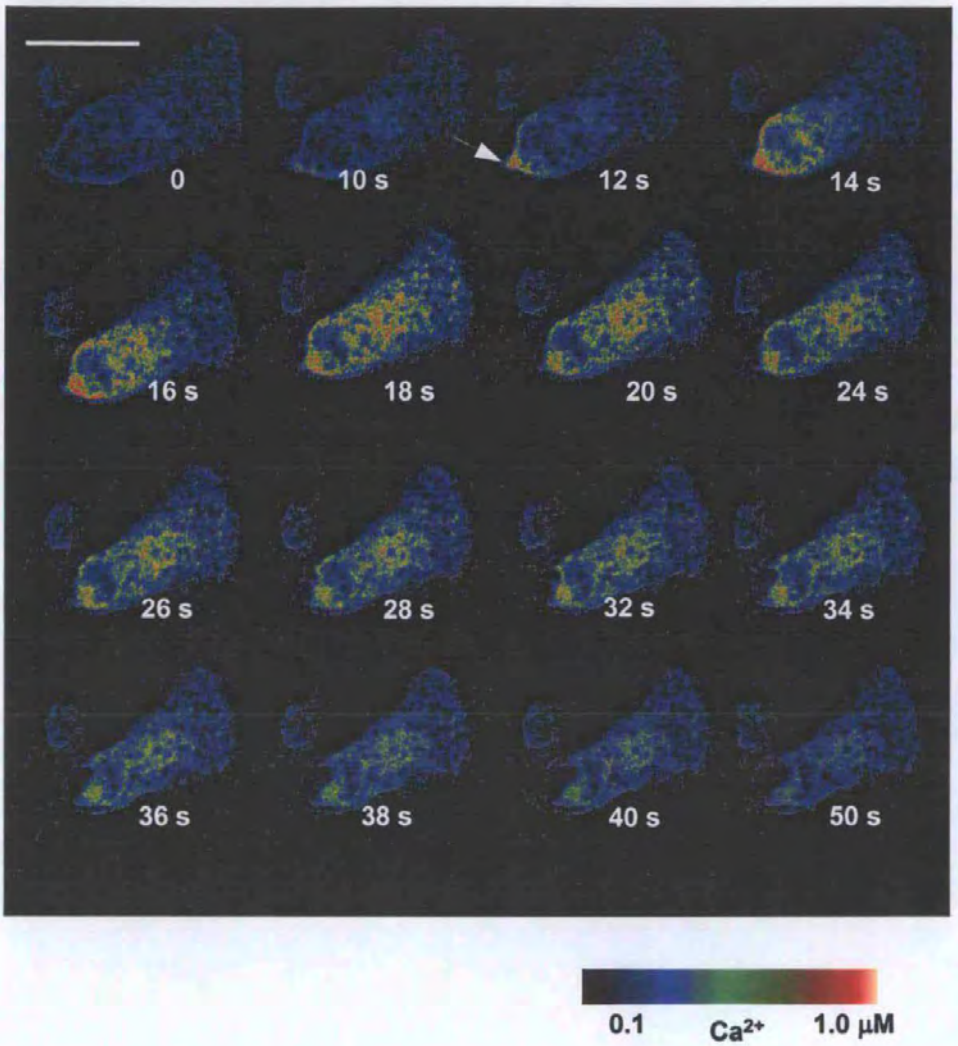

Figure 3.7. Confocal ratio images of a Ca^{2+}_{cyt} wave in response to hyper-osmotic treatment. Ca^{2+}_{cyt} elevation initiates from a point where the plasma membrane remains attached to the cell wall (arrow). Bar = 30 µm.

3.3.3. Hyper-osmotic stress and ROS production in discrete cellular compartments

Hyper-osmotic treatment also elicited an increase in ROS production in discrete intracellular compartments, monitored by DCF fluorescence in cells pre-incubated for 20 min in CM-$DCFH_2$-DA and subsequently washed for 20 min (see material and methods section). ROS started to increase within 120 s after hyper-osmotic treatment (Figure 3.9, n=25), followed by a more rapid production after 800 s and reaching a plateau after approximately 20 min. Although the time to onset of this component of intracellular ROS production varied from 40-120 s, this always occurred after the peak, i.e., downstream of, the hyper-osmotically-induced Ca^{2+} elevation and the rapid peripheral ROS production. By direct microinjection of CM-$DCFH_2$-DA into cells we were able to estimate the average cellular production of ROS during hyper-osmotic treatment to be equivalent to approximately 0.05 mmoles of H_2O_2 per liter of cell volume per minute.

3.3.4. Localisation of the oxidative burst

Embryos that were co-labeled with the fluorescent mitochondrial probe MitoTracker Red and CM-$DCFH_2$-DA showed a clear localization of ROS production to mitochondria but not to chloroplasts (Figure 3.10 A, n=7). TEM and confocal fluorescence images of identical sections labelled with Mitotracker Red confirmed, within the limits of resolution, the mitochondrial localization of the Mitotracker dye (Figure 3.10 B). This revealed discrete regions of dye fluorescence corresponding to groups of mitochondria. While the mitochondria were not all equally labelled with

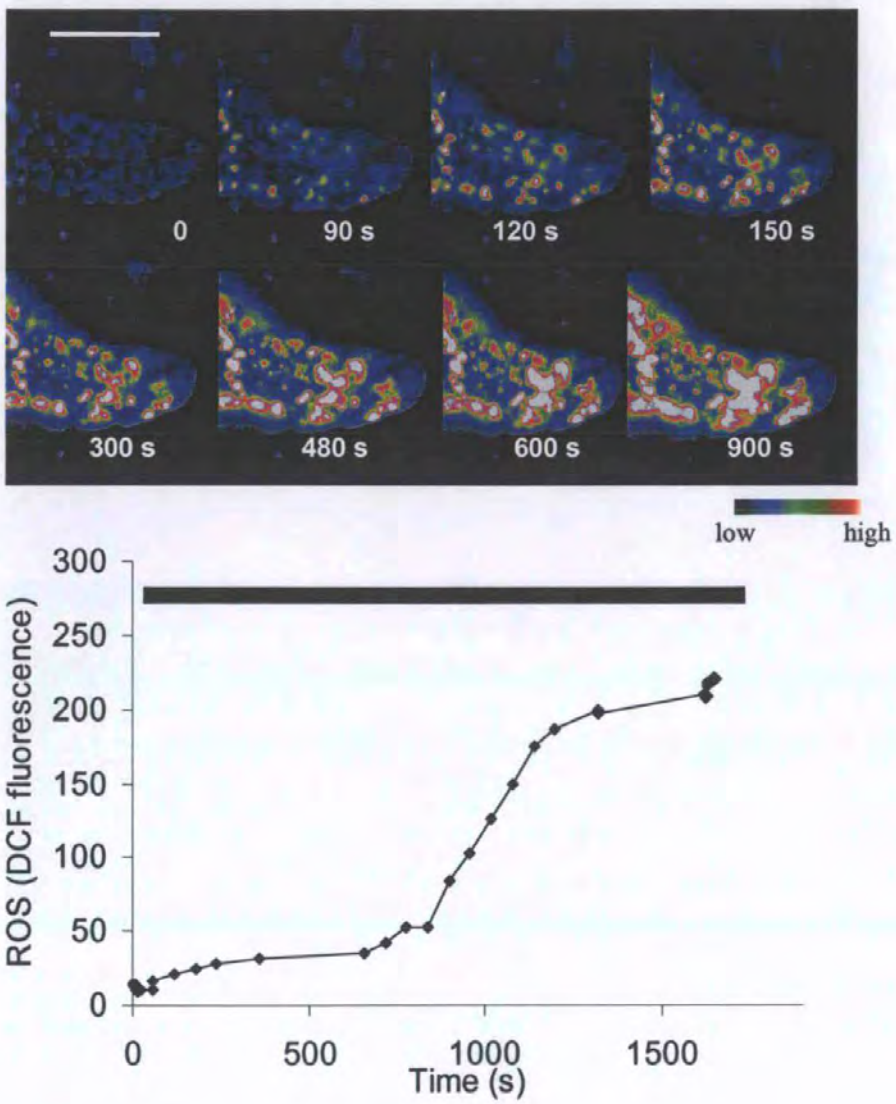

Figure 3.9. Intracellular ROS production A) Discrete localised intracellular ROS production during perfusion with hyper-osmotic solution (seawater + sorbitol 2 M). Cells were incubated for 20 min in 100 μM CM-$DCFH_2$-DA, followed by washing in seawater for 20 min prior to hyper-osmotic treatment. Bar = 20μm. **B)** Time course of average cellular ROS production during hyper-osmotic treatment.

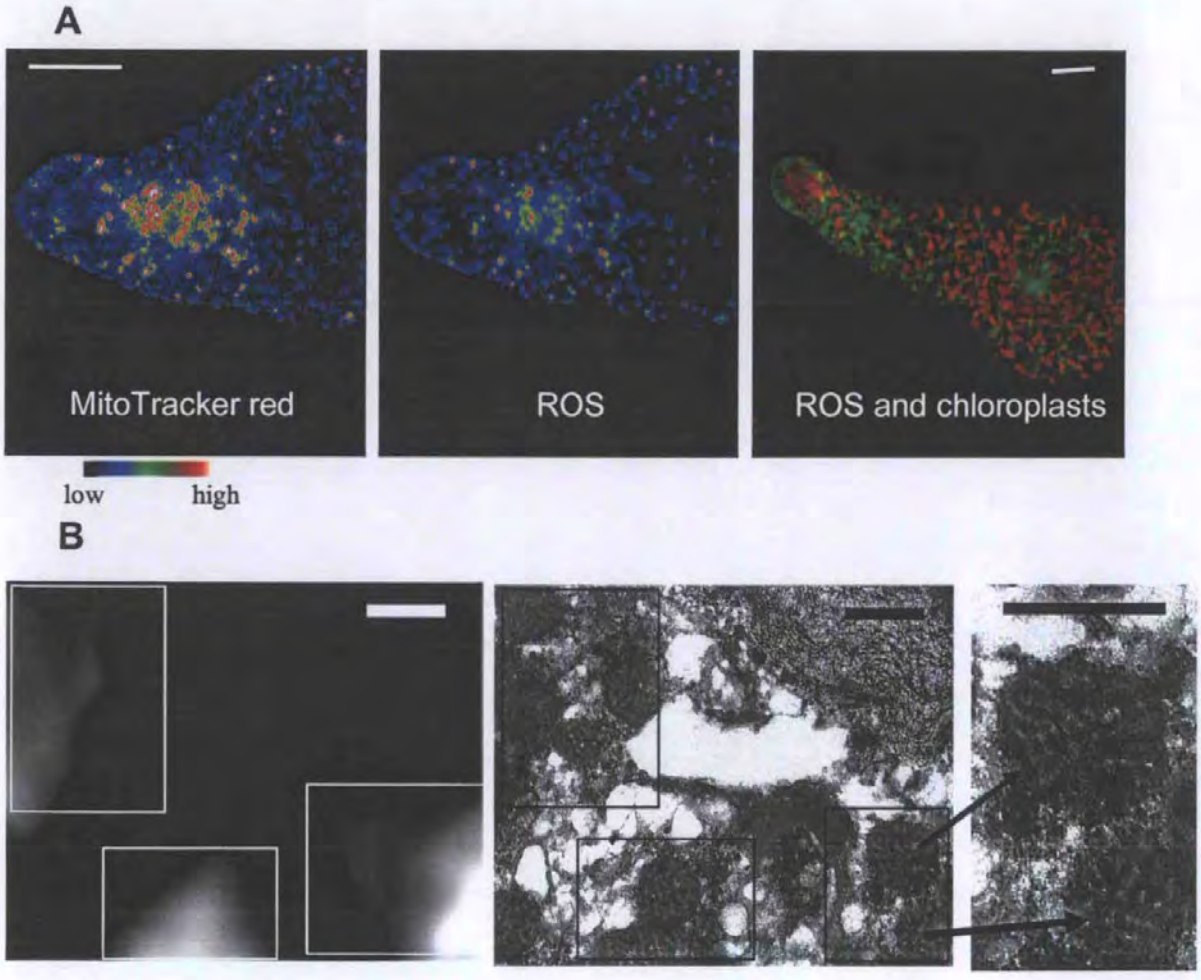

Figure 3.10. Intracellular localisation of ROS production. A) Co-localization of Mitotracker Red (left) and ROS production (centre). Cells were co-loaded with MitoTracker Red and CM-DCFH$_2$-DA. Right panel shows separate localization of chloroplasts (chlorophyll autofluorescence; red) and ROS production (green). Bar = 20 μm. **B)** Co-localization of Mitotracker red fluorescence (left) and mitochondria (TEM: right) in identical fixed sections. Bar = 1 μm. The mitochondrial cristae are clearly visible in the enlarged TEM view (right).

Mitotracker, dye fluorescence was not found in any other cell compartments. Dissipation of the mitochondrial proton-motive force with 1 μM FCCP completely abolished the hyper-osmotic shock-induced mitochondrial ROS production (Figure 3.11, n=5). This inhibition was reversible (not shown), suggesting a specific mitochondrial uncoupling and not a general cytotoxic effect.

3.3.5. Mitochondrial depolarisation and Ca^{2+}_m elevation

Monitoring fluorescence of tetramethyl rhodamine ester (TMRE) as an indicator of mitochondrial membrane potential ($\Delta\psi_m$) suggested the occurrence of mitochondrial depolarisation during hyper-osmotic shock (Figure 3.12, n=4), the time course of which was similar to that of the corresponding transient Ca^{2+}_{cyt} elevation. The mitochondrial Ca^{2+} reporter dye X-rhod-FF co-localized with MitoTracker Green in dual labelling experiments (Figure 3.13), allowing changes in mitochondrial Ca^{2+} (Ca^{2+}_m) to be monitored. An increase in Ca^{2+}_m was apparent approximately 20 s after hyper-osmotic treatment (Figure 3.13 A, B, n=15), i.e. closely following the peak of the Ca^{2+}_{cyt} transient.

3.3.6. Interdependence of Ca^{2+} and ROS production

3.3.6.1. Ca^{2+} dependence of ROS production

In order to determine whether Ca^{2+}_{cyt} elevation is essential for the mitochondrial ROS production, the Ca^{2+} chelator Br_2BAPTA was injected into the rhizoid cell. Br_2BAPTA has been shown to prevent osmotically-induced Ca^{2+} signals in *Fucus* rhizoids (Taylor et al., 1996). Br_2BAPTA abolished the hyper-osmotically-induced

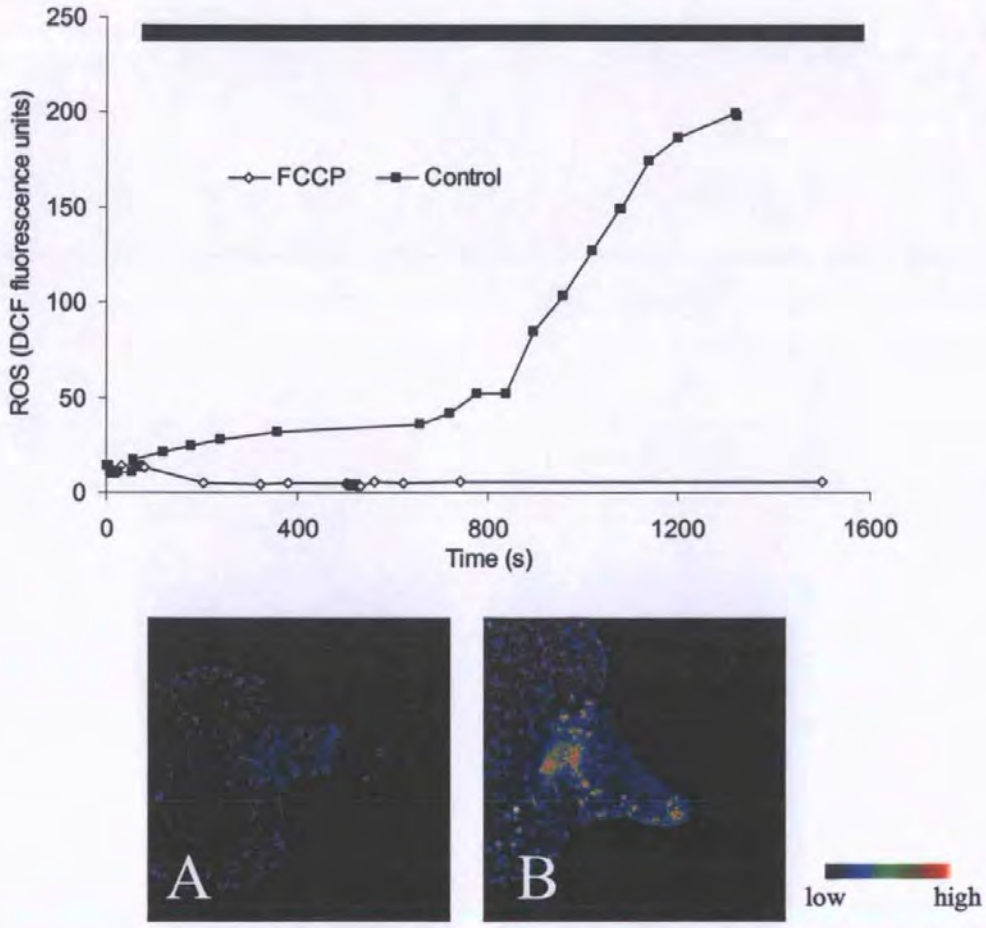

Figure 3.11. Effect of FCCP on hyper-osmotic-induced oxidative burst. Incubation in FCCP (1 μM, 1h pre-incubation) caused a complete inhibition of ROS production. Black bar indicates incubation in hyper-osmotic solution (in the presence of the inhibitor). **A)** Embryo submitted to hyper-osmotic stress in the presence of FCCP. **B)** Reversibility of the FCCP effect: FCCP was washed out and 1.5 h after cells were able to respond to hyper-osmotic shock with ROS production.

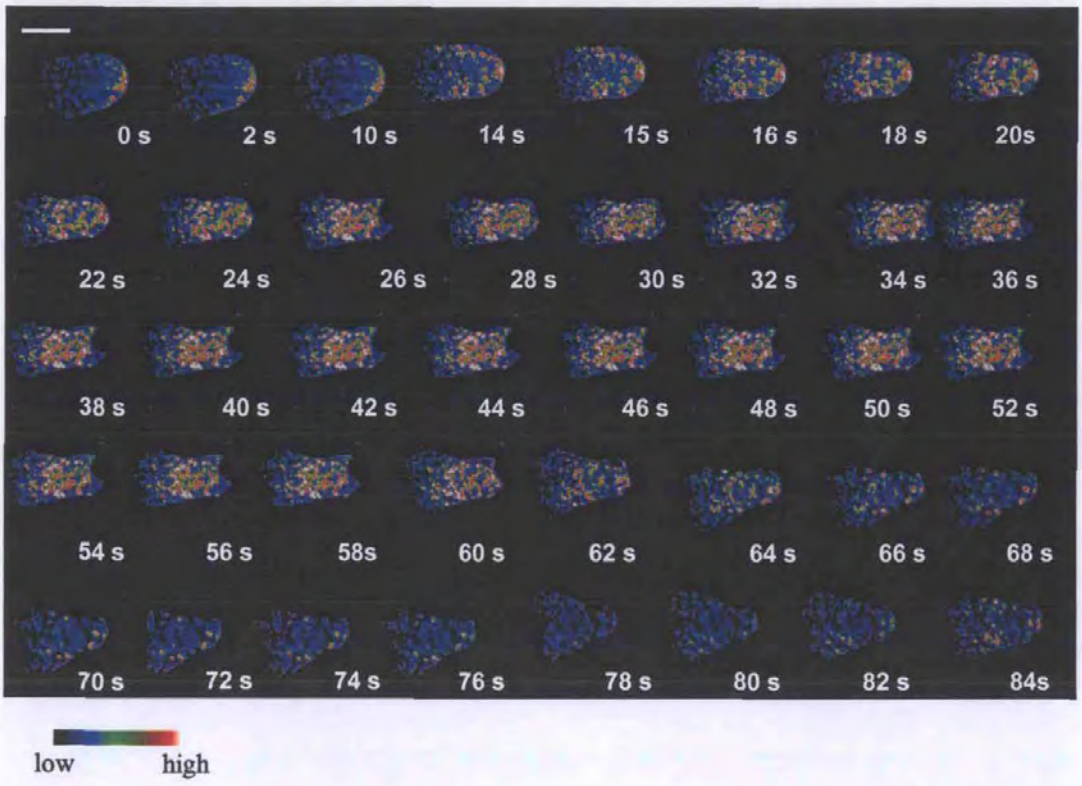

Figure 3.12. Mitochondrial changes in membrane potential during hyper-osmotic stress. Hyper-osmotic shock-induced depolarisation of the mitochondrial membrane potential ($\Delta\psi_m$) monitored by TMRE fluorescence. Bar = 30 μm.

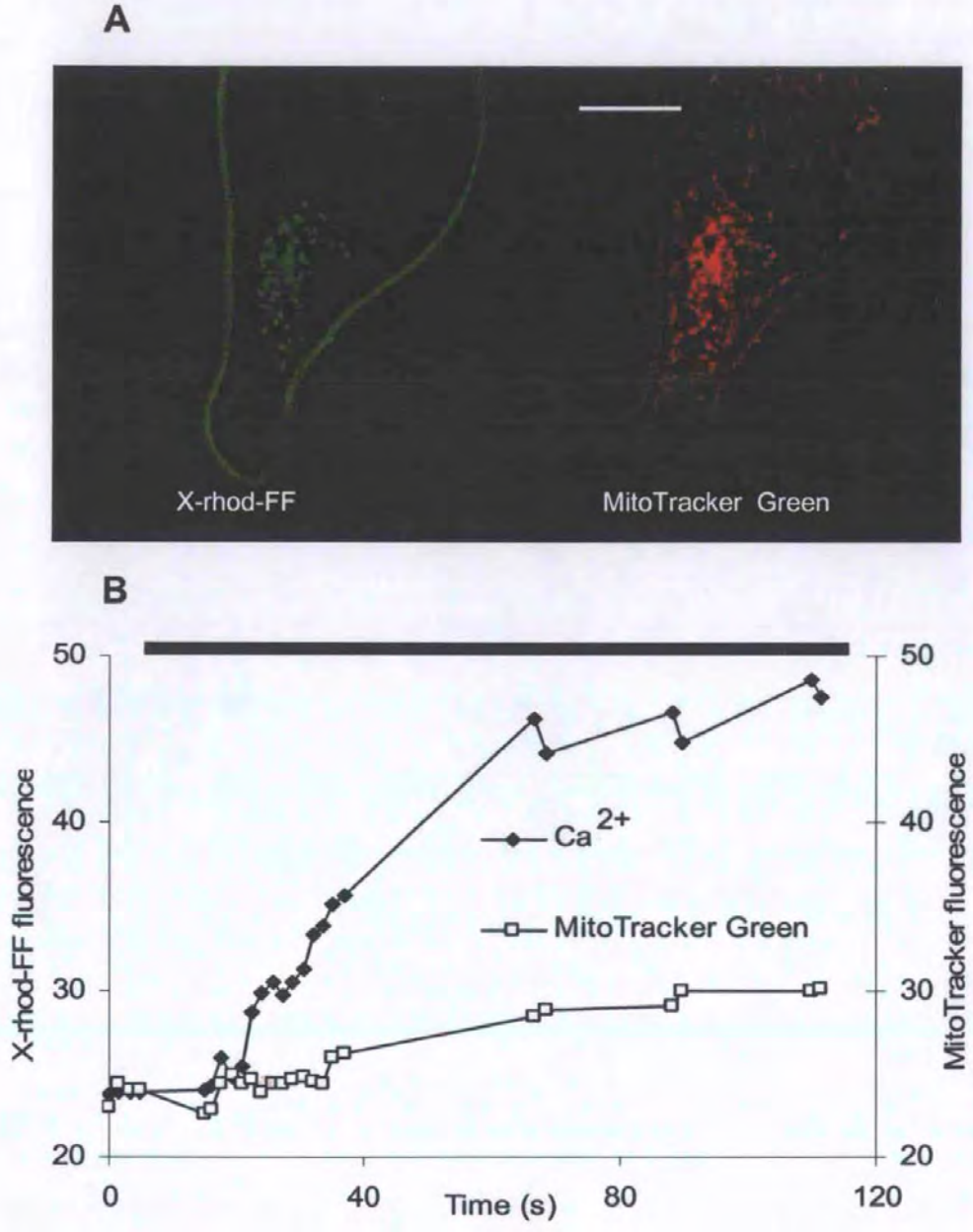

Figure 3.13. Mitochondrial Ca^{2+} dynamics during hyper-osmotic treatment. A) Co-localization of X-rhod-FF and MitoTracker Green in mitochondria. Bar = 30 μm. **B)** Mitochondrial Ca^{2+} elevation during hyper-osmotic treatment measured with X-rhod-FF. Dual labeling with MitoTracker Green allowed Ca^{2+}-independent fluorescence to be monitored. Average X-rhod-FF or MitoTracker Green fluorescence values were plotted from the peri-nuclear mitochondrial rich region. Black bar indicates hyper-osmotic treatment.

mitochondrial ROS production in the injected rhizoid cell but not in the adjacent non-Br_2BAPTA injected thallus cell (Figure 3.14, n=7). Thus, Ca^{2+}_{cyt} elevation is a necessary step for the mitochondrial ROS production.

The time course of early peripheral ROS production at the rhizoid apex was similar to that of the onset of Ca^{2+}_{cyt} elevation being detectable within a few seconds of hyper-osmotic treatment. Unlike mitochondrial ROS elevation, early peripheral ROS elevation was not inhibited in Br_2BAPTA-injected cells (Figure 3.15 A, n=12), indicating that it occurred independently or upstream of the Ca^{2+}_{cyt} wave. The phospholipase C (PLC) inhibitor U73122 blocked the hyper-osmotically-induced Ca^{2+} wave (Figure 3.16) and the mitochondrial ROS elevation (Figure 3.17) but did not block the peripheral ROS production (Figure 3.15 B, n=7). Interestingly, a prolonged elevation of ROS was observed in the rhizoid apex in the presence of U73122 (Figure 3.15 B). This contrasts with the more transient elevation of ROS in the rhizoid apex in Br_2BAPTA-buffered cells and may reflect the inability of U73122 to block a highly localised plasma membrane influx component of Ca^{2+} elevation leading to elevation of ROS in mitochondria near the cell apex. The inactive analog of U73122 (U73343) had no effect on ROS production (Figure 3.15 B).

3.3.6.2. Dependence of Ca^{2+} elevation on ROS production

The NADPH oxidase and peroxidase inhibitor diphenyleneiodonium (DPI) (Pugin et al., 1997; Frahry and Schopfer, 1998; Pei et al., 2000) brought about a complete inhibition of both peripheral and mitochondrial ROS elevation and abolished the Ca^{2+}_{cyt} wave (Figure 3.16 and 3.17, n=8). This raises the likelihood that the peripheral

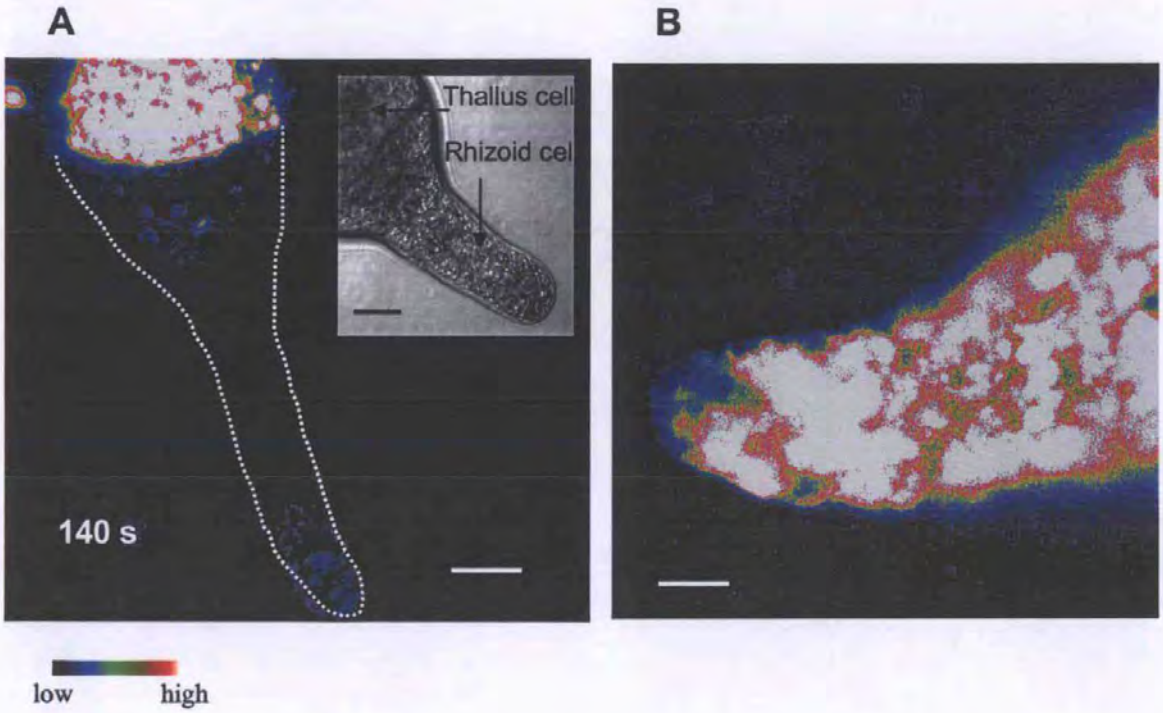

Figure 3.14. Interdependence between Ca^{2+}_{cyt} and ROS production. A) Injection of Br_2BAPTA (4 mM final intracellular concentration) into the rhizoid cell inhibited mitochondrial ROS production (monitored 140 s following hyper-osmotic treatment) in cells loaded for 20 min with CM-$DCFH_2$-DA but not in the adjacent non-injected thallus cell. Dotted line indicates the rhizoid cell. Bar = 30μm. **B)** Control cell, not Br_2BAPTA injected, showing a mitochondrial oxidative burst. Bar = 20μm.

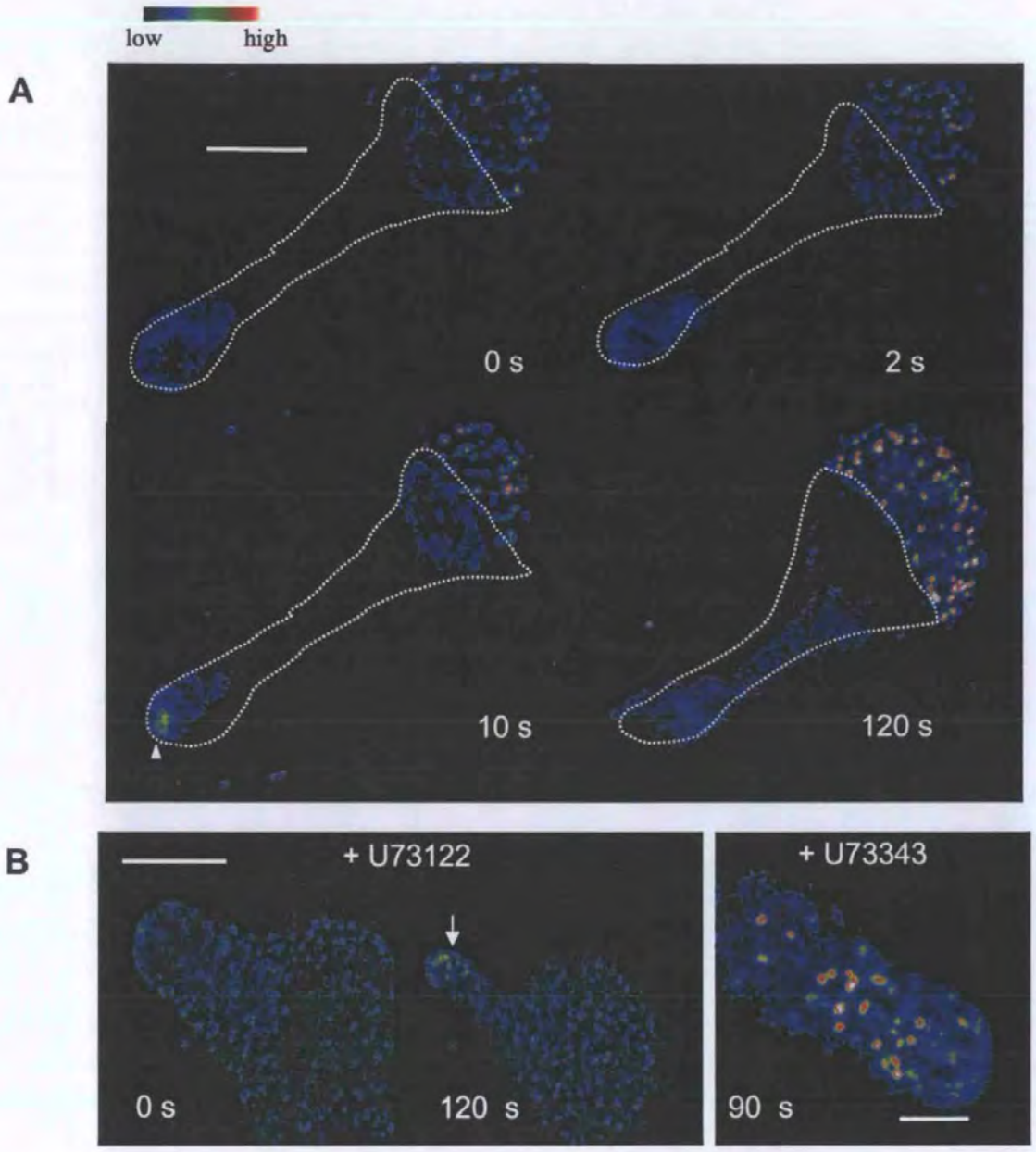

Figure 3.15. Interdependence between Ca^{2+}_{cyt} and ROS production A) Br_2BAPTA injection into the rhizoid cell did not prevent the early peripheral hyper-osmotically-induced ROS production (arrow). In the cell shown ROS production is apparent at the rhizoid apex at 2 and 10 s but declines to pre-treatment levels after 120 s. Bar = 40 μm. **B)** The PLC inhibitor U73122 inhibited the mitochondrial but not the peripheral hyper-osmotically-induced ROS production (left and middle sections). Cells were pre-incubated with U73122 for 2 h and the inhibitor was retained in the hyper-osmotic solution. The inactive analogue U73343 did not prevent mitochondrial ROS elevation (right section). Bar = 30 μm.

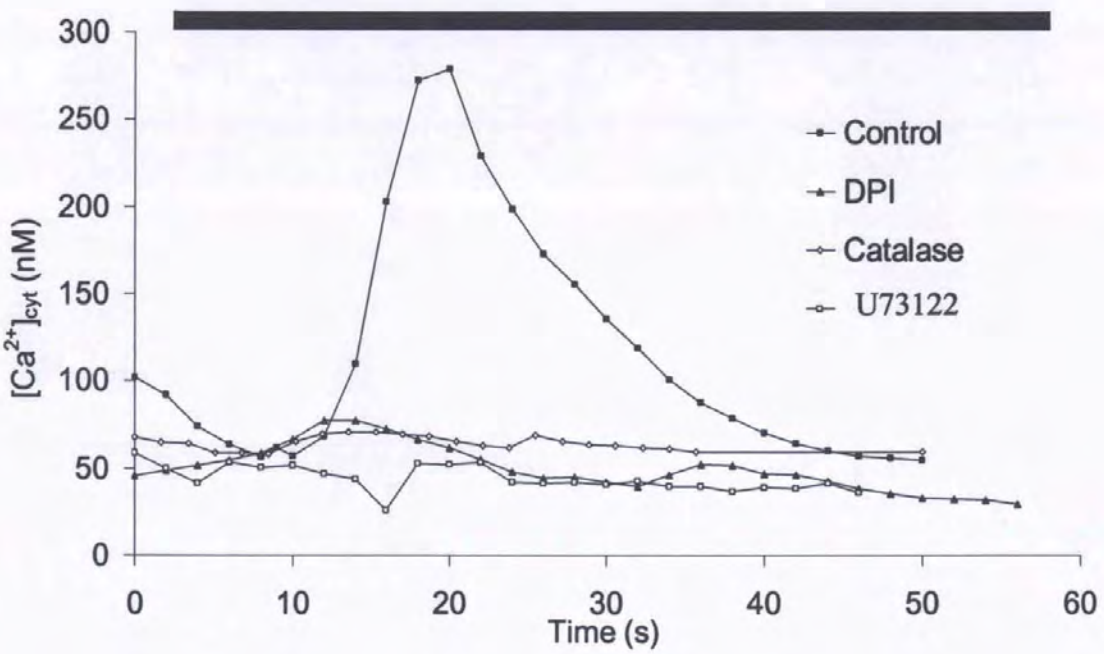

Figure 3.16. Effect of DPI, catalase and U73122 on hyper-osmotically-induced Ca^{2+}_{cyt} elevation in rhizoid cells. Calcium Green/Texas Red ratio values were averaged for the whole rhizoid cell. Bar indicates hyper-osmotic perfusion.

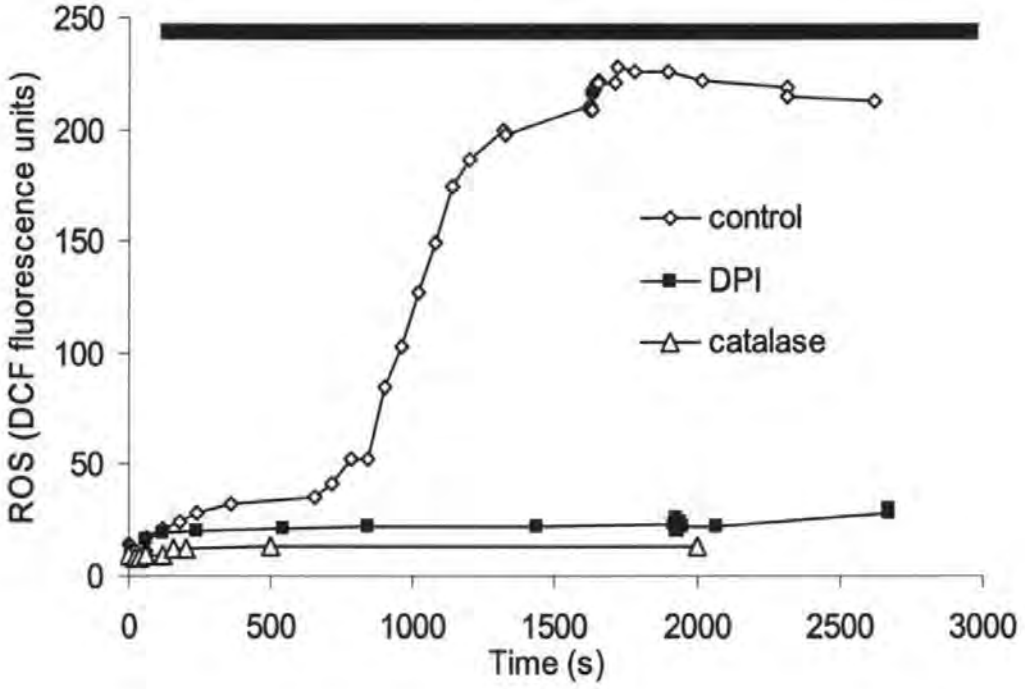

Figure 3.17. Effect of DPI and catalase on ROS production. DPI and externally applied catalase completely inhibited ROS production during hyper-osmotic shock. Cells were pre-incubated for 1 h in 10 μM DPI and for 30 min in 450 units/ml catalase and the inhibitors were retained in the perfusing hyper-osmotic solution. Bar indicates hyper-osmotic perfusion.

ROS elevation resulted from extracellular production of ROS following the activity of plasma membrane-associated NADPH oxidase, leading to diffusion of H_2O_2 into the cell. Interestingly, experiments showed that DPI decreases Ca^{2+}_{cyt} resting level from values of 81.3±3.0 nM before to 53.1±6.3 nM after incubation in DPI (n=5). The critical role of extracellular ROS production in initiating this cascade is further strongly supported by the dramatic inhibition of both the intracellular ROS production (n=20) and the Ca^{2+} wave (n=8) by the application of extracellular catalase (Figures 3.16, 3.17). External application of H_2O_2 produced a dose-dependent elevation of Ca^{2+}_{cyt} (Figure 3.18, n=4 for each concentration) reaching peak Ca^{2}_{cyt} levels of 600 ± 102 nM with 1 mM H_2O_2. However, in clear contrast to the hyper-osmotically-induced Ca^{2+}_{cyt} transient, this did not propagate as a wave, occurring instead as a global Ca^{2+}_{cyt} elevation spreading inwards from around the cell periphery. The Ca^{2+}_{cyt} elevation induced by external H_2O_2 was transient, lasting for approximately 60 s.

3.3.6.3. Ca^{2+}_{cyt} elevation and mitochondrial ROS production

To determine whether Ca^{2+} elevation alone was sufficient for mitochondrial ROS production, caged $Ins(1,4,5)P_3$ was used to elevate Ca^{2+}_{cyt} in the absence of any stimulus. Photorelease of $Ins(1,4,5)P_3$ caused an immediate elevation of Ca^{2+}_{cyt} (Figure 3.19 A) that lasted for up to 20 s (n=6). This Ca^{2+}_{cyt} elevation was sufficient to trigger a mitochondrial ROS production in the absence of any other stimulus (Figure 3.19 B; n=6). Significantly, the $Ins(1,4,5)P_3$-induced mitochondrial ROS production was not inhibited by DPI (Figure 3.19 C, n=3) indicating that the total inhibitory effect of DPI on the hyper-osmotic-induced ROS production and Ca^{2+}_{cyt} wave resulted from the specific inhibition of an upstream DPI-sensitive process.

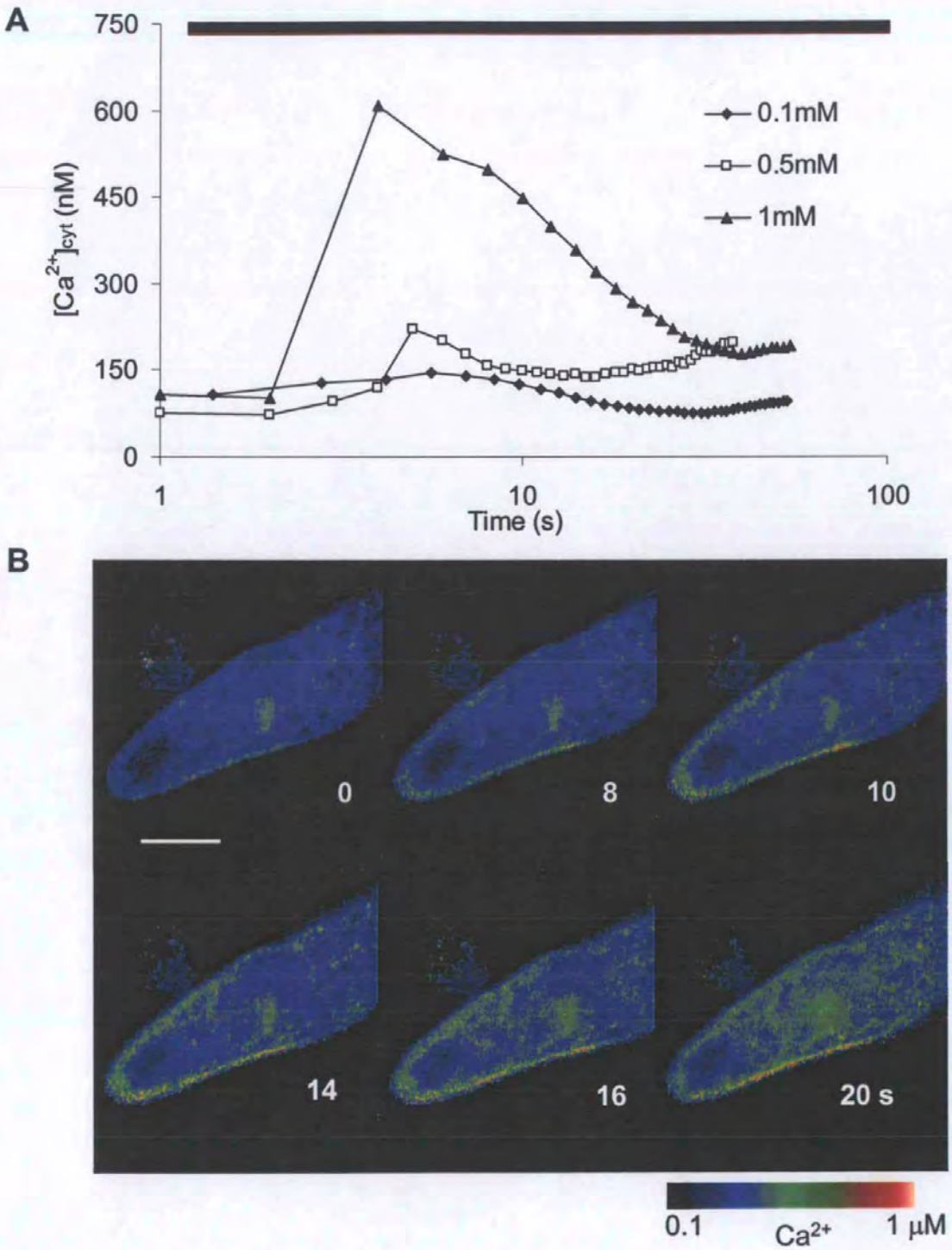

Figure 3.18. Changes in Ca^{2+}_{cyt} induced by extracellular H_2O_2. A) Externally applied H_2O_2 caused a transient dose-dependent elevation Ca^{2+}_{cyt} in rhizoid cells. Black bar indicates hyper-osmotic perfusion. **B)** Confocal ratio images of a Ca^{2+}_{cyt} elevation in response to externally applied 1 mM H_2O_2. Bar = 30 µm.

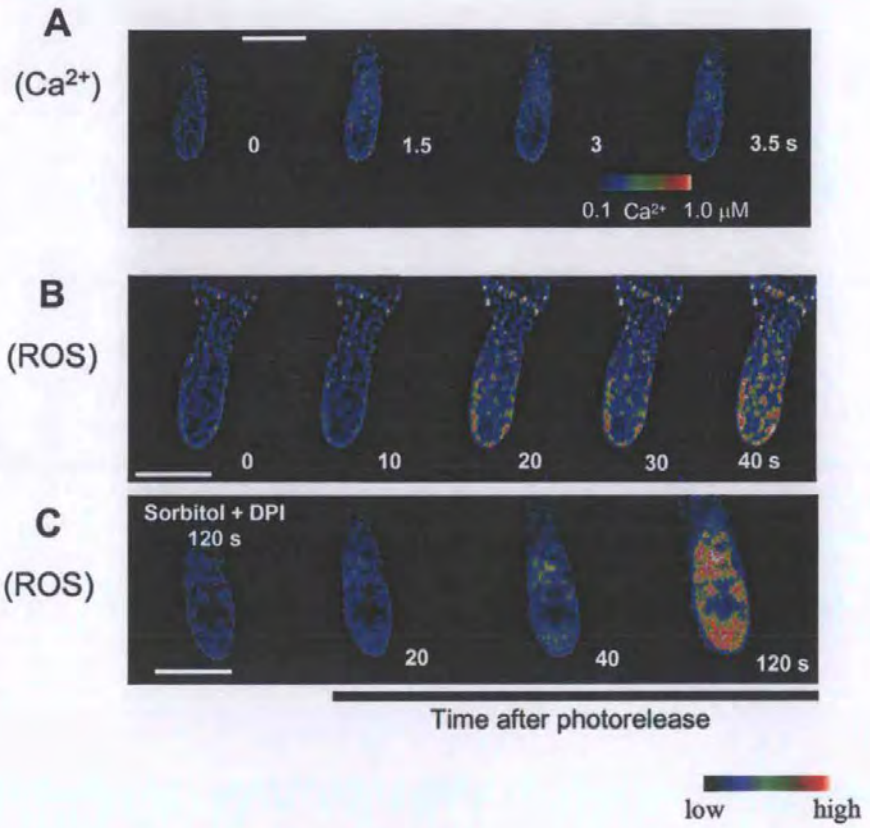

Figure 3.19. Ca^{2+}_{cyt} elevation is sufficient to induce mitochondrial ROS production. The left image of each sequence shows Ca^{2+} or ROS prior to photo-release of caged $Ins(1,4,5)P_3$. Images following $Ins(1,4,5)P_3$ release in **A-C** are identified by the bar at the bottom of the figure. **A)** Ca^{2+}_{cyt} elevation in response to photorelease of $Ins(1,4,5)P_3$ (1 s UV flash given at t = 0). Bar = 50 μm. **B)** ROS production induced by Ca^{2+}_{cyt} elevation in response to photorelease of $Ins(1,4,5)P_3$. Bar = 40 μm. **C)** DPI prevented the hyper-osmotically-induced (2 M sorbitol + seawater) but not the subsequent $Ins(1,4,5)P_3/Ca^{2+}$-induced mitochondrial ROS production. Bar = 40 μm.

3.3.6.4. Cation channel activation by ROS

Single channel recordings from cell-attached membrane patches of laser-derived spheroplasts from the rhizoid apex (Figure 3.20) consistently revealed the presence of cation-permeable channels with identical properties to those previously characterized as non-selective cation channels (Taylor et al., 1996), based on their conductance (28 pS) and reversal potential (-25 mV, assuming E_K of -50 mV, $[K^+]_{cyt}$ = 200 mM, Taylor et al., 1996) and spheroplast resting membrane potential of -60 mV (Berger and Brownlee, 1995) (Figure 3.20 B). In 16 out of 22 patches containing this type of channel activity, bath perfusion with 1 mM H_2O_2 in seawater produced a significant increase in channel activity. While the extent of channel activation varied from cell to cell, in the experiment shown, open probability averaged 0.01 prior to H_2O_2 addition and increased to 0.51 during the initial 10 s following H_2O_2 perfusion. While opening to only a single open current level was observed prior to H_2O_2 treatment, 4 open levels were apparent from the single channel trace and the associated amplitude histogram following H_2O_2 treatment (Figure 3.20). The effect of H_2O_2 was variable but transient, lasting between 10 and 30 s. This result is consistent with the transient nature of the H_2O_2-induced Ca^{2+} elevation.

3.4. DISCUSSION

The results show a clear and essential interaction between Ca^{2+} and ROS in short-term signalling in response to hyper-osmotic treatment. The velocity of propagation of the hyper-osmotically-induced Ca^{2+} wave reported here (ca. 15 $\mu m.s^{-1}$) was similar to that previously reported for hypo-osmotically-induced Ca^{2+} signals in *Fucus* rhizoid

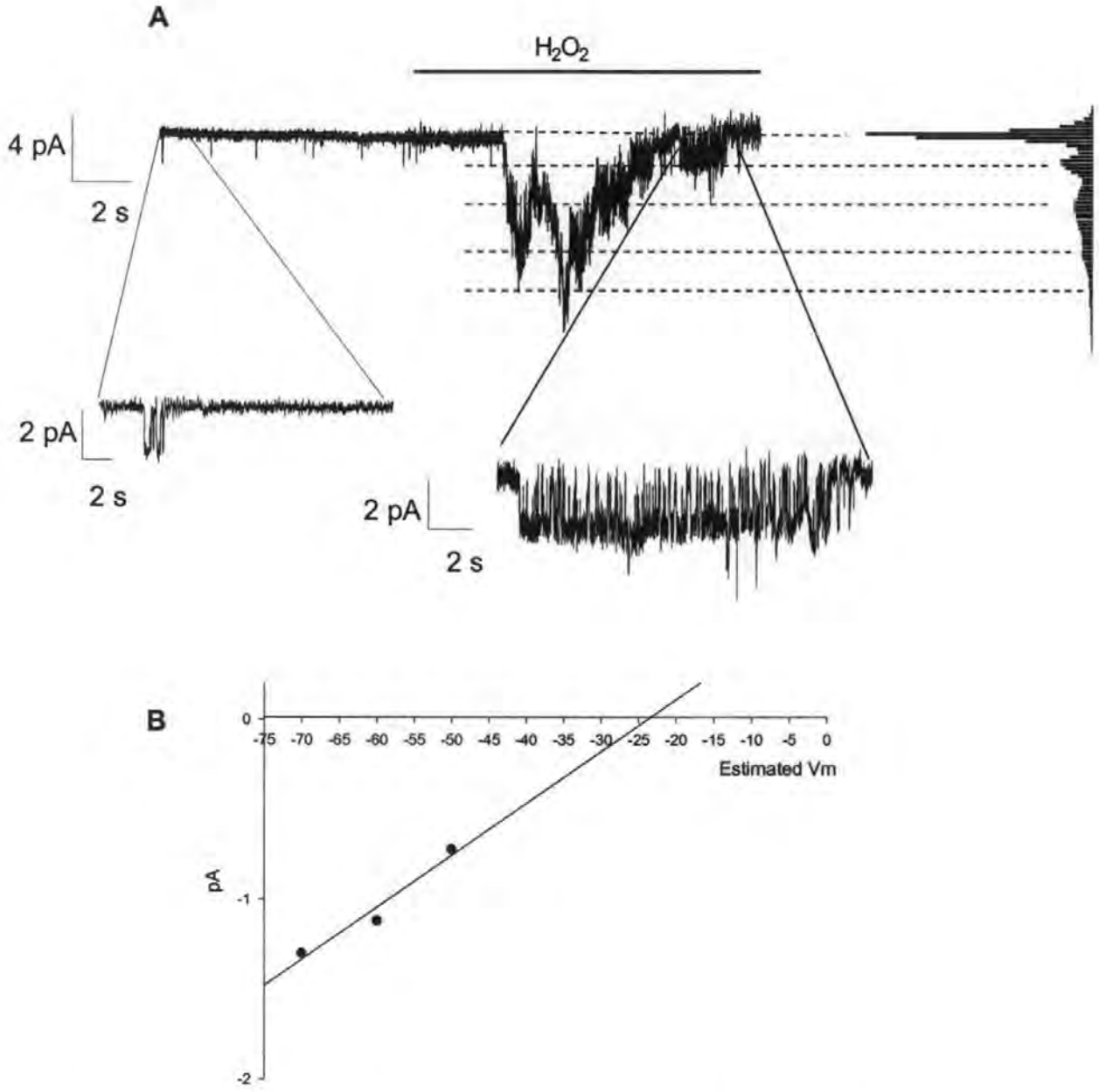

Figure 3.20. Changes in Ca^{2+}_{cyt} and channel activity induced by extracellular H_2O_2. A) Single channels recorded from a cell-attached membrane patch of a laser-derived spheroplast from the rhizoid apex. Prior to perfusion with H_2O_2, the patch showed single inward channels currents opening with low probability to a single level. A transient increase in channel activity was apparent within 4 s of 1 mM H_2O_2 perfusion. Four open levels induced by H_2O_2 are apparent in the channel trace and accompanying amplitude histogram (right). **B)** Representative cell attached I/V curve (n=3). Values were corrected for liquid junction potential (10 mV).

cells (Goddard et al., 2000). However, the pattern of propagation is different to that reported for hypo-osmotic treatments, which generate separate apical Ca^{2+} elevations and/or bi-directionally-propagating Ca^{2+} waves that initiate in the peri-nuclear region depending on the strength of the stimulus (Goddard et al., 2000). The hyper-osmotic Ca^{2+} wave thus provided a consistent signal against which to compare the patterns of ROS production in this signalling pathway. The hyper-osmotically-induced Ca^{2+} wave and the early peripheral ROS production both localize to the rhizoid apex at sites of adhesions between the plasma membrane and cell wall. However, while the Ca^{2+} wave was dependent on the extracellular production of ROS, as indicated by the complete inhibition of the Ca^{2+} wave by both DPI and extracellular application of catalase, the early peripheral ROS production was independent of the Ca^{2+}_{cyt} elevation. A role for ROS in spatial patterning of the Ca^{2+} wave was also indicated by the de-localized elevation of Ca^{2+}_{cyt} initiating from around the cell periphery in response to de-localized external H_2O_2 application. In addition, the rapid activation by H_2O_2 of non-selective plasma membrane cation channels in cell-attached recordings strongly suggests that the initial action of external ROS production is mediated via Ca^{2+} influx through these channels. The transient nature and rapid onset of both the H_2O_2-induced Ca^{2+}_{cyt} elevation and plasma membrane channel activation suggests that these two events are closely linked. However, the more prolonged Ca^{2+} elevation associated with hyper-osmotic treatment may require additional components that give rise to the propagating Ca^{2+} wave. The involvement of intracellular Ca^{2+} release via the activation of PLC and $Ins(1,4,5)P_3$ is evident from the inhibitory effects of U73122. However, the steps that lead from localised Ca^{2+} influx to the activation of Ca^{2+} release mechanism remain to be determined in detail. It will also be important to determine whether the production

of ROS at the growing rhizoid apex also underlies the Ca^{2+} gradient associated with rhizoid germination and growth (Brownlee and Wood, 1986; Taylor et al., 1996; Pu and Robinson, 1998). A role for H_2O_2 on the maintenance of Ca^{2+} cellular homeostasis is suggested by experiments that show a reduction in Ca^{2+} resting levels after incubation in DPI. The concentrations of H_2O_2 that elicited elevations in cytosolic Ca^{2+} (0.1-1.0 mM) are comparable with those shown to cause Ca^{2+} elevation and increased Ca^{2+} current in stomatal guard cell protoplasts (Pei et al, 2000). The actual H_2O_2 concentrations at the plasma membrane achieved during hyper-osmotic treatments are not known. While we have estimated an average cellular H_2O_2 production rate of 0.05 mmoles l^{-1} min^{-1}, the H_2O_2 concentration at localised sites of production are likely to be considerably higher than the μM range.

The mitochondrial membrane potential ($\Delta\psi_m$) drives ATP synthesis and provides a large driving force for divalent cation entry. Several studies have shown that when challenged with high cytosolic Ca^{2+} the mitochondria can contribute to Ca^{2+} homeostasis by providing an intracellular sink for Ca^{2+} (Rizzuto et al., 2000). The increase in cellular TMRE fluorescence in response to hyper-osmotic shock is consistent with the release of TMRE from the mitochondria in response to mitochondrial depolarization, resulting in reduced dye quenching (Zimmerman, 2000). X-rhod-FF was used as an indicator of Ca^{2+}_m. This is an analogue version of rhod-2, which has been used to monitor Ca^{2+}_m in both animal and plant cells (Subbaiah et al., 1998; Park et al., 2001). Its co-localization with Mitotracker in the present study confirmed its mitochondrial localization in *Fucus* rhizoid cells. The onset of Ca^{2+}_m elevation, coincident with the peak of the Ca^{2+}_{cyt} transient, i.e. 20 s following the

hyper-osmotic treatment suggests the occurrence of Ca^{2+} uptake by the mitochondria following cytoplasmic Ca^{2+} elevation, consistent with a role for mitochondria in buffering Ca^{2+}_{cyt} shown in a variety of animal cell types (Rizzuto et al., 2000; Zimmermann, 2000; Duchen, 2000). Moreover, recent reports show that uptake of Ca^{2+} by mitochondria can have a powerful impact on cellular Ca^{2+} signaling (Duchen, 2000), affecting for instance the generation and propagation of Ins(1,4,5)P_3-triggered Ca^{2+} waves (Zimmermann, 2000) and modulation of store-operated Ca^{2+} currents (Hoth et al., 1997). So far, evidence for the role of mitochondria in spatio-temporal Ca^{2+} signaling is largely lacking for plants or algae though mitochondria have been shown to represent a source of Ca^{2+} for signals elicited in response to anoxia (Subbaiah et al., 1998). It is clear from the present results that the onset of the increase in mitochondrial ROS production is coincident with the declining phase of the transient Ca^{2+}_{cyt} elevation, with the peak of the mitochondrial depolarisation and with the elevation of Ca^{2+}_{m} following hyper-osmotic treatment. Moreover, the mitochondrial ROS production shows an absolute dependence on Ca^{2+}_{cyt} elevation. In animal cells mitochondria may incur Ca^{2+}-induced respiratory impairment in response to Ca^{2+} loading that may potentiate ROS production (Grijalba et al., 1999). The total abolition of mitochondrial ROS production in Br_2BAPTA-injected rhizoid cells indicates a strong causal link between cytosolic Ca^{2+} elevation, mitochondrial Ca^{2+} uptake and ROS production.

The hyper-osmotically-induced mitochondrial ROS production and Ca^{2+}_{cyt} elevation were sensitive to DPI. In contrast, Ca^{2+}-induced mitochondrial ROS production following photorelease of caged Ins(1,4,5)P_3 was DPI-insensitive. Hyper-osmotically-

induced mitochondrial ROS production therefore appears to require the activity of an upstream DPI-sensitive process. Thus, an elevation of Ca^{2+}_{cyt} is necessary to induce mitochondrial ROS production and is preceded by peripheral cytosolic elevation of ROS, involving an initial extracellular production of ROS probably through a NADPH oxidase-like activity.

The results presented here indicate a sequence of events leading to mitochondrial ROS production involving an initial localised extracellular production of ROS at the level of the plasma membrane leading to Ca^{2+}_{cyt} elevation, Ca^{2+} uptake by mitochondria and mitochondrial ROS production. This is consistent with the demonstration of ROS production in response to absisic acid in *Arabidopsis* stomatal guard cells, which was shown to increase the activity of hyper-polarization dependent Ca^{2+} channels in the plasma membrane leading to Ca^{2+}_{cyt} elevation (Pei et al., 2000). That work showed a considerable delay (several minutes) between H_2O_2 addition and channel activation. The rapid onset of peripheral ROS production and Ca^{2+} elevation reported here indicates a direct and rapid modulation by ROS of the pathways leading to Ca^{2+}_{cyt}, wave propagation, involving both Ca^{2+} influx channels and release of Ca^{2+} from intracellular stores in endoplasmatic reticulum-rich cellular regions in *Fucus* rhizoid cells (Taylor et al., 1996; Goddard et al., 2000). In animal systems, few reports have clearly shown a direct activation of Ca^{2+}-permeable channels by H_2O_2. Some reports show indirect evidence (mainly through pharmacological tools) for regulation of cytoplasmatic Ca^{2+} by H_2O_2 (e.g. Wang and Joseph, 2000). Other reports indicate that H_2O_2 has a potent stimulatory effect on L-type Ca^{2+} currents (Thomas et al.,

1998), and on non-selective cation channels (Ji et al., 2002). A demonstration of the direct effect of ROS at the single channel level was not found in the literature.

In summary, the present work shows that ROS production in response to hyper-osmotic stress in embryonic cells of the alga *Fucus* comprises two distinct components (Figure 2.21 and 2.22). The first ROS component coincides closely with the origin of a Ca^{2+} wave in the peripheral cytosol at the growing cell apex, has an extracellular origin, and is necessary for the Ca^{2+} wave. Patch clamp experiments show that a non-selective cation channel is stimulated by H_2O_2, and may underlie the initial cytosolic Ca^{2+} elevation. The spatio-temporal pattern of the Ca^{2+} wave is thus determined by peripheral ROS production. The second, later ROS component localises to the mitochondria and is a direct consequence of the Ca^{2+} wave. The findings presented here provide an insight to ROS/Ca^{2+} signalling in showing that localized extracellular ROS production is required for the spatial patterning of a Ca^{2+} signal.

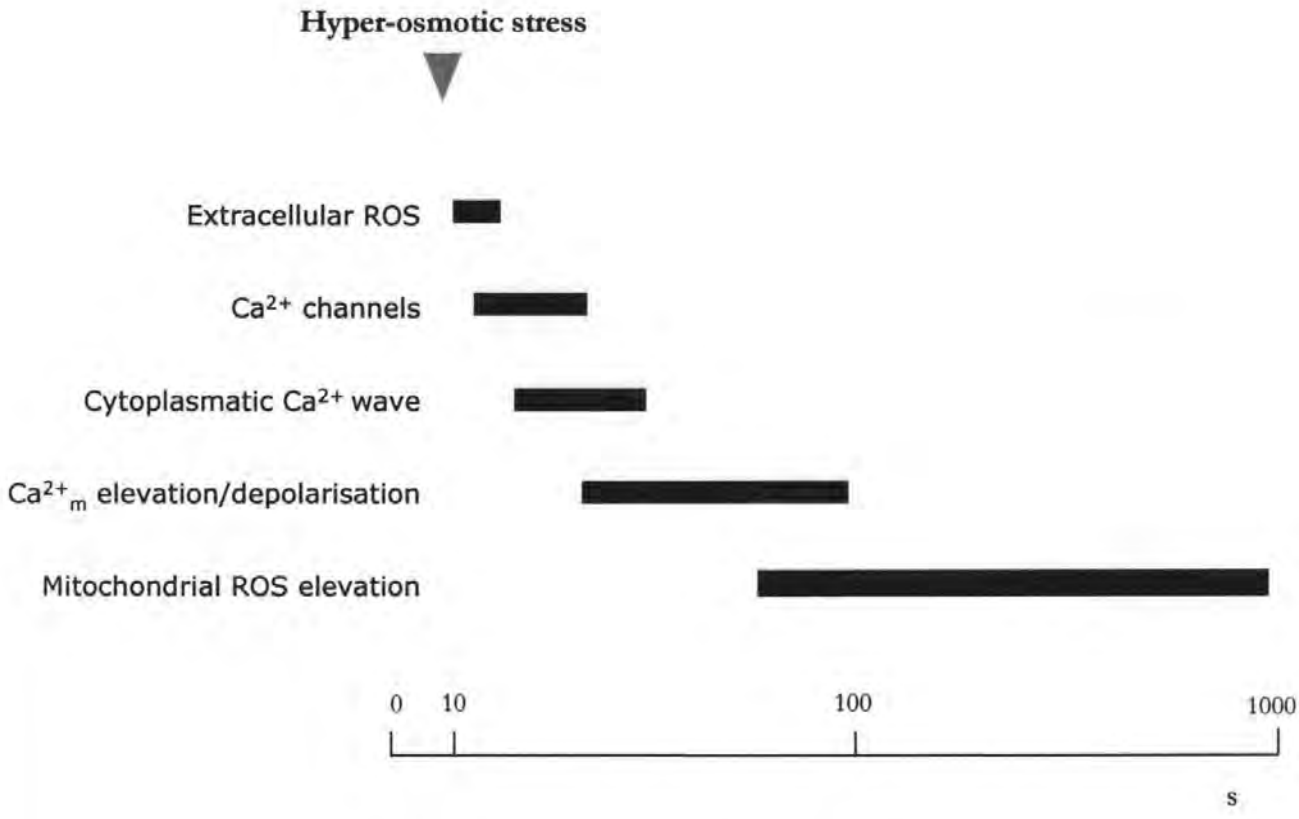

Figure 3.21. Proposed sequence of ROS and Ca^{2+} events following a hyper-osmotic shock in the *Fucus* rhizoid cell.

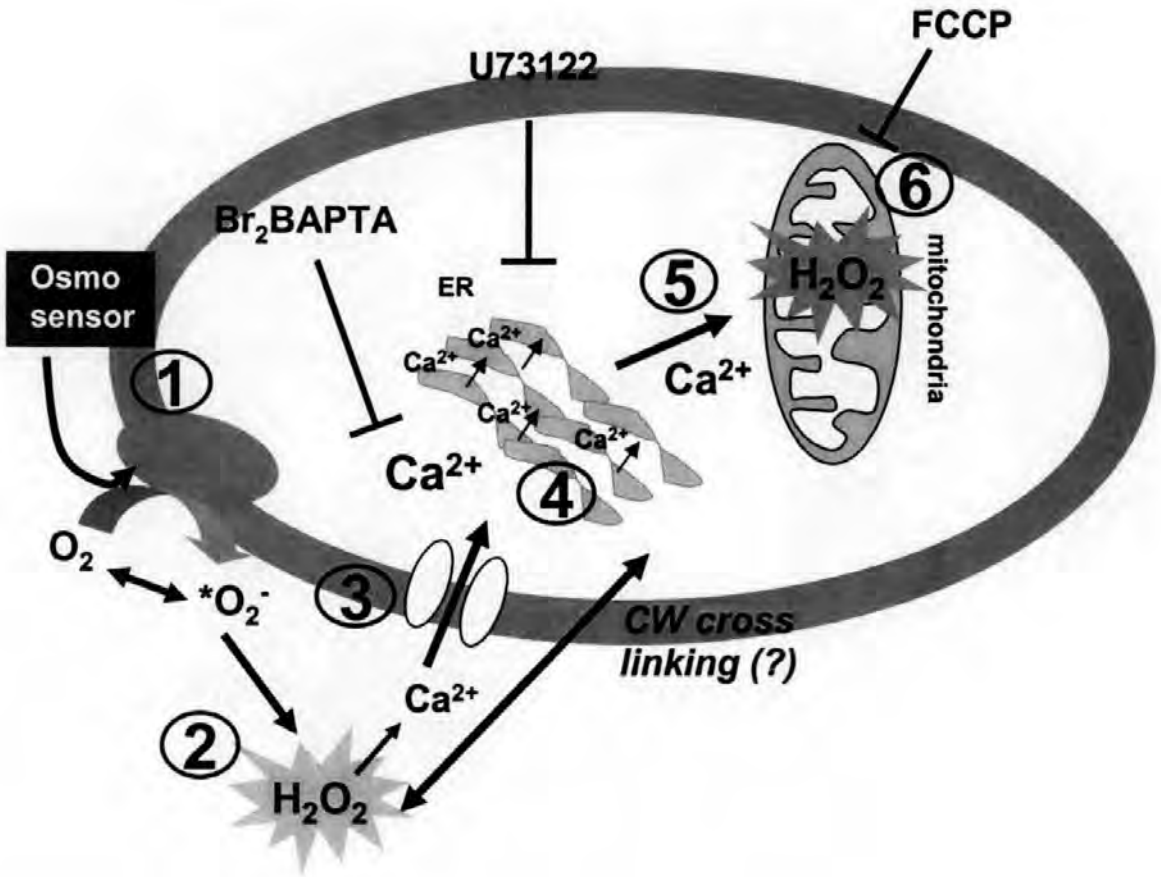

Figure 3.22. Proposed interactions between Ca^{2+} and ROS during hyper-osmotic stress in *Fucus* embryos. Osmotic change is sensed by an unidentified osmo-sensor (1), which induces a DPI-sensitive ROS production within 10 s (2). H_2O_2 is produced at the exterior side of the plasma membrane and may be involved in cell wall strengthening. H_2O_2 also diffuses into the cell leading to localized peripheral intracellular elevation. Localised external H_2O_2 production also increases Ca^{2+} channel activity (3). Downstream events include Ca^{2+} wave propagation over the following 10-60 s (4) followed by $Ca^{2+}{}_m$ elevation (5) and mitochondrial ROS production (6).

CHAPTER 4

DOWNSTREAM EFFECTS OF THE HYPER-OSMOTIC STRESS-INDUCED OXIDATIVE BURST: OSMOTIC ADAPTATION AND PROTEIN KINASE ACTIVATION

4.1. INTRODUCTION

This chapter presents the results of a preliminary study on the involvement of cell wall bromoperoxidase and protein kinases activities during hyper-osmotic stress in the *Fucus* embryo. These experiments were based on previous results regarding the participation of ROS and Ca^{2+} in the signal transduction pathway during hyper-osmotic stress (Chapter 3).

Because the early hyper-osmotically-induced ROS elevation was found to be localised at the cell periphery (Chapter 3), the hypothesis was that H_2O_2 produced by the DPI-sensitive process could affect the activity of cell wall enzymes involved in cross linking its components and therefore increase cell wall osmotic resistance. The first part of the present chapter thus addresses the question whether the peripheral oxidative burst after a hyper-osmotic stress is associated with cell wall strengthening mechanisms in the *Fucus* rhizoid.

Phosphorylation cascades induced by osmotic stress have been identified in animals, plants, yeasts and bacteria. Upon osmotic stress in bacterial or yeast cells, an osmosensor is activated which induces a MAPK cascade pathway (reviewed by Kultz and Burg, 1998; Hohmann et al., 2002). The activation of MAPK pathways by cell swelling has also been observed in mammals (Schliess et al., 1995). In plants a large number of reports associate ROS production during stress to MAPK cascade activation (e.g. Lingterink et al., 1997; Lebrun-Garcia et al., 1998; Yuasa et al., 2001). The second part of this chapter presents the preliminary results of an investigation on

the involvement of protein kinases, in particular MAPK, in the *Fucus* hyper-osmotic stress response.

4.1.1. Hyper-osmotic stress and osmotic adaptation

4.1.1.1. Cell wall deposition in Fucus *zygotes*

The *Fucus* zygote exhibits tip growth similar to pollen tubes and root hairs. Polar extension occurs by local vesicle fusion with the plasma membrane, process that adds new plasma membrane and secretes cell wall precursors and enzymes at the growing site (Steer and Steer, 1989). The nascent elongating wall must be flexible enough to expand under the force of turgor but strong enough to withstand lysis. In *Fucus* embryos, microtubules contribute to rhizoid tip morphology (Kropf et al., 1990) and both the F-actin cytoskeleton, which transport vesicles containing cell wall precursors, and microtubules have been shown to regulate *Fucus* tip growth (Kropf et al., 1990).

Eggs of fucoid brown algae have no cell wall, and following fertilisation the cell wall synthesis begins immediately. Initially, the cell wall is deposited uniformly, but during germination tip growth is initiated. The cell wall components and cytoskeleton of fucoid zygotes have been well characterised: the cell wall contains polysaccharides (alginic acid, fucans and cellulose), polyphenols and proteins (about 5%, Schoenwaelder and Wiencke 2000). Polyphenols, alginic acid and fucans are synthesised in the Golgi, transported to the plasma membrane in vesicles and secreted into the wall where they are stabilised and incorporated (Schoenwaelder and Wiencke, 2000). The highly sulphated fucan F2 is first deposited in the wall during the transition from diffuse growth (before polarisation) to tip polarised growth and is localised in the

rhizoid tip (Brawley and Quatrano, 1978). Polyphenols are also deposited preferentially into the rhizoid wall of germinated zygotes (Schoenwaelder and Wiencke, 2000). Cellulose is synthesised *in situ* by a cellulose synthase complex in the plasma membrane of the zygote (Peng and Jaffe, 1976). The microtubule cytoskeleton radiates out from the perinuclear centrosomes and extents into the cortex of the cell (Bisgrove and Kropf, 1998; Corellou and Brownlee, unpublished). A meshwork of F-actin is present in the cortex, and localised patches of F-actin are believed to function in establishing developmental polarity (Alessa and Kropf, 1999).

Recent studies on cell wall deposition during morphogenesis in *Fucus* embryos have shown that cytoskeleton and deposition of cellulose are involved in generating cell wall strength in growing zygotes. Cell wall strength has been shown to be dependent on F-actin in the apical cytoplasm, and cellulose and sulphated fucans in the cell wall (Bisgrove and Kropf, 2001).

4.1.1.2. Cell wall peroxidases and their functions in cell wall strengthening

Plants and bacteria contain haem-peroxidases that are capable of acting on a very wide range of substrates (Halliwell and Gutteridge, 1999). Oxidations by peroxidases can in almost all cases be represented by the following series of reactions, in which SH_2 is the substrate (Halliwell and Gutteridge, 1999):

Peroxidase + H_2O_2 =>Compound I

Compound I + SH_2 =>Compound II + SH^*

Compound II + SH_2 =>Peroxidase + SH^*

$SH^{\bullet} + SH^{\bullet} => S + SH_2$

Hydrogen peroxide removes two electrons to give compound I. Compound II is the intermediary state of the enzyme. The substrate-derived radicals then undergo a disproportionation reaction, one reducing the other to SH_2 and simultaneously oxidizing itself to S.

Several investigations on higher plants have indicated a close relationship between H_2O_2 production at peripheral cell sites, cell wall strengthening and peroxidase activity (e.g. Lin and Kao, 2001; Razem and Bernards, 2002). In higher plants, it has been shown that H_2O_2 localisation sites in the cell wall mirrors lignification sites (Olson and Varner, 1993; Ogawa et al., 1997). Lignification of plant cells involves the polymerisation of phenols and occurs through a series of enzymatic steps starting with a phenylalanine ammonia-lyase catalysed reaction to produce lignin precursors and terminating with a process that requires either H_2O_2 and a cell-bound peroxidase (Gross et al., 1977) to bring about polymerisation of the precursor units into lignin. The requirement for H_2O_2 and peroxidase for wound-induced suberization in potato tubers has also been demonstrated - H_2O_2 was found to be essential for the oxidation of polyphenols by cell wall peroxidases (Razam and Bernards, 2002). Studies with onion cell walls showed that peroxidase-driven reactions decrease extensibility by increasing the cross-linking reactions of several proteins and other polymers (Fry, 1986; Córdoba-Pedregosa et al., 1996; Schützendübel et al., 2001). It has been suggested that plant growth reduction is likely to result from cell wall stiffening processes related to formation of cross-links among cell wall polymers by peroxidases and related to increased levels of H_2O_2 (Lin and Kao, 2001). In contrast, a recent study

in maize seedlings suggests a role for ROS production and cell wall peroxidases in the loosening of cell wall components to allow auxin-induced elongation (Schopfer et al., 2002).

A role for H_2O_2 production in the activation of peroxidases is also reported in the animal kingdom. Ovoperoxidase, an enzyme secreted by sea urchin eggs, catalysis the formation of dityrosine residues in the fertilisation envelope. Fertilisation-envelope formation is initiated by a Ca^{2+} elevation, which triggers exocytosis of granules. The nascent envelope compounds cross-linking is catalysed by ovoperoxidase in a reaction that requires extracellularly generated H_2O_2. This production of H_2O_2 resembles the mammalian neutrophils oxidative burst. (Heinecke and Shapiro, 1990).

4.1.1.3. Biochemistry and functions of haloperoxidases

Of particular importance for marine algae is the subclass of peroxidases known as haloperoxidases. Haloperoxidases are a group of enzymes that are able to catalyse the halogenation of organic compounds in the presence of halide ions (iodide, bromide and chloride) and H_2O_2 (Butler, 1998). There are three distinct classes of these enzymes which carry out their reactions by different mechanisms: those which have a haem group, those which contain vanadium and those which contain no metals (Littlechild, 1999). Within the class of vanadium-haloperoxidase enzymes, both vanadium bromoperoxidase, which have been isolated from marine algae including *Fucus* and *Laminaria* (De Boer et al., 1986), and vanadium chloroperoxidases, isolated from terrestrial fungi, have been identified (reviewed by Butler, 1998). Many halogenated natural compounds have been isolated from marine algae, ranging from volatile halogenated hydrocarbons (bromoform, chloroform, etc) to chiral halogenated

terpenes, which have important anti-inflammatory, antimicrobial and pharmacological properties. The haloperoxidases present in brown algae are thought to be involved in the biosynthesis of these products (Butler, 1998).

Especially relevant for *Fucus* are the vanadium dependent bromoperoxidases (Jordan and Vilter, 1991) that specifically catalyse the oxidation of bromide or iodide by H_2O_2. The general reaction mechanism of bromoperoxidases (BPO) can be described as:

$$Br + H_2O_2 => BrHO + OH$$

$$BrOH + Br + H^+ => Br_2 + H_2O$$

They were first isolated from *Ascophyllum nodosum* (Weaver et al., 1985), and since then from other algae including *Fucus* (De Boer et al., 1986; Ohshiro et al., 1999). Bromoperoxidases are involved in the biosynthesis of halogenated organic compounds, which have various functions as intermediates in biosynthetic pathways, hormones or in relation to defence mechanisms (Fenical, 1982; Niedlman et al., 1986; Kupper et al., 1998). BPOs present in marine algae are also known to alleviate oxidative stress imparted by the presence of H_2O_2 (Pedersen et al., 1996). For example, BPO in the marine red algae *Corallina pilulifera* has the physiological function of producing bromoform to eliminate epiphytic organisms on its surface. In addition, Ohsawa et al. (2001) suggested that BPO can act as a potent substitute for catalase as it is used to efficiently eliminate H_2O_2. Other studies support this hypothesis, showing that H_2O_2 produced in green algae as a result of photosynthesis and respiration is detoxified by BPO through bromination of organic substrates (Manley and Barbero, 2001).

In addition to their role in defence mechanisms, haloperoxidases are thought to mediate cross-linking of the cell wall of *Fucus* (Vreeland et al., 1998). Phenolic cross linking of alginates occurs in early cell wall formation in *Fucus* and peroxidases may be involved in the catalysis of phenolic condensation onto alginate. In fact, polyphenols are amongst the compounds that can act as substrates for BPO (Itoh et al., 1988). BPO is present in both cytosolic and cell wall fractions of *Laminaria* sp. (Jordan et al., 1991). BPO is also present in the mucilage that surrounds *Fucus* embryos and is thought to be involved in adhesion to the substrate (reviewed by Vreeland et al., 1998).

4.1.2. MAPK cascades and hyper-osmotic stress

Mitogen-activated (MAP) protein kinases are well-conserved universal kinases among eukaryotes. They are key regulators in a wide range of signal transduction pathways that lead to a variety of responses, from cell cycle arrest and mating in *Saccharomyces cerevisae* to proliferation and differentiation in metazoans (reviewed by English et al., 1999; Chen et al., 2001). MAP kinases are activated through multi-step protein kinase cascades by dual phosphorylation on a tyrosine and threonine residue. Pathways involving MAPK are induced in response to a broad range of stimuli, such as growth factors, cytokines, hormones, irradiation, shear stress and osmotic shock.

4.1.2.1. MAPK pathways: activation modules involving three kinases

The basic assembly of MAPK pathways is a three-component module well conserved from yeast to humans. This includes three kinases that establish a sequential activation pathway, and comprise a MAPK kinase kinase (MAPKKK), MAPK kinase (MAPKK) and MAPK (Figure 4.1). The MAPKKK are serine/threonine kinases that

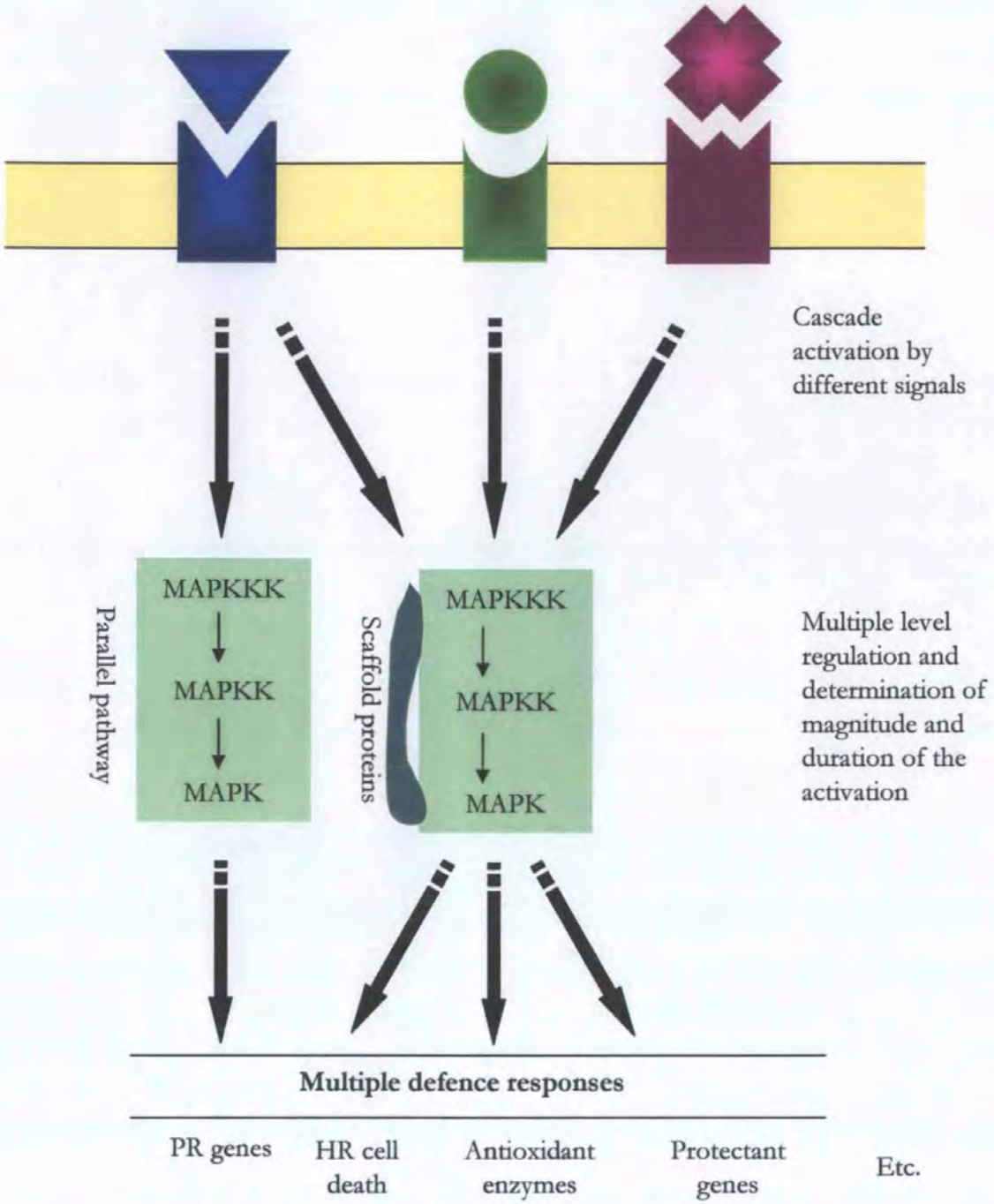

Figure 4.1. General scheme of the dynamic regulatory mechanisms involved in MAPK pathway and plant defence. Diagram represents a broad picture of how MAPK cascades may function and be regulated in plant defence. MAPK cascades are activated by several stimuli and several MAPK pathways can be used in parallel by a single stimulus (Cardinale et al., 2000; Kumar and Klessig, 2000). MAPK pathways bring together transduction pathways initiated by different signals and also deliver messages to diversified pathways to evoke transcription of genes and to affect the effectiveness of different proteins (Romais, 2001). Association with scaffold proteins makes the cascade efficient and increases specificity (Zhang et al., 2000).

After Xing et al., 2002

when activated phosphorylate and activate the next kinase in the module (MAPKK). The MAPKK are kinases that recognize and phosphorylate a Thr-X-Tyr (where X can be different amino acids) motif in the activation loop of MAPK. MAPKs are the final kinase in this three-component system and phosphorylate substrates on serine and threonine residues.

The regulation mechanism of this phosphorylation pathway is highly dynamic (Figure 4.1). In the MAPK signal transduction cascade, the active MAPK might allow the activation of other protein kinases, catalyse the phosphorylation of cytoskeletal components or activate transcription factors once translocated to the nucleus (reviewed by Xing et al., 2002). The cascades involve parallel or redundant components, signal convergence and divergence, positive and negative regulatory mechanisms and scaffold proteins. Figure 4.1 shows a summary of how MAPK may function and be regulated in plants.

Why have MAPK modules evolved to comprise three kinases? MAPK must be phosphorylated on both a threonine and tyrosine for their activation, a dual phosphorylation catalysed by a specific MAPKK. Very specific MAPKK and MAPK combinations are found in a MAPK module. Specific MAPKK recognise the tertiary structure of different MAPK, restricting their regulation of different MAPK subtypes. In contrast, MAPKKK are able to associate with a range of different MAPKK-MAPK combinations (Widmann et al., 1999). In mammalian cells there are more MAPKKK than MAPK, and MAPKK are the fewest members of the three-component module. The large number of MAPKKK allows for diversity of inputs from numerous stimuli to feed into specific MAPK pathways. Some kinases that appear to be MAPKKK may

regulate pathways not involving MAPK (such as direct regulation of NF-kB pathway). Thus, the regulation of MAPK pathways at the level of MAPKKK may represent branch points in regulation of signal pathways, at least in some cases (reviewed by Widmann et al., 1999; Garrington and Johnson, 1999). The diversity of regulatory domains in different MAPKKK gives the family of MAPK modules the flexibility to respond to a wide range of cellular stimuli. Emerging evidence indicates that the specificity of MAPKKK interactions is achieved in part by the use of scaffolding or anchoring proteins to co-ordinate MAPKKK binding to specific proteins for upstream inputs as well as specific downstream MAPKK-MAPK complexes. Scaffolding of multi-component regulatory systems is now recognised as an important mechanism for controlling signal transduction pathways (Pawson and Scott, 1997; Raab and Rapp, 2002).

4.1.2.2. Osmotic stress signalling in plant cells via MAPK cascades

MAPK family is thought to have evolved relatively soon after the origin of eukaryotes (Kultz and Burg, 1998). The fact that MAPK pathways transduce stress signals in both mammalian and plant cells indicates that there is a high degree of conservation between both types of organisms (Widmann et al., 1999). This hypothesis is reinforced for example by the fact that antibodies raised against mammalian MAPK (such as ERK 1, ERK2) also recognize plant MAPK (Cazalé et al., 1999).

Changes in cell volume caused by osmotic stress are accompanied by modifications in intracellular osmolyte concentration. Because cell volume and ion regulations are not instantaneous processes, osmotic stress may damage cellular macromolecules and impair cell function until compensatory adaptations counteract the imposed stress. An

efficient cellular signalling mechanism designed to respond and accommodate to these osmotic changes is, thus, fundamental. In yeast, the HOG1 MAPK pathway is activated in response to hyper-osmolarity and is responsible for increased production of osmolytes, such as glycerol, that are important for osmotic adjustment (Hohmann, 2002). It is possible that similar pathways also exist in plants, as indicated by osmotic stress activation of some MAPK pathway components. However, plant MAPK cascade outputs are still unclear.

Stress such as drought, cold, wounding or pathogen attacks have been shown to activate MAPK in several plant species and mediate the appropriate defence or survival mechanisms (see Table 4.3). Considerable progress has been made in understanding plant MAPKs, and various studies have demonstrated that MAPKs play a role in several aspects of development (Wilson et al., 1997), cell division (Banno et al., 1993; Calderini et al., 1998; Bogre et al., 1999), and the action of hormones, including auxin (Mizoguchi et al., 1994), abscisic acid (Knetsch et al., 1996), gibberellic acid (Huttly and Phillips, 1995), ethylene (Kieber et al., 1993; Chang, 1996), salicylic acid (Zhang and Klessig, 1997), and jasmonic acid (Seo et al,. 1995, 1999; Stratmann and Ryan, 1997). These results suggest that growth and/or development in plants may also be controlled, at least in part, by MAPK pathways. The increasing number of plant MAPK pathways that are currently being analysed (see Table 4.3) indicates that plant MAPK pathways mediate many different aspects of plant physiology. In particular, recent evidence has shown that MAPK cascades are involved as transducers of osmotic signals in plant cells and therefore important regulators in the adaptation to osmotic stress (see Table 4.3).

In plants, MAPK family is represented by a single subfamily (Kultz and Burg, 1998). This subfamily belongs to the ERK (extracellular-signal-regulated kinases) subgroup, hence the subfamily name is plant ERKs (PERKs). Several PERKs are strongly activated by osmotic stress. In *Medicago sativa*, drought activates MMK4, a PERK with a relative molecular mass of 44 kDa (Jonak et al., 1996). Other PERKs activated by osmotic stress include for example *Arabidopsis thaliana* ATMPK3 (Mizoguchi et al., 1996) and *Pisum sativa* PsMAPK (Popping et al., 1996). This latter is able to rescue yeast ΔHOG1 mutants in hyper-osmotic medium suggesting a close functional relationship between this PERK and a yeast stress-activated protein kinase (SAPK).

Parts of several MAPK modules that may be involved in osmotic stress signalling have been identified in alfafa (SIMKK-SIMK, Kiergerl et al., 2000) and in tobacco (NTMEK2-SIPK/WIPK, Yang et al., 2001; Zhang and Klessig, 2001). However, the *in vivo* function during stress signalling has not been established for any of the plant MAPK pathways. Osmotic stress can activate different MAPKs at different times after onset of stress and the activities of these MAPKs also last for different time periods (e.g. Mikolaczyk et al., 2000). Additionally, different levels of salt stress can activate distinct MAPK (Munnik et al., 1999). Three protein kinases of 50, 75 and 80 kDa were activated by hypo-osmotic stress in BY2 tobacco cells and were shown to be dependent on upstream phosphorylation and Ca^{2+} transduction steps (Takahashi et al., 1997). Activation of protein kinases by hyper-osmotic stress was also demonstrated for suspension cultured tobacco cells (Cazalé et al., 1999; Hoyos and Zhang, 2000). Hoyos and Zhang (2000) demonstrated that SIPK (stress induced protein kinase), a tobacco MAPK, is activated by hyper-osmotic stress and the authors suggested that SIPK could be the MAPK acting downstream of a plant osmosensor. In addition, they found a

Ca^{2+} and ABA-independent 40 kDa kinase, HOSAK (high osmolarity stress activated protein kinase) that is specifically activated by hyper-osmotic treatment.

Activation of protein kinases has also been shown in algal cells in response to osmotic shock. In *Lamprothamnium*, a Ca^{2+}-dependent kinase is activated in response to hypo-osmotic treatment (Yusa et al., 1997). In the halotolerant green alga *Dunaliella tertiolecta*, osmotic stress activates LAP kinase and HAP kinase (low- and high-pressure activated protein kinases) (Yuasa and Muto, 1996).

Interestingly, Ca^{2+} is the second messenger inducing the activation of MAPK in numerous animal cell types (reviewed by English et al., 1999). Intracellular free Ca^{2+} elevation is required for activation of ERK1 and ERK2 by several stimuli. A specific role for Ca^{2+} as an intermediate in MAPK cascades is also emerging for plant systems. Romeis et al. (1999) demonstrated that Ca^{2+} influx is necessary for MAPK activation upon fungal elicitor stimulation in tobacco cell cultures. Taylor et al. (2001) suggested a stress signal transduction pathway during soya bean oxidative burst that links elicitor stimulation, MAPK activation, Ca^{2+} entry and ROS production.

While the involvement of MAPK cascades in plant osmotic signalling has been well studied, the exact positioning and dependence of MAPK activation in relation to ROS production and Ca^{2+} dynamics is still not clear, and some differences between studies (probably related to plant species or stress applied) is evident (e.g. Yuasa et al. 2001; Desikan et al., 2001).

Table 4.1. *Examples of MAPK pathways during stress in several plant systems.*

MAPK	Treatment	Species	Notes	Reference
50 kDa 46 kDa	Hypo-osmotic	tobacco	Activation depended on Ca^{2+} influx. Activation downstream of oxidative burst	Cazalé et al., 1999
48 kD (SIPK) 40 kDa (HOSAK)	NaCl	tobacco	Activation is Ca^{2+} and ABA independent	Hoyos and Zhang, 2000
40 kDa (LAPK) 40 kDa (HAPK)	Hypo and hyper-osmotic	*Dunaliella*		Yuasa and Muto, 1996
ATMPK6	ROS	*Arabidopsis*	Activation by H_2O_2	Yuasa et al., 2001
SIMK (46 kDa) 38 kDa	Hyper-osmotic	alfafa	46 kDa is nuclear 38 kDa for extreme hyper-osmotic stress	Munnik et al., 1999
MMK4 (44 kDa)	Cold, drought	alfafa	Activation is ABA independent	Jonak et al., 1996
AtMPK4, AtMPK6	Low temperature, touch, wounding, low humidity, hyper-osmotic stress	*Arabidopsis*		Ichimura et al., 2000
OsMAPK2	Low temperature	rice		Huang et al., 2002
45 kDa	hydration	tobacco	Developmentally regulated	Wilson et al., 1997
44 kDa	auxin	*Arabidopsis*		Mockaitis and Howell, 2000
AMBP (45 kDa)	ABA	*P. sativum*		Burnett et al., 2000
47 kDa	Auxin, cytosolic acidification	tobacco	Cytoplasmatic acidification and not auxin induce activation of MAPK	Tena and Renaudin, 1998
SIPK (46 kDa)	Ozone/ROS	tobacco	Ca^{2+} dependent, downstream of ROS	Samuel et al., 2000
AtMPK4 AtMPK6	Harpin, H_2O_2	*Arabidopsis*	H_2O_2 activates only AtMPK6; activation independent of oxidative burst (sufficient, not necessary)	Desikan et al., 2001
44 kDa, 47 kDa	OGA, hypo-osmotic stress, fungal extract	soya bean	47 kD =>Ca^{2+} from internal stores =>44kD =>ROS	Taylor et al., 2001
SIPK (48 kDa) WIPK	Tobacco mosaic virus	tobacco	WIPK activation depends on disease resistance gene N	Zhang and Klessig, 1998a
SIPK (48 kDa)	Fungal elicitors	tobacco	Necessary for PAL gene activation	Zhang and Klessig, 1998b

48 kDa	Wounding, systemin, polygalacturonic acid, chitosan	tomato		Stratmann and Rayan, 1997
49 kDa	PA	*Glycine max*	SIMK-like; PA related to wound signalling	Lee et al., 2001
AtMPK6	Fungal, bacteria and plant elicitors	*Arabidopsis*	Activation simultaneous with medium alkalinisation	Nuhse et al., 2000
48 kDa	Fungal elicitors	tobacco	Activation upstream of medium alkalinisation and PAL activation	Zhang et al., 1998
39 kDa, 44 kDa	harpin	*Arabidopsis*	MAPK involved in defence gene expression and apoptosis	Desikan et al., 1999
39 kDa, 41 kDa, 45 kDa (ZmMPK5)	Senescence, recovery from cold stress	maize		Berberich et al., 1999
ERMK (45 kDa)	Fungal elicitor	parsley	Activation independent or upstream of ROS Ion channel activation dependent	Ligterink et al., 1997
ANP1 (MEK), AtMPK3, AtMPK6	H_2O_2	*Arabidopsis*	H_2O_2 induces ANP1 and further MAPK cascade MAPK cascade induces stress responsive genes	Kovtun et al., 2000
SIMK (46 kDa), MMK3, MMK2 (44 kDa), SAMK,	Yeast elicitor	alfafa	MMK3 activated during mitosis	Cardinale et al., 2000
50 kDa, 46 kDa	cryptogein	tobacco	Independent of ROS, dependent of Ca^{2+}	Lebrun-Garcia et al., 1998
48 kDa	ROS	*Arabidopsis*	MAPK involved in gene activation in response to redox cues	Grant et al., 2000
MMK3	metaphase	*Medicago*	MMK3 involved in cell cycle regulation	Bogre et al., 1999

4.1.3. Objectives

The specific objective of this preliminary work was to investigate if bromoperoxidases in *Fucus* embryos have a role in H_2O_2 detoxification during hyper-osmotic stress and to ascertain if BPO and H_2O_2 can have a function in increasing cell wall strength, thus protecting the cells against further osmotic shocks. In addition, this chapter describes

an introductory study on the involvement of protein kinases, in particular MAPK cascades, during *Fucus* embryo response to hyper-osmotic stress. In particular, the positioning of MAPK in relation to other critical cellular events (Ca^{2+} elevation and ROS production) in the stress-signalling pathway was analysed.

4.2. Material and Methods

4.2.1. Preparation of *Fucus* protein extracts

Fucus spiralis embryos were occasionally used because of availability in higher quantities than *F. serratus*. Moreover, *F. spiralis* were found to produce less polysaccharides during gamete release, making protein extraction easier. Because *F. spiralis* is a higher-intertidal shore species, therefore more adapted to osmotic stress changes, it was decided to use 3 M sorbitol as hyper-osmotic treatment. 3 M was chosen based on the strength of the osmotic solution that produced a decrease in cell volume upon stress comparable to the 2 M with *F. serratus* (not shown).

Embryos were cultured on plastic Petri dishes filled with 100 ml of filtered seawater in unidirectional light at 16°C. At the 2-cell stage, cells were treated with hyper-osmotic solution (seawater + 3 M sorbitol). At various times after stress and during recovery in seawater, cells were harvested by removing the liquid and scraping the embryos off the plate with a razor blade. Material was collected in eppendorf tubes. Seawater was further removed by centrifuging the eppendorfs for a few seconds and aspirating the remaining liquid. Material was then frozen in liquid nitrogen and stored at -80°C.

Protein extracts from treated cells were prepared using a modified protocol from Corellou et al. (2000). All steps were performed at 4°C. To prepare extracts from

treated cells, material was ground with mortar and pestle under liquid nitrogen, and mixed (vortex cycles) with 1.6 ml of extraction buffer (60 mM β-glycerophosphate, 15 mM nitrophenylphosphate, 25 mM MOPS pH 7.2, 1 mM phenylphosphate, 15 mM EGTA, 2 mM dithiothreitol (DTT), 15 mM $MgCl_2$, 1 mM Na_3VO_4, 1 mM NaF, 1 mM leupeptine, 1 mM aprotinin, 10 µg/ml SBTI, 100 µM benzamidine, 0.25 mg/ml Pefablock, 1% PVPP, 0.5% NP40) until cells were well disrupted. Material was then centrifuged at 10 000 g for 10 min and supernatants were collected in clean tubes. Proteins were concentrated using Centricon© and Microcon© centrifugal filter units (Millipore, Bedford, MA, USA) according to manufacturers guidelines.

4.2.2. Preparation of BPO protein extracts (improvement of the protein extraction method)

Fucus serratus embryos were grown on Petri dishes as described in 4.2.1. At 24 h AF they were submitted to hyper-osmotic stress (2 M sorbitol) and material was collected at different times (1 min, 5 min, 15 min 30 min after stress and after 1 h recovery in filtered seawater) as described above and frozen at -80°C. This new modified protocol permitted the use of *F. serratus* as it allowed the removal of excess polysaccharide mucous produced by this species.

Extraction buffer (15 mM EGTA, 20 mM KCl, 15 mM $MgCl_2$, 1% NP40, 2 mM PMSF, 1 mM leupeptine, 1 mM aprotinin) and a small quantity of sand were added to the samples, followed by quick vortex cycles. Extraction was then continued for 30 min at room temperature under agitation. Samples were then quickly frozen in liquid nitrogen and unfrozen at 25°C, and left for 2 h at 4°C under agitation. Cells were

broken by sonication followed by centrifugation at 10 000g 10 min at 4°C. This extraction procedure was repeated on the pellet to increase protein yield. PVPP was then added to the supernatant to eliminate polyphenols, under agitation at 4°C for 30 min, followed by centrifugation at 10 000g at 4°C for 15 min. 100 mM $CaCl_2$ was added to the supernatant to eliminate sugars, and left under agitation at 4°C for 1 h. Samples were centrifugation (10 000g, 4°C during 15 min) and supernatant precipitated with 3 volumes of acetone for 2 h at -20°C. After centrifugation (13 000g, 4°C during 15 min) the pellet was re-suspended in 50 mM Tris buffer pH9. 10 mM Na_3VO_4 was added to restore the activity of the BPO (Jordan et al., 1991).

Protein content was quantified using Bradford assay (BioRad, Hercules, CA, USA). Denaturing loading buffer (100 mM Tris HCl pH 6.8, 10% glycerol, 2% SDS, 0.1% bromophenol blue) was added, and extracts were loaded (same quantity of protein in each well) on SDS-PAGE 10% gels and run at 80 mV. Prestained markers (BioRad) were run parallel to the samples.

After electrophoresis, protein activity was restored in a renaturation buffer (Tris-glycine buffer pH 7.5 0.1% NP40) for at least 2 h with 4 changes of bath at 4°C. Data shown are representative of three replicate experiments.

4.2.3. Detection of bromoperoxidase activity

Detection of bromperoxidase activity was performed as described by Jordan et al., 1991. The method of detection is based on the oxidation of a substrate (o-dianosidine) by bromoperoxidases and H_2O_2 in the presence of halide ions (Br or I^-). After electrophoresis, gels were incubated for 1 h in solution 1 (1 mM o-dianosidine and 10

mM KI in 100 mM phosphate buffer pH 7.4) under constant agitation at room temperature in the dark. Gels were then transferred to solution 2 (10 mM H_2O_2) under agitation in the dark. Brown bands corresponding to BPO activity develop in few minutes.

4.2.4. Immunobloting using anti-BPO

Polyclonal antibodies raised against *Ascophyllum nodosum* bromoperoxidase (anti- A. n. I antibody), a kind gift from Hans Viler, Institute for Pharmaceutical Biology, University of Bonn, Germany, were used to recognize BPO in *Fucus* embryo protein extracts (Jordan and Vilter, 1990). Extracts were boiled for 10 min at 95°C and proteins were resolved on a 10% SDS-polyacrylamide denaturing gel and electrotransfered (0.025 M Tris and 0.192 M glycine) onto a PVDF membrane (Gelman, Ann Harbour, MI, USA). Proteins were stained with Ponceau Red to check the homogeneity of the transfer. Tris buffered saline 0.1% Tween (TBS) was used during all the further procedures. Membranes were blocked in TBS containing 5% skimmed milk and then incubated overnight at 4°C with the first antibody (anti-BPO) at 1:600 dilution. After extensive washing with TBS, proteins of interest were detected using ECF Western Blotting Kit (Amersham Pharmacia). The membranes were incubated in the secondary antibody (anti-rabbit fluorescein linked immunoglobulin 1:1000) in an orbital shaker for 1 h. Membranes were washed 3x with TBS, and then the signal was amplified by incubating membranes for 1 h in the anti-fluorescein alkaline phosphatase conjugate (1:2500) in an orbital shaker at room temperature. After washing 3x with TBS, membranes were incubated 10 min with the ECF substrate, at room temperature in the dark. Excess detection reagent was drained off and blots were

placed in absorbing paper (3MM, Whatman) for 20 min before scanning using a Storm 840 scanner (Molecular Dynamics Inc., Sunnyvale, CA, USA).

4.2.5. Cell wall strength experiments

Fucus serratus zygotes were grown in small plastic Petri dishes until 24 h-old. Treatments were carried out as described in Table 4.1 and 4.2. For each of the three replicate cultures, 100 embryos were counted, and results are representative of 2 independent experiments. Cell wall strength was measured by the capacity to withstand a hypo-osmotic shock (50% seawater) (Taylor et al., 1996; Bisgrove and Kropf, 2001).

4.2.6. In-gel kinase activity assay

In-gel kinase activity assays were performed using an adapted protocol from Zhang and Klessig (1997). Extracts from equal quantities of cells (60-80 µl of 1-2 mg/ml protein extracts) were electrophoresed on 10% (w/v) SDS-polyacrylamide gels with the kinase substrate myelin basic protein (MBP, Sigma, 0.25 mg/ml) embedded in the separating gel. Proteins were renaturated after electrophoresis by removing SDS with3x 30 min washes with washing buffer (25 mM Tris pH 7.5, 0.5 mM DTT, 0.1 mM Na_3VO_4, 5 mM NaF, 0.5 mg/ml BSA, 0.1% Triton X-100) at room temperature. This was followed by incubation in renaturation buffer (25 mM Tris pH 7.5, 1 mM DTT, 0.1 mM Na_3VO_4, 5 mM NaF) at 4°C overnight with three changes of buffer. The gel was first equilibrated at room temperature in reaction buffer (25 mM Tris pH 7.5, 2 mM EGTA, 12 mM $MgCl_2$, 1 mM DTT, 0.1 mM Na_3VO_4) and the reaction was started by addition of ATP (90 µM cold ATP and 50 µCi γ-^{32}P-ATP) for 60 min at 30°C. The reaction was stopped by transferring the gel into 5% trichloroacetic acid (50

ml/l) / 1% sodium pyrophosphate (10 g/l) and the gel was washed until no radioactivity was detected in the solution (5 x 30 min approximately). Gels were then dried and analysed with a Phosphorimager (Molecular Dynamics, Sunnyvale, CA, USA). Phosphorylation of substrate protein was quantified using ImageQuant (Molecular Dynamics).

4.2.7. Immunoblotting with anti-ERK

Proteins were resolved on a 10 or 12% SDS-polyacrylamide denaturing gel and electrotransfered (0.025 M Tris and 0.192 M glycine) onto a nitrocellulose membrane (Amersham Life Science, Buckingamshire, UK). Proteins were stained with Ponceau Red to check the homogeneity of the transfer. Tris buffered saline 0.1% Tween (TBS) was used during all the procedures. Membranes were blocked in TBS containing 5% skimmed milk and then incubated overnight at 4°C with the first antibody. A range of primary anti-MAPK antibodies was used to assess sensitivity and specificity of the reactions.

Anti-MAPK (ERK1, ERK-2):

Source: rabbit

Immunogen: a synthetic peptide corresponding to amino acids 317-339 derived from sub-domain XI of human MAPK (ERK1).

Notes: By immunoblotting, this antibody reacts with ERK1 and ERK2

Forms used in the present study:

- Unconjugated (M5670, Sigma) (whole serum) at a 1/8000 dilution
- Agarose conjugate (A3960, Sigma). Prepared using IgG fraction of M5670.

Anti-MAPK (ERK1) (M7927, Sigma):

Source: rabbit

Immunogen: A synthetic peptide corresponding to amino acids 351-368 of human ERK1. IgG fraction of antiserum.

Notes: By immunoblotting, the antibody reacts with ERK1 and ERK2. Dilution: 1:5000.

Monoclonal anti-MAPK activated (diphosphorylated ERK1, ERK-2):

Source: mouse

Immunogen: a synthetic peptide corresponding to the phosphorylated form of ERK-activation loop.

Forms used in the present study:

- unconjugated (M8159, Sigma) at 1:10000 dilution

Control blots were performed which consisted in incubating the membranes only in the secondary antibody to ensure specificity of reaction (not shown).

The membranes were washed 3 times in TBS and incubated in the secondary antibody (goat anti-rabbit IgG coupled to horseradish peroxidase, BioRad Laboratories Hercules, California). After extensive washing with TBS, proteins of interest were detected using enhanced chemiluminescence (ECL, Amersham) or alkaline phosphatase reagents when appropriate after exposure on an autoradiography film Hyperfilm MP (Amersham).

ERK sequence alignment was performed using the program Clustal W (version 1.81) Multiple Sequence Alignment (Thompson et al., 1994). ERK sequences access number were: ERK1 – XP055766; ERK2 – NP620407 and ERK5 – U25278.

4.2.8. Immunoprecipitation and *in vitro* assay of MAPK activity

All procedure steps were performed at 2-8°C. anti-ERK1,2 antibody coupled to agarose beads (A3960, Sigma) was diluted (1:6) in HNTG buffer (20 mM HEPES pH 7.5, 150 mM NaCl with 0.1% (w/v) Triton X-100, 10% (w/v) glycerol). Protein extract (1.6 ml) was incubated with 140 µl of the antibody at 4°C during 1.5 h with agitation. Agarose bead-protein complexes were washed 4x (centrifugation at 4000g 1 min 4°C) with HNTG with 1:1000 Pefablock. 20 µL of buffer K (60 mM β-glycerophosphate, 30 mM nitrophenylphosphate, 25 mM MOPS pH 7.5, 5 mM EGTA, 15 mM $MgCl_2$, 1 mM DTT, 0.1 mM vanadate), 5 µL MBP (6 mg/ml), 90 µM of cold ATP (stock 0.1 M at -20°C) and 0.2-0.4 µL ^{32}P ATP (2-4 µCi) were incubated at 30°C for 30 min and then vortexed every 3 min to re-suspend the beads and improve the reaction. 4x Laemmli buffer elution of the bead complex was added and boiled at 100°C during 10 min. MBP was resolved on a 15% separating gel. The gel was dried and analysed using Phosphorimager (Molecular Dynamics). Quantification of the relative kinase activities was performed using ImageQuant (Molecular Dynamics).

4.2.9. Inhibitors

Apigenin (Calbiochem) was dissolved in 0.1% DMSO to a final concentration of 10 µM in filtered seawater. Staurosporine (Sigma) was also dissolved in 0.1% DMSO to a final concentration of 1 µM in filtered seawater. For confocal laser scanning microscopy experiments (see Chapter 3) cells were pre-incubated in the inhibitors for 1 h before the beginning of the experiment, and the inhibitors were present in the perfused hyper-osmotic solution.

4.2.10. Confocal laser scanning microscopy

CM-DCFH$_2$-DA and Ca^{2+} labelling methods are described in detail in Chapter 3.

4.3. RESULTS

4.3.1. Peripheral ROS production and osmotic adaptation

Experiments were carried out to test cell wall resistance to osmotic shock in control and pre-treated embryos. Hypo-osmotic shock (from seawater to 50% seawater) caused a significant proportion (25%) of rhizoid cells to rupture in control embryos (Table 4.2). However, hyper-osmotic pre-treatment rendered embryos more tolerant to osmotic bursting in response to subsequent hypo-osmotic shock (Table 4.2, 4.3). Moreover, pre-treatment of embryos with 100 μM or 500 μM H_2O_2 also induced an increase in resistance to hypo-osmotic shock. DPI completely abolished the hyper-osmotic stress-induced osmotic adaptation. In contrast, treatment with the PLC inhibitor U73122 did not affect the acquisition of osmotic resistance.

Table 4.2. *Resistance to hypo-osmotic shock in pre-treated and control 24 h old embryos.*

[a]Pre-treatment	[d]Rhizoid cell bursting in response to subsequent hypo-osmotic shock (% of control)
Control (no pre-treatment)	100
[b]Sorbitol 2 M	13.5
Sorbitol 2 M+ U73122	19.2
Sorbitol 2 M + U73443	23.1
Sorbitol + DPI	101.9
DPI	100.7
[c]100 μM H_2O_2	30.8
[c]100 μM H_2O_2 + U73122	36.5
[c]100 μM H_2O_2 + U73343	38.5
500 μM H_2O_2	23.1
500 μM H_2O_2 + U73122	23.1
500 μM H_2O_2 + U73343	32.7
[e]BPO 100 units/ml	0
[e]BPO 500 units/ml	0

[a] Pre-treatments were given 1 h prior to a hypo-osmotic shock (50% seawater).

[b] Sorbitol pre-treatment was given for 30 min.

[c] H_2O_2 and U73122/U73343 were applied for 2 min (pre-treatment with U73122/U73343 for 2 h).

[d] A minimum of 100 embryos were counted per replicate. Bursting was recorded 5 min after hypo-osmotic shock. Values represent the average of 3 replicates and are representative of 2 independent experiments.

[e] Cells were incubated in BPO (purified extract dissolved in seawater) for 16 h (since 6 h AF). At BPO 500 units/ml 40% of the cells died, so the counting was performed in the surviving ones.

Table 4.3. *Resistance to hypo-osmotic shock in pre-treated and control 48 h old embryos*

[a] Pre-treatment	[d] Rhizoid cell bursting in response to subsequent hypo-osmotic shock (% of control)
Control (no pre-treatment)	100
[b] Sorbitol 2 M	33.3
Sorbitol + DPI	106.8
DPI for 1 h	105.4
[c] 100 μM H_2O_2	12.1
[c] 500 μM H_2O_2	21.2
[e] BPO 100 units/ml	0
[e] BPO 500 units/ml	0

[a] Pre-treatments were given to 48 h-old zygotes, 1 h prior to the hypo-osmotic shock (50% seawater).

[b] Sorbitol pre-treatment was given for 30 min.

[c] H_2O_2 was applied for 2 min.

[d] A minimum of 100 embryos were counted per replicate. Bursting was recorded 5 min following hypo-osmotic shock. Values represent the average of 3 replicates and are representative of 2 independent experiments.

[e] Cells were incubated in BPO for 24 h.

4.3.2. Bromoperoxidases and cell wall resistance

Table 4.2 and 4.3 show a dramatic effect of BPO in the acquisition of cell wall resistance to osmotic shock. Because BPO treatment in very young cells (6 h old) did not allow them to completely form a normal rhizoid cell (they germinated and divided but did not form an elongated rhizoid as the control cells), experiments were also performed in a later stage, i.e., at 24 h old, to be sure that the observed cell wall strengthening was not a matter of cell geometry. So, experiments were performed in which cells were continually incubated in BPO from 24 h AF and subsequent osmotic

resistance tests were made at 48 h AF. Table 4.3 shows the result of this experiment. Although some differences were observed in the percentage of bursting between 24 h old and 48 h old embryos (for example sorbitol 2 M pre-treatment induced more cell wall resistance in younger embryos), the general trend is consistent: sorbitol or H_2O_2 pre-treatment rendered embryos which resist better to subsequent hypo-osmotic shock. Although in young embryos BPO had some toxic effect at 500 units/ml (approximately 40% cell death) the cells that survived acquired very high osmotic resistance at all ages tested. Furthermore, continuous incubation in the presence of BPO considerably diminished rhizoid elongation (Figure 4.2).

4.3.3. BPO in-gel activity

To determine whether BPO activity changed after hyper-osmotic stress, an in-gel BPO activity assay was performed. Two protocols of protein extraction were tested:

The first one has been used for *Fucus* general protein extraction (Corellou et al., 2000a; 2000b). Using this protocol, native gel electrophoresis was performed to check changes in the activity of BPO. Five replicate experiments were performed, but problems with reproducibility of results were found. The crude extracts were very impure, with large amounts of polysaccharides, pigments and phenolic compounds that potentially interfered with the BPO activity detection.

Due to the problems found using the above protocol, a new extraction method was developed. The method is based on the fact that peroxidases, in particular bromoperoxidases, are highly resistant to conditions that cause inactivation of other proteins. For example, *Laminaria* sp. vanadium-dependent haloperoxidases are very

A

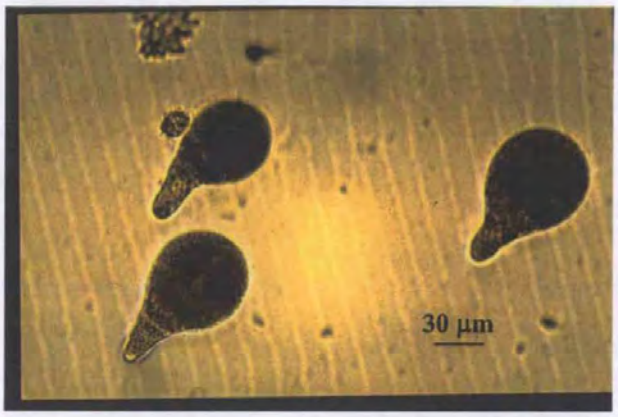

B

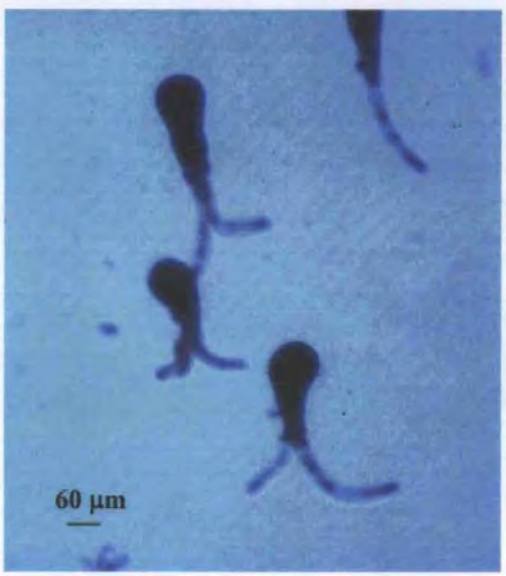

Figure 4.2. Effect of BPO on *Fucus* embryos early development. A) *Fucus* embryos at 72 h after fertilization continuously incubated in 100 units/ml BPO since 24 h AF. **B)** Control 72 h old embryos, grown in filtered seawater.

stable in the range 25-50°C, and an enhanced activity is observed at 40°C (Almeida et al., 2001). The extraction method used in combination with electrophoresis in denaturing conditions (which allowed determination of the size of the proteins) rendered gels more consistent and reproducible, and in which the activity of BPO could be further restored and qualitatively measured.

Figure 4.3 shows an activity gel assay based on protein fractionating by SDS- PAGE followed by regeneration of the BPO activity. This gel is representative of three independent replicates. Three bands with very close high molecular weighs (approximately 200 kDa) could be observed. The two lower bands seemed to be more intense after 5 min of hyper-osmotic treatment, and the intensity decreased 15 min after stress.

An *in vivo* BPO staining method using o-dianosidine (Fast Blue salts, Sigma) was also assayed. Because of the high quantity of *Fucus* embryos brown pigments, problems of accurate visualisation of the staining were found. Still, a preferential localisation of signal was observed at the rhizoid cell wall level, but the method was not precise enough to quantify the amount of BPO before and after hyper-osmotic stress (not shown).

4.3.4. Immunoblotting with anti-BPO

The antibody against BPO used in this study has been developed in *Ascophyllum nodosum*, another brown algae, but is known to react with BPO from *Fucus* sp. embryos (Delange, Station Biologique de Roscoff, unpublished). Figure 4.3 B shows a western blot obtained from crude protein extracts of *Fucus*. Although a high background was

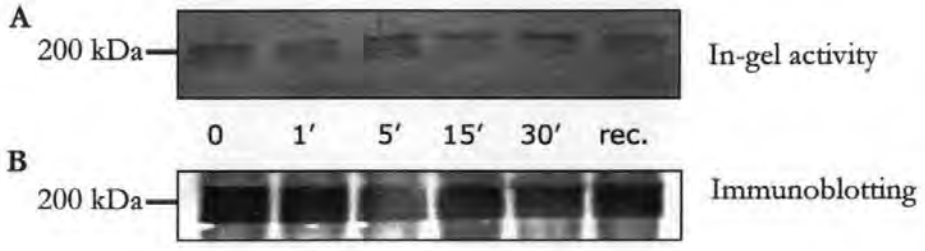

Figure 4.3. Bromoperoxidase in *Fucus* embryos at various times after hyper-osmotic stress. A) BPO in-gel activity assay. Protein extracted at different times after stress and recovery (rec) were resolved in a 10% denaturing gel and activity was restored in gel as described in material and methods section. **B)** Immunoblot with anti-BPO. After migration, proteins were electrotransfered to a PVDF membrane and probed with anti-BPO antibody using ECF Western Blotting kit (Amersham).

present, a group of bands could be seen at a molecular weight (approximately 200 kDa) comparable with the bands detected in the in-gel activity assay. The intensity of the bands was found not to change consistently (n=3) during hyper-osmotic stress treatment, indicating that the same amount of protein was present throughout all the times.

4.3.5. Detection of MBP kinase activity by in-gel assay

To investigate the involvement of protein kinases in the response to hyper-osmotic stress, cells were stimulated and the kinetics of the kinase activation was assessed by an in-gel assay using MBP as substrate (Figure 4.4). Two major signals were detected, at 48 and 120 kDa, respectively. The activity of p48 did not show significant change during osmotic stress. When a control in-gel assay was performed in the absence of MBP, the same 48 kDa protein was visible (Figure 4.5). A protein of 120 kDa was found to be activated progressively after hyper-osmotic stress showing a maximal activation after 30 min (activation factor of about 3.0 fold). During recovery (transfer of the embryos to filtered seawater), the activity of this protein decreased to that of unchallenged levels.

4.3.6. Immunoprecipitation of MAPK

Protein extracts were immunoprecipitated using the antibody anti-ERK1,2 coupled to agarose beads (A3960, Sigma). The immunoprecipitates were assayed for *in vitro* kinase activity using MBP as substrate. This method ensures better accessibility of the proteins to the substrate and is more reliable for detection of MAPK since proteins were previously purified by immunoprecipitation. The substrate MBP was then

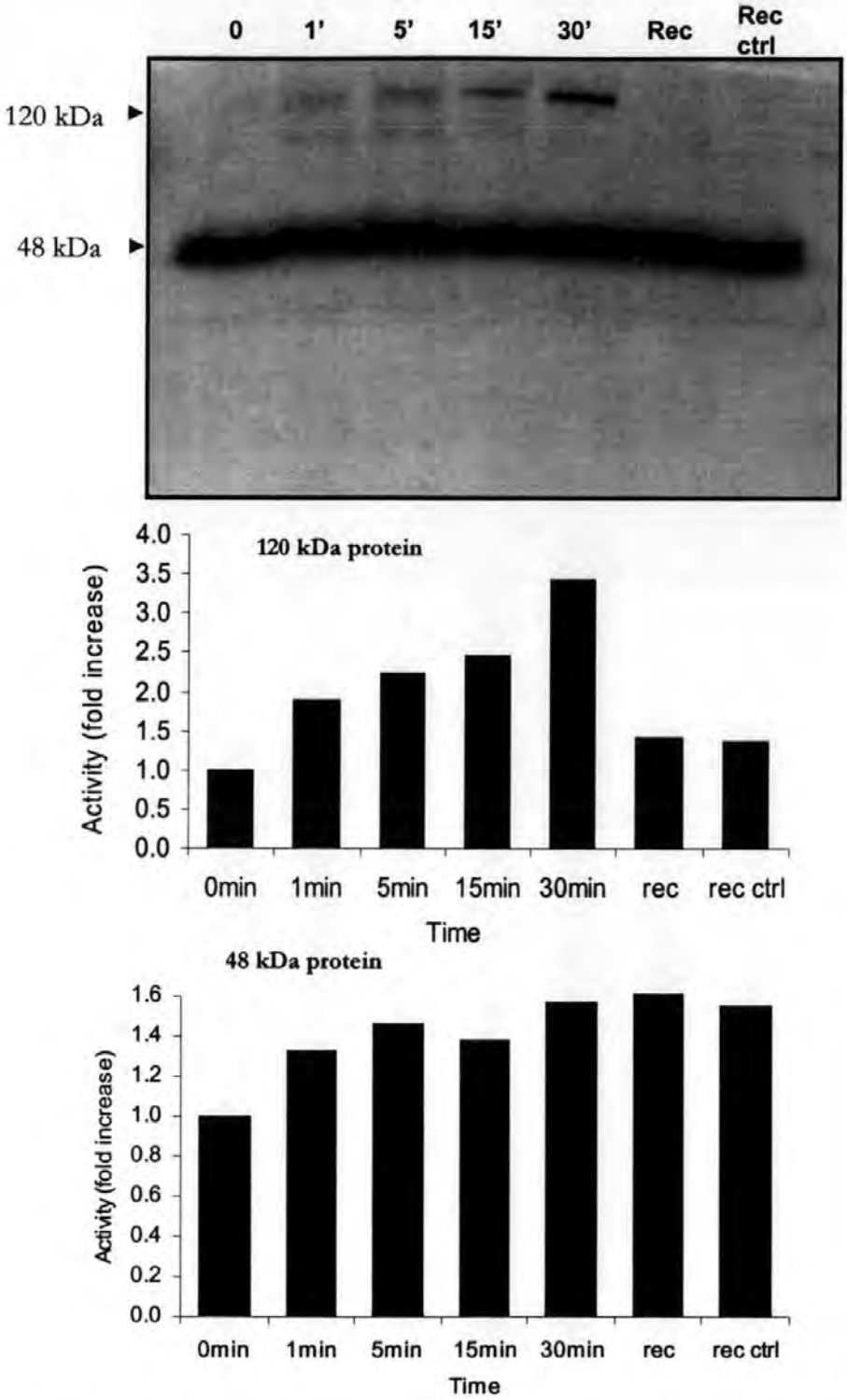

Figure 4.4. MAPK *in gel* assay. Protein extraction and in gel assay was performed as indicated in Material and Methods. Numbers indicate minutes after onset of the hyper-osmotic treatment. The 1 h recovery period is also indicated (*Rec*). Note the high activity of a 48 kD protein throughout all the times and the induction of the activity of a high molecular weight protein (120 kD). A control was included which consisted in 27 h old embryos to ensure that age of the embryos was not a interfering factor (*Rec. ctrl*). In the graphs, fold increase is in respect to time zero.

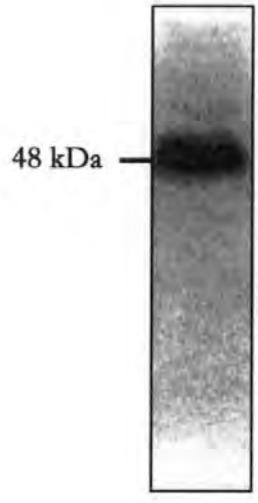

Figure 4.5. Control *in gel* assay in the absence of myelin basic protein. Note that the 48 kDa protein that was permanently detected in Figure 4.4 is present even in the absence of MAPK substrate.

resolved by SDS-PAGE and activity was quantified by phosphorimaging. MBP kinase activity increased by approximately 3-fold in the first 15 minutes following the hyper-osmotic shock (Figure 4.6). When cells were allowed to recover in filtered seawater, the activity progressively decreased and reached levels from unchallenged embryos after a 1 h-recovery period. A basal activity was observed even in the absence of hyper-osmotic stress.

4.3.7. Immunobloting with anti-ERK

Figure 4.7 shows immunoblots in which the antibody anti-ERK1 (M7927) was used. This antibody was raised against human ERK1. By immunoblotting, though, it cross-reacts both with ERK1 and ERK2. By using ECL detection, different bands between 29 kDa and 120 kDa were visible at all times before and after hyper-osmotic stress (Figure 4.7 A). To ensure that specific labelling of the bands was taking place with ECL, additional experiments were performed to compare bands detected by ECL with a another method, alkaline phosphatase (AP) (Figure 4.7 B). Approximately the same bands were found when either method was used. A 120 kDa protein could be detected by the antibody in all the gels shown. However, in Figure 4.7 A a lower band at approximately 29 kDa was visible, whereas it was less obvious in 4.7 B. In addition, a band at ~36 kDa (* in Figure 4.7 A) was also undetected in Figure 4.7 B. A Red Pouceau stained gel is shown in C.

Figure 4.8 shows a preliminary immunoblot obtained with the antibody diphosphorylated anti-ERK1,2 (M8159). Several proteins between 29-36 kDa that were recognised by the antibody seem to show an increase in intensity upon hyper-osmotic stress (*a* to *e*) althought care should be taken as the transfer seems not to be

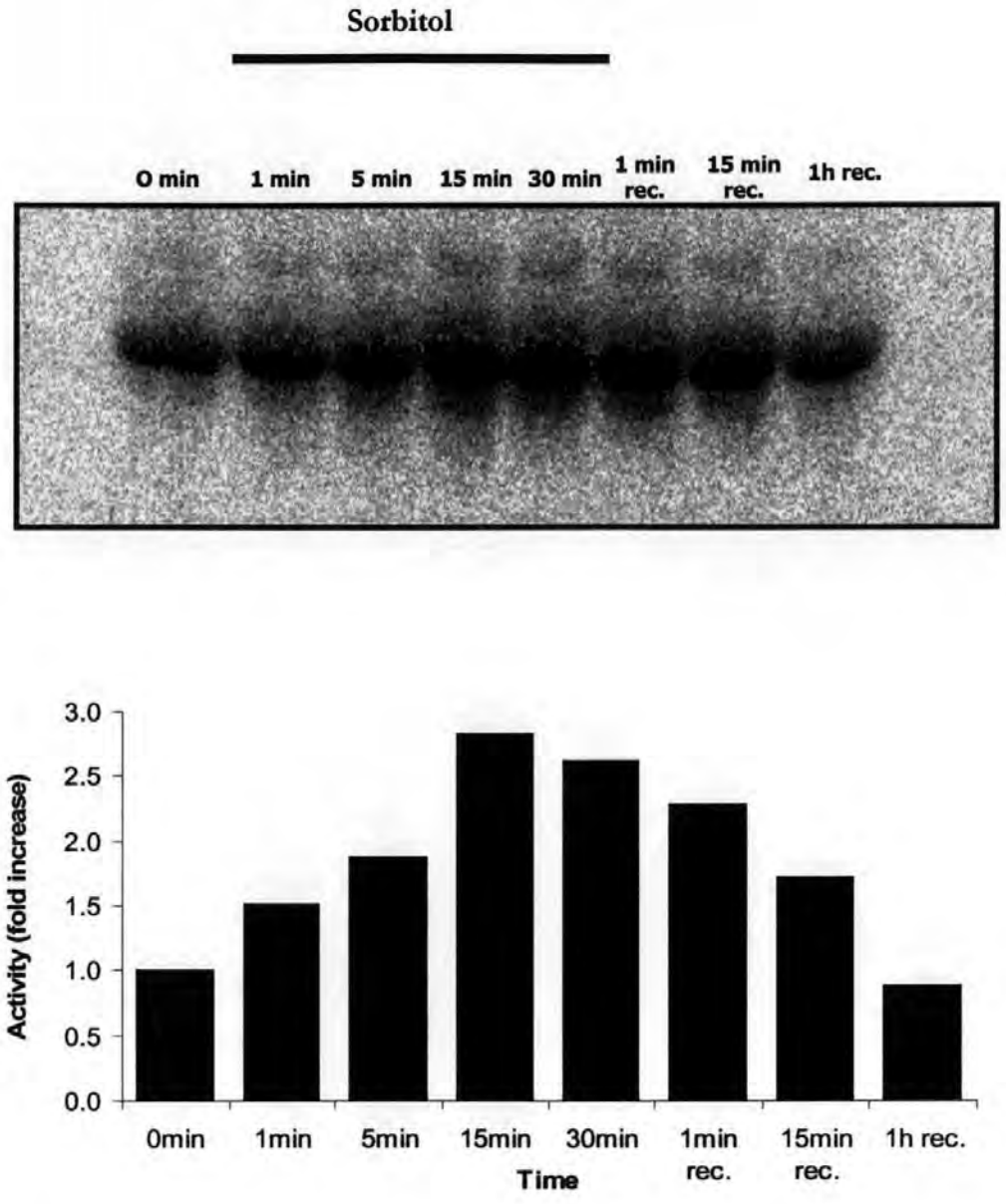

Figure 4.6. Kinase activity *in vitro* assay. Protein extracts prepared from hyper-osmotically stressed zygotes at different times were immunoprecipitated with anti-ERK1,2 conjugated to agarose. Activity was assayed *in vitro* by addition of MBP. The extent of MBP phosphorylation was evaluated by SDS-PAGE followed by phosphorimaging (Molecular Dynamics, Sunnyvale, CA). Each lane indicates the time after onset of the hyper-osmotic treatment and respective recovery in filtered seawater.

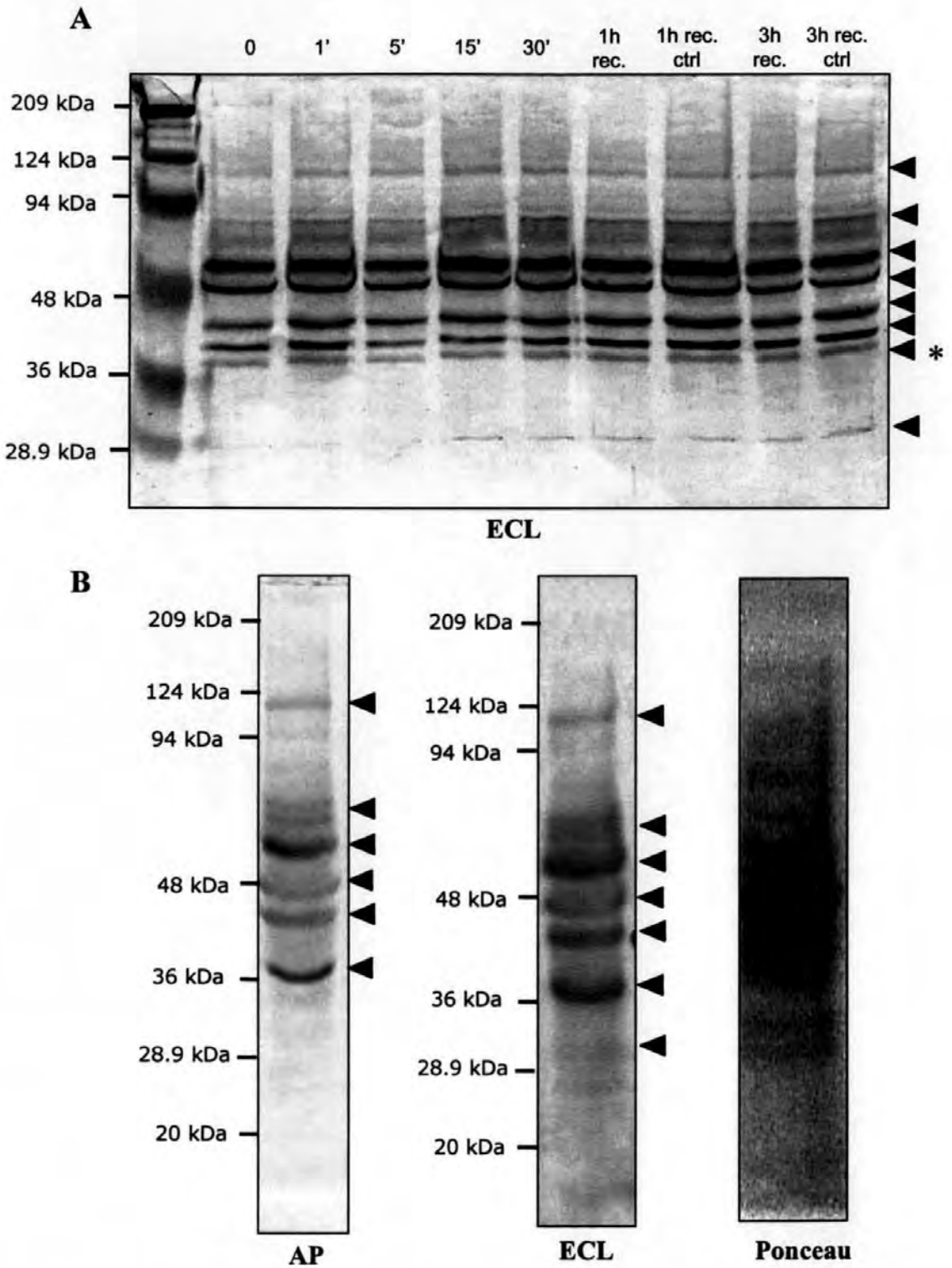

Figure 4.7. Immunodetection of MAPK in *Fucus* embryos using anti-ERK1 antibody. **A)** ECL detection of kinase activities during various times after hyper-osmotic stress and recovery in filtered seawater. Pre stained markers are shown in the first lane. **B)** Alkaline phosphatase (AP) and ECL detection of 15 min stressed *Fucus* embryos protein extracts. **C**) Red Ponceau staining.

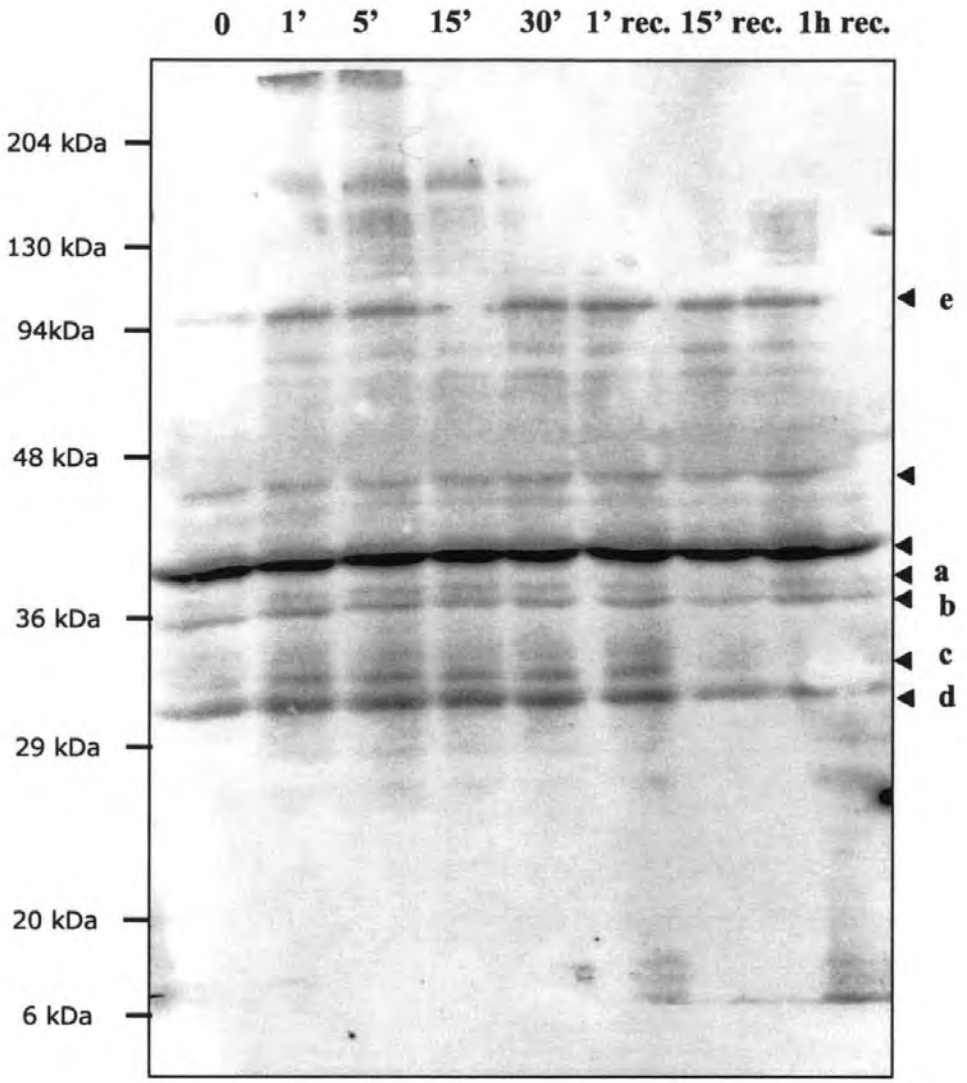

Figure 4.8. Immunoblot using anti-ERK-1,2 diphosphorylated (M8159). Bands represent activated forms of ERK. Bands indicated with **a, b, c, d** and **e** seem to have an increase in intensity during hyper-osmotic stress.

homogenous. These proteins seem to be activated between approximately 1 -5 min after stimulation. The presumptive activity was reduced to unchallenged levels 1-15 min after embryos were returned to filtered seawater.

A western blot of *Fucus* protein extracts probed with anti-ERK1,2 is shown in Figure 4.9. Both methods (AP and ECL) detected the presence of a large band between 29 and 36 kDa, that could correspond to the group of bands observed in Figure 4.8 (*b* to *d*). In addition, a band at approximately 94 kDa is recognised.

4.3.8. Effects of apigenin and staurosporine on Ca^{2+}_{cyt} elevation and ROS

When 10 μM apigenin was present during the immunoprecipitation and *in vitro* assay, a decrease in the activity of the MBP kinase was observed (Figure 4.10). Interestingly, when *Fucus* embryos were incubated in the presence of the same concentration of apigenin, the onset of the Ca^{2+}_{cyt} elevation in response to hyper-osmotic stress was not affected (Figure 4.11, n=3). Moreover, apigenin did not inhibit the mitochondrial oxidative burst in 70% of the cells tested, and had an inhibitory effect in the other 30% (Figure 4.12, n=7). In contrast, staurosporine completely abolished hyper-osmotic stress-induced ROS production in 100% of the cells tested (Figure 4.13, n=12).

4.4. Discussion

4.4.1. Peripheral ROS production and osmotic adaptation

The present study has shown a functional role for ROS in the response to abiotic stress, which was evident from experiments that monitored adaptation to osmotic

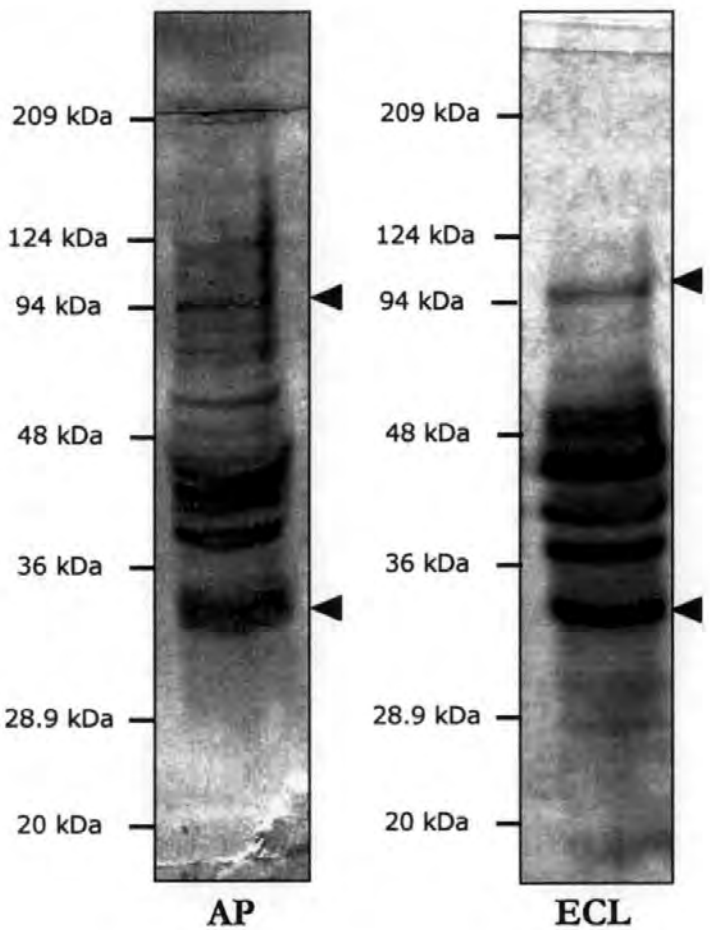

Figure 4.9. Western blots of *Fucus* protein extracts. Blots were probed with anti-ERK1,2 (M5670). Detection was carried out using two different methods, Alkaline Phosphatase (AP) and ECL (see Material and Methods).

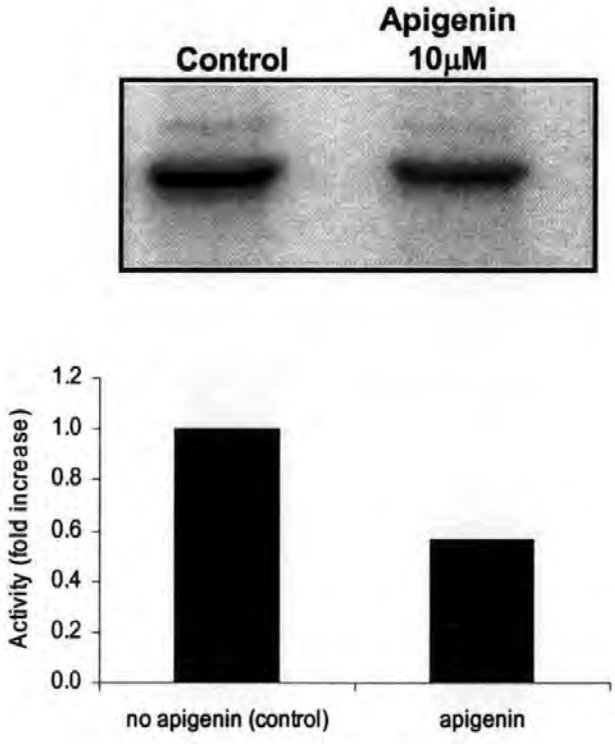

Figure 4.10. ***In vitro*** **effect of 10 μM apigenin on MAPK activity.** Extracts were immunoprecipitated with anti-ERK-1,2 coupled to agarose beads (Sigma) in the presence of myelin basic protein (MBP). Phosphorylated MBP was visualized by autoradiography.

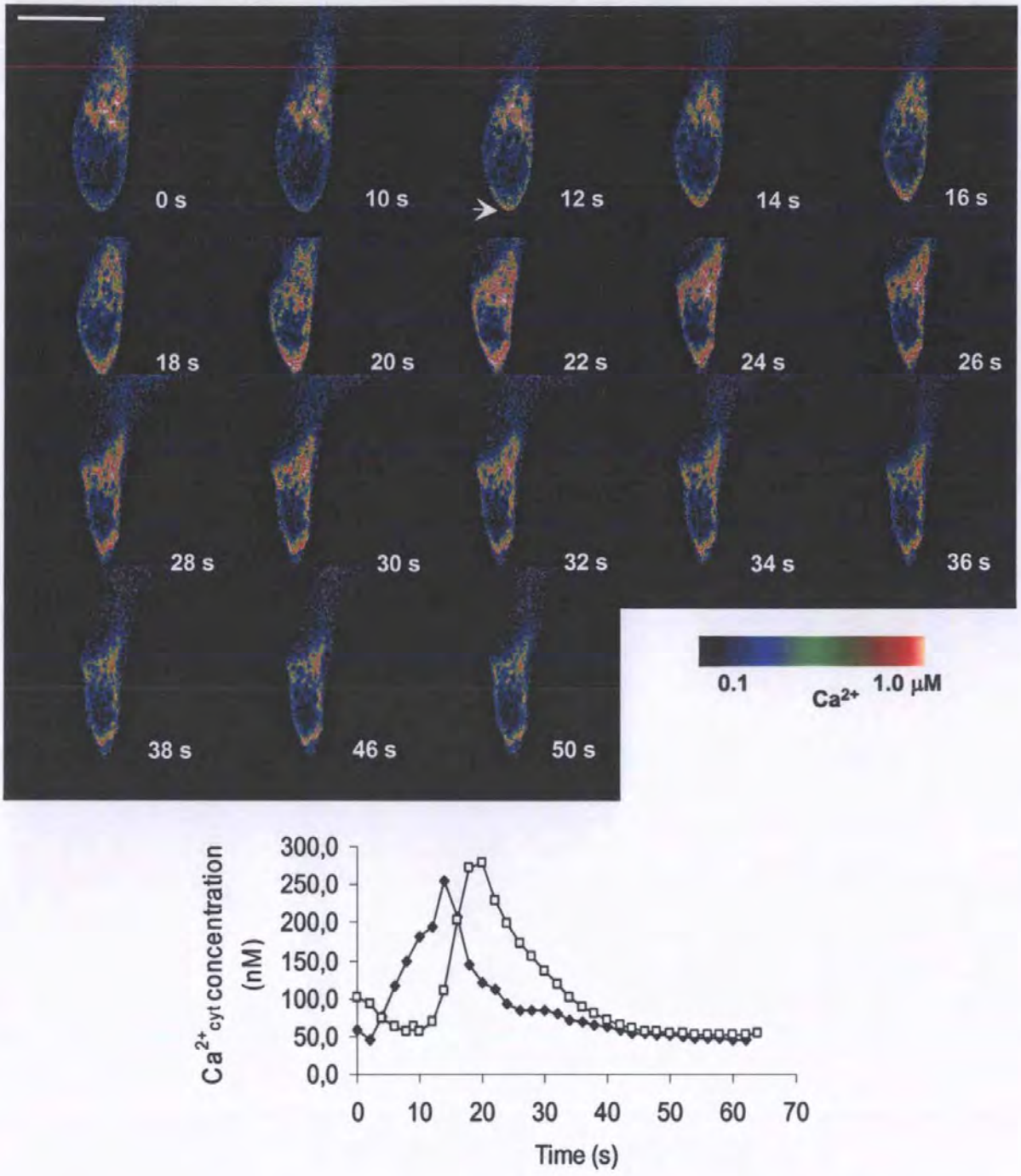

Figure 4.11. Ca^{2+} dynamics during hyper-osmotic treatment in the presence of apigenin. Cells were micro-injected with Calcium green/Texas red and pre-incubated for 1 h in 10 µM apigenin before the beginning of the experiment. **A)** Arrow indicates the on set of the Ca^{2+} elevation. Approximately 1.8 sec between images. **B)** Time course of Ca^{2+} elevation in presence of apigenin (full diamonds). Graph represents quantification of the fluorescence from the rhizoid represented in A. Bar = 30 µm. A control in the absence of apigenin (empty squares) is also shown.

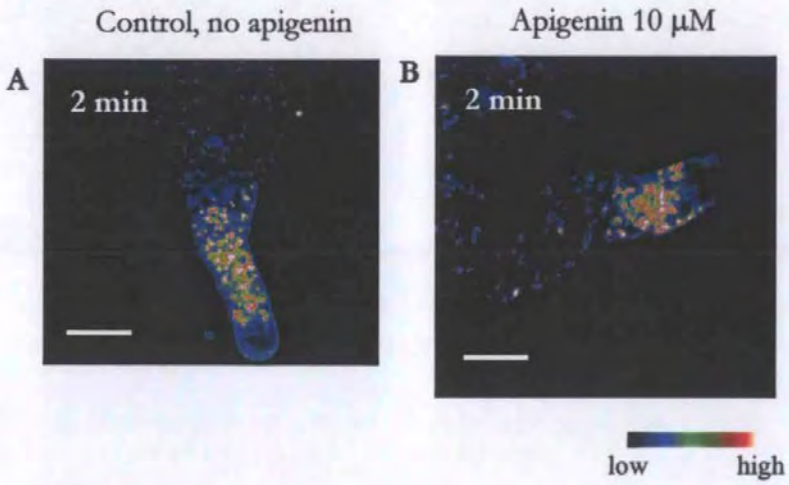

Figure 4.12. ROS production in response to hyper-osmotic stress in the presence of apigenin. A) Control cell (no apigenin) 2 min after onset of the hyper-osmotic treatment. **B)** Rhizoid of a representative cell, 2 min after onset of the hyper-osmotic treatment in the presence of 10 µM apigenin. Bar = 30 µM.

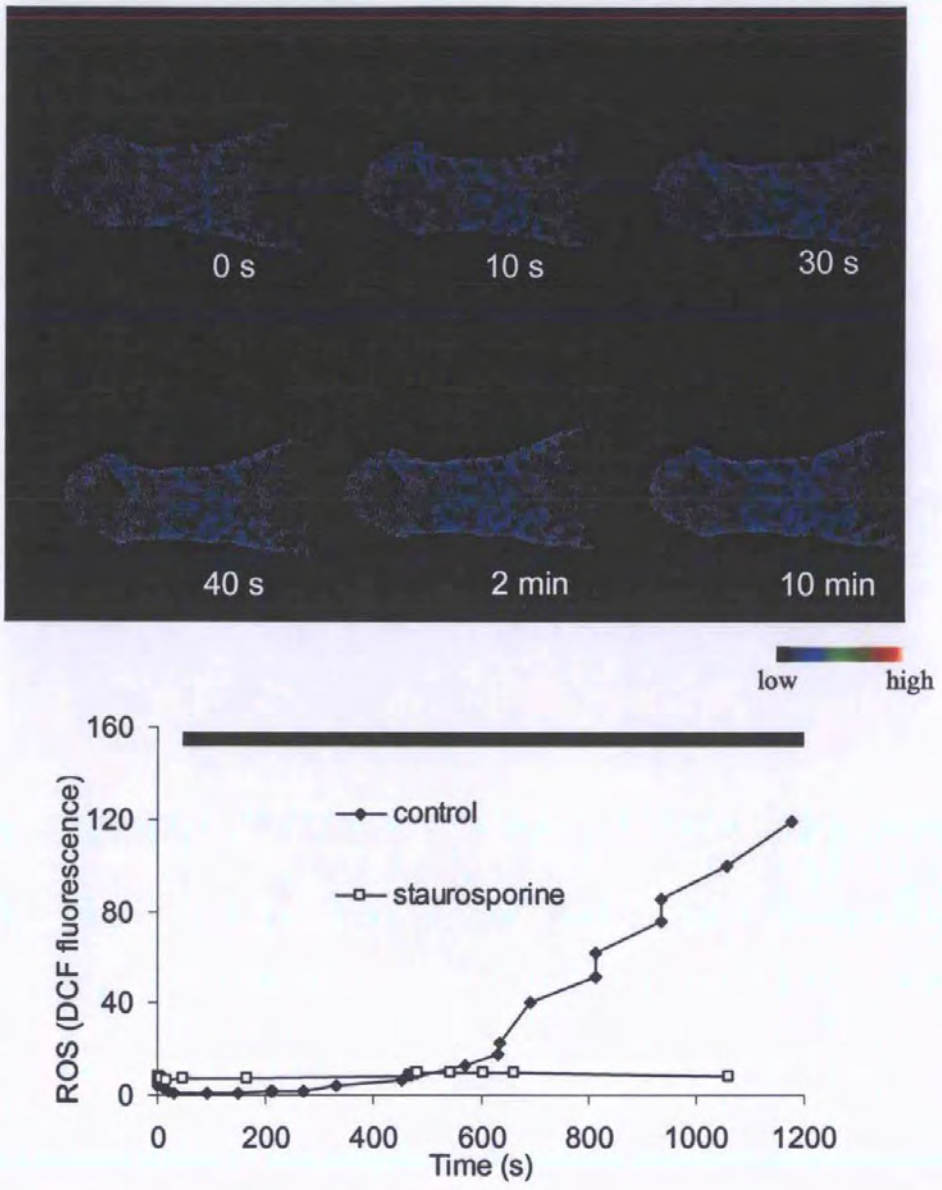

Figure 4.13. Effect of 1 µM staurosporine on *Fucus* rhizoid ROS production during hyper-osmotic treatment. Black bar indicates hyper-osmotic treatment (seawater + sorbitol 2 M).

treatments. Hypo-osmotic shock (from seawater to 50% seawater) caused a significant proportion of rhizoid cells to rupture in control embryos. However, hyper-osmotic pre-treatment rendered embryos more tolerant to osmotic bursting in response to subsequent hypo-osmotic shock indicating increased cell wall strength. Pre-treatment of embryos with 100 μM or 500 μM H_2O_2 also induced an increase in resistance to subsequent hypo-osmotic shock, suggesting a causal link between cell wall resistance and ROS production. This was further supported by the complete abolition of the osmotic adaptation by DPI pre-treatment. In contrast, PLC inhibitor U73122 (which blocks the hyper-osmotically-induced Ca^{2+} increase and subsequent mitochondrial ROS production but not the peripheral ROS production, Chapter 3) did not affect the acquisition of osmotic resistance, indicating that the early peripheral ROS production is sufficient to activate cell wall strengthening mechanisms.

The fact that hyper-osmotic or H_2O_2 pre-treatments rendered embryos more tolerant to osmotic bursting in response to subsequent hypo-osmotic shock is consistent with the widely reported role for ROS in increasing cross-linking of cell wall polymers leading to increased cell wall strength in response to stress (Bradley et al., 1992; Fry et. al., 2000). The activation of cell wall resistance mechanisms by hyper-osmotic treatment may function to counter the hypo-osmotic stress that is likely to occur during re-hydration on return to normal seawater following solute accumulation associated with hyper-osmotic adaptation.

4.4.2. Bromoperoxidases and cell wall resistance to osmotic stress

BPO was found to increase dramatically the capacity of embryos to withstand osmotic stress. Furthermore, the fact that continuous incubation in the presence of

BPO diminishes cell wall elongation, reinforces the hypothesis that BPO was involved in cell wall strengthening processes in the *Fucus* rhizoid. This result is consistent with other investigations that show that H_2O_2 produced at the cell periphery may be used by cell wall peroxidase enzymes to cross link cell wall components (Lin and Kao, 2001; Razam and Bernards, 2002).

4.4.3. BPO in-gel activity during hyper-osmotic stress

To determine whether BPO activity changed after hyper-osmotic stress, an in-gel assay was performed based on protein fractionating by SDS-PAGE followed by regeneration of the BPO activity. Consistently, three bands with very close high molecular weighs (approximately 200 kDa) could be observed. The molecular weight of BPO found here is higher than other algal species, as *Corallina officinalis* which BPO subunit has a molecular mass of 64 kDa (Sheffield et al., 1993). *Ascophyllum nodosum*, another Fucales, has a 106 kDa BPO form (Krenn et al., 1989). While it is possible that molecular weight of BPO can vary between algae, a possibility is that the enzyme was not completely denaturated by the method used in the present study and migrated as a multimer.

The three bands found here may correspond to different isoforms of the *Fucus* BPO, as vanadium haloperoxidases from other systems such as *Laminaria* are well known to present different isoforms (Jordan and Vilter, 1991; Almeida et al., 2001). However, studies showed that when electro-eluted separately and purified, the three *Fucus* BPO bands correspond to the same protein (Delange, Station Biologique de Roscoff, unpublished). This may suggest that the slightly different migrations may be due to some distinct modification of the protein, such as differential glycosylation

states. One possibility is that the different bands correspond to protein from distinct cellular location (e.g. cytosol versus cell wall). The two lower bands corresponding to BPO found in the present study seem to be more intense after 5 min of hyper-osmotic treatment, and the intensity decreases 15 min after stress. Although the method for BPO detection used here does not allow relative quantification of the enzyme activity, the results provide preliminary evidence that a small transient activation of BPO may take place a few minutes after hyper-osmotic stress.

4.4.4. Immunoblotting with anti-BPO

In parallel with the in-gel activity, denaturing gels for immunoblotting using anti-BPO were prepared. Western blot showed a group of bands at a molecular weight (approximately 200 kDa) comparable with the bands detected in the in-gel activity. The fact that the intensity of the bands did not change significantly during hyper-osmotic stress indicates that no *de novo* synthesis of BPO occurred upon stimulation, and suggests that BPO is already present before treatment but was positively regulated during stress, potentially by its substrate, H_2O_2. One possibility is that the enzyme has been mobilised from the cytosol to the cell wall after hyper-osmotic treatment. Further experiments using differential protein extraction procedures could be carried out to test this hypothesis.

4.4.5. Protein kinase activation and hyper-osmotic stress

4.4.5.1. Hyper-osmotic stress activated MBP phosphorylating kinases in Fucus *embryos*

The preliminary results presented here indicate that various protein kinases might have been activated by hyper-osmotic stress in *Fucus* embryos. Some lines of evidence

suggest that this group of kinases may belong to the MAP kinase family. They were recognised by several antibodies raised against MAPK, and activation was associated with phosphorylation of MBP based on immunoprecipitation with an anti-ERK1,2 antibody and *in vitro* kinase assay. Moreover, *in vitro* phosphorylating MBP kinase activity was reduced by apigenin, a MAPK inhibitor. However, care should be taken in drawing conclusions, as the results do not allow to determine which kinase recognised by the diphosphorylated anti-ERK1,2 was responsible for the MBP phosphorylation observed in the *in vitro* assay. Because the precipitated protein in the *in vitro* assay was not tested for size, and also because western blots with the antibodies may produce non specific bands, it is possible that a non-MAPK activity is precipitated and responsible for the MBP phosphorylation *in vitro*.

It is interesting to note that the kinetics of phosphorylation of some of the proteins detected by diphosphorylated anti-ERK1,2 paralleled the activation kinetics seen *in vitro*. However, more replicates would be necessary to rigorously ascertain the number, identity and activation dynamics of the set protein kinases found here.

The downstream functions of MAPK on the *Fucus* osmotic stress-signalling pathway remain to be determined. The location of an enzyme in the cell is a key determinant of its actions. In the case of MAPK their localisation is highly regulated although the underlying processes are still obscure (reviewed by English et al., 1999). In many cells, stimulation causes translocation of ERK1,2 to the nucleus where they activate transcription factors and regulate gene expression (reviewed by Kyriakis and Avruch, 2001). This possibility could be tested in *Fucus* by microinjection of anti-ERK1,2 conjugated to FITC and further confocal imaging during hyper-osmotic stress. In *Fucus*

embryos, MAPK could be responsible for activation of further stress adaptation-downstream responses, such as induction of osmotically active substances (similarly to the HOG1 pathway in yeast), induction of stress/resistance genes and cell wall strengthening-related compounds. Different MAPK are known to activate and regulate different types of transcription factors at the nucleus level (reviewed by Hohmann, 2002). The set of MBP phosphorylating kinases preliminarily reported here could be activating different transcription factors or regulating expression of several genes responsible for distinct downstream functions in cellular osmotic stress adaptation.

Interestingly, a high molecular weight protein (120 kDa) showed a clear increased activity upon hyper-osmotic stress. However, a control should be performed in the absence of osmotic stress (iso-osmotic control) to ensure that there is no effect of the experimental manipulation of the zygotes on this kinase activation.

Due to the presence of the constitutively abundant protein (presumably Rubisco), it is conceivable that MAPK with molecular weights around 48 kDa have been masked Further improvements of the protein extraction method, such as an ultra-centrifugation step to remove chloroplasts, could eventually solve this problem.

4.4.5.2. MAPK activation independent of Ca^{2+} and ROS elevation

An involvement of Ca^{2+} signalling upstream of MAPK cascade pathways has been proposed based on the observation that MAPK activation in tobacco was prevented by addition of Ca^{2+} channel blockers (Lebrun-Garcia et al., 1998). In plants, Ca^{2+} increases have been reported in response to several biotic and abiotic stimuli, indicating that Ca^{2+} is capable of fast transduction of stress signals (Chapter 3 and references therein). In particular, a Ca^{2+} increase is observed upon hypo- and hyper-

osmotic treatment in the *Fucus* rhizoid cell (Taylor et al., 1996; Coelho et al., 2002). Ca^{2+} has also been shown to be absolutely required for activation of a set of MAPKs in tomato cells stimulated by a pathogen elicitor, and the authors proposed that a specific Ca^{2+} signature is involved in MAPK activation (Link et al., 2002). The results presented here suggest that hyper-osmotic stress-induced Ca^{2+} elevation takes place upstream or independently of MAPK activation. Because H_2O_2 induces a different Ca^{2+} signature in *Fucus* compared with hyper-osmotic stress (Chapter 3), it would be interesting to test if the activation kinetics, number and identity of the MBP phosphorylating kinases activated by external addition of H_2O_2 and hyper-osmotic stress are comparable.

The present study also suggests that *Fucus* MAPK were activated downstream or independently of the mitochondrial oxidative burst. The order of such events during plant stress responses has been shown to vary considerable between different studies (see Table 4.3). For example, some investigations in higher plants indicate that MAPKs are activated upstream or independently of the oxidative burst (e.g., Lingterink et al., 1997) whereas others indicate that H_2O_2 directly activates MAPK cascades (Kovtun et al., 2000; Yuasa et al., 2001). The interpretation of several studies is however clouded by the lack of accurate measurement of H_2O_2 production and limited specificity of some inhibitors used. To improve the knowledge about the positioning of kinase activation relatively to mitochondrial ROS production and Ca^{2+}_{cyt} elevation in *Fucus*, more experiments could be performed using other MAPK inhibitors (such as PD98059). In addition, the effect of external H_2O_2 on the MBP phosphorylating kinases activation needs to be studied, as well as the effect of oxidative burst and Ca^{2+} blockers.

4.4.6. Conclusions

In conclusion, the results presented here suggest that H_2O_2 has a role in regulating cell wall resistance upon hyper-osmotic stress in the *Fucus* embryo probably through bromoperoxidases. However, additional experiments are required to establish the precise role of this enzyme. Firstly, a differential extraction of BPO from *Fucus* embryos cell wall and protoplasts would be important to establish if there is any mobilisation of the protein from the cytosolic to the cell wall fraction upon stimulation. Secondly, glycosylation studies could be carried out to see if the different bands correspond to differential targeting of the enzyme. In addition, purification of BPO could be performed to allow quantification of bromoperoxidase activity before and after stress by spectrophotometer assays. Moreover, the use of purified BPO extracts would obviate the problems of high background found in the western blots. Finally, cell wall isolation and further chemical analysis would permit assessment of the changes in the cell wall structure that may be responsible for the strengthening process that takes place upon hyper-osmotic stress.

Numerous studies have demonstrated that abiotic stimuli induce activation of several MAPKs in plant cells. It is indicated here that *Fucus* embryos may also respond to abiotic stress with an increase in MBP phosphorylating kinase activity that occurs downstream or independently of Ca^{2+}_{cyt} and mitochondrial ROS elevations.

This preliminary study in *Fucus* suggests that early ROS and Ca^{2+} signals in response to hyper-osmotic stress are associated with very specific downstream cellular responses. The results highlight the potential function of peripheral ROS at the *Fucus* rhizoid cell apex in direct adaptive responses to stress in addition to its role in

patterning Ca^{2+} signals (Chapter 3). Although questions remain to be answered, in particular those concerned with the identity of downstream targets and the specific nature of the activated kinases, this work opens some new perspectives in the study of *Fucus* osmotic stress signalling pathways.

CHAPTER 5

GENERAL DISCUSSION

This chapter provides a general overview of the cellular mechanisms and common features underlying the response of *Fucus* embryos to light and hyper-osmotic stress

5.1. Interaction between ROS and photoinhibition during abiotic stress

In their natural environment, inter-tidal algal species such as *Fucus*, experience dramatic fluctuations in light and external osmotic conditions. This study showed that ecologically relevant high irradiance levels, especially in the presence of ultraviolet A and B, and in combination with desiccation, constitute a physiological stress stimulus for *Fucus* embryos. Two photoinhibition responses were recognised. Firstly, a rapid decline of the photosynthetic efficiency associated with the xanthophyll cycle (photoprotection), followed by a slower second-phase decline, correlated with ROS production (sections 2.3.3. and 2.3.5.). Evidence is accumulating which shows a relationship between ROS production in the chloroplasts and photoinhibition of PSII (Kornyeyev et al., 2001). The data suggest that ROS production might have a positive feedback role in the inhibition of photosynthesis: excess photons during stress induce electron leakage from the chloroplast electron transport chain, potentially generating $^{*}O_2^-$ and H_2O_2. These molecules are likely to damage PSII components, leading to a further decrease in photosynthetic efficiency. Other sources for ROS production cannot be excluded. For example, the activity of NADPH oxidase could counter the effects of excess reductants (NADPH) arising from the chloroplast electron transport chain under high light, also leading to further ROS production. The results presented here do not allow conclusions to be drawn about the origin of ROS in response to high light, UV or hyper-osmotic stress. The general cellular responses to these stresses appear to be similar, i.e., a decrease in photosynthetic efficiency and an increase in

intracellular ROS production. However, various stresses could eventually have distinct targets in the cell. For example, UV-B radiation has been shown to induce ROS production in *Arabidopsis* via the activity of NADPH oxidase and peroxidase(s) (Mackerness et al., 2001), whereas it is assumed that high light induces ROS formation in the chloroplasts (e.g. Irihimovitch and Shapira, 2000). In *Fucus* embryos, hyper-osmotic stress has been shown to stimulate ROS elevation both at the plasma membrane level and in mitochondria (Coelho et al., 2002). High-resolution *in vivo* confocal imaging and double labelling experiments with specific cellular compartment fluorescent dyes would help to give a better insight on the origin of ROS during different stresses.

As a result of enhanced ROS production, a slower recovery of photosynthetic efficiency was observed, particularly with increased effective UV doses and combination of high light/hyper-osmotic treatment. However, *Fucus* embryos showed a remarkable ability to recover from the imposed stresses. Development of the embryos was only transiently affected by UV-B in combination or not with hyper-osmotic treatment (section 2.3.7.). This indicates that although the cellular physiology is dramatically affected, the embryos have well-developed mechanisms of acclimation to or recovery from these stresses. The re-allocation of energy and resources to adaptive molecular changes could be responsible for the transient decrease in growth rate observed, in particular when UV-B was present. It would be interesting to carry out experiments to investigate whether transcript levels of some key stress-related genes (such as antioxidant enzyme genes) are differently expressed and if the different stress factors used here induce distinct downstream molecular responses.

5.2. Spatial and temporal components of the hyper-osmotic stress-induced ROS elevation

The signal transduction events involved in the perception and response of cells to changes in external osmotic pressure are still ill defined, but numerous reports show that Ca^{2+} and ROS play an important role. Using fluorescent confocal laserscan microscopy, the spatio-temporal changes in ROS and Ca^{2+}_{cyt} that take place in two-cell embryos of *Fucus* during a hyper-osmotic shock were imaged *in vivo*. The results presented here show a tight functional coupling of Ca^{2+} and ROS during stress. Two components in the oxidative stress response could be found. A DPI-sensitive and Ca^{2+} elevation-independent early component, which takes place a few seconds after initiation of the hyper-osmotic stress, is localised at the plasma membrane level and is independent of Ca^{2+} elevation (section 3.3.1.). The second component takes place downstream of cytosolic Ca^{2+} elevation, is Ca^{2+} dependent and is located in the mitochondria (section 3.3.4.). Interestingly, a prolonged early peripheral elevation of ROS was observed in the rhizoid apex in the presence of the PLC inhibitor, U73122. This contrasts with the more transient elevation of ROS at the same site in Br_2BAPTA-buffered cells and may reflect the inability of U73122 to block a highly localised plasma membrane influx component of Ca^{2+} elevation leading to elevation of ROS in mitochondria near the cell apex.

While the role of Ca^{2+} elevation in inducing ROS production (and vice versa) in plant cells is already well established, the present work demonstrates the complexity of the plant stress response involving different cellular compartments and more than one second messenger.

5.3. ROS, Ca^{2+}_{cyt} elevation and plasma membrane Ca^{2+} channels

The transient increase in Ca^{2+}_{cyt} arising from hyper-osmotic treatment may be linked to the opening of Ca^{2+} channels in the plasma membrane induced by H_2O_2. Cell-attached patch clamp experiments showed a transient increase in the probability of opening of a cation channel with characteristics of a non-selective Ca^{2+} permeable channel upon perfusion with 1 mM H_2O_2 (section 3.3.6.4). The results indicate that ROS produced at the cell periphery through a DPI-sensitive process can pattern a Ca^{2+}_{cyt} signal. The highly localised nature of H_2O_2 production at the cell periphery during hyper-osmotic stress and further Ca^{2+} elevation in the form of a well-defined propagating wave reveals that the spatio-temporal pattern of a Ca^{2+} signal (Ca^{2+} signature) can be triggered by ROS production at very specific sites. It remains to be determined whether the production of ROS at the growing rhizoid apex also underlies the Ca^{2+} gradient associated with rhizoid germination and growth (Brownlee and Wood, 1986; Taylor et al., 1996; Pu and Robinson, 1998). Speculation can be made in terms of maintenance of a Ca^{2+}_{cyt} homeostasis at the cell apex by continuous controlled production of H_2O_2. The fact that DPI reduces the resting Ca^{2+}_{cyt} level reinforces that hypothesis, although more detailed investigations are required. Further experiments could be performed by monitoring ROS production at the cell apex throughout the developing stages of the rhizoid cell and using catalase and DPI to determine their effects on the Ca^{2+} gradient at the rhizoid apex, on zygote polarisation and on rhizoid growth. Additionally, electrophysiological characterisation of this H_2O_2-sensitive channel and simultaneous patch clamp and Ca^{2+} imaging would provide valuable information on the exact mechanism of Ca^{2+} entry and wave progression during hyper-osmotic stress.

While it is assumed that the main ROS involved in the hyper-osmotic stress response in *Fucus* embryos is H_2O_2, the possibility that $^{\bullet}OH$ radicals are implicated cannot be excluded. Indeed, an interaction between $^{\bullet}OH$ radicals and ion channel activity has recently been made evident (Az-ma et al., 2002).

5.4. Ca^{2+}_{cyt} wave and the role of mitochondria

The opening of the H_2O_2-activated Ca^{2+} permeable channels at the plasma membrane is associated with a cytoplasmatic Ca^{2+} elevation that progresses through the cell as a unidirectional wave (section 3.3.2.). A similar propagation upon stimulation with hypo-osmotic stress has been described, but the spatio-temporal pattern differed considerably depending on the strength of the hypo-osmotic stimulus (Goddard et al., 2000).

The amplitude of the Ca^{2+}elevation was maintained as the wave spread across the cell, suggesting that it progresses as an actively regenerative process and not simply by long-range passive diffusion following release from a point source. The propagating Ca^{2+} wave was associated with a propagating wave of mitochondrial depolarisation at a similar velocity (section 3.3.4.). This strongly indicates that mitochondria take up Ca^{2+} as the wave travels across the cell. To further confirm this, the mitochondrial Ca^{2+} reporter dye X-rhod-FF was used. X-rhod-FF co-localised with MitoTracker Green in dual labelling experiments, allowing changes in mitochondrial Ca^{2+} to be monitored during a stress stimulus. By this method it was confirmed that upon hyper-osmotic stress an elevation of mitochondrial Ca^{2+} took place, which coincided temporally with the declining phase of the cytoplasmatic Ca^{2+} wave and mitochondrial membrane depolarisation (section 3.3.5.).

The underlying mechanism of this potentially negative feedback control exerted by mitochondria upon the Ca^{2+} wave remains to be explored. Current models to account for the propagation of Ca^{2+} signals include a role for $Ins(1,4,5)P_3$ which induces a wave by diffusing through the cell, priming $Ins(1,4,5)P_3$ receptors and releasing Ca^{2+} as puffs from ER release sites (Wang et al., 1997). The rise in Ca^{2+}_{cyt} generates additional $Ins(1,4,5)P_3$ through Ca^{2+}-activation of phospholipase C (Berridge, 1993) providing a positive feedback step. Hypo-osmotic stress in *Fucus* is known to induce elemental Ca^{2+} elevations in ER-rich regions (Goddard et al., 2000), probably through a similar mechanism. The present results highlight the importance of mitochondria in the regulation of propagating Ca^{2+} waves. This role was first demonstrated in oocytes of *Xenopus* (Juaville et al., 1995), and has been corroborated since then by a number of reports in animal cells (Boitier et al., 1999). So far, evidence for the function of mitochondria in regulating spatio-temporal Ca^{2+} signalling is lacking in plants or algae, although mitochondria have been suggested to represent a source of Ca^{2+} for signals elicited in response to anoxia (Subbaiah et al., 1998).

In the *Fucus* rhizoid cell, the mode of propagation of the hyper-osmotically-induced Ca^{2+} wave is still a matter for speculation, but Ca^{2+} induced Ca^{2+} release from internal stores such as the ER is likely and $Ins(1,4,5)P_3$–induced Ca^{2+} release has been demonstrated (Goddard et al., 2000). New molecular techniques, such as post-transcriptional gene silencing (RNA interference; Vaucheret et al., 2001; Caplen et al., 2002), could be used to generate transient phospholipase C knockout zygotes which would allow more thorough investigations of the mode of progression of the Ca^{2+} wave during osmotic stress.

5.5. Distinct downstream roles of different components of ROS elevation

5.5.1. Peripheral ROS production and cell wall strength

A signalling role for H_2O_2 in the response to abiotic stress was evident from experiments that monitored adaptation to osmotic treatments. Thus, hyper-osmotic or H_2O_2 pre-treatments rendered embryos more tolerant to osmotic bursting in response to subsequent hypo-osmotic shock. This is consistent with the widely reported role for H_2O_2 in increasing the cross-linking of cell wall polymers leading to increased cell wall strength in response to stress (e.g. Brawley et al., 1996). Pre-treatment-induced tolerance was abolished by DPI but not by the inhibitor U73122 which blocks the Ca^{2+}_{cyt} increase and subsequent mitochondrial ROS production indicating that the early peripheral oxidative burst was sufficient to activate osmotic-tolerance mechanisms (section 4.3.1.). The induction of cell wall resistance mechanisms by hyper-osmotic treatment may function to counter the hypo-osmotic stress that is likely to occur during re-hydration on return to normal seawater following solute accumulation associated with hyper-osmotic adaptation.

Bromoperoxidases (BPO) are good candidates as mediators of the possible cell wall cross-linking in response to H_2O_2 produced at the cell periphery. While it was shown that the peripheral burst is sufficient for the activation of cell wall strengthening mechanisms, further in gel BPO experiments should be performed in the presence of U73122 to ensure that the increase in BPO activity found 5 min after stress still takes place. This would allow a more definitive conclusion to be made about the ability of peripheral ROS production to induce cell wall strengthening through BPO activation.

The information gained by the biochemical approach could be completed by the cloning of the BPO gene, which is currently being undertaken (Delange et al., Station Biologique de Roscoff). RNA interference techniques could then potentially be used to obtain transient BPO knockout embryos and therefore assess the role of bromoperoxidases in the regulation of *Fucus* cell wall mechanical properties and its connection with hyper-osmotic stress-induced H_2O_2 production.

However, the possibility that other cellular mechanisms may be responsible for the observed osmotic tolerance cannot be ruled out. These could include induction of more responsive solute loss mechanisms (e.g. plasma membrane ion channels) or changes in endo/exocytosis in relation to cell volume changes. The high-resolution measurement of cell volume changes upon hypo-osmotic treatment would help to understand the process of osmotic adaptation in *Fucus* embryos in more detail.

5.5.2. MAPK activation independent of Ca^{2+} wave and mitochondrial ROS elevation

The preliminary results presented here indicate that a rapid and transient protein kinase activation occurred in response to hyper-osmotic stress in *Fucus* embryos. *Fucus* protein kinases were found to efficiently phosphorylate myelin basic protein (MBP), a ubiquitous MAPK substrate, and reacted with antibodies raised against mammalian ERK isoforms.

Immunoblots suggested that a number of MAPK isoforms were expressed in *Fucus* embryos during hyper-osmotic stress (section 4.3.7.). Activation of separate plant MAPK species in response to different stress factors has been observed (Jonak et al., 1996; Munnik et al., 1999; Romeis et al., 1999). The activation of several MAPK in *Fucus* may represent a general stress response that could reflect the needs of the cells

under a range of environmental conditions. Thus, a comprehensive response may indeed apply to any stressful condition, preparing the cells to respond to a range of further stimuli. MAPK are undoubtedly involved in downstream regulation of gene expression (e.g. Grant et al., 2000; Lee et al., 2001). In the *Fucus* embryo, the set of MAPK induced by hyper-osmotic stress could be activating different nuclear transcription factors or regulating expression of different genes responsible for distinct downstream functions in cellular osmotic stress adaptation.

During hyper-osmotic stress, MAPK activation and the mitochondrial oxidative burst followed similar time courses, suggesting a relationship between mitochondrial ROS and MAPK. Taylor et al. (2001) similarly found a tight temporal correlation between MAPK and ROS during soya bean response to several biotic and abiotic stresses. Preliminary data presented here indicate that *in vitro* MBP phosphorylation was reduced by a MAPK inhibitor, apigenin. The same compound had no effect on either Ca^{2+}_{cyt} elevation or mitochondrial ROS production in response to hyper-osmotic stress, strongly suggesting that in *Fucus* embryos, MAPK activation is a downstream or independent event in the hyper-osmotic stress signal transduction pathway (section 4.3.8). However, to further define the positioning of the MAPK relative to mitochondrial ROS production and Ca^{2+}_{cyt} elevation more experiments should be performed using other inhibitors of MAPK. In addition, it would be interesting to ascertain the effect of external H_2O_2 on MAPK activation, as well as the effect of Ca^{2+} and oxidative burst inhibitors. This would allow a more thorough insight into the cellular signalling processes involving Ca^{2+}, ROS and MAPK during hyper-osmotic stress.

Moreover, the use of FITC anti-ERK1,2 could provide information on the temporal and spatial kinetics of the MAPK cascades activation during a stress response. In particular, an eventual migration of the activated MAPK to the nucleus upon stimulation could be visualised with high temporal and spatial resolution. Interestingly, certain MAPK were found to be associated with the microtubule cytoskeleton in animal cells (Rezka et al., 1995). Because cytoskeleton dynamics probably play an important role during cell shrinkage upon hyper-osmotic shock, it would be interesting to determine the interaction between MAPK and microtubules in the *Fucus* rhizoid. Further confocal microscopy dual labelling *in vivo* experiments could be performed, using fluorescent tubulin and FITC anti-ERK1,2 microinjected simultaneously. In addition, microinjection of FITC anti-ERK1,2 would potentially block MAPK activation during further hyper-osmotic osmotic stress with likely consequences at the cellular level including effects on the ability of the zygotes to withstand further osmotic shocks. Finally, molecular techniques would be valuable to gain more accurate information on the MAPK kinetics at the cellular level during the osmotic stress response. MAPK cascade analysis of transient knockout mutants (for example using the RNA interference technique) would help to elucidate the molecular mechanisms of the stress response and of adaptations to environmental changes in *Fucus* embyos.

5.6. Nature of the upstream osmosensor

The dynamics of osmo-sensing pathways have been well studied in yeast cells. In *Saccharomyces cerevisiae*, increases in external osmolarity evoke osmotic stress-induced signalling via the high-osmolarity glycerol (HOG) MAPK pathway. One of the upstream components of this signal transduction route is the putative osmosensor,

Sho1p (reviewed by Hohmann, 2002). Upon a shift to high osmolarity, yeast cells rapidly stimulate the HOG pathway, which orchestrates part of the transcriptional response. To date, surprisingly little is known about how plant cells detect osmotic changes. In *Arabidopsis*, the ATHK1 gene functions as an osmosensor and transmits the stress signal to a downstream MAPK cascade (Urao et al., 1999). Voltage-dependent K^+-channels are targets of osmotic sensing in *Vicea* faba guard cells, and the actin cytoskeleton may serve as the osmosensor (Liu and Luan, 1998). The nature of the *Fucus* embryo upstream element that senses the changes in the osmotic environment and activates the described sequence of cellular events is unknown. Previous work (Taylor et al. 1996) indicated that osmotic stress in *Fucus* embryos caused Ca^{2+} influx through stretch-activated channels and evoked a Ca^{2+}_{cyt} wave. However, Ca^{2+} influx through stretch-activated channels was found not to be sufficient to trigger a Ca^{2+}_{cyt} wave (Goddard, 2001). An additional component appears to be necessary. H_2O_2 production at the plasma membrane level is a very early component in the hyper-osmotic stress response, and a role for H_2O_2 in the amplification of the activity of stretch-activated channels (Taylor et al., 1996), inducing the Ca^{2+} wave progression and downstream osmotic signalling, is a possibility. The exact mechanism of osmotic sensing in *Fucus* appears to be extremely complex, but ROS and Ca^{2+} seem to hold predominant roles.

5.7. Proposed signal transduction pathway during hyper-osmotic stress

A simplified model for hyper-osmotic signal transduction pathways based on the results presented in this thesis is illustrated in Figure 5.1. ROS production in response to hyper-osmotic stress comprised two distinct components. The first ROS

component coincided closely with the origin of a Ca^{2+} wave in the peripheral cytosol at the growing cell apex, had an extracellular origin, and was necessary for the Ca^{2+} wave. Patch clamp experiments showed that a non-selective cation channel was stimulated by H_2O_2, and may underlie the initial cytosolic Ca^{2+} elevation. The second, later ROS component localizes to the mitochondria and is a direct consequence of the Ca^{2+} wave. The first, but not the second component was required for short-term adaptation to osmotic stress, probably through the activity of cell wall bromoperoxidases. Mitogen-activaed protein kinases may be involved in the hyper-osmotic stress response downstream or independently of the mitochondrial ROS production. The findings of this study stress that *Fucus* cells may provide a suitable physiological model to study the nature of stress-induced signalling pathways in eukaryotic cells.

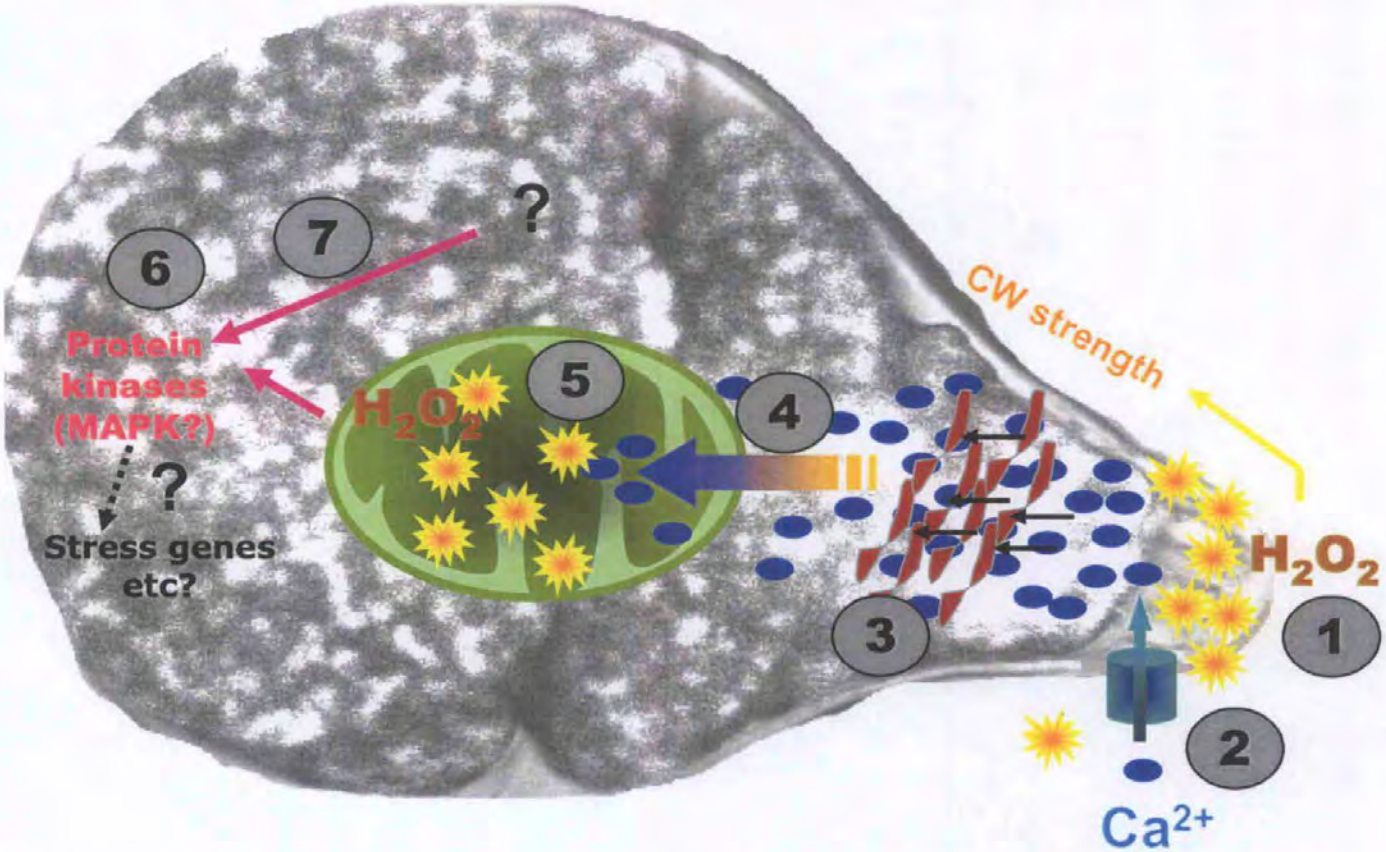

Figure 5.1. Proposed signalling pathway during hyper-osmotic stress in *Fucus* embryos. Osmotic change is sensed by an unidentified osmo-sensor, which induces a DPI-sensitive ROS production within 10 s (1). H_2O_2 is produced at the exterior side of the plasma membrane and may be involved in cell wall strengthening. H_2O_2 also diffuses into the cell leading to localized peripheral intracellular elevation. Localised external H_2O_2 production also increases Ca^{2+} channel activity (2). Downstream events include Ca^{2+} wave propagation over the following 10-60 sec (3) followed by $Ca^2{}_m$ elevation (4), mitochondrial ROS production (5), and protein kinase activation (6). An independent pathway for protein kinase activation is a possibility (7).

REFERENCES

Abe, J, Kusuhara, M, Ulevitch, R, Berk, B and Lee, J-D (1996) Big mitogen activated protein kinase 1 (BMK1) is a redox-sensitive kinase. J Biol Chem 271(28), 16586-16590

Alessa, L and Kropf, DL (1999) F-actin marks the rhizoid pole in living *Pelvetia compressa* zygotes. Development 126, 201-209

Allan, A and Fluhr, R (1997) Two distinct sources of elicited reactive oxygen species in tobacco epidermal cells. The Plant Cell 9, 1559-1572

Allan, GJ and Schroeder, JI (1998) Cyclic ADP-ribose and ABA signal transduction. Trends Plant Sci 3, 123-125

Allan, GJ, Muir, SR and Sanders, D (1995) Release of Ca^{2+} from individual plant vacuoles by both $InsP_3$ and cyclic ADP-ribose. Science 268, 735-737

Allen, VW and Kropf, DL (1992) Nuclear rotation and lineage specification in *Pelvetia* embryos. Development 115, 873-883

Almeida, M, Filipe, S, Humanes, M, Maia, MF, Melo, R, Severino, N, da Silva, JA, Frausto da Silva, JJ and Wever, R. (2001) Vanadium haloperoxidases from brown algae of the Laminariaceae family. Phytochemistry. 57(5):633-42.

Alscher RG, Erturk N and Heath LS (2002) Role of superoxide dismutases (SODs) in controlling oxidative stress in plants. J Exp Bot 53(372), 1331-41

Altamirano, J, Brodwick, MS and Alvarez-Leefmans, FJ (1998) Regulatory volume decrease and intracellular Ca^{2+} in murine neuroblastoma cells studied with fluorescent probes. J Gen Physiol 112, 145-160

Amsler, C and Neushul, M (1989) Chemostatic effects of nutrients on spores of the kelps *Macrocystis pyrifera* and *Pterygophora californica*. Mar Biol 102, 557-564

Apostol, I, Heinstein, P et al. (1989). Rapid stimulation of an oxidative burst during elicitation of cultured plant cells. Plant Physiol 90, 109-116.

Apte, SS, Mattei, MG, Seldin, MF and Olsen, BR (1995) The highly conserved defendor against the death 1 (DAD1) maps to human cromossome 14q11-q12 and mouse cromossome 14 and has plant and nematode homologues. FEBS Lett. 363, 304-306

Asada, K (1994) Mechanisms for scavenging reactive molecules generated in chloroplasts under light stress. In: Baker, N R and Boyer JD (eds) Photoinhibition of photosynthesis: from molecular mechanisms to the field pp 129-140 BIOS Scientific Publishers, Oxford

Asada, K (1999) The water-water cycle in chloroplasts: scavenging of active oxygens and dissipation of excess photons. Ann Rev Plant Physiol Plant Mol Biol 50, 601-639

Auh, C-K, and Murphy, TM (1995) Plasma membrane redox enzyme is involved in the synthesis of O_2^- and H_2O_2 by *Phythophthora* elicitor-stimulated rose cells. Plant Physiol 107, 1241-1247

Az-ma, T, Saeki, N and Yuge, O (2002) Cytosolic calcium movements of endothelium cells exposed to reactive oxygen intermediates: role of hydroxyl radical-mediated redox alteration of cell-membrane calcium channels. Br J Pharmacology 126(6), 1462-1470

Babior BM, Lambeth JD, Nauseef W. (2002) The neutrophil NADPH oxidase. Arch Biochem Biophys 397(2), 342-4

Bac, YS, Kang, SW, Seo, MS, Baines, IC, Teckle, E, Chock, PB and Rhee, SG (1997) Epidermal growth factor (EGF)-induced generation of hydrogen peroxide. J Biol Chem 272, 217-221

Badminton, MN, Kendall, JM, Rembold, CM and Campbell, AK (1998) Current evidence suggests independent regulation of nuclear calcium. Cell Calcium 23, 79-86.

Banno, H., Hirano, K., Nakamura, T., Irie, K., Nomoto, S., Matsumoto, K., and Machida, Y. (1993) *NPK1*, a tobacco gene that encodes a protein with a domain homologous to yeast BCK1, STE11 and BYR2 protein kinases. Mol Cell Biol 13, 4745-4752

Barry, PH and Lynch, JW (1991) Liquid junction potentials and small cell effects in patch clamp analysis. J Memb Biol 121, 101-117

Bartosz, G (1997) Oxidative stress in plants. Acta Physiol Plant 19, 47-64.

Batiza, AF, Schultz, T and Masson, PH (1996) Yeast respond to a hypootonic shock with a calcium pulse. J Biol Chem 271, 23357-23362

Baum, G, Long, JC, Jenkins, GI and Trewavas, AJ (1999) Stimulation of the blue light phototropic receptor NPH1 causes a transient increase in cytosolic calcium. PNAS USA 96, 13554-13559

Beach, K, Smith, C, Michael, T and Shin, H-W (1995) Photosynthesis in reproductive unicells of *Ulva fasciata* and *Enteromorpha flexuosa*: implications for ecological success. MEPS 125, 229-237

Bednarska, E and Butowt, R (1995) Calcium in pollen-pistil interaction in *Petunia-hybrida* hort.2. Localisation of Ca^{2+} ions and Ca^{2+}-ATPase in unpollinated pistil. Folia Histochimica et Cytobiologica 33, 43-52

Beers EP and McDowell JM (2001) Regulation and execution of programmed cell death in response to pathogens, stress and developmental cues. Curr Opin Plant Biol 4(6), 561-7

Bellgrove, A, Clayton, M and Quinn, G. (1997) Effects of secondarily treated sewage effluent on intertidal macroalgal recruitment processes. Mar Freshwater Res 48, 137-46.

Berberich, T, Sano, H and Kusano, T (1999) Involvement of a MAP kinase, ZmMPK5, in senescence and recovery from low temperature stress in maize. Mol Gen Genet 262(3), 534-542

Berger, F and Brownlee, C (1993) Ratio confocal imaging of free cytoplasmatic calcium gradients in polarising and polarised *Fucus* zygotes. Zygote, 1, 9-15

Berger, F. and Brownlee, C (1994) Cell fate determination by the cell wall in early *Fucus* development. Science 263, 1421-1423

Berger, F and Brownlee, C (1995) Physiology and development of protoplasts obtained from *Fucus* embryos using laser microsurgery. Protoplasma 186, 63-71.

Berridge, MJ (1993) Inositol triphosphate and calcium signalling. Nature 361, 315-325

Bestwick, C, I. Brown, et al. (1997) Localisation of hydrogen peroxide accumulation during the hypersensitive reaction of lettuce cells to *Pseudomonas syringae* pv phaseolicola. Plant Cell 9, 209-221

Bestwick, C., I. Brown, et al. (1998) Localized changes in peroxidase activity accompany hydrogen peroxide generation during the development of a non-host hypersensitive reaction in lettuce. Plant Physiol. 118, 1067-1078

Bewell, MA, Maathuis, FJM, Allen, GJ and Sanders, D (1999) Calcium-induced calcium release mediated by a voltage-activated cation channel in vacuolar vesicles from red beet. FEBS Lett 458, 41-44

Bilger, W and Björkman, O (1991) Temperature dependence of violoxanthin de-epoxidation and non-photochemical fluorescence quenching in intact leaves of *Gossypium hirsutum* L. Planta 184, 226-234.

Bilger, W, Schreiber, U and Bock, M (1995) Determination of the quantum efficiency of photosystem II and of non-photochemical quenching of chlorophyll fluorescence in the field. Oecologia 102, 425-432

Blokhina, OB, Chirkova, TV and Fagerstedt, KV (2001) Anoxic stress leads to hydrogen peroxide formation in plant cells. J Exp Bot 52(359), 1179-90

Blume, B, Nurnberger, T, Nass, N and Scheel D (2000) Receptor-mediated increase in cytoplasmic free calcium required for activation of pathogen defense in parsley. Plant Cell 12(8), 1425-40

Bogre, L, Calderini, O et al. (1999) A MAP kinase is activated late in plant mitosis and becomes localized to the plane of cell division. The Plant Cell 11, 101-113.

Bogre, L, Ligterink, E, Eberle-Bors, E and Hirt, H (1996) Mechanosensors in plants. Nature 383, 64-67

Bolwell, GP, Bindschedler, LV, Blee, KA, Butt, VS, Davies, DR, Gardner, SL, Gerrish, C, and Minibayeva, F (2002) The apoplastic oxidative burst in response to biotic stress in plants: a three-component system. J Exp Bot 53(372), 1367-76

Bolwell, GP, Butt, DR, Davies, C, and Zimmerlin, A (1995) The origin of the oxidative burst in plants. Free Radical Research 23, 517-532

Bonza, MC, Morandini, P, Luoni, L (2000) At-ACA8 encodes a plasma membrane localised calcium-ATPase of *Arabidopsis* with a calmodulin-binding domain at the N terminus. Plant Physiol 123, 1495-1505

Bootman, MD, Thomas, D, Tovey, SC, Berridge, MJ and Lipp, P (2000) Nuclear calcium signalling. Cell Mol. Life Sci 57, 371-378

Bouget, F-Y, Berger, F and Brownlee, C (1998) Position dependent control of cell fate in the *Fucus* embryo: role of intercellular communication. Development 125, 1999-2008

Bowie, A, and O'Neill, LA (2000) Oxidative stress and nuclear factor-kappaB activation: a reassessment of the evidence in the light of recent discoveries. Biochem Pharmacol 59, 13-23.

Bradley, D, Kjellbom, P and Lamb, C (1992). Elicitor- and wound-induced oxidative cross-linking of a proline-rich plant cell wall protein: a novel, rapid defence response. Cell 70, 21-30.

Brawley SH and Quatrano RS. (1979) Sulfation of fucoidin in *Fucus* embryos. IV. Autoradiographic investigations of fucoidin sulfation and secretion during differentiation and the effect of cytochalasin treatment. Dev Biol 73(2), 193-205

Brawley, S and Johnson, LE (1991) Survival of fucoid embryos in the intertidal zone depends upon developmental stage and microhabitat. J Phycol 27, 179-186.

Brawley, SH (1991) The fast block against polyspermy in fucoid algae is an electrical block. Dev Biol 144, 94-106

Brawley, SH and Robinson, KR (1985) Cytochalasin treatment disrupts the endogenous currents associated with cell polarisation in fucoid zygotes: studies of the role of F-actin in embryogenesis. J Cell Biol 100, 1173-1184

Brawley, SH, Wetherbee, R and Quatrano, RS (1976) Fine structural studies of the gametes and embryo of *Fucus vesiculosus* L. (Phaeophyta). II. The cytoplasm of the egg and young zygote. J Cell Sci 20, 255-271

Brinkhuis, B, Tempel, R and Jones, R (1976) Photosynthesis and respiration of exposed salt-marsh fucoids. Mar Biol (Berl) 34, 349-359.

Brisson, LF, Tebhaken, R and Lamb, CJ (1994) Function of oxidative cross-linking of cell wall structural proteins in plant disease resistance. Plant Cell 6, 1703-1712

Brownlee, C and Pulsford, A (1988) Visualization of the cytoplasmatic Ca^{2+} gradient in *Fucus serratus* rhizoids: correlation with cell structure and polarity. J Cell Sci 91, 249-256.

Brownlee, C and Wood, JW (1986) A gradient of cytoplasmatic free calcium in growing rhizoid cells of *Fucus serratus*. Nature, 320, 624-626

Bush, DS (1993) Regulation of cytosolic calcium in plants. Plant Physiol 103, 7-13

Butler A (1998) Vanadium haloperoxidases. Curr Opin Chem Biol 2(2), 279-85

Caplen, N (2002) A new approach to the inhibition of gene expression. Trends Biotech, 20, 49-54

Cardinale, F. Jonak, C et al. (2000) Differential activation of four specific MAPK pathways by distinct elicitors. J Biol Chem 275(47), 36734-36740

Carpaneto, A, Cantu, AM and Gambale, F (2001). Effects of cytoplasmatic magnesium on slowly activating channels in isolated vacuoles of *Beta vulgaris*. Planta 213, 457-468

Cazalé, A.-C., M.-A. Rouet-Mayer, et al. (1998) Oxidative burst and hypoosmotic stress in tobacco cell suspensions. Plant Physiol 116, 659-669.

Cazalé, A-C., M-J Droillard, et al. (1999) MAP kinase activation by hypoosmotic stress of tobacco cell suspensions: towards the oxidative burst response? Plant J 19(3), 297-307.

Cessna, SG and Low, PS (2001) Activation of oxidative burst in aequorin transformed *Nicotiana tabacum* cells is mediated by protein kinase and anion channel dependent release of Ca^{2+} from internal stores. Planta 214 (1), 126-134

Chandra, S, Cessna, SG, Yahraus, T, Devine, R and Low, PS (2000) Homologous and heterologous desensitization and synergy in pathways leading to the soybean oxidative burst. Planta 211(5), 736-42

Chandra, S, and Low, P (1997) Measurement of Ca^{2+} fluxes during elicitation of the oxidative burst in aequorin-transformed tobacco cells. J Biol Chem 272, 28274-28280

Chandra, S, Martin, G et al. (1996) The Pto kinase mediates a signalling pathway leading to the oxidative burst in tomato. PNAS USA 93, 13393-13397

Chandra, S, Heinstein, PF et al. (1996) Activation of phospholipase A by plant defence elicitors. Plant Physiol 110, 979-986

Chang, C (1996) The ethylene signal transduction pathway in *Arabidopsis*: An emerging paradigm? Trends Biochem Sci 21, 129-133

Chapman, V (1966) The physiological ecology of some New Zealand seaweeds. Proc Int Seaweed Symp 5:29-54

Chen, Z, Gibson, TB, Robinson, F, Silvestro, L, Pearson, G, Xu, B, Wrig, A, Vanderbilt, C and Cobb, MH (2001) MAP kinases. Chem Rev 101(8), 2449-2476

Chen, Z, Silva, H and Klessig, DF (1993) Active oxygen species in the induction of plant systemic acquired resistance by salicylic acid. Science 262, 1883-1886

Cobbold, PH and Rink, TJ (1997) Fluorescence and bioluminescence measurements of cytoplasmatic free calcium. Biochem J 248, 313-328

Cockell, CS (1998) Ultraviolet radiation, evolution and the π-electron system. Biological Journal of the Linnean Society 63, 449-457

Collén, J and Davison, IR (1997) *In vivo* measurement of reactive oxygen production in the brown alga *Fucus evanescens* using 2,7-dichlorohydrofluorescein diacetate. Journal of Phycology 33, 643-648

Corellou, F, Brownlee, C, Detivaud, L, Kloareg, B and Bouget, F-Y (2001b). Cell cycle in the Fucus zygote parallels a somatic cell cycle but displays a unique translational regulation of cyclin-dependet kinases. The Plant Cell 13, 585-598

Corellou, F, Brownlee, C, Kloareg, B and Bouget, F-Y (2001a) Cell cycle-dependent control of polarised develoipment by a ciclin-dependent kinase-like protein in the *Fucus* zygote. Development 128, 4383-4392

Corpas, FJ, Barroso, JB and del Rio, L (2001) Peroxisomes as a source of reactive oxygen species and nitric oxide signal molecules. Trends Plant Sci. 6(4), 145-150

Coyle, JT and Puttfarcken, P (1993) Oxidative stress, glutamate, and neurodegenerative disorders. Science 262, 689-695

Crawford, DR; Abramova, NE and Davies, KJ (1998) Oxidative stress causes a general, calcium-dependent degradation of mitochondrial polynucleotides. Free Rad Bio Med 25(9), 1106-1111

Crayton, MA, Wilson, E and Quatrano, RS (1974) Sulphatation of fucoidan in *Fucus* embryo. II Separation from initiation of polar growth. Dev Biol 39, 164-167

Creed, JC,. Norton, TA and. Kain, JM (1997) Intraspecific competition in *Fucus serratus* germlings: the interaction of light, nutrients and density. J Exp Mar Biol Ecol, 212, 211-223

Dangl, JL, Dietrich, RA and Richberg, MH (1996) Death don't have no mercy: cell death programmes in plant-microbe interactions. Plant Cell 8, 1793-1807

Davison, I, Johnson, LE, and Brawley, SH (1993) Sub-lethal stress in the intertidal zone: tidal emersion inhibits photosynthesis and retards development in embryos of the brown alga *Pelvetia fastigiata*. Oecologia 96, 483-492

Davison, IR and Pearson, G (1996) Stress tolerance in intertidal seaweeds. J Phycol 32, 197-211

Davison, PA, Hunter, CN, Horton, P (2002) Overexpression of beta-carotene hydroxylase enhances stress tolerance in *Arabidopsis*. Nature 418(6894), 203-206

Day, B, Bergamini, S, Tyurina, YY, Carta, G, Tyurin, VA and Kagan, VE (1998) β-carotene - an antioxidant or a target of oxidative stress in cells? In Quinn and Kagan [Eds.] Subcellular Biochemistry. NY, Plenum Press 30, 209-217

Demers, S, Roy, S, Gagnon, R and Vignault, C (1991) Rapid light-induced changes in cell fluorescence and in xanthophyll-cycle pigments of *Alexandrium excavatum* (Dinophyceae) and *Thalassiosira pseudonana* (Bacillariophyceae): a photoprotection mechanism. MEPS 76, 185-93

Demmig, B, Winter, K, and Czygan, F-C (1987) Photoinhibition and zeaxanthin formation in intact leaves: a possible role of the xanthophyll cycle in the dissipation of the excess light energy. Plant Physiol 84, 214-224

Demmig-Adams, B (1990) Carotenoids and photoprotection in plants: a role for the xanthophyll zeaxanthin. Bioch Biophys Acta 1020, 1-24

Demmig-Adams, D, and Adams, W (1992) Photoprotection and other responses of plants to high light stress. Ann Rev Plant Pysiol Plant Mol Biol 43, 599-626

Desikan, R, Hancock, JT, Neill, SJ, Coffey, MJ, Jones, OT (1996) Elicitor-induced generation of active oxygen in suspension cultures of *Arabidopsis thaliana*. Biochem Soc Trans 24(2), 199S

Desikan, R, Neill, SJ and Hancock, JT (2000) Hydrogen peroxide-induced gene expression in *Arabidopsis thaliana*. Free Rad Biol Med 28, 773-778

Desikan, R, Clarke, A et al. (1999) Harpin induces mitogen-activated protein kinase activity during defense responses in *Arabidopsis thaliana* suspension cultures. Planta 210(1), 97-103

Desikan, R, Hancock, JT, Ichimura, K, Shinozaki, K and Neill, SJ (2001). Harpin induces activation of the *Arabidopsis* mitogen activated protein kinases AtMPK4 and AtMPK6. Plant Physiol. 126(4), 1579-1587

Devlin, W and Gustine, D (1992) Involvement of the oxidative burst in phytoalexin accumulation and the hypersensitive reaction. Plant Physiol 100, 1189-1195

DeWald, DB, Torabinejad, J, Jones, CA, Shope, JC, Cangelosi, AR, Thompson, JE, Prestwich, GD and Hama, H (2001) Rapid accumulation of phosphatidylinositol 4,5-biphsphate and inositol 1,4,5-triphspohate correlates with calcium mobilisation in salt-stressed *Arabidopsis*. Plant Physiol 126, 759-769

Doke, N (1983) Involvement of superoxide anion generation in the hypersensitive response of potato tuber tissues to infection with an incompatible race of *Phythophora infestans* and to the hyphal cell wall components. Physiol Plant Pathol 23, 345-357

Doke, N and Miura, Y (1995) *In vitro* activation of NADPH-dependent O_2^- -generating system in a plasma membrane rich fraction of potato tuber tissues by treatment with an elicitor from *Phytophora infestans* or with digitonin. Physiol Mol Plant Pathol 46, 17-28

Dring, MJ and Brown, FA (1982) Photosynthesis of intertidal brown algae during and after periods of emersion: a renewed research for physiological causes of zonation. MEPS 8, 301-308.

Dring, MJ, Makarov, V, Schoshina, E, Lorenz, M and Lüning, K (1996) Influence of ultraviolet radiation on chlorophyll fluorescence and growth in different life-history stages of three species of *Laminaria* (Phaeophyta). Mar Biol 126, 183-191

Drobak, BK and Watkins, PAC (2000) Inositol (1,4,5) triphosphate production in plant cells: an early response to salinity and hyper-osmotic stress. FEBS Lett 481, 240-244

Duchen, MR (2000) Mitochondria and calcium: from cell signalling to cell death. J Physiol 529, 57-68

Durner, J, Wendehenne, D, and Klessig, DF (1998) Defence gene induction in tobacco by nitric oxide, cyclic GMP and cyclic ADP-ribose. PNAS USA 95, 10328-10333

English, J, Pearson, G et al. (1999) New insights into the control of MAP kinase pathways Experimental Cell Research 253, 255-270

Epperlein, MM, Noronha-Dutra, AA and Strange, RN (1986) Involvement of the hydroxyl radical in the abiotic elicitation of phytoalexins in legumes. Physiol Mol Plant Pathol 28, 67-77

Ettinger, WF, Clear, AM, Fanning, KJ and Peck, ML (1999) Identification of a Ca^{2+}/H^+ antiport in the plant chloroplast thylakoid membrane. Plant Physiol 119, 1379-1385

Falkovki, PG and Raven J (1997) Aquatic Photosynthesis. Blackwell Science Oxford UK

Falkovki, PG, Green, R and Kolber Z (1994) Light utilisation and photoinhibition of photosynthesis in marine phytoplankton. In: Baker, N R and Boyer JD (eds.) Photoinhibition of photosynthesis: from molecular mechanisms to the field. BIOS Scientific Publishers, Oxford

Finkel, T (1998) Oxygen radicals and signalling. Curr Opin Cell Biol 10, 248-253

Fletcher, R and Callow, M (1992) The settlement, attachment and establishment of marine algal spores. Br Phycol J 27, 303-329

Forster RM and Lüning, K (1996) Photosynthetic response of *Laminaria digitata* to ultraviolet A and B radiation. *In* Figueroa, F.L., Jimenez, C., Perez-Llorens, L., Niell, F.X. [Eds.] Underwater light and algal photobiology. Sci Mar 60 (Supl. 1), 65-71

Foyer CH, Lelandais M, and Kunert KJ (1994) Photooxidative stress in plants. Physiol Plant 92, 696-717

Frahry, G and Schopfer, P (1998) Inhibition of $O_2^{\cdot}$ reducing activity of horseradish peroxidase by diphenyleneiodonium. Phytochemistry 48, 223-227

Franklin, LA and Forster, RM (1997) The changing irradiance environment: consequences for marine macrophyte physiology, productivity and ecology. Eur J Phycol 32, 207-232

Frohnmayer, H, Loyall, L, Blatt, MR and Grabov, S (2001) A millisecond UV-B irradiation evokes prolonged elevation of cytosolic free calcium and stimulates gene expression in transgenic parsley cell cultures. Plant J 20, 109-117

Fry, SC (1986) Cross-linking of matrix polymers in the growing cell wall of angiosperms. Ann Rev Plant Physiol 37, 165-186

Fry, SC, Willis, SC and Patterson, AE (2000) Evidence for covalent linkage between xyloglucan and acidic pectins in suspension-cultured rose tissue. Planta 211, 275-286

Garcia-Ruiz, C, Colell, A, Morales, A, Kaplowitz, N and Fernandez-Checa, JC (1995) Role of oxidative stress generated from the mitochondrial electron transport chain and mitochondrial glutathione status in loss of mitochondrial function and activation of transcription factor nuclear factor-kappa B: studies with isolated mitochondrial and rat hepatocytes. Mol Pharmacol 48(5), 825-834

Garrington, TP and Johnson, GL (1999) Organization and regulation of mitogen-activated protein kinase signaling pathways. Curr Opinion Plant Biol 11, 211-218

Gehring, CA, Williams, DA, Cody, SH and Parish, RW (1990) Phototropism and geotropism in maize coleoptiles are spatially correlated with increases in cytosolic free calcium. Nature 345, 528-530

Genty, B, Briantais, J-M and Baker, N (1989) The relationship between the quantum yield of photosynthetic electron transport and quenching of chlorophyll fluorescence Bioch Bioph Acta 990, 87-92

Gille, G. and Sigler, K. (1995) Oxidative stress and living cells. Folia Microbiologia 40, 131-152

Glazener, J, Orlandi, E et al. (1996) The active oxygen response of cell suspensions to imcompatible bacteria is not sufficient to cause hypersensitive cell death Plant Physiol 110, 759-763

Goddard, H, Manison, N, Tomos, D, and Brownlee, C (2000) Elemental propagation of calcium signals in response-specific patterns determined by environmental stimulus strength. PNAS 97, 1932-1937

Gonzalez-Flecha, A and Bovaris, A (1995) Mitochondrial sites of hydrogen peroxide in reperfused rat kidney cortex. Biochem Biophys Acta 1243, 361-366

Goodman, RN and Novaky, AJ (1994) The hypersensitive response reaction in plants to pathogens: a resistance phenomon. St. Paul, MN: American Phytopathological Society

Goodner, B and Quatrano, RS (1993) *Fucus* embryogenesis: a model to study the establishment of polarity. Plant Cell 5, 1471-1481

Grant, J and Loake, G (2000) Role of reactive oxygen intermediates and cognate redox signalling in disease resistance. Plant Physiol 124, 21-29

Grant, J, Yun, B-W et al. (2000) Oxidative burst and cognate redox signalling reported by luciferase imaging: identification of a signal network that functions independently of ethylene, SA and Me-JA but is dependent on MAPKK activity. Plant J 24(5), 569-582

Green, R and Fluhr, R (1995) UV-B-induced PR-1 accumulation is mediated by active oxygen species. Plant Cell 7, 203-212

Greenberg, JT. (1996) Programmed cell death: a way of life for plants. PNAS USA 93(22), 12094-12097

Grijalba, MT, Vercesi, AE and Schreier, S (1999) Ca^{2+}- induced increased lipid packing and domain formation in submitochondrial particles: a possible early step in the mechanism of Ca^{2+}-stimulated generation of reactive oxygen species by the respiratory chain. Biochemistry 38, 13279-87

Groom, QJ, Torres, MA, Fordham-Skelton, AP, Hammond-Kosack, KE, Robinson, NJ, Jones, JD. (1996) rbohA, a rice homologue of the mammalian gp91phox respiratory burst oxidase gene. Plant J 10(3), 515-22

Groom, QJ and Baker, NR (1992) Analysis of light induced depressions of photosynthesis in leaves of a wheat crop during the winter. Plant Physiol 100, 1217-1223

Grynkiewicz, G, Poenie, M and Tsien, RY (1985) A new generation of Ca^{2+} indicators with greatly improved fluorescence properties. J Biol Chem 260, 3440-3450

Guan, LM, Zhao, J and Scandalios, JG (2000) Cis-elements and trans-factors that regulate expression of the maize Cat1 antioxidant gene expression in response to ABA and osmotic stress: H_2O_2 is the likely intermediary signalling molecule for the response. Plant J 22(2), 87-95

Guo, Z, Du, X and Iacovitti, L (1998) Regulation of tyrosine hydroxylase gene expression during differentiation of strial neurons: changes in transcription factors binding the AP-1 site. J. Neurosci 18(20), 8163-8174

Hable, WE and Kropf, DL (2000) Sperm entry induces polarity in fucoid zygotes. Development 127, 493-501

Halliwell, B and Gutteridge, JMC (1999) Free radicals in Biology and Medicine. 3nd ed. Clarendon Press, Oxford University Press pp 968

Hamilton, DWA, Hills, A, Kohler, B and Blatt, MR (2000) Ca^{2+} channels at the plasma membrane of stomatal guard cells are activated by hyper-polarisation and abscisic acid. PNAS USA 97, 4967-4972

Hammond-Kosack, KE and Jones, JDG (1996) Resistance gene-dependent plant defence responses. Plant Cell 8, 1773-1791

Hanelt D, Li, L and Nultsch, W (1994) Tidal dependence of photoinhibition in marine macrophytes in the South China Sea. Botanica Acta 107, 66-72

Hanelt, D, Uhrmacher, S and Nultsch, W (1995) The effect of photoinhibition of photosynthetic oxygen production in the brown algae *Dictyota dichotoma*. Botanica Acta 108, 99-105

Harding, S and. Roberts, D (1998) Incompatible pathogen infection results in enhanced reactive oxygen and cell death responses in transgenic tobacco expressing a hyperactive mutant calmodulin. Planta 206, 253-258

Harker, M, Berkaloff, C, Lemoine, Y, Britton, G, Young, AJ, Duval, J-C, Rmiki, N-E and Rousseau, B (1999) Effects of high light and desiccation on the operation of the xanthophyll cycle in two marine brown algae. Eur J Phycol 34, 35-52

Harvaux, M, and Kloppstech, K. (2001) The protective functions of carotenoid and flavonoid pigments against excess visible radiation at chilling temperature investigated in *Arabidopsis* npq and tt mutants. Planta 213(6), 953-66

Havaux, M, Bonfils, JP, Lutz, C, Niyogi, KK. (2000) Photodamage of the photosynthetic apparatus and its dependence on the leaf developmental stage in the npq1 *Arabidopsis* mutant

deficient in the xanthophyll cycle enzyme violaxanthin de-epoxidase. Plant Physiol 124(1), 273-84

He, YY, Hader, DP. (2002a) UV-B-induced formation of reactive oxygen species and oxidative damage of the cyanobacterium *Anabaena sp.*: protective effects of ascorbic acid and N-acetyl-L-cysteine. J Photochem Photobiol 66(2), 115-24

He, YY, Hader, DP. (2002b) Involvement of reactive oxygen species in the UV-B damage to the cyanobacterium *Anabaena sp.* J Photochem Photobiol 66(1), 73-80

Heinecke, JW and Shapiro, BM (1990) Superoxide peroxidase activity of ovoperoxidase, the cross-linking enzyme of fertilization. J Biol Chem 265(16), 9241-6

Hideg, E and Vass, I (1996) UV-B induced free radical production in plant leaves and isolated thylakoid membranes. Plant Science 115, 251-260

Hideg, E, Spetea, C and Vass, I (1994) Singlet oxygen and free radical production during acceptor- and donor-side-induced photoinhibition. Studies with spin-trapping EPR spectroscopy. Bioch Biophys Acta 1186, 143-152

Hirayama, S, Ueda, R and Sugata, K (1995) Detection of hydroxyl radical in intact cells of *Chlorella vulgaris*. Free Rad Res 23, 51-59

Hohmann, S (2002) Osmotic stress signalling and osmoadaptation in yeasts. Microbiol Mol Biol Rev 66(2), 300-72

Hoth, M, Fanger, C and Lewis, R (1997). Mitochondrial regulation of store-operated calcium signalling in T lymphocytes. J Cell Biol 137, 633-648

Hoyos, ME and Zhang, S (2000) Calcium-independent activation of salicylic acid-induced protein kinase and a 40-kilodalton protein kinase by hyperosmotic stress. Plant Physiol 122, 1355-1363

Huang, HJ, Fu, SF, Tai, YH, Chou, WC, Huang, DD (2002) Expression of Oryza sativa MAP kinase gene is developmentally regulated and stress-responsive. Physiol Plant 114(4), 572-580

Huckelhoven, R, Dechert, C, Trujillo, M, Kogel, KH. (2001) Differential expression of putative cell death regulator genes in near-isogenic, resistant and susceptible barley lines during interaction with the powdery mildew fungus. Plant Mol Biol 47(6), 739-48

Hurst, SR and Kropf, DL (1991) Ionic requirement for establishment of an embryonic axis in *Pelvetia* zygotes. Planta 185, 27-33

Huttly, A., and Phillips, A.L. (1995) Gibberellin-regulated expression in oat aleurone cells of two kinases that show homology to MAP kinase and a ribosomal protein kinase. Plant Mol Biol 27, 1043-1052

Ichimura, K, Mizoguchi, T et al. (2000) Various abiotic stresses rapidly activate *Arabidopsis* MAP kinases ATMPK4 and ATMPK6. Plant J 24(5), 655-666

Irihimovitch, V and Shapira, M (2000) Glutathione redox potential modulated by reactive oxygen species regulates translation of Rubisco large subunit in the chloroplast. J Bio Chem 275(21), 16289-16295

Ishida H, Shimizu S, Makino A, Mae T (1998) Light-dependent fragmentation of the large subunit of ribulose-1,5-bisphosphate carboxylase/oxygenase in chloroplasts isolated from wheat leaves Planta 204(3), 305-9

Itoh, N, Hasan, AKMQ, Izumi, Y and Yamada, H (1988). Eur J Biochem 172, 477-485

Jabs, T, Dietrich, RA and Dangl, J (1996) Initiation of runaway cell death in an *Arabidopsis* mutant by extracellular superoxide. Science 273, 1853-1856

Jaffe , L (1968) Localisation in the developing *Fucus* egg and the general role of localising currents. Adv Morphol 7, 295-328

Jeffrey SW, Mantoura, RFC and Wright, SW (1997) Phytoplankton pigments in oceanography: Guidelines to modern methods. *SCOR UNESCO* Monographs on oceanographic methodology, UNESCO Publishing, 661 pp

Ji, G, O'Brien, CD, Feldman, M, Manevich, Ylim, P, Sun, J, Albelda, S M, Kotlikoff, MI (2002) PECAM-1 (CD31) regulates a hydrogen peroxide-activated nonselective cation channel in endothelial cells. J Cell Biol 157(1), 173-184

Jimenéz, C, Figueroa, FL, Salles, S, Aguilera, J, Mercado, J, Viñela B, Flores-Moya, A, Lebert, M and Hader, D-P (1998) Effects of solar radiation on photosynthesis and photoinhibition in red macrophytes from the intertidal system of Southern Spain. Bot Mar 41, 329-338

Jonak, C, Kiegerl, S et al. (1996) Stress signalling in plants: a mitogen-activated protein kinase pathway is activated by cold and drought. PNAS USA 93: 11274-11279

Jones, A (2000) Does the plant mitochondrion integrate cellular stress and regulate programmed cell death? Trends Plant Sci 5(5), 225-30

Jones, LW and Kok B (1966) Photoinhibition of chloroplast reactions. 1) Kinetics and action spectrum. Plant Physiol 41, 1037-1043

Jordan, P and Vilter, H (1990) Native bromoperoxidases do not bind to nitrocellulose: use of DEAE-cellulose as an alternative in blotting. Electrophoresis 11, 653-655.

Jordan, P, Kloareg, B and Vilter, H (1991) Detection of vanadate-dependent bromoperoxidases in protoplasts from the brown algae *Laminaria digitata* and *L. saccharina*. J Plant Physiol 137, 520-524

Kaiser, W (1979) Reversible inhibition of the Calvin cycle and activation of oxidative pentose phosphate cycle in isolated intact chloroplasts by hydrogen peroxide. Planta 145, 377-382.

Kalinich, JF, Ramakrishnan, N and McClain, DE (1997) The antioxidant Trolox enhances the oxidation of 2',7'-dichlorofluorescin to 2',7'-dichlorofluorescein. Free Rad Res 26, 37-47.

Karentz, D, Cleaver, J and Mitchell, D (1991) Cell survival characteristics and molecular responses of Antartic phytoplancton to ultraviolet-B radiation. J Phycol 27, 326-341

Kawalleck, P, Schmelzer, E, Hahlbrock, K and Somssich, IE (1995) Two pathogen presponsive genes in parsley encoding a tyrosine rich hydroxyproline-rich glycoprotein (hrgp) and an anionic peroxidase. Mol Gen Genet 247, 444-452

Kawamitsu, Y and Boyer J (1999) Photosynthesis and carbon storage between tides in a brown alga, *Fucus vesiculosus*. Mar Biol 133, 361-369

Kawano, T, Sahashi, N et al. (1998) Salicylic acid induces extracellular superoxide generation followed by an increase in cytosolic calcium ion in tobacco suspension culture: the earliest events in salicylic acid signal transduction Plant Cell Physiol 39(7), 721-730

Keller, HE (1995) Objective lenses for confocal microscopy. In Pawley, JB (ed.) Handbook of biological confocal microscopy, 2nd edition. Plenum Press, New York, London, 632 pp

Keller, T, Damude, H et al. (1998) A plant homolog of the neutrophil NADPH oxidase $gp91^{phx}$ subunit gene encodes a plasma membrane protein with Ca^{2+} binding motifs. Plant Cell 10, 255-266.

Kendrick, G and Walker, D (1994) Role of recruitment in structuring beds of *Sargassum spp.* (Phaeophyta) at Rottnest Island, Western Australia. J Phycol. 30, 200-208.

Kernyeyev, D, Logan, BA, Payton, P, Allan, R and Holaday, AS (2001) Enhanced photochemical light utilization and decreased chilling-induced photoinhibition of photosystem II in cotton overexpressing genes encoding chloroplast-targeted antioxidant enzymes. Physiol Plant 113(3), 323-331

Kerr, JFR, Wyllie, JY and Currie, AT (1972) Apoptosis: a basic biological phenomenon with wide-ranging implications in tissue kinetics. Br J Cancer 26, 239-257

Kieber, JJ, Rothenberg, M, Roman, G, Feldmann, KA, and Ecker, JR (1993) CTR1, a negative regulator of the ethylene response pathway in *Arabidopsis*, encodes a member of the raf family of protein kinases. Cell 72:427-441

Kiegerl, S, Cardinale, F, Siligan, C, Gross, A, Baudouin, E Liwosz, A Eklöf, S, Till, S, Bögre, L, Hirt, H and Meskiene, H (2000) SIMKK, a Mitogen-activated protein kinase (MAPK) kinase, is a specific activator of the salt stress–induced MAPK, SIMK. Plant Cell, 12, 2247-2258

Kirst, GO (1989) Salinity tolerance of eukaryotic marine algae. Ann Rev Plant Physiol Plant Mol Biol 40, 21-53.

Kloareg, B and Quatrano, RS (1988) Structure of the cell walls of marine algae and ecophysiological functions of the matrix polysaccharides. Oceanogr Mar Biol Ann Rev. 26, 259-315

Klusener, B, Boheim, G, Liss, H, Engelberth, J and Weiler, EW (1995) Gadolinium-sensitive, voltage-dependent calcium-release channels in the endoplasmatic-reticulum of a higher plant mechanoreceptor organ. EMBO J 14, 2708-2714

Knetsch, MLW, Wang, M, Snaar-Jagalska, BE, and Heimovaara-Dijkstra, S (1996) Abscisic acid induces mitogen-activated protein kinase activation in barley aleurone protoplasts. Plant Cell 8, 1061-1067

Knight, H and Knight, MR (2001) Abiotic stress signalling pathways: specificity and cross-talk. Trends Plant Sci 6, 262-267

Knight, H, Trewavas, AJ and Knight, MR (1996) Cold calcium signaling in *Arabidopsis* involves two cellular pools and a change in calcium signature after acclimation. Plant Cell 8 489-503

Knight, H, Trewavas, AJ and Knight, MR (1997). Cold calcium signalling in *Arabidopsis thaliana* responding to drought and salinity. Plant J 12, 1067-1078

Knight, MR, Campbell, AK, Smith SM and Trewavas, AJ (1991) Transgenic plant aequorin reports the effects of touch and cold-shock and elicitors on cytoplasmatic calcium. Nature 352, 524-526

Knight, MR, Smith SM and Trewavas, AJ (1992) Wind-induced plant motion immediately increases cytosolic calcium. PNAS USA 89, 4967-4971

Krenn, BE, Tromp, MGM and Wever, R. (1989) The brown algae Ascophyllum nodosum contains two different vanadium bromoperoxidases. J Biol Chem 264, 19287-19292

Koehler, LD and Linskens, HF (1967). Incorporation of protein and RNA precursors into fertilised *Fucus* eggs. Protoplasma 64, 209-212.

Kok, B (1948). On the inhibition of photosynthesis by intense light. Biochim Biophys Acta 21, 234-244

Kornyeyev, D, Logan, BA, Payton, P, Allen, RD, Holaday, AS (2001) Enhanced photochemical light utilization and decreased chilling-induced photoinhibition of photosystem II in cotton overexpressing genes encoding chloroplast-targeted antioxidant enzymes. Physiol Plant 113(3), 323-331

Kovtun, Y, W-L Chiu, et al. (2000) Functional analysis of oxidative stress-activated mitogen-activated protein kinase cascade in plants. PNAS USA 97(5), 2940-2945

Kraay, GW, Zapata, M and Veldhuis, MJW (1992) Separation of chlorophylls c1, c2 and c3 of marine phytoplankton by reversed-phase-C18-high-performance liquid chromatography. J Phycology 28, 708-712

Krause, GH, Weis, E (1991). Chlorophyl fluorescence and photosynthesis: the basics. Annual Rev Plant Physiol 42: 313-349

Kroon, BMA (1994) Variability of photosystem II quantum yield and related processes in *Chlorella pyrenoidsa* (Chlorophyta) acclimated to an oscillating light regime simulating a mixed photic zone. J Phycol 30, 841-852

Kropf, DL (1997) Induction of polarity in fucoid zygotes. Plant Cell 9, 1011-1020

Kropf, DL and Quatrano, RS (1987) Localisation of membrane-associated calcium during development of fucoid algae using chlorotetracycline. Planta 171, 158-167

Kropf, DL (1989) Calcium and early development in fucoid algae. Biol Bull 176, S5-8

Kropf, DL (1994) Cytoskeletal control of cell polarity. Dev Biol 165, 361-371

Kropf, DL, Berge, SK, Quatrano, RS (1989) Actin localisation during *Fucus* embryogenesis. Plant Cell 1, 191-200

Kropf, DL, Kloareg, B and Quatrano, RS (1988) Cell wall is required for fixation of the embryonic axis in *Fucus* zygotes. Science 239, 187-190

Kropf, DL, Maddock, A and Gard, DL (1990) Microtubule distribution and function in early *Pelvetia* development. J Cell Sci 97, 545-552

Kultz, D and Burg, M (1998) Evolution of osmotic stress signalling via MAP kinase cascades. J Exp Biol 201, 3015-3021.

Kumar, D and Klessig, D (2000) Differential induction of tobacco MAP kinases by the defence signals nitric oxide, salicylic acid, ethylene and jasmonic acid. Mol Plant Interact 13, 347-351

Kuo, ML and Yang, NC (1995) Reversion of v-H-ras-transformed NIH 3T3 cells by apigenin through inhibiting MAPK and its downtream oncogenes. Biochem Biophys Res Comm 212(3) 767-775

Kupper, FC, Schweigert, N, Legendre, J-M, Vilter, H and Kloareg, B (1998). Iodine uptake in Laminariales involves extracellular, haloperoxidase-mediated oxidation of iodide. Planta 207, 163-171

Ladyzhenskaya, EP, Dardzhaniya, LG and Korableva, NP (1991) Effect of gibberellic acid on calcium content in subcellular fractions of potato tuber cells. Soviet Plant Physiol 38, 521-528

Lamb, C. and Dixon, R. (1997) The oxidative burst in plant disease resistance. Ann Rev Plant Physiol Plant Mol Biol 48, 251-275

Lamote, M, Schoefs, B, Duval, JC and Lemoine, Y (1998) Development of the photosynthetic apparatus in *Fucus serratus* embryos. In Garab, G. (ed) Photosynthesis: mechanisms and effects. Vol. IV: 3245-3248. Proc. XIth International Congress on Photosynthesis. Kluwer Academic Publishers. 5 volumes; 4396 pp

Lawlor, DW (1993) Photosynthesis: molecular, physiological and environmental processes. London: Longman Scientific 1993

Lebrun-Garcia, A, Ouaked, F, Chiltz, A, and Pugin, A (1998) Activation of MAPK homologues by elicitors in tobacco cells, Plant J 15, 77-83

Lebrun-Garcia, A, Bourque, S et al. (1999) Involvement of plasma membrane proteins in plant defence responses. Analysis of the cryptogein signal transduction in tobacco. Biochimie 81, 663-668

Lee, S, Hirt, H et al. (2001) Phophatidic acid activates a wound-activated MAPK in *Glycine max*. Plant J 26(5), 479-486

Leitsch J, Schnettger B, Critchley, C and Krause, G.H. (1994) Two mechanisms of recovery from photoinhibition in vivo: Reactivation of photosystem II related and unrelated to D1-protein turnover. Planta 194, 15-21

Lesser, MP (1996) Elevated temperatures and ultraviolet radiation cause oxidative stress and inhibit photosynthesis in symbiotic dinoflagellates. Limn Oceanog 41, 271-283

Levine, A, Pennell, RI, Alvarez, ME, Palmer, R and Lamb, C (1996) Calcium mediated apoptosis in a plant hypersensitive disease resistance response. Curr Biol 6, 427-437

Levine, A, Tenhaken, R et al. (1994) H_2O_2 from the oxidative burst orchestrates the plant hypersensitive disease resistance response. Cell 79: 583-593.

Levring, T (1952) Remarks on the submicroscopical structure of eggs and spermatozoids of *Fucus* and related genera. Physiologia Pl. 5 528-539

Li, YY, Yeh, E, Hays, T et al. (1993) Disruption of mitotic spindle orientation in a yeast dynein mutant PNAS USA 90, 10096-10100

Lichtenthaler, HK (1998) The stress concept in plants: an introduction. An NY Acad Sci 851:187-198

Ligterink, W, Kroj, T et al. (1997) Receptor-mediated activation of a MAP kinase in pathogen defence of plants. Science 276, 2054-2057

Lin, CC and Kao, CH (2001) Abscisic acid induced changes in cell wall peroxidase activity and hydrogen peroxide levels in roots of rice seedlings. Plant Sci 160(2), 323-329

Littlechild, J (1999) Haloperoxidases and their role in biotransformation reactions. Curr Opin Chem Biol 3(1), 28-34

Lobban, CS and Harrison, PJ (1994) Seaweed ecology and physiology. Cambridge University Press. 366 pp

Loggini, B, Andrea, S, Brugnoli, E and Navari-Izzo, F (1999) Antioxidative defense system, pigment composition and photosynthetic efficiency in two wheat cultivars subjected to drought. Plant Physiol 119, 1091-1099

Lopez-Huertas, E, Charlton, WL, Johnson, B, Graham, IA and Baker, A (2000) Stress induces peroxisome biogenesis genes. EMBO J 19(234), 6770-6777

Love, J, Brownlee, C and Trewavas, AJ (1997) Ca^{2+} and calmodulin dynamics during photopolarisation in *Fucus serratus* zygotes. Plant Physiol 115, 249-261

Low, P and Merida, J (1996) The oxidative burst in plant defense: function and signal transduction. Physiol Plant 96, 533-542

Lu, C and Vonshak, A (2002) Effects of salinity stress on photosystem II function in cyanobacterial *Spirulina platensis* cells. Physiol. Plant 114(3), 405-413

MacCarrone M, Van Zadelhoff G, Veldink GA, Vliegenthart JF, Finazzi-Agro A. (2000) Early activation of lipoxygenase in lentil (*Lens culinaris*) root protoplasts by oxidative stress induces programmed cell death. Eur J Biochem 267(16), 5078-84

Mackenzie, S and McIntosh, L. (1999) Higher plant mitochondria Plant Cell 11(4), 571-86

Mackerness, S, John, C, Jordan, B, and Thomas, B (2001) Early signalling components in ultraviolet-B responses: distinct roles for different reactive oxygen species and nitric oxide, FEBS Lett, 489, 237

Madsen, TV and Maberly, SC (1990) A comparison of air and water as environments for photosynthesis by the intertidal algae *Fucus spiralis* (Phaeophyta). J Phycol 26, 24-30

Major, KM and Davison, I (1998) Influence of temperature and light on growth and photosynthetic physiology of *Fucus evanescens* (Phaeophyta) embryos. Eur J Phycol 33, 129-138

Malanga, G and Puntarulo, S (1995) Oxidative stress and antioxidant content in *Chlorella vulgaris* after exposure to ultraviolet-B radiation. Physiol Plant 94, 672-79

Malanga, G., Calmanovici, G. and Puntarulo, S. (1997) Oxidative damage to chloroplasts from *Chlorella vulgaris* exposed to ultraviolet-B radiation. Physiol Plant. 101, 455-462

Malhó, R, Moutinho, A, van der Luit, A and Trewavas, AJ (1998) Spatial characteristics of calcium signalling: the calcium wave as a basic unit in plant cell calcium signalling. Phil Trans R Soc Lond B353, 1463-1473

Manes, F, Donato, E and Vitale M (2001) Physiological responses of *Pinus halepensis* under ozone and water stress conditions. Physiol Plant 113 (2) 249-257

Manley, SL, and Barbero, Pe (2001) Physiological constrains of bromoform (CHBr3) production by *Ulva lactuca* (Chlorophyta). Limnol Oceanogr 46(6) 1392-1399

Marrè, M, Amicucci, E et al. (1998) The respiratory burst and electrolyte leakage induced by sulphydryl blockers in *Egeria densa* leaves are associated with H2O2 production and are dependent on Ca^{2+} influx. Plant Physiol. 118, 1379-1387.

Marshall, CJ (1995) Specificity of receptor tyrosine kinase signalling: transient versus susttained extracellular-regulated protein kinase activation. Cell 80, 179-185

Martinec, J, Feltl, T, Scanlon, CH, Lumsden, PJ and Machackova, I (2000) Subcellular localisation of a high affinity binding site for D-myo-inositol 1,4,5-triphosphate from *Chenopodium rubrum*. Plant Physiol 124, 475-483

Maxwell, D, Wang, Y and McIntosh, L (1999) The alternative oxidase lowers mitochondrial reactive oxygen production in plant cells. PNAS USA 96, 8271-8276

Maxwell, K, and Johnson, GN (2000) Chlorophyll fluorescence--a practical guide. J Exp Bot 51(345), 659-68

May, MJ, Hammond-Kosack, KE and Jones, JDG (1996) Involvement of reactive oxygen species, glutathione metabolism and lipid peroxidation in the CF-gene dependent defense response of tomato cotyledones induced by race specific elicitors of *Cladosporium fulvum*. Plant Physiol 110, 1367-1369

McAinsh, MR, Brownlee, C and Hetherington, AM (1990) Absisic acid-induced elevation of guard cell cytosolic Ca^{2+} precedes stomatal closure. Nature 343, 186-188

McAinsh, MR, Brownlee, C and Hetherington, AM (1992). Visualizing changes in cytosolic-free Ca^{2+} during the response of stomatal guard-cells to abcisic acid. Plant Cell 4, 1113-1122

McAinsh, MR and Hethrerington, AM (1998) Encoding specificity in calcium signalling systems. Trends Plant Sci 3, 32-36

McCook, IJ and Chapman, ARO (1997) Patterns and variation in natural succession following massive ice-scour of a rocky intertidal seashore. J Exp Mar Biol Ecol 214, 121-147

McDowell, JM, Dangl, JL (2000) Signal transduction in the plant immune response. Trends Biochem Sci 25(2), 79-82

McIntosh, L, Eichler, T, Gray, G, Maxwell, D, Nickels, RN and Wong, Y (1998) Biochemical and genetic controls exerted by plant mitochondria. Biochem Biophys Acta 1365, 278-284

McLachlan, J (1974) Effects of temperature and light on growth and development of embryos of *Fucus edentatus* and *F. distichus*. Can J Bot 52, 943-51

McLachlan, J and Bidwell, R (1978) Photosynthesis of eggs, sperm, zygotes and embryos of *Fucus serratus*. Can J Bot 56, 371-373

Mehdy, M (1994) Active oxygen species in plant defence against pathogens. Plant Physiology 105, 467-472.

Mellersh, DG, Foulds, IV, Higgins, VJ, Heath, MC. (2002) H_2O_2 plays different roles in determining penetration failure in three diverse plant-fungal interactions. Plant J 29(3), 257-68

Mellersh, DG, Heath, MC (2001) Plasma membrane-cell wall adhesion is required for expression of plant defence responses during fungal penetration. Plant Cell 13(2), 413-24

Meneguzzo, S, Navari-Izzo, F and Izzo, R (1999) Antioxidative responses of shoots and roots of wheat to increasing NaCl concentrations. J Plant Physiol 155:274-280

Michaeli, R, Philosoph-Hadas, S, Riov, J, Shahak, Y, Ratner, K and Meir, S (2001) Chilling-induced leaf abscission of *Ixora coccinea* plants. III. Enhancement by high light via oxidative processes. Physiol Plant 113(3), 338-345

Mikolajczyk, M, Olubunmi, SA, Muszynska, G, Klessig, DF and Dobrowolska, G (2000) Osmotic stress induces rapid activation of a salicylic acid-induced protein kinase and a homolog of portien kinase ASK1 in tobacco cells. Plant Cell 12, 165-178

Miller, AJ, Callaham, DA, Gross, DJ and Hepler, PK (1992). Free Ca^{2+} gradient in growing pollen tubes of *Lilium* J Cell Sci 101, 7-12

Minibayeva, F, Kolesnikov, O and Gordon, L (1998) Contribution of plasma membrane redox system to the superoxide production by wheat root cells. Protoplasma 205, 101-106

Mittler, R, Shulaev, V, Seskar, M and Lamb, C (1996) Inhibition of programmed cell death in tobacco plants during pathogen-induced hypersensitive response at low oxygen pressure. Plant Cell 8, 1991-2001

Mittler, R, Feng, X et al: (1998) Post-transcriptional suppression of cytosolic ascorbate peroxidase expression during pathogen-induced programmed cell death in tobacco. Plant Cell 10, 461-473

Mizoguchi, T, Irie, K et al. (1996) A gene encoding a MAPKKK is induced simultaneously with genes for a MAPK and a S6 ribosomal protein kinase by touch, cold, and water stress in *Arabidopsis thaliana*. PNAS 93: 765-769

Moller, IM (2001) Plant mitochondria and oxidative stress: Electron transport, NADPH turnover, and metabolism of reactive oxygen species. Annu Rev Plant Physiol Plant Mol Biol 52, 561-591

Morel, F, Doussiere, J and Vignais, PV (1991). The superoxide-generating oxidase of phagocytic cells: physiological, molecular and pathological aspects. Eur J Biochem 201, 523-546

Morel, Y and Barouki, R (1999) Repression of gene expression by oxidative stress. Biochem J 342, 481-496.

Muller, DG and Gassmann, G (1978) Identification of the sex attractant in the marine algae *Fucus vesiculosus*. Naturwissenschaften 65S:389

Munnik, T, Ligterink, W et al. (1999) Distinct osmo-sensing protein kinases pathways are involved in signalling moderate and severe hyoer-osmotic stress. Plant J 20(4), 381-388.

Murata,Y, Pei, Z-M, Mori, I and Schroeder, J (2001) Abscisic Acid Activation of Plasma Membrane Ca^{2+} Channels in Guard Cells Requires Cytosolic NAD(P)H and Is Differentially Disrupted Upstream and Downstream of Reactive Oxygen Species Production in *abi1-1* and *abi2-1* Protein Phosphatase 2C Mutants. Plant Cell 13, 2513-2523

Navari-Izzo, F, Pinzino, C, Quartacci, MF, Sgherri, CL (1999) Superoxide and hydroxyl radical generation, and superoxide dismutase in PSII membrane fragments from wheat. Free Rad Res 31 (suppl.) 3-9

Navari-Izzo, F, Quartacci, MF and Sgherri, CLM (1997) Desiccation tolerance in higher plants related to free radical defences. Phyton (Austria) 37:203-214

Navas, P and Córdoba, F (1996) Role of apoplastic and cell wall peroxidases on the stimulation of root elongation by ascorbate. Plant Physiol 112, 1119-1125

Navazio, L, Bewell, MA, Siddiqua, A, Dickinson, GD, Galione, A and Sanders, D (2000). Calcium release from the endoplasmatic reticulum of higher plants elicited by NADP metabolite nicotinic acid adenine dinucleotide phosphate. PNAS USA 97, 8693-8698

Navazio, L, Mariani, P and Sander, D (2001) Mobilisation of Ca^{2+} by cyclic ADP-ribose from the endoplasmatic reticulum of cauliflower florets. Plant Physiol 125, 2129-2138

Neher, E (1992). Correction of liquid junction potentials in patch clamp experiments. Methods in Enzymology 207, 123-131

Nishiyama, Y, Yamamoto, H, Allakhverdiev, S I, Inaba, M, Yokota, A and Murata, N (2001) Oxidative stress inhibitos the repair of photodamage to the photosynthetic machinary. EMBO J20(20), 5587-5594

Noctor, G, Veljovic-Jovanovic, S and Foyer, CH (2000) Peroxide processing in photosynthesis: antioxidant coupling and redox signalling. Philos Trans R Soc Lond B Biol Sci 355(1402), 1465-75

Norton, T, (1983) The resistance to dislodgement of *Sargassum muticum* germlings under defined hydrodynamic conditions. J Mar Biol Ass UK 63, 181-193.

Nuccitelli, R (1978) Ooplasmic segregation and secretion in the *Pelvetia* egg is accompanied by a membrane-generated electrical current. Dev Biol 62, 13-33

Nuccitelli, R. and Jaffe, L. F. (1974). Spontaneous current pulses through developing fucoid eggs. PNAS 71, 4855-4859

Nuhse, TS, Peck, SC et al. (2000) Microbial elicitors induce activation and dual phosphorylation of the *Arabidopsis thaliana* MAPK6. J Biol Chem 275(11), 7521-7526

Ogawa, K, Kanematsu, S, Asada, K (1997) Generation of superoxide anion and localization of CuZn-superoxide dismutase in the vascular tissue of spinach hypocotyls: their association with lignification. Plant Cell Physiol 38(10), 1118-26

Ohsawa, N, Ogata, Y, Okada, N and Itoh, N (2001) Physiological function of bromoperoxidase in the red marine alga *Corallina pilulifera*: production of bromoform as an allochemical and the simultaneous elimination of hydrogen peroxide. Phytochem 58, 683-692

Ohshiro, T, Nakano, S, Takahashi, Y, Suzuki, M, Izumi, Y (1999) Occurrence of bromoperoxidase in the marine green macroalgae *Ulvella lens* and emission of volatile brominated methane by the enzyme. Phytochem 52, 1211-1215

Oike, M, Droogmans, G and Nilius, B (1994). Mechanosensitive Ca 2+ transients in endothelial cells from human umbilical vein. PNAS USA 91, 2940-2944

Okazaki, Y, Yoshimoto, Y, Hiramoto, Y and Tazawa, M (1987) Turgor regulation and cytoplasmatic free Ca^{2+} in the algae *Lamprothamnium*. Protoplasma 140, 67-71

Olsen, PD and Varner, JE (1993). Hydrogen peroxide and lignification. Plant J 4, 887-892

Oltmanns, F (1922) In: Morphologie und Biologie der Algen. Jena. Jena Verlag

Orozco-Cárdenas, M, Narváez-Vasquez, J and Ryan, C (2001) Hydrogen peroxide acts as a second messenger for the induction of defense genes in tomato plants in response to wounding, systemin and methyl jasmonate, Plant Cell, 13, 179-188

Ort, DR (2001) When there is too much light. Plant Physiol 125, 29-32

Osiewacz, HD (2002) Mitochondrial functions and aging. Gene 286(1), 65-71

Osmond, C (1994) What is photoinhibition? Some insights from comparisons of shade and sun plants. In Baker, N and Bowyer, N (eds.) Photoinhibition of photosynthesis, from molecular mechanisms to the field. BIOS Scientific Publ., Oxford, pp.1-24

Otero P, Viana M, Herrera E and Bonet B (1997) Antioxidant and prooxidant effects of ascorbic acid and flavonoids on LDL submitted to different degrees of oxidation. Free Rad Res 27, 619-626

Palenik B, Price, NM and Morel, FMM (1991) Potential effects of UV-B on the chemical environment of marine organisms: a review. Env Poll 70, 117-130

Papadakis, A and Roubelakis-Angelakis, K. (1999) The generation of active oxygen species differs in tobacco and grapevine mesophyll protoplasts. Plant Physiol 121, 197-205

Park, MK, Ashby, MC, Erdemli, G, Petersen, OH and Tepikin, AV (2001) Perinuclear, perigranular and sub-plasmalemmal mitochondria have distinct functions in the regulation of cellular calcium transport. EMBO J 20(8), 1863-1874

Pastori, Y and del Rio, LA (1997) Natural senescence of pea leaves – an activated oxygen-mediated function for peroxisomes. Plant Physiol 113, 411-418

Patsikka, E, Kairavuo, M, Sersen, F, Aro, EM and Tyystjarvi (2002) Excess copper predisposes photosystem II to photoinhibition in vivo by outcompeting iron and causing decrease in leaf chlorophyll. Plant Physiol 129(3), 1359-1367

Pawley, J.B. (1995) Handbook of biological confocal microscopy. 2nd edition, Plenum Press, New York, London, 632 pp.

Pawson, T and Scott, JD (1997) Signalling through scaffold, anchoring and adapter proteins. Science 278, 2075-2080

Payton, P, Webb, R, Kornyeyev, D, Allen, R, Holaday, AS (2001) Protecting cotton photosynthesis during moderate chilling at high light intensity by increasing chloroplastic antioxidant enzyme activity. J Exp Bot 52(365), 2345-54

Pearson, G and Davison, IR (1994) Freezing stress and osmotic dehydration in *Fucus distichus* (Phaeophyta): evidence for physiological similarity. J. Phycol. 30, 257-267

Pearson, G and Davison, IR (1993) Freezing rates and duration determine the physiological response of intertidal fucoids to freezing. Mar Biol 115, 353-362

Pearson, G and Brawley, SH (1996) Reproductive ecology of *Fucus distichus* (Phaeophyceae): an intertidal algae with successful external fertilisation. MEPS 143, 211-223

Pedersen, M, Collen, J, Abrahamsson, K and Ekdahl, A (1996) Production of halocarbons from seaweeds: an oxidative stress reaction? Sci Mar 60: 257-263

Pei, Z-M, Murata, Y, Benning, G, Thomine, S, Klusener, B, Allen, G, Grill, E and Schroeder, JI (2000) Calcium channels activated by hydrogen peroxide mediate abscisic acid signalling in guard cells. Nature 406, 731-734

Pei, ZM, Ward, JM and Schroeder, JI (1999) Magnesium sensitises slow vacuolar channels to physiological cytosolic calcium and inhibits fast vacuolar channels in fava bean guard cell vacuoles. Plant Physiol 121, 977-986

Pellinen, R, Palva, T et al. (1999) Subcellular localisation of ozone-induced hydrogen peroxide production in birch (*Betula pendula*) leaf cells. Plant J 20(3), 349-356

Peng, HB and Jaffe, LF (1976) Cell wall formation in *Pelvetia* embryos. A freeze fracture study. Planta 133, 57-71

Peng, M and Kuc, J (1992). Peroxidase-generated hydrogen peroxide as a source of anti-fungal activity *in vitro* and on tobacco leaf disks. Phytopathology 82, 696-699

Perera, IY, Heilmann, I and Boss, WF (1999). Transient and sustained increase in inositol 1,4,5, triphosphate precede the differential growth response in gravistimulated maize pulvini. PNAS USA 96, 5838-5843

Platt T, Gallegos C and Harrison WG (1980) Photoinhibition of photosynthesis in natural assemblages of marine phytoplankton. J Mar Res 38, 687-701

Popov, V, Simonian, R, Skulachev, V, and Starkov, A (1997) Inhibition of the alternative oxidase stimulates H_2O_2 production in plant mitochondria. FEBS Lett 415(1), 87-90

Popping, B, Gibbonds, T and Watson, MD (1996). The *Pisum sativa* MAP kinase homologue (PsMAPK) rescues the *Saccharomyces cerevisae* HOG1 deletion mutant under conditions of high osmotic stress. Plant Mol Biol 31, 355-363

Potikha TS, Collins CC, Johnson DI, Delmer DP and Levine A (1999) The involvement of hydrogen peroxide in the differentiation of secondary walls in cotton fibers Plant Physiol 119(3), 849-58

Poyton, RO, and McEwen, JE (1996). Crosstalk between nuclear and mitochondrial genomes Annu Rev Biolchem 65, 563-607

Price, A, Taylor, A et al. (1994) Oxidative stress signals in tobacco increase cytosolic calcium. Plant Cell 6, 1301-1310.

Pu, R and Robinson, K (1998) Cytoplasmatic calcium gradients and calmodulin in the early development of the fucoid algae *Pelvetia compressa*. J Cell Sci 111, 3197-3207

Pu, RS, Wozniak, M and Robinson, KR (2000) Cortical actin filaments form rapidly during photopolarization and are required for the development of calcium gradients in *Pelvetia compressa* zygotes. Dev Biol 222, 440-449

Pugin, A, Frachisse, J-M, Tavernier, E, Bligny, R, Gout, E, Douce, R and Guern, J (1997) Early events induced by the elicitor cryptogein in tobacco cells: involvement of a plasma membrane NADPH oxidase and activation of glycolysis and the pentose phosphate pathway. Plant Cell 9, 2077-2091

Puntarulo, S, Sanchez, R and Bovaris, A (1988) Hydrogen peroxide metabolism in soybean embryonic axes at the onset of germination. Plant Physiol 86, 626-630

Quatrano, R and Shaw, SL (1997) Role of the cell wall in the determination of cell polarity and the plane of cell division in *Fucus* embryos. Trends Plant Sci 2, 15-21

Quatrano, RS (1974) Developmental biology: development in marine organisms. In: Experimental Marine Biology 303-344

Quatrano, RS (1972) An ultrastructural study of the determined site of rhizoid formation in *Fucus* zygotes. Exp Cell Res 70, 1-12

Quatrano, RS, Brian, L, Aldridge, J and Schultz, T (1991) Polar axis fixation in *Fucus* zygotes: components of the cytoskeleton and extracellular matrix. Development 1, S11-16

Quillet-Mary A, Jaffrezou JP, Mansat V, Bordier C, Naval J, Laurent G. (1997) Implication of mitochondrial hydrogen peroxide generation in ceramide-induced apoptosis. J Biol Chem 272(34), 21388-21395

Raab, T and Rapp, UP (2002) KSR – a regulator and scaffold protein of the MAPK pathway. Sci STKE 11(136), PE28

Rajasekhar, V, Lamb, C et al. (1999) Early events in the signal pathway for the oxidative burst in soybean cells exposed to avirulent *Pseudomonas syringae* pv *glycinea*. Plant Physiol 120, 1137-1146

Rathore, KS, Cork, RJ and Robinson, KR (1991) A cytoplasmatic gradient of Ca^{2+} is correlated with the growth of Lily pollen tubes. Dev Biol 148, 612-619

Razem FA, Bernards MA (2002) Hydrogen peroxide is required for poly(phenolic) domain formation during wound-induced suberization. J Agric Food Chem 50(5), 1009-1015

Reed, D, Amsler, C and Ebeling, A. (1992) Dispersal in kelps: factors affecting spore swimming and competency. Ecology 73(5), 1577-1585

Reed, D, (1990) The effects of variable settlement and early competition on patterns of kelp recruitment. Ecology 71(2), 776-787

Reed, R, Davison, L, Chudek, J and Foster, R (1985) The osmotic role of mannitol in the Phaeophyta: an appraisal. Phycologia 24, 35-47

Reichheld, J-P, Vernoux, T, Lardon, F, Van Montagu, M and Inzé, D (1999) Specific checkpoints regulate plant cell cycle progression in response to oxidative stress. Plant J 17, 647-656

Ren D, Yang H, Zhang S. (2002) Cell death mediated by MAPK is associated with hydrogen peroxide production in Arabidopsis. J Biol Chem 277(1), 559-65

Rizzuto, R Bernardi, P and Pozzan, T (2000) Mitochondria as all-round players of the calcium game. J Physiol 529, 37-47

Roberts, JM (1993) Turning DNA replication on and off. Curr Opin Cell Biol 5, 201-206

Roberts, S and Brownlee, C (1995) Calcium influx, fertilisation potential and egg activation in *Fucus serratus*. Zygote 3, 191-197

Roberts, SK, Berger, F and Brownlee, C (1993). The role of Ca^{2+} in signal transduction following fertilisation in *Fucus serratus*. J Exp Biol 184, 197-212.

Robinson, K and Jaffe, LF (1975) Polarising fucoid eggs drive calcium current through themselves. Science 187, 70-72

Robinson, KR (1996). Calcium and photopolarisation of *Pelvetia* zygotes. Planta 198, 378-384

Romeis, T (2001). Protein kinases in the plant defence response. Curr Opin Plant Biol 4, 407-414

Romeis, T, Piedras, P et al. (1999) Rapid Avr-9 and Cf-9-dependent activation of MAP kinases in tobacco cell cultures and leaves: convergence of resistance gene, elicitor, wound and salicylate responses. Plant Cell 11, 273-287

Romeis, T, Piedras, P et al. (2000) Resistance gene-dependent activation of a calcium-dependent protein kinase in the plant defence response. Plant Cell 12, 803-815

Rothstein, A and Mack, E (1990) Volume activated K^+ and Cl^- pathways of dissociated MDCK cells. Am J Physiol 258, C827-834

Royall, JA and Ischiropoulos, H (1993) Evaluation of 2,7-dichlorofluorescein and dihydrorhodamine 123 as fluorescent probes for intracellular H_2O_2 in cultured endothelial cells. Arch Biochem Biophys 302, 348-355.

Ruban, AV, Horton, P (1999) The xanthophyll cycle modulates the kinetics of nonphotochemical energy dissipation in isolated light-harvesting complexes, intact chloroplasts, and leaves of spinach Plant Physiol 119(2), 531-42

Sagi, M, Fluhr, R. (2001) Superoxide production by plant homologues of the gp91(phox) NADPH oxidase. Modulation of activity by calcium and by tobacco mosaic virus infection. Plant Physiol 126(3), 1281-90

Sairam, RK, Deshmukh, PS and Saxena, DC (1998) Role of antioxidant systems in wheat genotypes tolerance to water stress. Biol Plant 41, 387-394.

Samuel, MA, Miles, GP et al. (2000) Ozone treatment rapidly activates MAP kinase signalling in plants. Plant J 22(4), 367-376.

Samuilov, VD, Bezryadnov, B, Gusev, MV, Kitashov, AV and Fedorenko, TA (2001) Hydrogen peroxide inhibits photosyntheic electron transport in cells of cyanobacteria. Biochemistry (Mosc) 66(6) 640-645

Sanders D, Pelloux J, Brownlee C, Harper JF (2002) Calcium at the crossroads of signaling. Plant Cell 14 Suppl, S401-17

Sanders, D, Brownlee, C and Harper, JF (1999) Communicating with calcium. Plant Cell 11, 691-706

Santabarbara S, Bordignon E, Jennings RC, Carbonera D. (2002) Chlorophyll triplet states associated with photosystem II of thylakoids. Biochemistry 41(25), 8184-94

Santela, L and Kyozuka, K (1997). Effects of 1-methyladenine on nuclear Ca 2+ transients and meiosis resumption in starfish oocytes are mimicked by the nuclear injection of inositol 1,4,5-triphosphate and cADP-ribose. Cell Calcium 22, 1-20

Satoh, K, Smith, C and Fork, D (1983) Effects of salinity on primary processes of photosynthesis in the red alga *Porphyra perforata*. Plant Physiol 73, 643-647

Sauer, N, Corbin, DR, Keller, B and Lamb, C (1990) Cloning and characterisation of a wiund-specific hydroxyproline-rich glycoprotein in *Phaseolis vulgaris*. Plant Cell Environ 13, 257-266

Schoenwaelder, MEA and Wiencke, C (2000) Phenolic compounds in embryos during development of several northern hemisphere fucoids. Plant Biol 2, 24-33

Schofield, O, Evens, T and Millie, DF (1998) Photosystem II quantum yields and xanthophyll-cycle pigments of the macroalgae *Sargassum natans* (Phaeophyceae): responses under natural sunlight. J Phycol 34, 104-112

Schofield, O, Evens, T and Millie, DF (1998) Photosystem II quantum yields and xanthophyll-cycle pigments of the macroalgae *Sargassum natans* (Phaeophyceae): responses under natural sunlight. J Phycol 34:104-112

Schopfer P, Liszkay A, Bechtold M, Frahry G, Wagner A (2002) Evidence that hydroxyl radicals mediate auxin-induced extension growth. Planta 214(6), 821-8

Schopfer P (2001) Hydroxyl radical-induced cell-wall loosening in vitro and in vivo: implications for the control of elongation growth. Plant J 28(6), 679-88

Schopfer, P (2002). Hydroxyl radical-induced cell wall loosening *in vitro* and *in vivo*. Implications for the control of elongation growth. Plant J 28(6): 678-688

Schopfer, P, Plachy, C, and Frahry, G, (2001) Release of reactive oxygen intermediates (superoxide radicals, hydrogen peroxide and hydroxyl radicals) and peroxidase in germinating radish seeds controlled by light, giberellin and abscisic acid, Plant Physiol 125, 1591-1600

Schreiber, U, Schliwa, U and Bilger, B (1986) Continuous recording of photochemical and non-photochemical quenching with a new type of modulation fluorometer. Photosynthetic Research 10, 51-62

Schützendübel, A, Schwanz, P, Teichmann, T, Gross, K, Langenfeld-Heyser, R, Godbold DL., and Polle., A (2001) Cadmium-induced changes in antioxidative systems, hydrogen peroxide content, and differentiation in scots Pine roots. Plant Physiol 127, 887-898

Schwacke, R and Hager, A (1992) Fungal elicitors induce a transient release of active oxigen species from cultured spruce cells that is dependent on calcium and protein kinase activity. Planta 187, 136-141.

Schwarze, SR, Weindruch, R and Aiken, JM (1998). Oxidative stress and aging reduce COX I RNA and cytochrome oxidase activity in *Drosophila*. Free Rad Biol Med 25(6), 740-747

Scully, NM, McQueen DJ, Lean, DRS, Cooper, WJ (1996) Hydrogen peroxide formation: the interaction of ultraviolet radiation and dissolved organic carbon in lake waters along a 43-75°N gradient. Limnol Ocean41, 540-548

Seo, S, Okamoto, M, Seto, H, Ishizuka, K, Sano, H, and Ohashi, Y (1995) Tobacco MAP kinase: A possible mediator in wound signal transduction pathways. Science 270, 1988-1992

Seo, S, Sano, H, and Ohashi, Y (1999) Jasmonate-based wound signal transduction requires activation of WIPK, a tobacco mitogen-activated protein kinase. Plant Cell 11, 289-298

Sgherri CL, Pinzino C, Samaritani E, Navari-Izzo F (1999) Activated oxygen generation from thylakoids: a novel spin trap. Free Radic Res 31 Suppl, S199-204

Shackelford, RE, Kaufmann, WK and Paules, RS (2000) Oxidative stress and cell cycle checkpoint function. Free Rad Biol Med 28, 1387-404

Shaw, SL and Quatrano, RS (1996a) Polar localisation of a polar dihydropyridine receptor on living *Fucus* zygotes. J Cell Sci. 109, 335-342

Shaw, SL and Quatrano, RS (1996b) The role of targeted secretion in the establishment of cell polarity and the orientation of the division plane in *Fucus* zygotes. Development 122, 2623-2630

Shen, B, Jensen, RG and Bohnert, HJ (1997) Mannitol protects against oxidation by hydroxyl radicals. Plant Physiol 115, 527-532

Sheng, J, D'Ovidio, R and Mehdy, MC (1991) Negative and positive regulation of a novel proline-rich protein mRNA by fungal elicitors and wounding. Plant J 3, 345-354

Shirasu, K, Nakajima, H et al. (1997) Salicylic acid potentiates an agonist-dependent gain control that amplifies pathogen signals in the activation of defence mechanisms. Plant Cell 9, 261-270

Siefermann-Harms, D (1987) The light harvest and protective functions of carotenoids in photosynthetic membranes. Physiol Plant 69, 561-68

Smidsrød, O and Christensen, BE (1991) Molecular structure and physical behaviour of seaweed colloids as compared with microbial polysaccharides. In Guiry, M.D. & Blunden, G. (eds.) Seaweed resources in Europe: uses and potential. 8, 185-217

Smirnoff, N (1993) The role of active oxygen in the response of plants to water deficit and desiccation. New Phytol 125:27-58.

Soedjak HS and Butler, A (1991) Mechanism of dioxygen formation catalyzed by vanadium bromoperoxidase from *Macrocystis pyrifera* and *Fucus distichus*: steady state kinetic analysis and comparison to the mechanism of V-BrPO form *Ascophyllum nodosum* Biochim Biophys Acta 1079, 1-7

Sokal, RR and Rohlf, FJ (1995) Biometry: The principles and practice of statistics in biological research, 3rd edition. W.H. Freeman and Company, New York, 871pp

Spekssnijder, JA, Miller, AL, Weisenseel, MH, Chen, T-H and Jaffe, LF (1989) Calcium buffer microinjections block fucoid egg development by facilitating calcium diffusion. PNAS USA 86, 6607-6611

Sheffield, DJ, Harry, TR, Smith, AJ and Rogers, LJ (1995). *Corallina officinalis* bromoperoxidase immobilised on agarose. Phytochemistry 38, 1103-1107

Steer, MW and Steer, JM (1989). Pollen tube tip growth. New Phytol 111, 323-358

Stratmann, GW and Ryan, C (1997). Myelin basic protein kinase activity in tomato leaves is induced systemically by wounding and increases in repsonse to systemin and oligosaccharide elicitors. PNAS USA 94, 11085-11089

Strid A, Chow WS and Anderson JM (1994) UV-B damage and protection at the molecular level in plants. Photosynthetic Research 39, 475-489

Subbaiah, CC, Bush, DS et al. (1998) Mitochondrial contribution to the anoxic Ca^{2+} signal in maize suspension-cultured cells. Plant Physiol 118, 759-771

Sugimoto, A, Hozak, RR, Nakashima, T, Nishimoto, T and Rothman, JH (1995) Dad-1, and endogenous programmed cell death supressor in *Caenohabditis elegans* and vertebrates. EMBO J 14, 4434-4441

Surroca, A and Wolff, D (2000) Inositol 1,4,5-triphosphate but not ryanodine-receptor agonists induces calcium release from rat liver Golgi apparatus membrane vesicles. J Membr Biol 177, 243-249

Susin, SA, Zamzami, N and Kroemer, G (1998) Mitochondria as regulators of apoptosis: doubt no more. Biochem Biophys Acta 1366(1-2), 151-165

Suzuki, K, Yano, A and Shinshi, H (1999) Slow and prolonged activation of the p47 protein kinase during hypersensitive cell death in a culture of tobacco cells. Plant Physiol 119, 1465-1472

Takahashi, K, Isobe, M and Muto, S (1997) An increase in cytosolic calcium ion concentration precedes hypoosmotic shock activation of protein kinases in tobacco cell suspension culture cells. FEBS Lett 401, 202-206

Tan, S, Sagara, Y, Liu, Y, Maher, P and Schubert, D (1998). The regulation of reactive oxygen species production during programmed cell death. J Cell Biol 141, 1423-1432

Taylor, A and Brownlee, C (1992) Localized patch clamping of plasma membrane of a polarized plant cell. Plant Physiol 99, 1686-1688

Taylor, AR, Manison, N, Fernandez, C. Wood, J and Brownlee, C (1996) Spatial organization of calcium signalling involved in cell volume control in the *Fucus* rhizoid. Plant Cell 8, 2015-2031

Taylor, AR, Manison, NFH et al. (1996) Spacial organization of calcium signalling involved in cell volume control in the *Fucus* rhizoid. Plant Cell 8, 2015-2031

Taylor, A, Kim, J et al. (2001) Involvement of mitogen-activated protein kinase activation in the signal-transduction pathways of the soya bean oxidative burst. Biochem J 355, 795-803

Taylor, AR and Brownlee, C (1993) Calcium and potassium currents in the *Fucus* egg. Planta 189, 109-119

Taylor, LP and Hepler, PK (1997) Pollen germination and tube growth. Ann Rev Plant Physiol Plant Mol Biol 48, 461-491

Tazawa, M, Shimada, K and Kikuyama, M (1995) Cytoplasmic hydration triggers a transient increase in cytoplasmatic Ca^{2+} concentration in *Nitella flexilis*. Plant Cell Physiol 36, 335-340

Tena, G and Renaudin, J-P (1998) Cytosolic acidification but not auxin at physiological concentration is an activator of MAP kinases in tobacco cells. Plant J 16(2), 173-182

Tenhaken R, Levine A, Brisson LF, Dixon RA, Lamb C (1995) Function of the oxidative burst in hypersensitive disease resistance. PNAS USA 92(10), 4158-63

Thomas, GP, Sims, SM, Cock, MA and Karmazyn, M (1998) Hydrogen peroxide-induced stimulation of L-type calcium current in guinea pig ventricular myocytes and its inhibition by adenosine A1 receptor activation. J Pharmacol Exp Ther 286(3), 1208-1214

Thomas, MV (1982) Techniques in calcium research. Academic Press, London.

Thompson, JD, Higgins, DG and Gibson, TJ (1994) CLUSTAL W: improving the sensitivity of progressive multiple sequence alignment through sequence weighting, positions-specific gap penalties and weight matrix choice. Nucleic Acids Res 22, 4673-4680

Torres MA, Onouchi H, Hamada S, Machida C, Hammond-Kosack KE, Jones JD (1998) Six *Arabidopsis thaliana* homologues of the human respiratory burst oxidase (gp91phox). Plant J 14(3), 365-70

Tschiersch, H and Ohmann, E (1994) Photoinhibition in *Euglena gracilis*: Involvement of reactive oxygen species Planta 191, 316-323

Tsuji, H, Nakazono, M, Saisho, D, Tsutsumi, N and Hirai, A (2000) Transcript levels of the nuclear-encoded respiratory genes involved in oxygen deprivation: evidence for involvement of calcium in expression of alternative oxidase 1a gene. FEBS Lett 471 (2-3), 201-204

Uhrmacher, S, Hanelt, D and Nultsch, W (1995) Zeaxanthin content and the degree of photoinhibition are linearly correlated in the brown alga *Dictyota dichotoma*. Mar Biol 123, 159-165

Underwood, AJ and Fairweather, PG (1989) Supply-side ecology and benthic marine assemblages. Trends Ecol. Evol 4, 16-20

Urao, T, Yakubov, B et al. (1999) A transmembrane hybrid-type histidne kinase in *Arabidopsis* fuctions as an osmosensor. Plant Cell 11, 1743-1764.

Vadas, R, Wright, W and Miller, S (1990) Recruitment of *Ascophyllum nodosum* wave action as a source of mortality. MEPS 61, 263-272

Vadas, S, Johnson, S and Norton, TA (1992) Recruitment and mortality of early post-settlement stages of benthic algae. Br Phycol J 27, 331-335.

Vaucheret, H, Béclin, C, and Fagard, M, (2001) Post-transcriptional gene silencing in plants, J Cell Sci 114, 3083-3090

Very, AA and Davies, JM (2000) Hyper-polarisation-activated calcium channels at the tip of *Arabidopsis* rood hairs. PNAS USA 97, 9801-9806

Vranova E, Inze D and Van Breusegem F. (2002) Signal transduction during oxidative stress. J Exp Bot 53(372), 1227-36

Vreeland, V and Epstein, L (1996) Analysis of plant-substratum adhesives. *In* Linskens, H.F. & Jackson, J.F. (eds.) Modern methods of plant analysis. Plant cell wall analysis. 17, 95-116

Vreeland, V Grotkopp, E, Espinosa, S, Quiroz, D, Laetsch, WM and West, J (1993) The pattern of cell wall adhesive formation by *Fucus* zygotes. Hydrobiologia 261, 485-491

Wagner, AM (1995) A role for active oxygen species as second messengers in the induction of alternative oxidase gene expression in *Petunia hybrida* cells. FEBS Lett 368, 339-342

Wang, H and Joseph, J (2000) Mechanisms of hydrogen peroxide-induced calcium dysregulation in PC12 cells. Free Rad Biol Med 28(8), 1222-1231

Wang, Z, Tymianski, M, Jones, OT and Nedergaard, M (1997). Impact of cytoplasmatic calcium buffering on the spatio temporal characteristics of intracellular calcium signals in astrocytes. J. Neurosci. 17, 7359-7371

Weaver, R, Plat, H de Boer, E (1985) Isolation procedure and some properties of the bromoperoxidase from *Ascophyllum nodosum*. Biochim Biophys Acta 830, 181-186

Weis E, and Berry J (1987) Quantum efficiency in photosystem II in relation to energy-dependent quenching of chlorophyll fluorescence. Biochim Biophys Acta 894, 198-208.

Weisenseel, MH, Jaffe, LF (1972) Membrane potential and impedance of developing fucoid eggs. Dev Biol. 27, 555-574

Weyand, M, Hecht, HJ, Kieb, M, Liaud, MF, Vilter, H and Schomburg (1999) X.ray structure determination of a vanadium-dependent ghaloperoxidase from *Ascophyllum nodosum* as 2.0 A resolution. J. Mol Biol. 293, 595-611

White, OJ (2000) Calcium channels in higher plants. Biochim Biophys Acta 1465, 171-189

Widmann, C, Gibson, S et al. (1999) Mitogen-activated protein kinase: conservation of a three-kinase module from yeast to human. Physiol Rev 79(1), 143-180

Wilson, C, Voronin, V et al. (1997) A developmentally regulated MAP kinase activated by hidration in tobacco pollen. Plant Cell 9, 2093-2100

Wiltens, P, Schreiber, U and Vidaver, W (1978) Chlorophyll fluorescence induction: an indicator of photosynthetic activity in marine algae undergoing desiccation. Can J Bot 56, 2787-2794

Wojtaszek, P (1997) Oxidative burst: an early plant response to pathogen infection. Biochem J 322 (Pt 3), 681-92

Wright, SW, Jeffrey, SW, Mantoura, RFC, Llewellyn, CA, Bjørnland, T, Repeta, D and Welschmeyer, N (1991) Improved HPLC method for the analysis of chlorophylls and carotenoids from marine phytoplankton. MEPS 77, 183-196

Wright, PJ and Reed, RH (1990) Effects of osmotic stress on gamete size, rhizoid initiation and germling growth in fucoid algae. Br Phycol J 25, 149-155

Wu, G, Shortt, BJ et al. (1995) Disease resistance conferred by expression of a gene encoding H_2O_2-generating glucose oxidase in transgenic potato plants. The Plant Cell 7, 1357-1368.

Xing, T, Higgins, VJ, Blumwald, E (1997) Race-specific elicitors of *Cladosporium fulvum* promote translocation of cytosolic components of NADPH oxidase to the plasma membrane of tomato cells. Plant Cell 9(2), 249-59

Xing, T, Ouellet, T, Miki, B (2002). Towards genomic and proteomic studies of protein phosphorylation in plant-pathogen interactions. Trends Plant Sci 7(5), 224-230

Xu, H and Heath, M. (1998) Role of calcium in signal transduction during the hypersensitive response caused by basidiospore-derived infection of the Cowpea rust fungus. The Plant Cell 10, 585-597

Yahrous, T, Chandra, S et al. (1995) Evidence for a mechanically induced oxidative burst. Plant Physiol 109, 1259-1266

Yamanouchi, S (1909) Mitosis in *Fucus*. Bot Gaz 47, 173-197

Yang, KY, Liu, Y and Zhang, S (2001) Activation of a mitogen-activated protein kinase pathway is involved in disease resistance in tobacco. PNAS USA 98(2), 741-6

Yang, T and Poovaiah, BW (2002) Hydrogen peroxide homeostasis: activation of plant catalase by calcium/calmodulin. PNAS USA 99(6), 4097-4102

Yang, Y, Shah, J and Klessig, DF (1997) Signal perception and transduction in plant defence responses. Genes Dev 11, 1621-1639

Yoshioka H, Sugie K, Park HJ, Maeda H, Tsuda N, Kawakita K, Doke N (2001) Induction of plant gp91 phox homolog by fungal cell wall, arachidonic acid, and salicylic acid in potato. Mol Plant Microbe Interact 14(6), 725-36

Yuasa, K and Maeshima, M (2001) Organ specificity of a vacuolar Ca^{2+}-binding protein RVCaB in radish and its expression under Ca^{2+}-deficient conditions. Plant Mol Biol 47(5), 633-40

Yuasa, T, Ichimura, K, Mizogushi, T and Shinozaki, K (2001) Oxidative stress activates ATMPK6 an Arabidopsis homologue of MAP kinase. Plant Cell Phyisiol 42(9), 1012-1016

Yuasa, T and Muto, S (1996) Activation of a 40-kDa protein kinases in response to hypo- and hyperosmotic shock in the halotolerant green alga *Dunaliella tertiolecta*. Pant Cell Physiol 37(1), 35-42.

Zhang S and Klessig DF (1998b) The tobacco wounding-activated mitogen-activated protein kinase is encoded by SIPK PNAS USA 95(12), 7225-30

Zhang, S, Sheng, J, Liu, Y and Mehdy, MC (1993). Fungal elicitor-induced bean proline-rich protein mRNA down-regulation is due to destabilisation that is transcript and translation dependent. Plant Cell 5, 1089-1099

Zhang, S and Klessig, DF (1998a) Resistance gene *N*-mediated *de novo* synthesis and activation of a tobacco mitogen-activated protein kinase by tobacco mosaic virus infection. PNAS USA 95, 7433-7438

Zhang, S and Klessig, D (2001) MAPK cascades in plant defense signalling. Trends Plant Sci 6(11), 520-527

Zhang, S, Du, H et al. (1998) Activation of the tobacco SIP kinase by both a cell wall-derived carbohydrate elicitor and purified proteinaceous elicitins from *Phytophthora* spp. Plant Cell 10: 435-449

Zhang, X, Lin, Z, Dong, F, Gao, J, Galbraith, D and Song, C-P, (2001) Hydrogen peroxide is involved in abscisic acid-induced stomatal closure in *Vicia faba*, Plant Physiol, 126, 1438

Zhou, X and Mopper, K (1990) Determination of photochemically produced hydroxyl radicals in seawater and freshwater. Mar Chem 30, 71-88

Zhu, H Bannenberg, P Moldéus, GL, and Shertzer, HG (1994) Oxidation pathways for the intracellular probe 2′,7′-dichloroflurescein. Acta Toxicol. 68, 582-587

Zhu, H, Ming, H, Bannenberg, GL, Moldéus, P and Shertzer, HG (1996) Effects of glutathione and pH on the oxidation of biomarkers of oxidative stress. Arch Toxicol 70:628-634

Zimmermann, B (2000) Control of $Ins(1,4,5)P_3$-induced Ca^{2+} oscillations in permeabilized blowfly salivary gland cells: contribution of mitochondria. J Physiol 525, 707-719.

APPENDICES

The Plant Cell, Vol. 14, 2369–2381, October 2002, www.plantcell.org © 2002 American Society of Plant Biologists

Spatiotemporal Patterning of Reactive Oxygen Production and Ca^{2+} Wave Propagation in Fucus Rhizoid Cells

Susana M. Coelho,[a,b] Alison R. Taylor,[a] Keith P. Ryan,[a] Isabel Sousa-Pinto,[c] Murray T. Brown,[b] and Colin Brownlee[a,1]

[a] Marine Biological Association of the United Kingdom, Citadel Hill, PL1 2PB Plymouth, United Kingdom
[b] Department of Biological Sciences, University of Plymouth, Drake Circus, PL4 8AA Plymouth, United Kingdom
[c] Centro Interdisciplinar de Investigação Marinha e Ambiental, Universidade do Porto, Rua do Campo Alegre, 4100 Porto, Portugal

Both Ca^{2+} and reactive oxygen species (ROS) play critical signaling roles in plant responses to biotic and abiotic stress. However, the positioning of Ca^{2+} and ROS (in particular H_2O_2) after a stress stimulus and their subcellular interactions are poorly understood. Moreover, although information can be encoded in different patterns of cellular Ca^{2+} signals, little is known about the subcellular spatiotemporal patterns of ROS production or their significance for downstream responses. Here, we show that ROS production in response to hyperosmotic stress in embryonic cells of the alga *Fucus serratus* consists of two distinct components. The first ROS component coincides closely with the origin of a Ca^{2+} wave in the peripheral cytosol at the growing cell apex, has an extracellular origin, and is necessary for the Ca^{2+} wave. Patch-clamp experiments show that a nonselective cation channel is stimulated by H_2O_2 and may underlie the initial cytosolic Ca^{2+} increase. Thus, the spatiotemporal pattern of the Ca^{2+} wave is determined by peripheral ROS production. The second, later ROS component localizes to the mitochondria and is a direct consequence of the Ca^{2+} wave. The first component, but not the second, is required for short-term adaptation to hyperosmotic stress. Our results highlight the role of ROS in the patterning of a Ca^{2+} signal in addition to its function in regulating cell wall strength in the Fucus embryo.

INTRODUCTION

Reactive oxygen species (ROS) are produced by plant and animal cells in response to a range of stimuli (Bac et al., 1997; Minibayeva et al., 1998; Tan et al., 1998; Grant and Loake, 2000). Such oxidative bursts can underlie antimicrobial activity or downstream responses such as modulation of gene expression and cell cycle control (Finkel, 1998; Reichheld et al., 1999; Bowie and O'Neill, 2000; Desikan et al., 2000; Shackelford et al., 2000). In plants and animals, the activity of a plasma membrane NADPH oxidase is implicated as an important source of ROS. Superoxide generation at the external surface of the cells is followed by a rapid dismutation to H_2O_2, which readily crosses membranes. Inhibitors of the animal NADPH oxidase, including the suicide substrate inhibitor diphenyleneiodonium (DPI), also block the elicitor-stimulated oxidative burst in plant cells (Levine et al., 1994; Desikan et al., 1996; Pugin et al., 1997), and molecular and physiological data indicate functional and mechanistic similarities between the animal and plant NADPH oxidase related–oxidative burst. Abscisic acid has been shown to increase ROS in guard cells (Pei et al., 2000), and ROS was shown to be an intermediary in the pathway leading to abscisic acid–induced antioxidant (*CAT1*) gene expression (Guan et al., 2000). In addition to plasma membrane NADPH oxidase, mitochondria, peroxisomes, and chloroplasts are potential powerful intracellular generators of ROS (Pastori and del Rio, 1997; Morel and Barouki, 1999). Plant mitochondria can produce high levels of ROS when the activity of the enzyme alternative oxidase is suppressed (Maxwell et al., 1999). Allan and Fluhr (1997) studied ROS generation using the fluorescent dye dichlorofluorescein and showed an accumulation of oxidized dye in the chloroplasts and nucleus in intact tobacco epidermal cells, which suggests the production of ROS in these compartments. However, little information is available on the subcellular spatiotemporal dynamics of ROS production in response to specific stimuli.

A close relationship between stress-induced Ca^{2+} signals and ROS production is becoming increasingly clear from studies in both plant and animal cells. Both the Ca^{2+} dependence of H_2O_2 production (Grant and Loake, 2000) and the modulation of plasma membrane Ca^{2+} channels and

[1] To whom correspondence should be addressed. E-mail cbr@mba.ac.uk; fax 01752633102.
Article, publication date, and citation information can be found at www.plantcell.org/cgi/doi/10.1105/tpc.003285.

cytosolic Ca^{2+} (Ca^{2+}_{cyt}) by H_2O_2 (Pei et al., 2000) have been demonstrated. However, essential spatiotemporal data that would allow mechanistic interpretations of the interdependence of Ca^{2+} and ROS signals is lacking.

Two-celled *Fucus serratus* embryos comprise a polarized growing rhizoid cell and a thallus cell and experience regular and dramatic natural changes in their external osmotic conditions. Hypoosmotic or hyperosmotic treatment is known to cause transient increases of Ca^{2+} that initiate in the apical rhizoid region (Taylor et al., 1996), and the spatiotemporal patterns of hypoosmotically induced Ca^{2+} signals vary with stimulus strength (Goddard et al., 2000). These Ca^{2+} signals were shown to involve both Ca^{2+} influx across the plasma membrane and the release of Ca^{2+} from intracellular stores.

We used the suitability of Fucus embryos for microinjection, patch-clamp, and cellular Ca^{2+} imaging to understand the relationship between Ca^{2+} and ROS in the stress-signaling response pathway after hyperosmotic treatment. We demonstrate a close interdependence between Ca^{2+} and ROS signals during hyperosmotic stress. We show that there are two components in the hyperosmotic stress response. An initial ROS increase, at the plasma membrane level, is initiated a few seconds after hyperosmotic treatment and is required for the generation of a Ca^{2+}_{cyt} wave. A slower, Ca^{2+}-dependent component of ROS production is localized to the mitochondria. These results also indicate a functional role, specific to the peripheral component of ROS production, in the short-term adaptive response to hyperosmotic stress.

RESULTS

Hyperosmotic Stress Elicits Rapid Production of ROS at the Rhizoid Apex

The fluorescent probe chloromethyl-2′,7′-dichlorodihydrofluorescein diacetate (CM-$DCFH_2$-DA) was used to measure intracellular ROS production by Fucus embryos. Oxidation of $DCFH_2$ by ROS yields the fluorescent DCF. Although the oxidizing agent is believed to be either $OH^{\bullet}$ or H_2O_2 (Zhu et al., 1994), it is assumed that the main ROS reported is H_2O_2 (Pei et al., 2000). In cells that were loaded with CM-$DCFH_2$-DA to visualize both early cytosolic and mitochondrial ROS production (see Methods), hyperosmotic treatment (transfer from seawater to seawater plus 2 M sorbitol) induced a fast (within a few seconds) peripheral production of ROS at the rhizoid cell apex, particularly noticeable at sites of membrane–cell wall adhesions (Figure 1B; $n = 10$). After ~40 s, ROS production also was detectable in more discrete areas in subapical regions, becoming more evident after 120 s (Figure 1B). The time course of ROS production clearly showed an earlier onset in the peripheral region compared with the subapical region (Figure 1C).

Hyperosmotic Stress Elicits a Transient Ca^{2+}_{cyt} Increase and ROS Production in Discrete Intracellular Compartments

Hyperosmotic treatment induced a transient Ca^{2+}_{cyt} increase in rhizoid cells within 10 to 12 s, coincident with a reduction in cell volume (Figures 1D and 1E; $n = 10$). This Ca^{2+}_{cyt} transient reached peak average cellular levels of 483 ± 45.2 nM within 10 s of the onset of the Ca^{2+} increase before returning to resting levels during the subsequent 24 to 40 s. Confocal ratio images revealed that the hyperosmotically induced Ca^{2+} transient initiated at a discrete location in the rhizoid apex, where the plasma membrane remained attached to the cell wall during cytoplasmic shrinkage, and propagated through the cell as a unidirectional wave with an estimated velocity of 15 μm/s, reaching peak levels of at least 1 μM (Figure 1E). The apical Ca^{2+} gradient also was apparent on return to seawater (Figure 1E, a and b). Smaller excursions at resting Ca^{2+} were observed occasionally, occurring either spontaneously or in response to return to seawater after hyperosmotic treatment. In Figure 1D, these are apparent as a small decrease from 100 to 50 nM Ca^{2+}_{cyt} at the beginning of the trace and small transient increases after the return to seawater. These small changes in resting Ca^{2+} probably were related to growth or turgor regulation (Taylor et al., 1996).

Hyperosmotic treatment also elicited an increase in ROS production in discrete intracellular compartments, as monitored by DCF fluorescence in cells preincubated for 20 min in CM-$DCFH_2$-DA and washed subsequently for 20 min. ROS started to increase within 120 s after hyperosmotic treatment (Figures 1F and 1G; $n = 25$), followed by a more rapid production after 800 s, and reached a plateau after ~20 min. Although the time to onset of this component of intracellular ROS production varied from 40 to 120 s, this always occurred after the peak (i.e., downstream) of the hyperosmotically induced Ca^{2+} increase and the fast peripheral ROS production. By direct microinjection of CM-$DCFH_2$-DA into cells, we were able to estimate the average cellular production of ROS during hyperosmotic treatment to be equivalent to ~0.05 mmol of H_2O_2 per liter of cell volume per minute.

Localization of the Oxidative Burst

Embryos that were colabeled with the fluorescent mitochondrial probe MitoTracker Red and CM-$DCFH_2$-DA showed a clear localization of ROS production to mitochondria but not to chloroplasts (Figure 2A; $n = 7$). Transmission electron microscopy and confocal fluorescence imaging of identical sections labeled with MitoTracker Red confirmed, within the limits of resolution, the mitochondrial localization of the MitoTracker dye (Figure 2B). Although the mitochondria were not all labeled equally with MitoTracker dye, fluorescence was not found in any other cell compartments. Dissipation

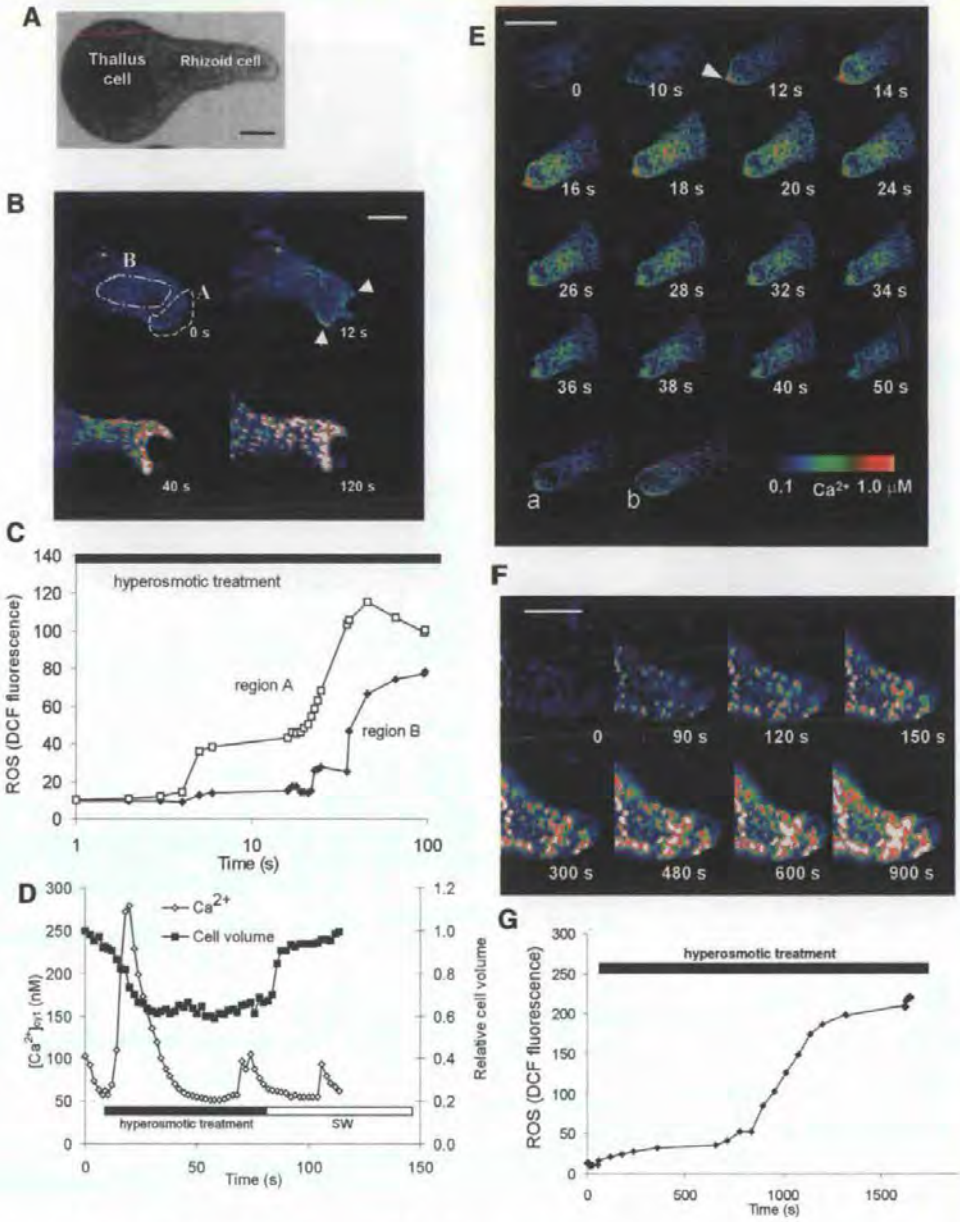

Figure 1. Time Course of Intracellular ROS Production and Ca^{2+}_{cyt} Dynamics during Hyperosmotic Treatment (Transfer from Seawater to Seawater Plus 2 M Sorbitol) in a Fucus Embryo Rhizoid Cell.

(A) Bright-field image of a two-celled Fucus embryo showing rhizoid and thallus cells. Bar = 30 μm.

(B) Early peripheral ROS production at the rhizoid apex during hyperosmotic shock. ROS production initiates at plasma membrane–wall adhesion sites (arrowheads). Cells were incubated for 20 min in 100 μM CM-$DCFH_2$-DA, immediately followed by hyperosmotic treatment. A and B represent apical and subapical regions from which mean fluorescence was plotted in **(C)**. Bar = 20 μm.

(C) Time course of DCF fluorescence in apical and subapical regions after hyperosmotic shock in the cell shown in **(B)** showing clear temporal separation of the onset of ROS production in each region.

(D) Time course of average Ca^{2+}_{cyt} increase during hyperosmotic treatment. Cell volume was computed simultaneously from transmitted light images.

(E) Confocal ratio images of a Ca^{2+}_{cyt} wave in response to hyperosmotic treatment. Ca^{2+}_{cyt} increase initiates from a point at which the plasma membrane remains attached to the cell wall (arrowhead). Localized Ca^{2+} increase at the extreme rhizoid apex was observed at 1 min (a) and 60 min (b) after return to seawater. Bar = 30 μm.

(F) Discrete localized intracellular ROS production during perfusion with hyperosmotic solution. Cells were incubated for 20 min in 100 μM CM-$DCFH_2$-DA, followed by washing in seawater for 20 min before hyperosmotic treatment. Bar = 20 μm.

(G) Time course of average cellular ROS production during hyperosmotic treatment.

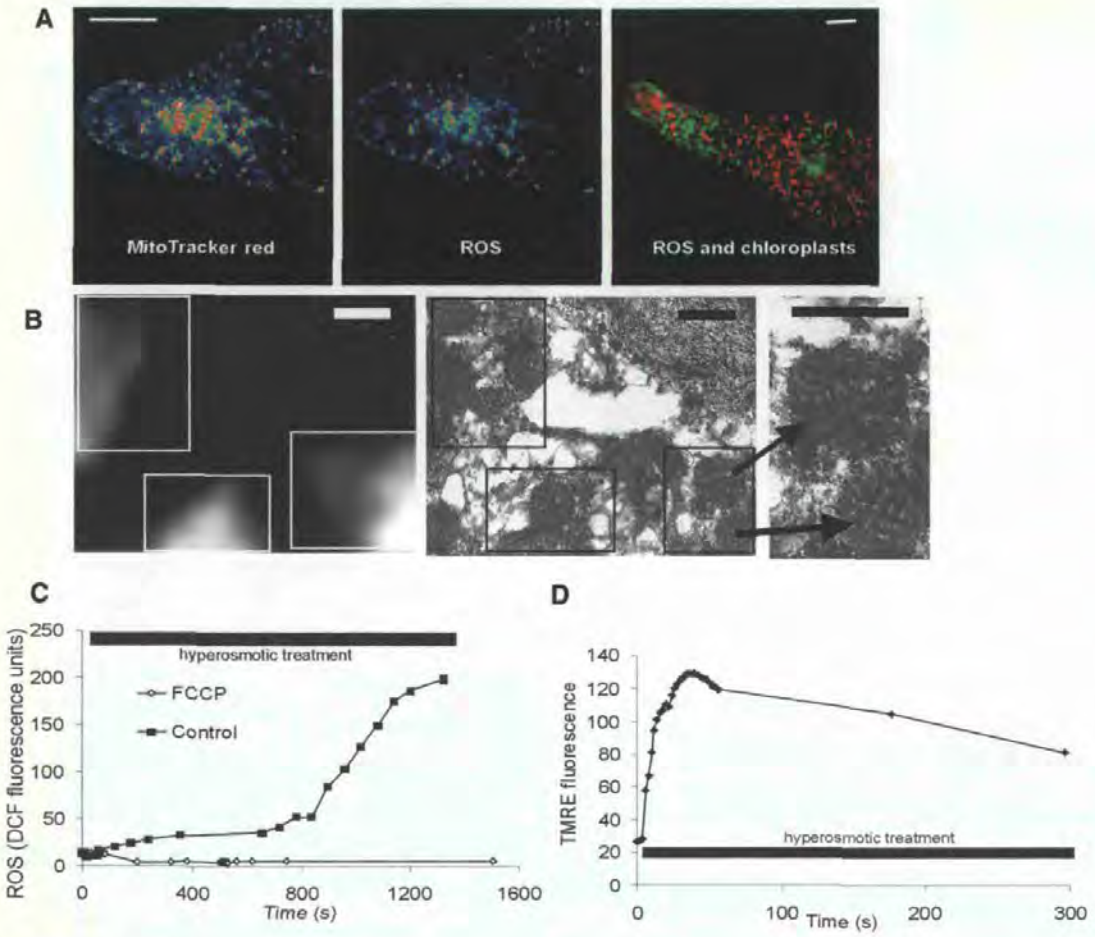

Figure 2. Mitochondrial ROS Increase.

(A) Colocalization of MitoTracker Red (left) and ROS production (center). Cells were coloaded with MitoTracker Red and CM-DCFH$_2$-DA. At right, a separate localization of chloroplasts (chlorophyll autofluorescence; red) and ROS production (green) is shown. Bar = 20 μm.

(B) Colocalization of MitoTracker Red fluorescence (left) and mitochondria (transmission electron microscopy; right) in identical fixed sections. The mitochondrial cristae are clearly visible in the enlarged transmission electron microscopy view (right). Bars = 1 μm.

(C) Carbonylcyanide *p*-trifluoromethoxyphenyl hydrazone (FCCP; 1 μM; 1 h of preincubation) caused a complete inhibition of ROS production.

(D) Hyperosmotic shock–induced depolarization of the mitochondrial membrane potential monitored as increased cellular TMRE fluorescence.

of the mitochondrial proton motive force with 1 μM carbonylcyanide *p*-trifluoromethoxyphenyl hydrazone completely abolished the hyperosmotic shock–induced mitochondrial ROS production (Figure 2C; $n = 5$). This inhibition was reversible (data not shown), suggesting a specific mitochondrial uncoupling effect.

The pattern of tetramethyl rhodamine ester (TMRE) accumulation also was identical to that of MitoTracker Green and CM-DCFH$_2$-DA (data not shown). Monitoring of the fluorescence of TMRE as an indicator of mitochondrial membrane potential suggested the occurrence of mitochondrial depolarization during hyperosmotic shock (Figure 2D; $n = 4$), the time course of which was similar to that of the corresponding transient Ca^{2+}_{cyt} increase. The mitochondrial Ca^{2+} (Ca^{2+}_m) reporter dye X-rhod-FF colocalized with MitoTracker Green in dual-labeling experiments (Figure 3A), allowing changes in Ca^{2+}_m to be monitored. An increase in Ca^{2+}_m was apparent ~20 s after hyperosmotic treatment (Figures 3A and 3B; $n = 15$)—that is, soon after the peak of the Ca^{2+}_{cyt} transient.

Interdependence of Ca^{2+} and ROS Production

To determine whether Ca^{2+}_{cyt} increase *is essential* for mitochondrial ROS production, the Ca^{2+} chelator dibromo gly-

cine, N_1N^1-(1,2-ethanediylbis(oxy-2,1-phenylene)) bis(N-carboxymethyl))-tetrapotassium salt (Br_2BAPTA) was injected into the rhizoid cell. Br_2BAPTA has been shown to prevent osmotically induced Ca^{2+} signals in Fucus rhizoids (Taylor et al., 1996). Br_2BAPTA abolished hyperosmotically induced ROS production in the injected rhizoid cell but not in the adjacent non-Br_2BAPTA-injected thallus cell (Figure 4A; $n = 7$). Thus, Ca^{2+}_{cyt} increase is a necessary step for mitochondrial ROS production.

The time course of early peripheral ROS production at the rhizoid apex was similar to that of the onset of Ca^{2+}_{cyt} increase, being detectable within a few seconds of hyperosmotic treatment. Unlike mitochondrial ROS increase, early peripheral ROS increase was not inhibited in Br_2BAPTA-injected cells (Figure 4B; $n = 12$), indicating that it occurred independently or upstream of the Ca^{2+}_{cyt} wave. The phospholipase C inhibitor U73122 blocked the hyperosmotically induced Ca^{2+} wave (Figure 4E) and the mitochondrial ROS increase but did not block peripheral ROS production (Figure 4C; $n = 7$). Interestingly, a prolonged increase of ROS was observed in the rhizoid apex in the presence of U73122 (Figure 4C). This contrasts with the more transient increase of ROS in the rhizoid apex in Br_2BAPTA-buffered cells and may reflect the inability of U73122 to block the highly localized plasma membrane influx component of Ca^{2+} increase, leading to an increase of ROS in mitochondria near the cell apex. The inactive analog of U73122 (U73343) had no effect on ROS production (data not shown).

We then investigated whether ROS production could lead to Ca^{2+}_{cyt} increase. The NADPH oxidase and peroxidase inhibitor DPI (Pugin et al., 1997; Frahry and Schopfer, 1998; Pei et al., 2000) brought about a complete inhibition of both peripheral and mitochondrial ROS increase and abolished the Ca^{2+}_{cyt} wave (Figures 4D and 4E; $n = 8$). This raises the likelihood that the peripheral ROS increase resulted from the extracellular production of ROS by the activity of plasma membrane–associated NADPH oxidase, leading to diffusion of H_2O_2 into the cell. The critical role of extracellular ROS production in initiating this cascade is further strongly supported by the dramatic inhibition of both intracellular ROS production ($n = 20$) and the Ca^{2+} wave ($n = 8$) by the application of extracellular catalase (Figures 4D and 4E). External application of H_2O_2 produced a dose-dependent increase of Ca^{2+}_{cyt} (Figures 5A and 5B; $n = 4$ for each concentration), reaching Ca^{2+}_{cyt} peak levels of 600 ± 102 nM with 1 mM H_2O_2. However, in clear contrast to the hyperosmotically induced Ca^{2+}_{cyt} transient, this did not propagate as a wave, occurring instead as a global Ca^{2+}_{cyt} increase spreading inward from around the cell periphery.

Single-channel recordings from cell-attached membrane patches of laser-derived spheroplasts from the rhizoid apex (Figure 5C) consistently revealed the presence of cation-permeable channels with properties identical to those characterized previously as nonselective cation channels (Taylor et al., 1996), based on their conductance (28 pS), reversal potential (−25 mV; assuming E_K of −50 mV, $[K^+]_{cyt} = 200$ mM) (Taylor et al., 1996), and spheroplast resting membrane potential of −60 mV (Berger and Brownlee, 1995). In 16 of 22 patches containing this type of channel activity, bath perfusion with 1 mM H_2O_2 in seawater produced a significant increase in channel activity. Although the extent of channel activation varied from cell to cell, in the experiment shown in Figure 5C, open probability averaged 0.01 before H_2O_2 addition and increased to 0.51 during the initial 10 s after H_2O_2 perfusion. Although opening to only a single open current

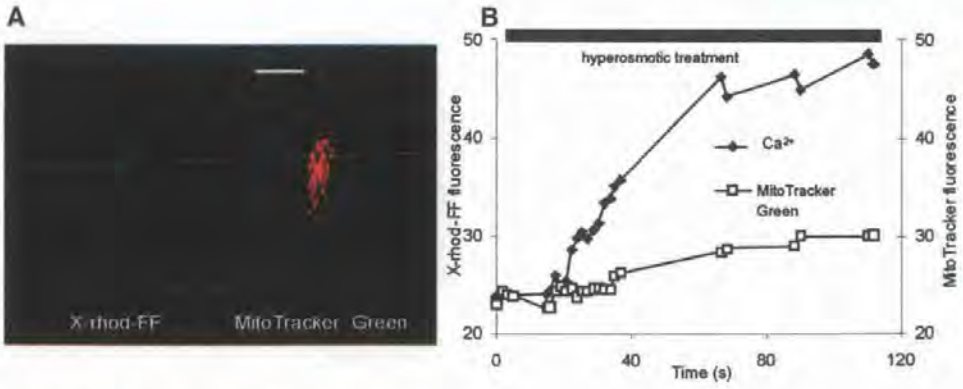

Figure 3. Ca^{2+}_m Dynamics during Hyperosmotic Treatment.

(A) Colocalization of X-rhod-FF and MitoTracker Green in mitochondria. Bar = 30 μm.

(B) Ca^{2+}_m increase during hyperosmotic treatment (black bar at top) measured with X-rhod-FF. Dual labeling with MitoTracker Green allowed Ca^{2+}-independent fluorescence to be monitored. Average X-rhod-FF or MitoTracker Green fluorescence values were plotted from the perinuclear mitochondria-rich region.

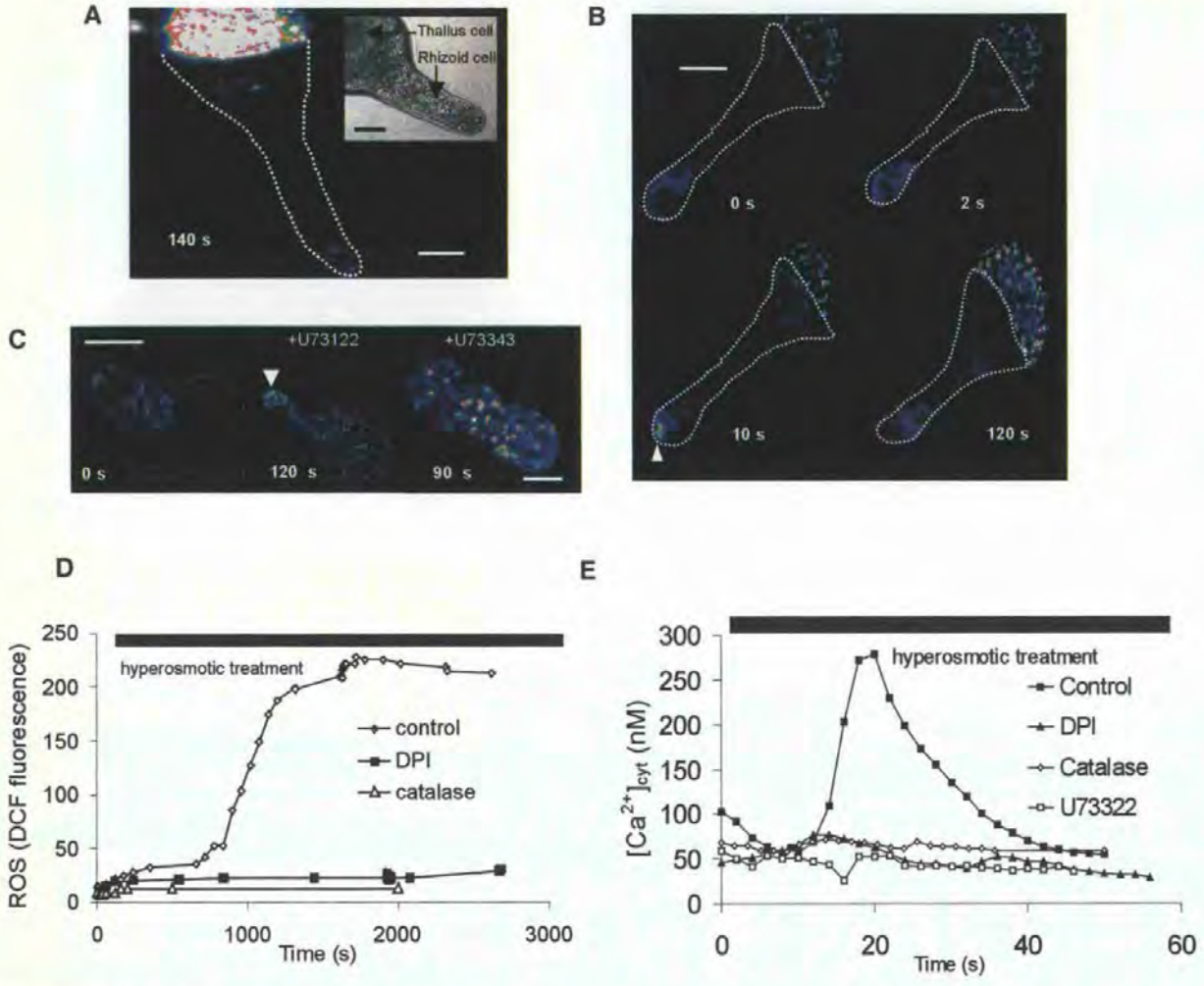

Figure 4. Interdependence between Ca^{2+}_{cyt} and ROS Production.

(A) Injection of Br_2BAPTA (4 mM final intracellular concentration) into the rhizoid cell inhibited mitochondrial ROS production (monitored at 140 s after hyperosmotic treatment) in cells loaded for 20 min with CM-$DCFH_2$-DA but not in the adjacent noninjected thallus cell. The dotted line indicates the rhizoid cell. Bar = 30 μm.

(B) Br_2BAPTA injection into the rhizoid cell did not prevent early peripheral hyperosmotically induced ROS production (arrowhead). In the cell shown, ROS production was apparent at the rhizoid apex at 2 and 10 s but declined to pretreatment levels after 120 s. Bar = 40 μm.

(C) The phospholipase C inhibitor U73122 inhibited mitochondrial but not peripheral hyperosmotically induced ROS production (left and middle). Cells were preincubated with U73122 for 2 h, and the inhibitor was retained in the hyperosmotic solution. The inactive analog U73343 did not prevent mitochondrial ROS increase. Bar = 30 μm.

(D) DPI and externally applied catalase completely inhibited ROS production during hyperosmotic shock. Cells were preincubated for 1 h in 10 μM DPI and for 30 min in 450 μg/mL catalase, and the inhibitors were retained in the perfusing hyperosmotic solution. The black bar at top indicates hyperosmotic perfusion.

(E) DPI, catalase, and U73122 abolished the hyperosmotically induced Ca^{2+}_{cyt} increase in rhizoid cells. Calcium green/Texas red ratio values were averaged for the whole rhizoid cell. The black bar at top indicates hyperosmotic perfusion.

level was observed before H_2O_2 treatment, four open levels were apparent from the single-channel trace and the associated amplitude histogram after H_2O_2 treatment (Figure 5C). The effect of H_2O_2 was variable but transient, lasting between 10 and 30 s.

Ca^{2+}_{cyt} Increase Is Sufficient to Induce Mitochondrial ROS Production

To determine whether Ca^{2+} increase alone was sufficient for mitochondrial ROS production, we used caged inositol

1,4,5-triphosphate [Ins(1,4,5)P_3] to increase Ca^{2+}_{cyt} in the absence of any stimulus. Photorelease of Ins(1,4,5)P_3 caused an immediate increase of Ca^{2+}_{cyt} (Figure 6A) that lasted for up to 20 s (n = 6). This Ca^{2+}_{cyt} increase was sufficient to trigger mitochondrial ROS production in the absence of any other stimulus (Figure 6B; n = 6). Significantly, the Ins(1,4,5)P_3-induced mitochondrial ROS production was not inhibited by DPI (Figure 6C; n = 3), indicating that the total inhibitory effect of DPI on hyperosmotically induced ROS production and the Ca^{2+}_{cyt} wave resulted from the specific inhibition of an upstream DPI-sensitive process.

Peripheral ROS Production Is Involved in Osmotic Adaptation

A functional role for ROS in the response to abiotic stress was evident from experiments that monitored the adaptation

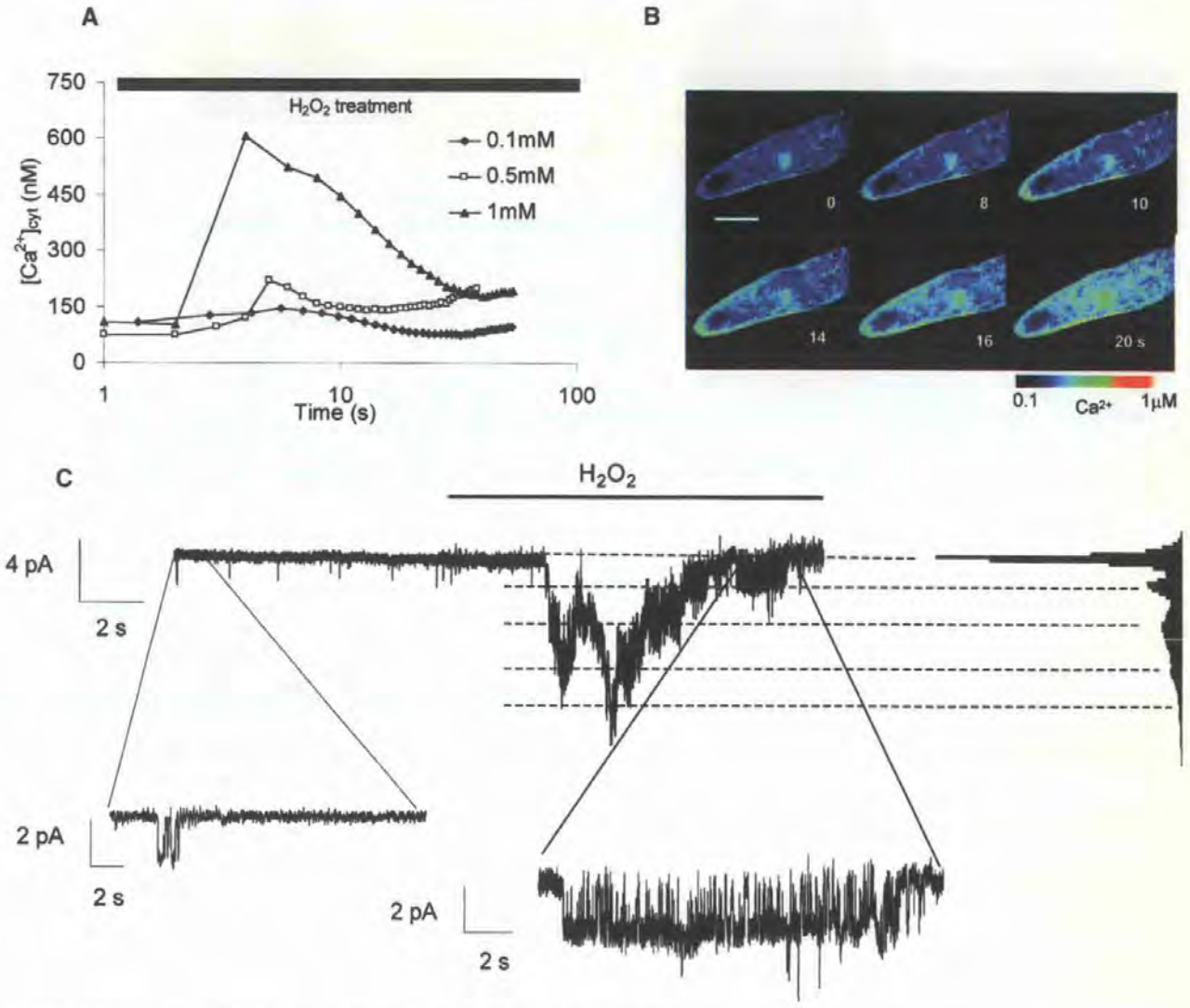

Figure 5. Changes in Ca^{2+}_{cyt} and Channel Activity Induced by Extracellular H_2O_2.

(A) Externally applied H_2O_2 caused a transient dose-dependent increase in Ca^{2+}_{cyt} in rhizoid cells.

(B) Confocal ratio images of a Ca^{2+}_{cyt} increase in response to externally applied 1 mM H_2O_2. Bar = 30 μm.

(C) Single channels recorded from a cell-attached membrane patch of a laser-derived spheroplast from the rhizoid apex. Before perfusion with H_2O_2, the patch showed single inward channel currents opening with low probability to a single level. A transient increase in channel activity was apparent within 4 s of 1 mM H_2O_2 perfusion. Four open levels induced by H_2O_2 are apparent in the channel trace and the accompanying amplitude histogram (right).

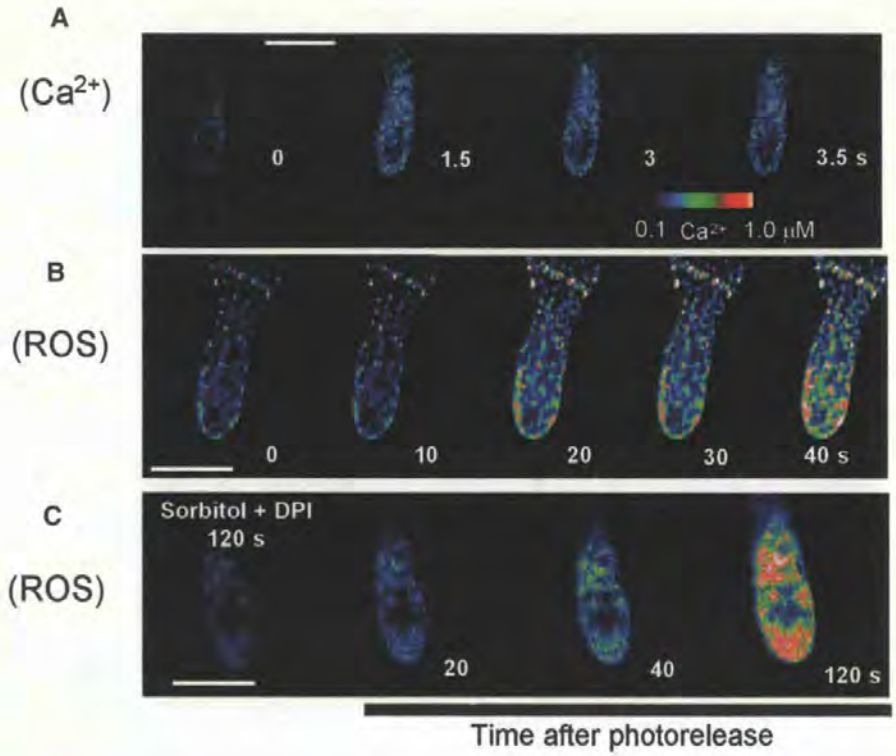

Figure 6. Ca^{2+}_{cyt} Increase Is Sufficient to Induce Mitochondrial ROS Production.

The left image in each sequence shows Ca^{2+} or ROS before photorelease of caged Ins(1,4,5)P_3. Images after Ins(1,4,5)P_3 release are identified by the bar at bottom.

(A) Ca^{2+}_{cyt} increase in response to photorelease of Ins(1,4,5)P_3 (1-s UV light flash given at time 0). Bar = 50 μm.

(B) ROS production induced by Ca^{2+}_{cyt} increase in response to photorelease of Ins(1,4,5)P_3. Bar = 40 μm.

(C) DPI prevented the hyperosmotically induced (sorbitol plus seawater) but not the subsequent Ins(1,4,5)P_3/Ca^{2+}-induced mitochondrial ROS production. Bar = 40 μm.

to osmotic treatments. Hypoosmotic shock (from 100% to 50% seawater) caused a significant proportion (25%) of rhizoid cells to rupture. However, hyperosmotic pretreatment rendered embryos more tolerant to osmotic bursting in response to subsequent hypoosmotic shock (Table 1), indicating increased cell wall strength. Pretreatment of embryos with 100 or 500 μM H_2O_2 also induced increases in resistance to subsequent hypoosmotic shock, suggesting that the osmotic adaptation induced by hyperosmotic pretreatment is related to ROS production. This was further supported by the complete abolition of this osmotic adaptation by DPI. By contrast, treatment of the embryos with the phospholipase C inhibitor U73122 (which blocks the hyperosmotically induced Ca^{2+} increase [Figure 4] and subsequent mitochondrial ROS production but not peripheral ROS production) did not affect the development of osmotic resistance, indicating that early peripheral ROS production is sufficient to activate cell wall resistance mechanisms.

DISCUSSION

Our results show a clear and essential interaction between Ca^{2+} and ROS in short-term signaling in response to hyperosmotic treatment. The velocity of propagation of the hyperosmotically induced Ca^{2+} wave reported here (~15 μm/s) was similar to that reported previously for hypoosmotically induced Ca^{2+} signals in Fucus rhizoid cells (Goddard et al., 2000). However, the pattern of propagation is different from that reported for hypoosmotic treatments, which generate separate apical Ca^{2+} increases and/or bidirectionally propagating Ca^{2+} waves that initiate in the perinuclear region depending on the strength of the stimulus (Goddard et al., 2000). Thus, the hyperosmotic Ca^{2+} wave provided a consistent signal against which to compare the patterns of ROS production in this signaling pathway. The hyperosmotically induced Ca^{2+} wave and the early peripheral ROS production both localize to the rhizoid apex at sites of adhesions be-

tween the plasma membrane and the cell wall. However, although the Ca^{2+} wave was dependent on the extracellular production of ROS, as indicated by the complete inhibition of the Ca^{2+} wave by both DPI and the extracellular application of catalase, early peripheral ROS production was independent of the Ca^{2+}_{cyt} increase.

A role for ROS in the spatial patterning of the Ca^{2+} wave also was indicated by the delocalized increase of Ca^{2+}_{cyt} initiating from around the cell periphery in response to delocalized external H_2O_2 application. In addition, the rapid activation by H_2O_2 of nonselective plasma membrane cation channels in cell-attached recordings strongly suggests that the initial action of external ROS production is mediated via Ca^{2+} influx through these channels. It remains to be determined whether the production of ROS at the growing rhizoid apex also underlies the Ca^{2+} gradient associated with rhizoid germination and growth (Brownlee and Wood, 1986; Taylor et al., 1996; Pu and Robinson, 1998). The concentrations of H_2O_2 that elicited increases in Ca^{2+}_{cyt} (0.1 to 1.0 mM) are comparable to those shown to cause Ca^{2+} increases and increased Ca^{2+} current in stomatal guard cell protoplasts (Pei et al., 2000). The actual H_2O_2 concentrations at the plasma membrane during hyperosmotic treatments are not known. Although we have estimated an average cellular H_2O_2 production rate of 50 $\mu mol \cdot L^{-1} \cdot min^{-1}$, the H_2O_2 concentrations at localized sites of production are likely to be considerably higher than the micromolar range.

The mitochondrial membrane potential drives ATP synthesis and provides a large driving force for divalent cation entry. Several studies have shown that, when challenged with high Ca^{2+}_{cyt}, the mitochondria can contribute to Ca^{2+} homeostasis by providing an intracellular sink for Ca^{2+} (Rizzuto et al., 2000). The increase in cellular TMRE fluorescence in response to hyperosmotic shock is consistent with the release of TMRE from the mitochondria in response to mitochondrial depolarization, resulting in reduced dye quenching (Zimmermann, 2000). We used X-rhod-FF as an indicator of Ca^{2+}_{m}. This is an improved version of rhod-2, which has been used to monitor Ca^{2+}_{m} in both animal and plant cells (Subbaiah et al., 1998; Park et al., 2001). Its colocalization with MitoTracker in the present study confirmed its mitochondrial localization in Fucus rhizoid cells. The onset of Ca^{2+}_{m} increase, coincident with the peak of the Ca^{2+}_{cyt} transient (i.e., 20 s after the hyperosmotic treatment), suggests the occurrence of Ca^{2+} uptake by the mitochondria after cytoplasmic Ca^{2+} increase, consistent with the role for mitochondria in buffering Ca^{2+}_{cyt} shown in a variety of animal cell types (Duchen, 2000; Rizzuto et al., 2000; Zimmermann, 2000). Moreover, recent reports show that the uptake of Ca^{2+} by mitochondria has a powerful impact on cellular Ca^{2+} signaling (Duchen, 2000), affecting the generation and propagation of $Ins(1,4,5)P_3$-triggered Ca^{2+} waves (Zimmermann, 2000) and the modulation of store-operated Ca^{2+} currents (Hoth et al., 1997).

To date, evidence for the role of mitochondria in spatiotemporal Ca^{2+} signaling is largely lacking for plants and algae, although mitochondria have been shown to represent a source of Ca^{2+} for signals elicited in response to anoxia (Subbaiah et al., 1998). We also show here that the onset of the increase in mitochondrial ROS production is coincident with the declining phase of the transient Ca^{2+}_{cyt} increase, with the peak of the mitochondrial depolarization, and with the increase of Ca^{2+}_{m} after hyperosmotic treatment. Moreover, mitochondrial ROS production shows an absolute dependence on Ca^{2+}_{cyt} increase. In animal cells, mitochondria may incur Ca^{2+}-induced respiratory impairment in response to Ca^{2+} loading that may potentiate ROS production (Grijalba et al., 1999). The total abolition of mitochondrial ROS production in Br_2BAPTA-injected rhizoid cells indicates a strong causal link between Ca^{2+}_{cyt} increase, Ca^{2+}_{m} uptake, and ROS production. Thus, an increase of Ca^{2+}_{cyt} is necessary to induce mitochondrial ROS production and is preceded by a peripheral cytosolic increase of ROS, involving an initial extracellular production of ROS, probably through a NADPH oxidase–like activity.

The hyperosmotically induced mitochondrial ROS production and Ca^{2+}_{cyt} increase were sensitive to DPI. By contrast, Ca^{2+}-induced mitochondrial ROS production after photorelease of caged $Ins(1,4,5)P_3$ was DPI insensitive. Therefore, hyperosmotically induced mitochondrial ROS production appears to require the activity of an upstream DPI-sensitive process.

A functional role for ROS in the response to abiotic stress was evident from experiments that monitored adaptation to

Table 1. Resistance to Hyperosmotic Shock in Pretreated and Control Embryos

Pretreatment[a]	Rhizoid Cell Bursting in Response to Subsequent Hypoosmotic Shock (% of Control)[b]
Control (no pretreatment)	100
2 M Sorbitol[c]	13.5
2 M Sorbitol + U73122	19.2
Sorbitol + DPI	101.9
100 μM H_2O_2[d]	30.8
100 μM H_2O_2 + U73122[d]	36.5
500 μM H_2O_2	23.1
500 μM H_2O_2 + U73122	23.1

[a] Pretreatments were given 1 h before a hypoosmotic shock (50% seawater).

[b] A minimum of 100 embryos were counted per replicate. Bursting was recorded at 5 min after hypoosmotic shock. Values represent the average of three replicates and are representative of two independent experiments.

[c] Sorbitol pretreatment was given for 30 min.

[d] H_2O_2 and U73122 were applied for 2 min (pretreatment with U73122 for 2 h).

The hyperosmotically induced mitochondrial ROS production and Ca^{2+}_{cyt} increase were sensitive to DPI. By contrast, Ca^{2+}-induced mitochondrial ROS production after photorelease of caged $Ins(1,4,5)P_3$ was DPI insensitive. Therefore, hyperosmotically induced mitochondrial ROS production appears to require the activity of an upstream DPI-sensitive process.

A functional role for ROS in the response to abiotic stress was evident from experiments that monitored adaptation to

osmotic treatments. Thus, hyperosmotic or H_2O_2 pretreatments rendered embryos more tolerant to osmotic bursting in response to subsequent hypoosmotic shock (Table 1). This is consistent with the widely reported role for ROS in increasing cross-linking of cell wall polymers, leading to increased cell wall strength in response to stress (Bradley et al., 1992; Fry et al., 2000). This was abolished by DPI but not by the inhibitor U73122, which blocks the Ca^{2+}_{cyt} increase and subsequent mitochondrial ROS production (Figures 4C and 4E), indicating that the early peripheral oxidative burst is sufficient to activate cell wall resistance mechanisms. The activation of cell wall resistance mechanisms by hyperosmotic treatment may function to counter the hypoosmotic stress that is likely during rehydration on return to normal seawater after solute accumulation associated with hyperosmotic adaptation.

Our results indicate a sequence of events leading to mitochondrial ROS production that involves an initial localized extracellular production of ROS at the level of the plasma membrane leading to Ca^{2+}_{cyt} increase, Ca^{2+} uptake by mitochondria, and mitochondrial ROS production (Figure 7). This is consistent with the demonstration of ROS production in response to abscisic acid in Arabidopsis stomatal guard cells, which was shown to increase the activity of hyperpolarization-dependent Ca^{2+} channels in the plasma membrane, leading to Ca^{2+}_{cyt} increase (Pei et al., 2000). The rapid onset of peripheral ROS production and Ca^{2+} increase reported here indicates a direct and rapid modulation by ROS of the pathways leading to propagation of a Ca^{2+}_{cyt} wave, involving both Ca^{2+} influx channels and release of Ca^{2+} from intracellular stores in endoplasmic reticulum–rich cellular regions in Fucus rhizoid cells (Taylor et al., 1996; Goddard et al., 2000).

These findings provide an insight into ROS/Ca^{2+} signaling in showing that localized extracellular ROS production is required for the spatial patterning of a Ca^{2+} signal. Good evidence exists for differing roles of spatially distinct Ca^{2+} signals in Fucus (Goddard et al., 2000). Although additional work is needed to establish the significance of mitochondrial ROS production in this system, peripheral ROS at the cell apex is involved in both Ca^{2+} wave generation and direct adaptive responses to stress.

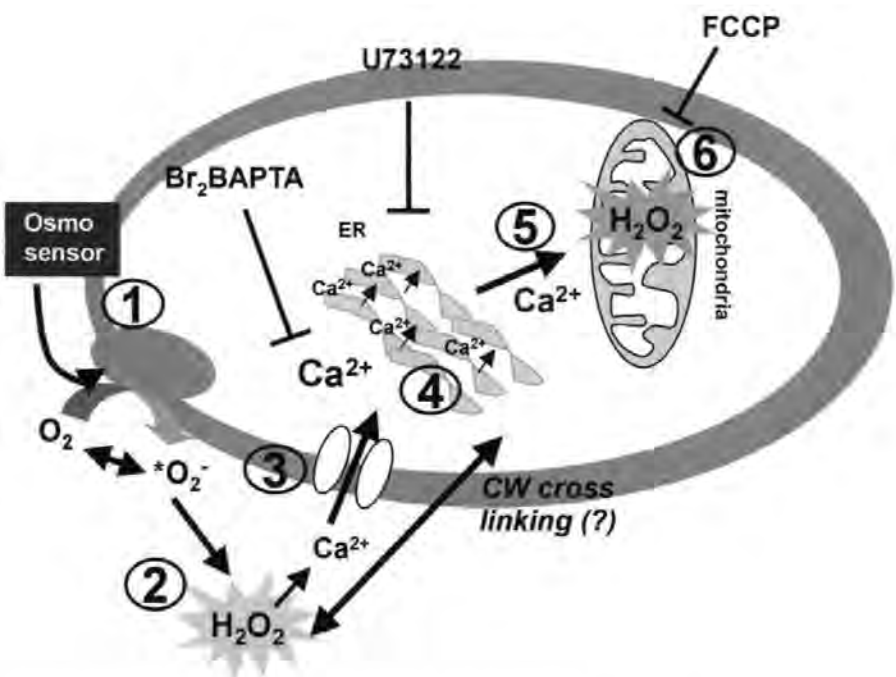

Figure 7. Proposed Signaling Pathway during Hyperosmotic Stress in Fucus Embryos.

Osmotic change is sensed by an unidentified osmosensor (1), which induces DPI-sensitive ROS production within 10 s (2). H_2O_2 is produced at the exterior side of the plasma membrane and may be involved in cell wall strengthening. H_2O_2 also diffuses into the cell, leading to a localized peripheral intracellular increase. Localized external H_2O_2 production also increases Ca^{2+} channel activity (3). Downstream events include Ca^{2+} wave propagation during the subsequent 10 to 60 sec (4), followed by Ca^{2+}_{m} increase (5) and mitochondrial ROS production (6). FCCP, carbonylcyanide *p*-trifluoromethoxyphenyl hydrazone.

METHODS

Embryo Culture

Fucus serratus embryos were cultured on glass cover slips fitted to the base of culture dishes in filtered seawater for 24 h in unidirectional light at 16°C, as described previously (Goddard et al., 2000). All experiments were performed using two-celled embryos. Dishes were perfused during experiments on the stage of a Nikon Diaphot 300 inverted microscope (Tokyo, Japan) with a gravity perfusion system that allowed rapid solution changeover.

Cytosolic Ca^{2+} Measurements

Cytosolic Ca^{2+} ($Ca^{2+}{}_{cyt}$) was measured in rhizoid cells using Calcium green–dextran (10 kD) ratioed against Texas red–dextran (10 kD; Molecular Probes, Eugene, OR) (Goddard et al., 2000). Dyes were dissolved to a final concentration of 1 mM in an artificial intracellular solution (200 mM KCl, 10 mM Hepes, and 550 mM mannitol, pH 7.0), pressure microinjected (Taylor et al., 1996; Goddard et al., 2000) using pipettes fabricated from 1.2-mm filamented borosilicate glass, and dry beveled (Taylor et al., 1996). In some cells, the Ca^{2+} chelator dibromo glycine, N_1N^1-(1,2-ethanediylbis(oxy-2,1-phenylene)) bis(N-carboxymethyl))-tetrapotassium salt (intracellular concentration of 4 mM) was microinjected along with the Ca^{2+} dyes to buffer $Ca^{2+}{}_{cyt}$ changes. Ca^{2+} dyes were injected to a final intracellular concentration of 10 to 50 μM. Embryos were incubated in 0.1 to 0.2 M sorbitol to reduce internal turgor pressure during microinjection and recovered in seawater for >1 h before measurements were taken. Images were acquired using a Bio-Rad 1024 confocal microscope (Hemel Hampstead, UK) equipped with a krypton/argon laser. Calcium green and Texas red were excited at 488 nm (523 nm emission) and 567 nm (605 nm emission), respectively. Images were acquired using TIMECOURSE software (Bio-Rad) and ratioed using TIMECOURSE (Bio-Rad) or LUCIDA (Kinetic Imaging, Liverpool, UK) software. Calcium green/Texas red fluorescence ratio (R) values were calibrated from R_{min} and R_{max} (Grynkiewicz et al., 1985). Dye-loaded cells were perfused alternatively with Ca^{2+}-free seawater (containing 0.1 mM EGTA) and 50 mM Ca^{2+}-seawater to obtain R_{min} and R_{max} values, respectively. All calibration solutions contained 100 μM ionomycin (Calbiochem, Nottingham, UK). $Ca^{2+}{}_{cyt}$ values were calculated using the formula $[Ca^{2+}]_{cyt} = K_d(R - R_{min})/(R_{max} - R)$. The K_d of Calcium green = 190 nM.

Intracellular Reactive Oxygen Species Measurements

Reactive oxygen species (ROS) production was monitored as oxidation of 5- (and 6-) chloromethyl-2′,7′-dichlorodihydrofluorescein diacetate (CM-$DCFH_2$-DA; Molecular Probes). Different dye-loading protocols were used to visualize preferentially either early peripheral cytosolic ROS production or longer term mitochondrial production. For visualization of early ROS increases in both the cytosol and the mitochondria, embryos were incubated in 100 μM CM-$DCFH_2$-DA in 1% ethanol for 20 min. Dye was retained in the experimental solution throughout the experiment. For preferential visualization of mitochondrial ROS production, cells were washed in seawater for 20 min before experiments. This removed dye from the cytosolic, but not the mitochondrial, compartment. Confocal images were obtained after excitation at 488 nm and emission at 522 nm. Because CM-$DCFH_2$-DA is a nonratiometric dye, we checked for any changes in fluorescence caused by a decrease in cell volume during hyperosmotic shock by simultaneously monitoring the fluorescence of microinjected Texas red–dextran (see above).

To estimate intracellular ROS production in nonstressed cells and during hyperosmotic shock, we used an in vivo calibration protocol. First, an in vitro calibration curve of the fluorescence of droplets of CM-$DCFH_2$ (chemically hydrolyzed from CM-$DCFH_2$-DA as indicated by the manufacturer) mixed with known concentrations of H_2O_2 (calibration curve A) was constructed together with an in vitro calibration curve of the fluorescence of droplets of various known concentrations of Texas red (calibration curve B). Rhizoid cells were injected with equal proportions of Texas red–dextran and CM-$DCFH_2$-DA. The average cellular fluorescence of each dye was monitored before and after hyperosmotic shock treatment. The concentration of Texas red, and thus the concentration of DCFH, was determined from calibration curve B. Using calibration curve A, we calculated the intracellular total ROS production that gave rise to the observed fluorescence.

Mitochondrial Localization

Mitochondria were localized after incubation with 0.1 μM MitoTracker Red (Molecular Probes) for 30 min or 0.2 μM MitoTracker Green (Molecular Probes) for 1.5 h. Mitochondrial membrane potential was monitored using the lipophilic cationic probe tetramethylrhodamine ester (TMRE; 0.1 μM for 5 min) (Molecular Probes). Each dye was dissolved in 0.1% DMSO in filtered seawater. To confirm the mitochondrial localization of MitoTracker dyes, embryos labeled with MitoTracker red or MitoTracker green were fixed, embedded, and sectioned for transmission electron microscopy as described previously (Brownlee and Pulsford, 1988) but without osmium after fixation. Confocal fluorescence images of sections mounted on 3- × 1-mm slot grids (0.1 to 0.5 μm) were acquired, and sections were exposed subsequently to osmium vapor from a drop of osmium tetroxide in a closed petri dish. They were then stained in 4% methyl acetate and lead citrate and viewed with a JEOL 200 CX electron microscope. This allowed the direct identification of fluorescent cellular structures.

TMRE enters mitochondria in a membrane potential–dependent manner. Mitochondrial accumulation of TMRE has been shown to cause the quenching of fluorescence, whereas mitochondrial depolarization induces TMRE release from mitochondria and a consequent increase in cellular fluorescence (Zimmermann, 2000). Thus, changes in TMRE fluorescence have been used to monitor mitochondrial membrane potential changes. TMRE fluorescence was monitored with the confocal microscope at 568-nm excitation and 605-nm emission. Cells loaded simultaneously with CM-$DCFH_2$-DA and MitoTracker red or with X-rhod-FF ((Molecular Probes; see below) and MitoTracker green were scanned at 488/568 nm (excitation wavelengths) and 522/605 nm (emission wavelengths).

Inhibitors

The mitochondrial uncoupler carbonylcyanide *p*-trifluoromethoxyphenyl hydrazone (Sigma, Poole, UK) was dissolved in 0.1% DMSO and filtered seawater (final concentration of 1 μM). The NADPH oxidase inhibitor diphenyleneiodonium (Sigma) was dissolved in 0.1% DMSO to a final concentration of 10 μM in filtered seawater. Cells were exposed to inhibitors for 1 h before the beginning of the experiment, and inhibitors also were included in the perfusing solutions.

The phospholipase C inhibitor U73122 or its inactive analog U73343 was dissolved in 0.1% DMSO and filtered seawater (final concentration of 10.0 μM), and cells were preincubated for 2 h. Catalase (Sigma) was used at a concentration of 450 μg/mL.

Mitochondrial Ca^{2+}

X-rhod-FF was used to monitor mitochondrial Ca^{2+} changes. X-rhod-FF has a net positive charge, which facilitates its sequestration inside mitochondria by potential-driven uptake. Cells were loaded with 2 μM X-rhod-FF AM (0.1% DMSO) for 1.5 h. The residual extracellular and cytosolic dye was eliminated by washing in seawater for 2 h. The mitochondrial localization of the dye was checked by coloading the cells with MitoTracker green. Confocal images of X-rhod-FF fluorescence were obtained at 568 nm (excitation) and 605 nm (emission).

Inositol 1,4,5-Triphosphate Photorelease

Rhizoid cells were microinjected with a mixture of caged inositol 1,4,5-triphosphate [Ins(1,4,5)P_3] (Calbiochem; final intracellular concentration of 10 μM) and Calcium green–dextran and Texas red–dextran as described above. To monitor ROS production, cells were injected with Ins(1,4,5)P_3 and Texas red–dextran (final intracellular concentration of 10 to 50 μM) and then incubated with CM-DCFH_2-DA as described above. Photorelease was achieved with a UV light–pulsed nitrogen laser (10-ns pulses, 20 Hz for 1 s) (VSL337; Laser Science, Cambridge, MA) delivered via the microscope objective and focused to an adjustable spot via a beam expander and adjustable focusing lens (Goddard et al., 2000). Laser intensity was adjusted with a diaphragm in the delivery optics to a level that caused the photorelease of Ins(1,4,5)P_3 but did not by itself induce an oxidative burst. Control cells were microinjected only with Texas red–dextran, loaded with CM-DCFH_2-DA, and exposed to identical laser excitation.

Patch Clamping

Spheroplasts were obtained from the apices of Fucus rhizoid cells using laser microsurgery of the cell wall, as described previously (Taylor and Brownlee, 1992; Taylor et al., 1996). Cell-attached recordings were made from apical protoplasts using conventional patch-clamp techniques (Taylor et al., 1996). The reference electrode consisted of an Ag/AgCl pellet in a holder containing seawater and was connected to the bath via a 3% agar bridge. Patch pipettes were fabricated from borosilicate glass (GC150TF; Clark, Pangbourne, UK) with a Narishige pipette puller (P-833; Narishige, Tokyo, Japan). Electrodes were dipped briefly in 0.001% polylysine solution (Sigma) before back filling with ultrafiltered pipette solution (30 mM $CaCl_2$, 30 mM KCl, and 10 mM Hepes, pH 7.8). Patch-clamp recordings were obtained with an Axopatch 1D amplifier (Axon Instruments, Foster City, CA), filtered at 5 kHz, and analyzed with PCLAMP software (Axon Instruments).

Upon request, all novel materials described in this article will be made available in a timely manner for noncommercial research purposes. No restrictions or conditions will be placed on the use of any materials described in this article that would limit their use for noncommercial research purposes.

ACKNOWLEDGMENTS

Supported by Fundação para a Ciência e Tecnologia, Portugal (S.M.C.), and the Biotechnology and Biological Science Research Council and the Natural Environment Research Council, United Kingdom (C.B. and A.R.T.).

Received March 22, 2002; accepted June 26, 2002.

REFERENCES

Allan, A., and Fluhr, R. (1997). Two distinct sources of elicited reactive oxygen species in tobacco epidermal cells. Plant Cell **9,** 1559–1572.

Bac, Y.S., Kang, S.W., Seo, M.S., Baines, I.C., Teckle, E., Chock, P.B., and Rhee, S.G. (1997). Epidermal growth factor (EGF)-induced generation of hydrogen peroxide. J. Biol. Chem. **272,** 217–221.

Berger, F., and Brownlee, C. (1995). Physiology and development of protoplasts obtained from *Fucus* embryos using laser microsurgery. Protoplasma **186,** 63–71.

Bowie, A., and O'Neill, L.A. (2000). Oxidative stress and nuclear factor-kappaB activation: A reassessment of the evidence in the light of recent discoveries. Biochem. Pharmacol. **59,** 13–23.

Bradley, D., Kjellbom, P., and Lamb, C. (1992). Elicitor- and wound-induced oxidative cross-linking of a proline-rich plant cell wall protein: A novel, rapid defense response. Cell **70,** 21–30.

Brownlee, C., and Pulsford, A. (1988). Visualization of the cytoplasmic Ca^{2+} gradient in *Fucus serratus* rhizoids: Correlation with cell structure and polarity. J. Cell Sci. **91,** 249–256.

Brownlee, C., and Wood, J.W. (1986). A gradient of cytosolic free calcium in growing rhizoid cells of *Fucus serratus*. Nature **320,** 624–626.

Desikan, R., Hancock, J.T., Coffey, M.J., and Neill, S.J. (1996). Generation of active oxygen in elicited cells of *Arabidopsis thaliana* is mediated by a NADPH oxidase-like enzyme. FEBS Lett. **382,** 213–217.

Desikan, R., Neill, S.J., and Hancock, J.T. (2000). Hydrogen peroxide-induced gene expression in *Arabidopsis thaliana*. Free Radical Biol. Med. **28,** 773–778.

Duchen, M.R. (2000). Mitochondria and calcium: From cell signaling to cell death. J. Physiol. **529,** 57–68.

Finkel, T. (1998). Oxygen radicals and signaling. Curr. Opin. Cell Biol. **10,** 248–253.

Frahry, G., and Schopfer, P. (1998). Inhibition of O_2^- reducing activity of horseradish peroxidase by diphenyleneiodonium. Phytochemistry **48,** 223–227.

Fry, S.C., Willis, S.C., and Patterson, A.E. (2000). Evidence for covalent linkage between xyloglucan and acidic pectins in suspension-cultured rose tissue. Planta **211,** 275–286.

Goddard, H., Manison, N., Tomos, D., and Brownlee, C. (2000). Elemental propagation of calcium signals in response-specific patterns determined by environmental stimulus strength. Proc. Natl. Acad. Sci. USA **97,** 1932–1937.

Grant, J., and Loake, G. (2000). Role of reactive oxygen intermediates and cognate redox signaling in disease resistance. Plant Physiol. **124,** 21–29.

Grijalba, M.T., Vercesi, A.E., and Schreier, S. (1999). Ca^{2+}-induced increased lipid packing and domain formation in submitochondrial particles: A possible early step in the mechanism of Ca^{2+}-stimulated generation of reactive oxygen species by the respiratory chain. Biochemistry **38,** 13279–13287.

Grynkiewicz, G., Poenie, M., and Tsien, R.Y. (1985). A new generation of Ca^{2+} indicators with greatly improved fluorescence properties. J. Biol. Chem. **260,** 3440–3450.

Guan, L.M., Zhao, J., and Scandalios, J.G. (2000). *Cis*-elements and *trans*-factors that regulate expression of the maize *Cat1* antioxidant gene expression in response to ABA and osmotic stress: H_2O_2 is the likely intermediary signaling molecule for the response. Plant J. **22,** 87–95.

Hoth, M., Fanger, C., and Lewis, R. (1997). Mitochondrial regulation of store-operated calcium signaling in T lymphocytes. J. Cell Biol. **137,** 633–648.

Levine, A., Tenhaken, R., Dixon, R., and Lamb, C. (1994). H_2O_2 from the oxidative burst orchestrates the plant hypersensitive disease resistance response. Cell **79,** 583–593.

Maxwell, D., Wang, Y., and McIntosh, L. (1999). The alternative oxidase lowers mitochondrial reactive oxygen production in plant cells. Proc. Natl. Acad. Sci. USA **96,** 8271–8276.

Minibayeva, F., Kolesnikov, O., and Gordon, L. (1998). Contribution of plasma membrane redox system to the superoxide production by wheat root cells. Protoplasma **205,** 101–106.

Morel, Y., and Barouki, R. (1999). Repression of gene expression by oxidative stress. Biochem. J. **342,** 481–496.

Park, M.K., Ashby, M.C., Erdemli, G., Petersen, O.H., and Tepikin, A.V. (2001). Perinuclear, perigranular and sub-plasmalemmal mitochondria have distinct functions in the regulation of cellular calcium transport. EMBO J. **20,** 1863–1874.

Pastori, Y., and del Rio, L.A. (1997). Natural senescence of pea leaves: An activated oxygen-mediated function for peroxisomes. Plant Physiol. **113,** 411–418.

Pei, Z.-M., Murata, Y., Benning, G., Thomine, S., Klusener, B., Allen, G., Grill, E., and Schroeder, J.I. (2000). Calcium channels activated by hydrogen peroxide mediate abscisic acid signalling in guard cells. Nature **406,** 731–734.

Pu, R., and Robinson, K.R. (1998). Cytoplasmic calcium gradients and calmodulin in the early development of the fucoid alga *Pelvetia compressa*. J. Cell Sci. **111,** 3197–3207.

Pugin, A., Frachisse, J.-M., Tavernier, E., Bligny, R., Gout, E., Douce, R., and Guern, J. (1997). Early events induced by the elicitor cryptogein in tobacco cells: Involvement of a plasma membrane NADPH oxidase and activation of glycolysis and the pentose phosphate pathway. Plant Cell **9,** 2077–2091.

Reichheld, J.-P., Vernoux, T., Lardon, F., Van Montagu, M., and Inzé, D. (1999). Specific checkpoints regulate plant cell cycle progression in response to oxidative stress. Plant J. **17,** 647–656.

Rizzuto, R., Bernardi, P., and Pozzan, T. (2000). Mitochondria as all-round players of the calcium game. J. Physiol. **529,** 37–47.

Shackelford, R.E., Kaufmann, W.K., and Paules, R.S. (2000). Oxidative stress and cell cycle checkpoint function. Free Radical Biol. Med. **28,** 1387–1404.

Subbaiah, C.C., et al. (1998). Mitochondrial contribution to the anoxic Ca^{2+} signal in maize suspension-cultured cells. Plant Physiol. **118,** 759–771.

Tan, S., Sagara, Y., Liu, Y., Maher, P., and Schubert, D. (1998). The regulation of reactive oxygen species production during programmed cell death. J. Cell Biol. **141,** 1423–1432.

Taylor, A., and Brownlee, C. (1992). Localized patch clamping of plasma membrane of a polarized plant cell. Plant Physiol. **99,** 1686–1688.

Taylor, A.R., Manison, N., Fernandez, C., Wood, J., and Brownlee, C. (1996). Spatial organization of calcium signaling involved in cell volume control in the *Fucus* rhizoid. Plant Cell **8,** 2015–2031.

Zhu, H., Bannenberg, G.L., Moldéus, G.L., and Shertzer, H.G. (1994). Oxidation pathways for the intracellular probe 2′,7′-dichlorofluorescein. Acta Toxicol. **68,** 582–587.

Zimmermann, B. (2000). Control of Ins(1,4,5)P_3-induced Ca^{2+} oscillations in permeabilized blowfly salivary gland cells: Contribution of mitochondria. J. Physiol. **525,** 707–719.

Plant, Cell and Environment (2001) **24**, 801–810

Cellular responses to elevated light levels in *Fucus spiralis* embryos during the first days after fertilization

S. COELHO,[1,2] J. W. RIJSTENBIL,[1] I. SOUSA-PINTO[3] & M. T. BROWN[2]

[1]*Netherlands Institute of Ecology, Centre for Estuarine and Coastal Ecology (NIOO-CEMO), PO Box 140, NL-4400 AC Yerseke, The Netherlands,* [2]*Department of Biological Sciences, University of Plymouth, Plymouth, PL4 8AA, UK and* [3]*Department of Botany, Faculty of Sciences, University of Porto, R. do Campo Alegre, 1191, P-4150 Porto, Portugal*

ABSTRACT

Cellular responses of 1-, 2- and 4-d-old *Fucus spiralis* embryos subjected to a single dose of elevated photosynthetically active photon flux density (PPFD), with or without ultraviolet (UV) radiation, were investigated by measuring the effects on the effective quantum yield of photosystem II (ΔF / F_m') and intracellular production of active oxygen species (AOS). Production of AOS was determined by the *in vivo* conversion of 5-(and-6)-chloromethyl-2′,7′-dichlorodihydrofluorescein diacetate (CM-DCFH$_2$-DA) to the fluorescent compound dichlorofluorescein (DCF) using confocal laser scan microscopy (CLSM) and image analysis. The role of xanthophyll cycle pigments in photoprotection was also assessed. A rapid decline in ΔF / F_m' was observed under all elevated light conditions. A correlation was found between non-photochemical quenching and the de-epoxidation ratio zeaxanthin/(zeaxanthin + violoxanthin). Active oxygen formation increased with PPFD and was higher in older embryos and when UVB was present. Two photoinhibition responses were recognized: (i) a rapid decline of the PSII yield due to the violoxanthin–zeaxanthin cycle (photoprotection), and (ii) a slower second-phase decline, correlated with active oxygen production. Electron transport rate (ETR) increased with embryo age, and was correlated with AOS production. As a result of enhanced AOS production, there was a slow recovery of the PSII yield, in particular with increased effective UV dose. In general, embryos were able to recover from the imposed light conditions, but UVB had a more damaging effect. Overall, our data suggest that under natural conditions, embryos of *F. spiralis* are susceptible to elevated light levels, and that UVB radiation is an important stress factor.

Key-words: Active oxygen; chloromethyl dichlorodihydrofluorescein diacetate (CM-DCFH$_2$-DA); confocal laser scan; oxidative stress; xanthophyll cycle.

Abbreviations: ΔF / F_m', effective quantum yield of PSII; AOS, active oxygen species; CLSM, confocal laserscan microscope; CM-DCFH2-DA, chloromethyl dichlorodihydrofluorescein diacetate; DCF, dichlorofluorescein; PAM, pulse–amplitude modulation; PPFD, photosynthetically active photon flux density; PSII, photosystem II; qP, photochemical quenching; qN, non-photochemical quenching; SA, sun + UVA; SAB, sun + UVA + UVB; shade, 15 μmol m^{-2} s^{-1} PPFD; sun, 300 μmol m^{-2} s^{-1} PPFD; UV, ultraviolet; *V*, violoxanthin concentration; *Z*, zeaxanthin concentration.

Correspondence: Murray T. Brown. E-mail: mtbrown@plymouth.ac.uk

INTRODUCTION

Fucoid brown algae (Phaeophyceae) are important members of marine intertidal communities in the north Atlantic Ocean. Variability in their recruitment and regeneration of the *Fucus* canopy are major influences on the rate of succession and the abundance of other species (McCook & Chapman 1997). Despite the importance of stress tolerance in intertidal seaweeds, the underlying mechanisms that confer such tolerance are still poorly understood (Davison & Pearson 1996). To date, most studies have focused on adult stages, but the mechanisms by which *Fucus* embryos withstand the prevailing physical forces in the intertidal zone (light, tidal movement, waves) are key determinants of their ability to survive and establish a population. The impact on embryonic stages in the first days after settlement may be particularly severe. It has become apparent that the response of early life history stages to the environmental conditions cannot necessarily be predicted from knowledge of the adult canopy (Davison, Johnson & Brawley 1993). Although fucoid embryos are easily manipulated in laboratory culture and their early development has been well characterized (Kropf & Quatrano 1987; Kropf 1997), relatively little is known about their stress physiology.

Fucus embryos develop under shade conditions, typically in rock crevices and under the protection of the adult canopy, so exposure to an elevated light climate – especially during emersion – is likely to result in photoinhibition. Variable fluorescent techniques are suitable tools for studying photosynthetic inhibition as activity of the PSII reaction centre (i.e. the rate of production of electrons by the water-splitting system of PSII) is measured. The PAM method is based on the principle that under *in vivo* conditions, fluorescence changes originate almost exclusively from chlorophyll *a* and the associated antenna pigments in PSII (see Genty, Briantais & Baker 1989; Schofield, Evens & Millie 1998). The potential inhibition of photosynthesis due to light stress can be minimized through several physi-

ological mechanisms (Schofield *et al.* 1998), including the involvement of the xanthophyll cycle pigment pool in dissipating excess energy from the reaction centres (Kroon 1994).

It is also known that excess light, cold, heat and drought can trigger increased production of harmful AOS such as hydrogen peroxide (H_2O_2), superoxide radicals ($*O_2^-$) and hydroxyl radicals (*OH) (Foyer, Lelandais & Kunert 1994). Intracellular production of deleterious active oxygen species occurs in all organisms but is more problematic in phototrophs because they produce these metabolites during photosynthetic metabolism (Halliwell & Gutteridge 1989). Oxidative stress can be countered by a set of antioxidative enzyme-mediated reactions. How the oxiradical attack and the antioxidant defence evolve during the first (decisive) days after fertilization of *Fucus* eggs is not known.

The aim of this study was to assess the impact of experimental light conditions on the physiology of developing *Fucus spiralis* L. embryos during the first 4 d after fertilization. This was achieved by investigating: (i) protection mechanisms against sunlight, using the PAM technique to measure photosynthetic performance and high-performance liquid chromatography (HPLC) to quantify the xanthophyll cycle and other relevant pigments; (ii) the intracellular production of active oxygen species in response to elevated PPFD using the fluorescent label CM-$DCFH_2$-DA in combination with CLSM and quantitative image analysis, and (iii) the ability of embryos to recover from oxidative stress under more favourable, dim-light, conditions.

MATERIALS AND METHODS

Plant material and growth conditions

Receptacles of mature *F. spiralis* were collected from the compact intertidal seaweed belt, growing on concrete substrata along the shoreline of the Oosterschelde basin (29‰ salinity) near Yerseke (south-west Netherlands), from September 1998 to April 1999. Receptacles were stored at 4 °C in the dark until they were used (within 1 week). To achieve synchronous release of gametes, receptacles were incubated in filtered seawater (0·45 μm) under strong white light at 15 °C. The gamete solution was then filtered through a 120 μm nylon mesh to discard debris and oogonia. Time of fertilization was considered to be 30 min after gamete release. Fertilized eggs were then pipetted onto the surface of high-precision coverslips for CLSM (Assistent; Glaswarenfabrik Karl Hecht, Sondheim/Rhoen, Germany; 170 ± 10 μm thick, 25 mm diameter) and placed inside small Petri dishes containing 8 mL filtered seawater, where they attached and grew. For the analysis of chlorophyll fluorescence and xanthophyll cycle pigments, the embryos were grown onto cellulose nitrate filters in small Petri dishes. Attached zygotes were incubated at 15 °C under 15 μmol m^{-2} s^{-1} PPFD (4π-sensor QSL-100; Biospherical Instruments, Inc., San Diego, CA, USA) on a 12 : 12 h light : dark cycle. Seawater was replaced daily. Replicate cultures (n = 3–5) were maintained for each treatment.

Light conditions and experimental protocol

In the south-west Netherlands, the reproductive season for *F. spiralis* is autumn/winter. The control/low PPFD (15 μmol m^{-2} s^{-1}) was selected on the basis of *in situ* measurements taken during a cloudy day at 1000 and 1600 h in February, when the adult canopy almost completely covers the embryos. These were considered to be the standard growth conditions for the first days after fertilization. The elevated PPFD (300 μmol $m^{-2}s^{-1}$) was chosen based on *in situ* measurements at noon on a sunny day in February, when the adult canopy was partially removed and the embryos were exposed to higher light levels. In nature, fertilization occurs during daytime low tide (Pearson & Brawley 1996), so the first potential exposure to high light is ~24 h after fertilization, at the next daytime low tide.

Experiments were conducted under four different light regimes: shade/control (Philips TLD18W33 fluorescent lamps; Philips, Eindhoven, The Netherlands), sun, SA and SAB. A ZABU UVD clear acrylate sheet (Wientjes BV, Roden, The Netherlands) was used to filter out UVC radiation (below 285 nm) under all light conditions, a Mylar filter was used to cut off UVB radiation (below 320 nm) and a plexiglass filter was used to remove UVA radiation (below 380 nm). A PPFD spectrum (250–700 nm) was scanned with a spectroradiometer equipped with a 2π cosine-corrected sensor (MACAM Photometrics SR-9910-PC; Macam Photometrics Ltd, Livingston, UK). The biologically effective dose of Jones & Kok (1966) was 2·1 W m^{-2} (SAB), 0·6 (SA), 0·1 (sun) and 0 (shade) and was calculated using a weighting factor, $WF_\lambda = 1000*e^{-0.023*\lambda}$ (R^2 = 1), derived from the plot in Forster & Lüning (1996) that sets $WF_{300} = 1$. For the calculation of this effective dose, λ = 280–400 nm are considered, using the formula $BED_{J/K} = {}^{\lambda = 280-400}\Sigma\ (WF_\lambda * Q_\lambda)$, in which Q_λ is the PPFD (W m^{-2}) at wavelength λ (nm).

Fluorescence measurements

In vivo light-modulated chlorophyll fluorescence was monitored in 1-, 2- and 4-d-old photosynthetically competent embryos (Brawley, Quatrano & Wetherbee 1977) with a pulse–amplitude modulation apparatus (PAM 2000 Walz; Heinz Walz GmbH, Effeltrich, Germany), based on the principles described by Schreiber, Evens & Bilger (1986). The saturating pulse method provides information on processes related to the quantum yield of PSII in response to light stress. Yield is usually determined under steady-state illumination, in which the effective quantum yield of PSII is close to the overall quantum yield of photosynthesis. The effective quantum yield was determined according to the equation $\Delta F / F_m' = (F_m' - F_s) / F_m'$ (Genty *et al.* 1989), where ΔF is the difference between the respective maximal fluorescence F_m' of light-adapted algae and the ambient fluorescence level (current steady-state fluorescence, F_s). The effective quantum yield was used as the photoinhibition parameter since it is correlated with oxygen production (Hanelt, Li & Nultsch 1994; Hanelt, Uhrmacher & Nultsch

1995). Changes in chlorophyll fluorescence in photochemical quenching were calculated according to the expression $qP = (F_m' - F_t) / (F_m' - F_o')$; in non-photochemical quenching, $qN = 1 - (F_m - F_o') / (F_m - F_o)$. Zygotes were well dispersed over the cellulose nitrate filter to ensure that all embryos were submitted to similar light conditions. The PAM fibre was placed carefully over the attached population of embryos and the fluorescence yield was measured at a minimum of five different positions on the filter (i.e. five measurements for each data point, which correspond to independent embryos in the dish population). The measurements were performed at short intervals (≈ 5 min) during 60 min exposure under each light condition. The change in yield during a 60–180 min recovery period, under shade, was also assessed.

Chlorophyll fluorescence was also used to analyse the light response curves (photosynthesis versus PPFD curves) of *F. spiralis* embryos during their early development stages, from 3 h after fertilization to 10 d. Zygotes were obtained as described before, and the growing embryos were incubated in shade, 15 °C and a 12 h photoperiod. Samples were exposed to increasing PPFDs of actinic red light (650 nm); PPFDs ranged from 10 to 504 μmol m^{-2} s^{-1} with, in total, 20 PPFD values. The material was dark-adapted before the beginning of the measurements. The light response curves were fitted by the model equations given by Platt, Gallegos & Harrison (1980). Relative electron transport rates (rel. ETR) were calculated by multiplying quantum yield by PPFD (rel. ETR = $\Delta F / F_m' \times$ PPFD) and plotted against PPFD. Alpha (α) (initial slope under light-limited conditions), and P_{max} (gross photosynthesis under saturating light) were also determined.

Pigment analysis

For pigment (violoxanthin, zeaxanthin, β-carotene, chlorophyll *a*) analysis of embryos exposed to SAB, samples were obtained at short intervals during the 60 min period of exposure to elevated light, and also during recovery under dim light. Frozen samples (–80 °C) of *F. spiralis* embryos, grown onto cellulose nitrate filters, were extracted in 90% methanol in 0·5 M ammonium acetate, the pigments separated and concentrations determined by HPLC following the procedures of Wright *et al.* (1991) and Kraay, Zapata & Veldhuis (1992). Methanol extracts were injected into a PC-controlled (Millennium 2·15 software; Waters, Milford, MA, USA) HPLC system (Waters) equipped with a reversed-phase column (Nova-Pak C18, 4 μm, 15 cm; Waters Wat086344). Gradient-mixing HPLC pumps delivered three mobile-phase solvents: ammonium acetate/methanol, 90% acetonitril and 100% ethyl acetate. A photodiode array detector was used (Waters), in which the absorption characteristics of the eluted pigments were matched with those described in Jeffrey, Mantoura & Wright (1997). Antheraxanthin, the xanthophyll intermediate of violaxanthin and zeaxanthin, could not be detected. Commercially available standards of the pigments were used (DHI Water & Environment, Hørsholm, Denmark). Pigment concentrations of β-carotene, violaxanthin and zeaxanthin were normalized to the chlorophyll *a* peak area. The relative pool of xanthophyll cycle pigments was estimated as $Z / (Z + V)$. Values of $Z / (Z + V)$ were plotted against qN to characterize the relationship between the de-epoxidized xanthophyll cycle pigments and non-photosynthetic energy dissipation (Schofield *et al.* 1998).

Quantitative detection of active oxygen species

The formation of DCF from $DCFH_2$-DA is currently used for the assessment of oxidative stress in microalgae and seaweeds (Lesser 1996; Malanga & Puntarulo 1995; Collén & Davison 1997). $DCFH_2$-DA is a non-polar, non-fluorescent compound that diffuses across membranes. Within the cell, acetate is cleaved off by esterases to give 2′,7′-dichlorohydrofluorescein ($DCFH_2$), a polar compound that can only leak from disrupted cells or via active membrane transport. Oxidation of $DCFH_2$ by active oxygen species (Royall & Ischiropoulos 1993) yields a fluorescent compound, DCF. The oxidizing agent is either *OH, which may be formed from H_2O_2 and Fe^{2+} in the Fenton reaction, or H_2O_2, which may react with $DCFH_2$ via peroxidases (Zhu *et al.* 1994). Here, intracellular active oxygen production was studied by measuring the oxidation of the label CM-$DCFH_2$-DA (Molecular Probes, Eugene, OR, USA), a chloromethyl derivate of $DCFH_2$-DA; the use of this minimizes the risk of $DCFH_2$ leakage from living cells as its thiol-reactive chloromethyl group links CM-DCF with intracellular thiols (e.g. glutathione). Subsequent $DCFH_2$ oxidation yields DCF that is trapped inside the cell. *Fucus spiralis* embryos grown under dim light on high-precision CLSM coverslips (~50 per coverslip) were loaded with a CM-$DCFH_2$-DA working stock solution (100 μM). Working solutions of CM-$DCFH_2$-DA were stored in the dark under a nitrogen atmosphere to avoid DCF formation. Loading of the label (30 min, 15 °C, dim light) was terminated by rinsing the sample with filtered seawater (0·2 μm) to remove the excess label not incorporated into cells. Embryos were then submitted to each condition (defined earlier) for 30 min. Following exposure, the coverslips with the attached embryos were mounted in a sample chamber (Attofluor; Molecular Probes), filled with 0·27 mL filtered seawater. Finally, 0·01 mL ascorbate solution (1 mg mL^{-1}, pH 8) was added. This compound is both an antifading reagent, preventing bleaching of DCF fluorescence, and an antioxidant, stopping further oxidation of $DCFH_2$ in cells (Pawley 1995). Stock solutions of CM-$DCFH_2$-DA, filtered seawater and ascorbate were prepared fresh daily.

Confocal laser scan microscopy and image analysis

A laser scan unit (Leica TCS NT; Leica Microsystems GmbH, Mannheim, Germany) was built on an inverted microscope (Leica-IRB). The Ar/Kr laser was set at half-maximum; the 488 nm excitation line was chosen, and set at 15% intensity by an optacoustic device (AOTF). With a 25

× 0·75NA/oil objective (Leica UV-PLFLUO), the emission pinhole set at 90 μm matching 1 airy disc unit (Pawley 1995), and using high-precision bottom in the sample chamber (Keller 1995), an optimum theoretical thickness of 2·4 μm was calculated for the focal plane (z-slice). In these analyses, the intersection (z) intervals were set at 1·5 μm to minimize loss of digital information. Via a beam splitter (RSP580), the green and red fluorescence from the focal plane were separated using emission filters BP530/30 and LP590 (Leica), respectively. Both green fluorescence emitted at 530 nm by DCF and red autofluorescence were measured using photomultiplier detectors. Simultaneously, three digital images were taken: (i) green emission of DCF; (ii) red emitted by chloroplasts, and (iii) transmitted light image. A daily calibration procedure was introduced using standardized fluorescent spheres (Focal Check, 15 μm; Molecular Probes). For conversion of the relative fluorescent units to real concentrations of DCF, standard solutions of DCF (Sigma-Aldrich Chemie, Zwijndrecht, The Netherlands) were used to build a calibration line (R^2 = 0·997). Using the image analysis programme QWIN (Leica), an automated scanning procedure was written in QUIPS language. This routine controls the CLSM scanning software, the xy-stage and the z-focus of the objective. After marking the xyz position of 10 embryos (randomly) in each sample, an automatic scanning and image analysis was started. Per sample, a file was made containing all data. This file was imported into Microsoft Excel (Microsoft Corp., Seattle, WA, USA) for further calculations of the mean grey value of the DCF per embryo per sample. Finally, the average DCF concentration per sample was calculated. For each experimental condition, 30–40 independent embryos were used. In the figures, DCF concentrations (μM) are presented (± SD) and values of AOS represent a production rate, μM DCF (30 min)$^{-1}$.

Statistical analysis

Data were analysed, using the statistical programme Statistica® version 6·0 (Statsoft, Tulsa, OK, USA), by two- or three-way analysis of variance (ANOVA), with multiple comparisons determined using the Sheffé test (Sokal & Rohlf 1995). Since measurements taken at days 1, 2 and 4 were performed on different batches of embryos, the factor 'time', when included in the analysis, is treated as an independent variable. Differences were considered to be significant at a probability of 5% ($P \leq 0{\cdot}05$). Correlation coefficients were determined according to Sokal & Rohlf (1995).

RESULTS

Effects of elevated light on photosynthetic efficiency

The impact of 1 h exposure to 300 μmol m^{-2} s^{-1} on $\Delta F / F_m'$ was dramatic (Fig. 1). Values decreased within 3 min of embryos being transferred from shade to any of the three

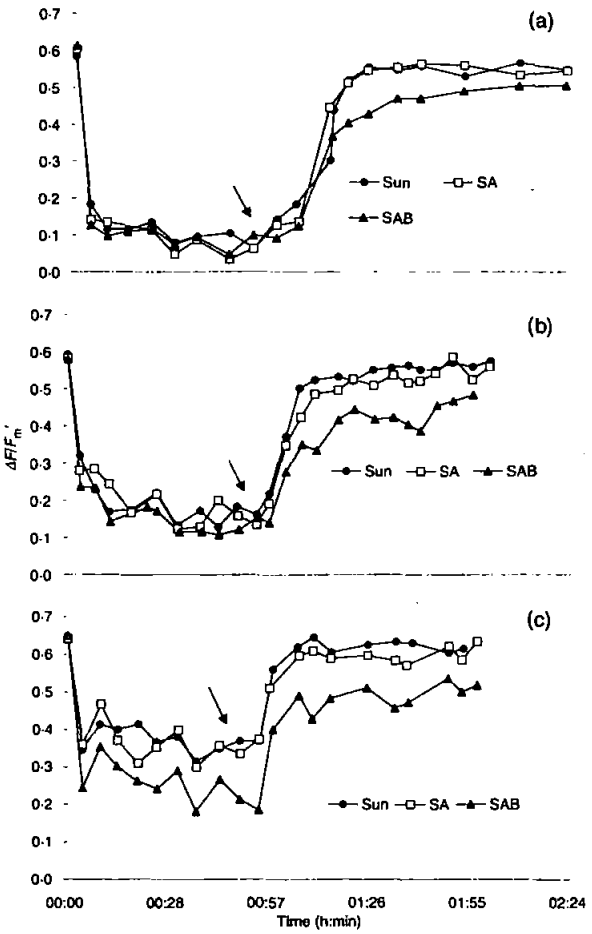

Figure 1. Chlorophyll fluorescence measurements of *F. spiralis* embryos at different stages of development and exposed to shade, sun, SA and SAB conditions. A population of embryos was grown in filters submersed in filtered seawater and the effective quantum yield was measured in at least five different regions of the filter approximately every 5 min for 1 h and also during a 1 h recovery period under low light. Arrows indicate the start of the recovery period. (a) 1 d old; (b) 2 d old; (c) 4 d old.

elevated light conditions (sun/SA/SAB). The steepest decline was in 1-d-old embryos: after a 10 min exposure period, $\Delta F / F_m'$ decreased, on average, to 20 and 55% of the initial value in the youngest and oldest embryos, respectively; 2-d-old embryos had intermediate values. Reduction in $\Delta F / F_m'$ was consistently more pronounced in the presence of UVB: 17, 24 and 43% of the initial values in 1-, 2- and 4-d-old embryos, respectively. The initial decrease in $\Delta F / F_m'$ (0–8 min) was followed by a second, slower decline (≈ 8–45 min). At the end of the 1 h exposure, 1-d-old embryos had 12% of their initial value of $\Delta F / F_m'$, 2-d-old had 28% and 4-d-old 54%. A rapid recovery in $\Delta F / F_m'$ occurred on transfer from sun and SA to shade, reaching pre-exposure values within 1 h. After exposure to UVB, recovery was significantly slower ($F_{12,141} = 2{\cdot}1$, $P = 0{\cdot}02$), and after 1 h embryos had recovered to 87% of the initial $\Delta F / F_m'$. Complete recovery was achieved only after 3 h (Fig. 1).

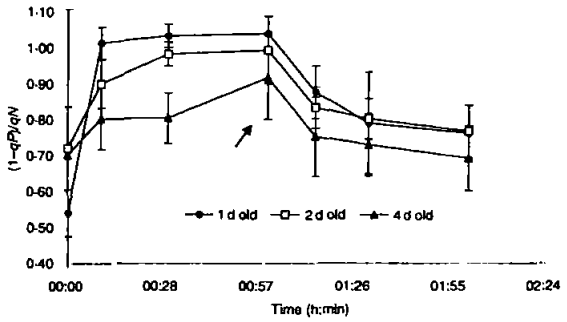

Figure 2. $(1-qP)/qN$ in *F. spiralis* embryos during incubation under SAB and during a 1 h recovery period. Arrow indicates the start of the recovery period under dim light. Values represent means of at least five measurements.

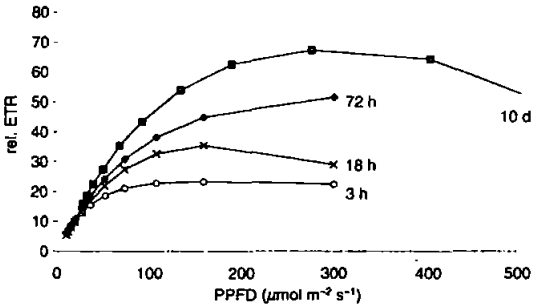

Figure 4. Photosynthetic light response curves of *F. spiralis* embryos at different stages of development. Curves were fitted using the equations of Platt *et al.* (1980). P_{max} varies between 23·3 (3h old) and 67·4 (10d old). Alpha varies between 0·68 (2h old) and 1·75 (10d old).

The photoinhibition observed under elevated PPFD was further evaluated by examining changes in qP and qN of chlorophyll fluorescence. The quantitative indication of the fraction of active PSII centres that are closed by the background light at the moment of the F_m' measurement can be defined as $(1-qP)$. This value indicates the capacity of electron flow, and the ratio $(1-qP)\ /\ qN$ provides a more appropriate measure of the capacity of photoprotection to excess light than analysing the parameters qN and $(1-qP)$ separately (Jiménez *et al.* 1998). The ratio $(1-qP)\ /\ qN$ increased with time of exposure and decreased slowly as the embryos recovered under more favourable conditions. Despite having a lower initial value of $(1-qP)\ /\ qN$, 24-h-old embryos displayed the largest increase in this ratio (Fig. 2), while 4-d-old embryos increased the least (age–time interaction $F_{4,37} = 2{\cdot}89$, $P = 0{\cdot}035$).

Xanthophyll cycle pigments

After exposure to SAB for 1 h, both photoinhibition and changes in the xanthophyll cycle pigment ratios were observed. Figure 3 shows the $Z\ /\ (V+Z)$ values plotted against qN. The correlation between these parameters improves with the age of the embryos. The concentration of β-carotene did not change significantly during these experiments (results not shown).

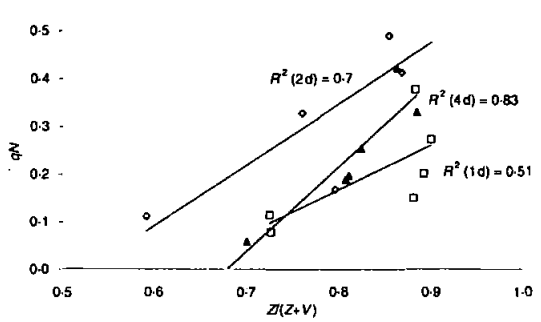

Figure 3. Photoinhibition of *F. spiralis* embryos. Correlation between qN and the ratio $Z/V+Z$ of embryos sampled at different times during the treatment (SAB).

Although exposure to elevated light caused a steep decline in $\Delta F\ /\ F_m'$, considerable electron transport was still possible. The light response curves of the different developmental stages, from 3 h after fertilization to 10 d old, are shown in Fig. 4. As embryos developed, there was an increase in α and P_{max}. From these observations it is estimated that saturation PPFD ranged from 150 to 300 μmol m^{-2} s^{-1} at the respective ages investigated here.

Effects of elevated light on active oxygen production

The production of AOS, as measured by the formation of DCF, increased with PPFD (Figs 5 and 7). In 1-d-old embryos, the increase followed approximately a logarithmic curve up to 300 μmol m^{-2} s^{-1}, whereas in older embryos (2 d and 4 d), the increase was more linear. In accordance with the ETR increase observed in Fig. 4, this may be attributable to the progressive development of the photosynthetic apparatus in the embryo cells. From Figs 6 and 7, it is clear that after 30 min exposure to all high-light treatments, CM-DCFH$_2$-DA was oxidized by active oxygen produced in *F. spiralis* cells, relative to the initial condition

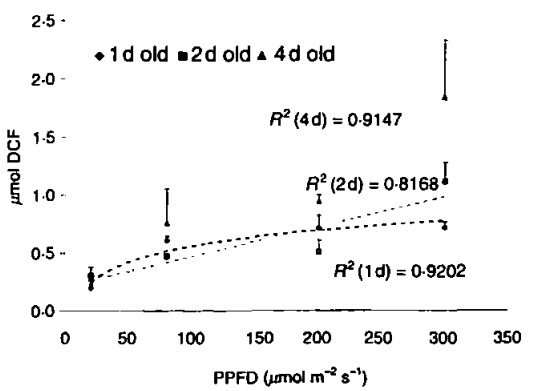

Figure 5. DCF production by *F. spiralis* embryos in response to increasing light levels. Values represent mean + SD (n=30–40).

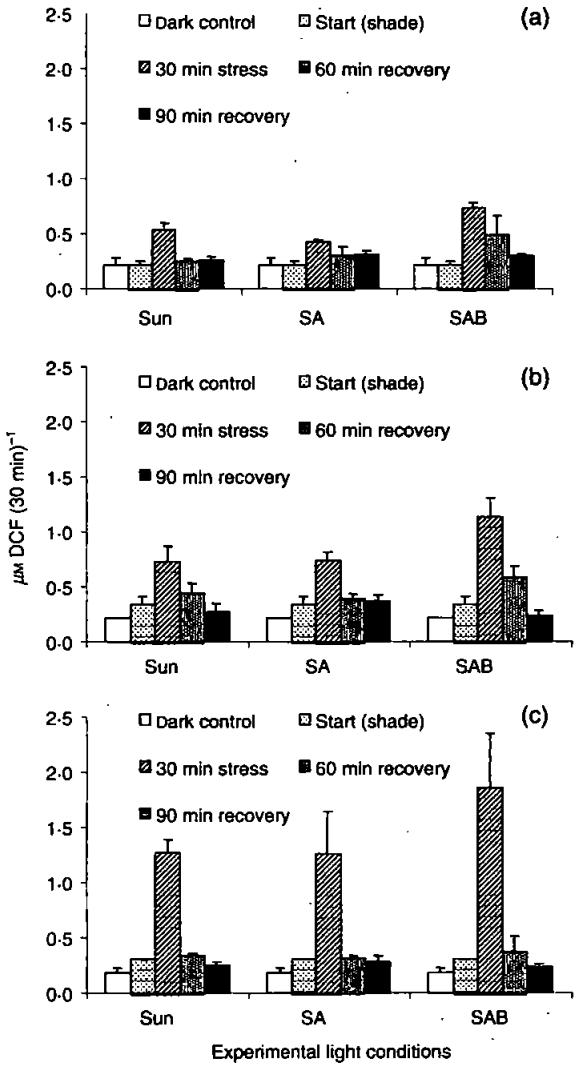

Figure 6. DCF production (corresponding to AOS production) in *F. spiralis* embryos: in the dark (dark control), in low light [start (shade)], exposed for 30 min to experimental high-light conditions (sun, SA, SAB), after different recovery periods (60 min and 90 min) and under low light (shade). Values represent mean + SD (n = 30–40). There is a significant effect of age ($F_{2,990}$ = 62·79, P < 0·0001), light ($F_{4,990}$ = 195·48, P < 0·0001) and the interaction age × light ($F_{8,990}$ = 11·81, P < 0·0001) on (a) 1-, (b) 2- and (c) 4-d-old embryos.

(15 μmol m^{-2} s^{-1}). When all embryos were transferred from shade to higher PPFD, there was a significant increase in DCF formation, with more produced under SAB than under either sun or SA.

The response of the embryos depended upon their stage of development. Older embryos (4 d) had the highest values of DCF formation, while 1-d-old ones had the lowest values (Figs 5, 6 and 7). On transfer to shade conditions, production of AOS continued for some time – in some situations even after 60 min [this is most evident in 1- and 2-d-old embryos previously exposed to UVB (Fig. 6)]. AOS production in all embryos, no matter their stage of development (1–4 d) or treatment, returned to control values after 90 min under shade conditions.

An increase in both AOS production (in terms of DCF) and electron transport rate (rel. ETR = PPFD × $\Delta F / F_m'$) with the stage of development of the embryos were observed. There is a correlation (n = 15; R^2 = 0·75; P < 0·001) between AOS production rates and relative ETR calculated from PPFD (400–700 nm) (results not shown). Thus, active oxygen production seems to be proportional to the electrons generated in PSII, regardless of the age of the embryo. Comparing the trends of recovering $\Delta F / F_m'$ values in Fig. 1, it can be seen that when UVB is present, (SAB) recovery occurs very slowly. During recovery from exposure to elevated light, the index of photoprotection [(1 – qP) / qN] decreases gradually again (Fig. 2) to around 0·7, but does not reach the initial values in the case of the UVB treatment (SAB).

DISCUSSION

Treatment with 300 μmol m^{-2} s^{-1} (with or without ultraviolet radiation) induced measurable cellular responses in *F. spiralis* embryos. The quality and quantity of the light used here falls within the natural ranges encountered at the site of collection (under the adult canopy). Embryos subjected to elevated PPFD (with or without ultraviolet radiation) quickly reduced their effective quantum yield and this was maintained at a low value during incubation under high-light conditions. Changes in $\Delta F / F_m'$ have been related to photoinhibition effects. Photoinhibition can result from two different mechanisms (Demmig, Winter & Czygan 1987). The first is dynamic photoinhibition, which implicates photoprotection. The second type of photoinhibition is more permanent: this (semi) permanent decrease in photosynthetic capacity is known to cause photodamage to PSII reaction centres (Bilger & Björkman 1991). The results presented here suggest that dynamic photoinhibition was dominant in *Fucus* embryos challenged with 300 μmol m^{-2} s^{-1}. Reductions in $\Delta F / F_m'$ were readily overcome after transfer to more favourable conditions (dim light), indicating that the reduction in the photosynthetic effective quantum yield is more a photoprotective mechanism than a chronic inhibition. The younger embryos (1 d) seem to have a lower capacity for non-photochemical quenching. This is in agreement with the results obtained when qN is plotted against the relative pool of xanthophyll cycle pigments for the different aged embryos. The non-destructive dissipation of excitation energy into heat via pathways other than photochemistry leads to fluorescence quenching (Demmig *et al.* 1987), and is recognized as an efficient protective mechanism. The site of energy-dependent dissipation during dynamic photoinhibition is generally believed to be the LHCII antenna complex of PSII, associated with the reversible de-epoxidation of violoxanthin to zeaxanthin in the xanthophyll cycle. In spite of the attempt by cells to protect themselves against excess light energy through the dissipation mechanism of de-epoxidation, significant changes in photosynthesis were measured.

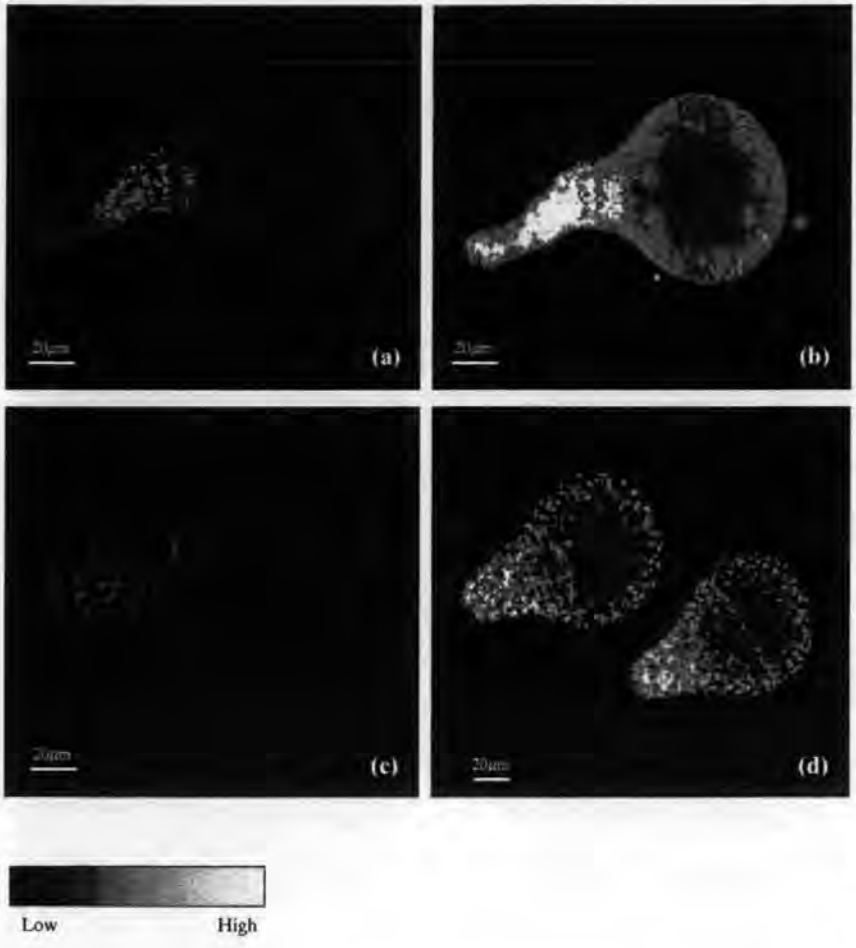

Figure 7. *Fucus spiralis* embryos grown under sun, 15 °C and 12 h photoperiod (z-section, 40×). Embryos were loaded with 100 μM CM-DCFH$_2$-DA as described in Material and methods. (a) 4-d-old embryos showing basal active oxygen species production (shade); (b) production of active oxygen species in 4-d-old embryos exposed for 30 min to sun conditions; (c) 1-d-old embryos in low light (shade); (d) 1-d-old embryos exposed for 30 min to sun conditions. Note that the images illustrate one 2-μm-thick section of the embryo, with the rhizoid cell in focus. Fluorescence intensity is more or less evenly distributed throughout the whole embryo, but because the thallus cell is out of focus, the labelling appears more concentrated in the rhizoid.

A slower, second-phase decline in ΔF / F_m' occurred from 8 min to about 45 min under all high-light treatments. Although the slopes of the curves for each age became steeper with effective UV, dose there was no overall correlation between these two parameters. The slopes of the ΔF / F_m' curves seem to increase with the DCF production (measured during 30 min exposure period) for all ages and all light treatments tested. This suggests that the further reduction in ΔF / F_m' could be due to production of AOS under high light. These data support the hypothesis that AOS are involved in the response of *F. spiralis* embryos to high light. Exposure to UVB produced a very strong oxidative stress response, with embryos incubated under 300 μmol m^{-2} s^{-1} with UVA + UVB producing the highest levels of AOS. Similar changes in active oxygen production in response to UV radiation have been reported in *Chlorella vulgaris* (Malanga & Puntarulo 1995). Semi-permanent inhibition of photosynthesis may be a result of both increased light and UV damage. UV radiation, and in particular UVB, reacts photochemically with atmospheric oxygen to form AOS in cells and in the aquatic environment (Palenik, Price & Morel 1991; Scully *et al.* 1996; Zhou & Mopper 1990). Active oxygen-generating reactions also occur as a result of the photochemical interaction between UVB and organic molecules (Malanga, Calmanovici & Puntarulo 1997; Gille & Sigler 1995; Cockell 1998). In cells, toxic hydroxyl radicals (*OH), formed from hydrogen peroxide and superoxide radicals in the Haber–Weiss reaction, are reactive with a variety of UV-absorbing biomolecules (sensitizers) that are essential for algal photosynthesis (Strid, Chow & Anderson 1994). Hideg, Spetea & Vass (1994) observed that in light-stressed thylakoid isolates, *OH radicals at PSII could cause photoinhibition on the electron donor side; this (UVB) light-induced *OH production was dependent on the electron donation from manganese ions in the water-splitting complex of PSII. In the photosystems, these oxiradicals are mainly damaging to the thylakoid membrane structure, most pigments (carotenoids, chlorophyll) and the D1 protein in the PSII core (Hideg & Vass 1996); other proteins (enzymes in the dark reactions), DNA and membrane lipids can also be damaged by UVB-induced oxiradicals (Foyer *et al.* 1994). Enhanced *OH formation can lower the photosynthetic efficiency of algae at elevated PPFDs, as well as under UVB (Tschiersch & Ohmann 1993; Hirayama, Uega & Suama 1995).

On return of the embryos to dim light, a rapid, first-phase recovery took place. Recovery depended upon the age of the embryos and the previous stress situation. Following photoinhibition of photosynthesis, a reversible increase in relative zeaxanthin content and a concomitant

decrease of violoxanthin was observed in the embryos previously exposed to UVB. This trend was less evident in 1-d-old embryos, but its significance increased with age.

The role of β-carotene as a biologically significant antioxidant is highly controversial. Results of some studies suggest that β-carotene plays a significant role *in vivo* by protecting the PSII reaction centre against photooxidative damage by scavenging superoxide, at least in higher plants (Siefermann-Harms 1987). Others (Day *et al.* 1998) have concluded that β-carotene was ineffective in exerting protection and had no antioxidant effect. In this study, there is no evidence for variation in β-carotene concentration that would suggest any role in protection against light stress. Uhrmacher, Hanelt & Nultsch (1995) too could find no change in the concentration of β-carotene during 2 h exposure of *Dictyota dichotoma* to high PPFD, despite the importance of xanthophyll cycle pigments in the photoprotection of this species.

An increase in the ratio $(1 - qP) / qN$ indicates that high light had a relatively greater impact on the electron flow rate (by the ongoing closure of reaction centres) than it had on the increase of the non-photochemical quenching (which is due mainly to protective energy dissipation). Consequently, a higher $(1 - qP) / qN$ value would also indicate a greater susceptibility to light stress (Jiménez *et al.* 1998), as shown in Fig. 2. Thus, according to these results, older embryos showed a higher capacity for photoprotection than younger ones. Embryos also converted $DCFH_2$ to DCF in total darkness, although to a lesser extent. Collén & Davison (1997) have observed this in adult *Fucus*; they suggested that there is a basal rate of non-photosynthetic active oxygen production. One-day-old embryos had the highest production of active oxygen species in darkness and 4-d-old ones the lowest. Dark production of oxiradicals can be explained by respiration of storage products. It has been suggested that growth and photosynthesis are uncoupled in the embryonic stages of *Fucus* (Major & Davison 1998), presumably because of the utilization of stored compounds such as mannitol (Davison *et al.* 1993). Mannitol may act as an oxiradical scavenger (Shen, Jensen & Bohnert 1997), but perhaps also as a radical producer; many 'antioxidant' molecules can serve as intermediates that produce active oxygen (Kalinich, Ramakrishnan & McClain 1997; Otero *et al.* 1997). In embryos, 80 μmol m^{-2} s^{-1} was sufficient to increase active oxygen production (Fig. 5), whereas in adult *Fucus evenescens*, there was a limited increase of DCF production at 100 μmol m^{-2} s^{-1} (Collén & Davison 1997). This would suggest that embryos are more sensitive to PPFD than more developed stages.

Active oxygen production (conversion of $DCFH_2$ into DCF) increased significantly, almost linearly, with the age of the embryos under all conditions tested ($P < 0.001$). This is most likely due to older embryos having a more developed photosynthetic machinery and greater pigment synthesis (McLachlan 1974; McLachlan & Bidwell 1978; Davison *et al.* 1993; Lamote *et al.* 1998), a view supported by the light response curves that show an increase in α and P_{max} (Fig. 4).

During recovery, particularly from SAB, there was excess active oxygen – even after 60 min in 15 μmol m^{-2} s^{-1}. This might be explained by continued inhibition of the dark reactions, whereby the pool of NADPH is high and PSI (ferredoxin) remains in a very reduced state. This could result in cyclic electron transport (Mehler reaction), and hence extra production of $^*O_2^-$ and H_2O_2 that would lead, indirectly, to $DCFH_2$ oxidation. However, detailed studies are required to verify this.

In conclusion, the data presented here indicate that a single, ecologically relevant dose of PPFD, with and without ultraviolet A or B, can affect the cellular physiology of *F. spiralis* embryos. Two photoinhibition responses are recognized: firstly, a rapid decline of the PSII yield ($\Delta F / F_m'$) that is probably due to the violaxanthin–zeaxanthin cycle (photoprotection), followed by a slower, second-phase decline that is most likely a direct consequence of active oxygen production. In the developing photosynthetic apparatus, ETRs increase with the age of the early life stages. Active oxygen production rates are directly coupled with ETR (although other electron-consuming processes such as photorespiration cannot be excluded), and photoprotection increases with age. As a result of enhanced active oxygen production, a slow repair of the PSII yield is observed, particularly with increased effective UV doses associated with the experimental high-light conditions. In the absence of UVB, embryos were generally able to recover quickly from the imposed high-light exposure. Overall, our data suggest that under natural conditions, embryos of *F. spiralis* are susceptible to high light, and that solar UVB radiation is an important stress factor for these early stages.

ACKNOWLEDGMENTS

The authors wish to thank Dr Rod Forster and Dr Jacco Kromkamp for their help with the PAM measurements and Jan Sinke for help with the HPLC. We are also grateful to Dr Gareth Pearson and Dr Jonas Collén for their comments on an earlier draft of the manuscript, to Dr Chris Rickett for his advice on the statistical analyses and to the referees for their suggestions. S.C. is supported by a scholarship from FCT, Portugal. Publication no 2807, NIOO Centre for Estuarine and Coastal Ecology, Yerseke, The Netherlands.

REFERENCES

Bilger W. & Björkman O. (1991) Temperature dependence of violoxanthin de-epoxidation and non-photochemical fluorescence quenching in intact leaves of *Gossypium hirsutum* L. *Planta* **184**, 226–234.

Brawley S.H., Quatrano R.S. & Wetherbee R. (1977) Fine-structural studies of the gametes and embryo of *Fucus vesiculosus* L. (Phaeophyta): III. cytokinesis and the multicellular embryo. *Journal of Cell Science* **24**, 275–294.

Cockell C.S. (1998) Ultraviolet radiation, evolution and the π-electron system. *Biological Journal of the Linnean Society* **63**, 449–457.

Collén J. & Davison I.R. (1997) *In vivo* measurement of active oxygen production in the brown alga *Fucus evanescens* using 2,7-dichlorohydrofluorescein diacetate. *Journal of Phycology* **33**, 643–648.

Davison I., Johnson L.E. & Brawley S.H. (1993) Sublethal stress in the intertidal zone: tidal emersion inhibits photosynthesis and retards development in embryos of the brown alga *Pelvetia fastigiata*. *Oecologia* **96**, 483–492.

Davison I.R. & Pearson G. (1996) Stress tolerance in intertidal seaweeds. *Journal of Phycology* **32**, 197–211.

Day B., Bergamini S., Tyurina Y.Y., Carta G., Tyurin V.A. & Kagan V.E. (1998) β-carotene – an antioxidant or a target of oxidative stress in cells? In *Subcellular Biochemistry* (eds P.J. Quinn & V.E. Kagan), pp. 209–217. Plenum Press, New York.

Demmig B., Winter K. & Czygan F.-C. (1987) Photoinhibition and zeaxanthin formation in intact leaves: a possible role of the xanthophyll cycle in the dissipation of the excess light energy. *Plant Physiology* **84**, 214–224.

Forster R.M. & Lüning K. (1996) Photosynthetic response of *Laminaria digitata* to ultraviolet A and B radiation. *Scientia Marina* **60** (suppl.) 185–193.

Foyer C.H., Lelandais M. & Kunert K.J. (1994) Photooxidative stress in plants. *Physiologia Plantarum* **92**, 696–717.

Genty B., Briantais J.-M. & Baker N. (1989) The relationship between the quantum yield of photosynthetic electron transport and quenching of chlorophyll fluorescence. *Biochimica et Biophysica Acta* **990**, 87–92.

Gille G. & Sigler K. (1995) Oxidative stress and living cells. *Folia Microbiologia* **40**, 131–152.

Halliwell B. & Gutteridge J.M.C. (1989) *Free Radicals in Biology and Medicine* 2nd edn. Oxford University Press, Oxford.

Hanelt D., Li L. & Nultsch W. (1994) Tidal dependence of photoinhibition in marine macrophytes in the South China Sea. *Botanica Acta* **107**, 66–72.

Hanelt D., Uhrmacher S. & Nultsch W. (1995) The effect of photoinhibition of photosynthetic oxygen production in the brown algae *Dictyota dichotoma*. *Botanica Acta* **108**, 99–105.

Hideg E., Spetea C. & Vass I. (1994) Singlet oxygen and free radical production during acceptor- and donor-side-induced photoinhibition. Studies with spin-trapping EPR spectroscopy. *Biochimica et Biophysica Acta* **1186**, 143–152.

Hideg E. & Vass I. (1996) UV-B induced free radical production in plant leaves and isolated thylakoid membranes. *Plant Science* **115**, 251–260.

Hirayama S., Ueda R. & Sugata K. (1995) Detection of hydroxyl radical in intact cells of *Chlorella vulgaris*. *Free Radical Research* **23**, 51–59.

Jeffrey S.W., Mantoura R.F.C. & Wright S.W. (1997) *Phytoplankton Pigments in Oceanography: Guidelines to Modern Methods*. SCOR UNESCO monographs on oceanographic methodology. UNESCO Publishing, Paris.

Jiménez C., Figueroa F.L., Salles S., Aguilera J., Mercado J., Viñela B., Flores-Moya A., Lebert M. & Häder D.-P. (1998) Effects of solar radiation on photosynthesis and photoinhibition in red macrophytes from the intertidal system of Southern Spain. *Botanica Marina* **41**, 329–338.

Jones L.W. & Kok B. (1966) Photoinhibition of chloroplast reactions: I. Kinetics and action spectrum. *Plant Physiology* **41**, 1037–1043.

Kalinich J.F., Ramakrishnan N. & McClain D.E. (1997) The antioxidant Trolox enhances the oxidation of 2′,7′-dichlorofluorescin to 2′,7′-dichlorofluorescein. *Free Radical Research* **26**, 37–47.

Keller H.E. (1995) Objective lenses for confocal microscopy. In *Handbook of Biological Confocal Microscopy* (ed. J.B. Pawley) 2nd edn, pp. 111–126. Plenum Press, New York.

Kraay G.W., Zapata M. & Veldhuis M.J.W. (1992) Separation of chlorophylls c1, c2 and c3 of marine phytoplankton by reversed-phase-C18-high-performance liquid chromatography. *Journal of Phycology* **28**, 708–712.

Kroon B.M.A. (1994) Variability of photosystem II quantum yield and related processes in *Chlorella pyrenoidsa* (Chlorophyta) acclimated to an oscillating light regime simulating a mixed photic zone. *Journal of Phycology* **30**, 841–852.

Kropf D.L. (1997) Induction of polarity in fucoid zygotes. *The Plant Cell* **9**, 1011–1020.

Kropf D.L. & Quatrano R.S. (1987) Localisation of membrane-associated calcium during development of fucoid algae using chlorotetracycline. *Planta* **171**, 158–167.

Lamote M., Schoefs B., Duval J.C. & Lemoine Y. (1998) Development of the photosynthetic apparatus in *Fucus serratus* embryos. In *Photosynthesis: Mechanisms and Effects* Vol. IV (ed. G. Garab), pp. 3245–3248. Proceedings of the XIth International Congress on Photosynthesis. Kluwer Academic Publishers, Dordrecht, The Netherlands.

Lesser M.P. (1996) Elevated temperatures and ultraviolet radiation cause oxidative stress and inhibit photosynthesis in symbiotic dinoflagellates. *Limnology and Oceanography* **41**, 271–283.

Major K.M. & Davison I. (1998) Influence of temperature and light on growth and photosynthetic physiology of *Fucus evanescens* (Phaeophyta) embryos. *European Journal of Phycology* **33**, 129–138.

Malanga G., Calmanovici G. & Puntarulo S. (1997) Oxidative damage to chloroplasts from *Chlorella vulgaris* exposed to ultraviolet-B radiation. *Physiologia Plantarum* **101**, 455–462.

Malanga G. & Puntarulo S. (1995) Oxidative stress and antioxidant content in *Chlorella vulgaris* after exposure to ultraviolet-B radiation. *Physiologia Plantarum* **94**, 672–679.

McCook I.J. & Chapman A.R.O. (1997) Patterns and variation in natural succession following massive ice-scour of a rocky intertidal seashore. *Journal of Experimental Marine Biology and Ecology* **214**, 121–147.

McLachlan J. (1974) Effects of temperature and light on growth and development of embryos of *Fucus edentatus* and *F. distichus*. *Canadian Journal of Botany* **52**, 943–951.

McLachlan J. & Bidwell R. (1978) Photosynthesis of eggs, sperm, zygotes and embryos of *Fucus serratus*. *Canadian Journal of Botany* **56**, 371–373.

Otero P., Viana M., Herrera E. & Bonet B. (1997) Antioxidant and prooxidant effects of ascorbic acid and flavonoids on LDL submitted to different degrees of oxidation. *Free Radical Research* **27**, 619–626.

Palenik B., Price N.M. & Morel F.M.M. (1991) Potential effects of UV-B on the chemical environment of marine organisms: a review. *Environmental Pollution* **70**, 117–130.

Pawley J.B. (1995) *Handbook of Biological Confocal Microscopy* 2nd edn. Plenum Press, New York.

Pearson G. & Brawley S.H. (1996) Reproductive ecology of *Fucus distichus* (Phaeophyceae): an intertidal algae with successful external fertilisation. *Marine Ecology Progress Series* **143**, 211–223.

Platt T., Gallegos C. & Harrison W.G. (1980) Photoinhibition of photosynthesis in natural assemblages of marine phytoplankton. *Journal of Marine Research* **38**, 687–701.

Royall J.A. & Ischiropoulos H. (1993) Evaluation of 2,7-dichlorofluorescein and dihydrorhodamine 123 as fluorescent probes for intracellular H_2O_2 in cultured endothelial cells. *Archives of Biochemistry and Biophysics* **302**, 348–355.

Schofield O., Evens T. & Millie D.F. (1998) Photosystem II quantum yields and xanthophyll-cycle pigments of the macroalgae *Sargassum natans* (Phaeophyceae): responses under natural sunlight. *Journal of Phycology* **34**, 104–112.

Schreiber U., Schliwa U. & Bilger B. (1986) Continuous recording of photochemical and non-photochemical quenching with a new type of modulation fluorometer. *Photosynthesis Research* **10**, 51–62.

Scully N.M., McQueen D.J., Lean D.R.S. & Cooper W.J. (1996) Hydrogen peroxide formation: the interaction of ultraviolet radiation and dissolved organic carbon in lake waters along a 43–75° N gradient. *Limnology and Oceanography* **41**, 540–548.

Shen B., Jensen R.G. & Bohnert H.J. (1997) Mannitol protects against oxidation by hydroxyl radicals. *Plant Physiology* **115**, 527–532.

Siefermann-Harms D. (1987) The light harvest and protective functions of carotenoids in photosynthetic membranes. *Physiologia Plantarum* **69**, 561–568.

Sokal R.R. & Rohlf F.J. (1995) *Biometry: the Principles and Practice of Statistics in Biological Research* 3rd edn. W.H. Freeman, New York.

Strid A., Chow W.S. & Anderson J.M. (1994) UV-B damage and protection at the molecular level in plants. *Photosynthesis Research* **39**, 475–489.

Tschiersch H. & Ohmann E. (1993) Photoinhibition in *Euglena gracilis*: involvement of reactive oxygen species. *Planta* **191**, 316–323.

Uhrmacher S., Hanelt D. & Nultsch W. (1995) Zeaxanthin content and the degree of photoinhibition are linearly correlated in the brown algae *Dictyota dichotoma*. *Marine Biology* **123**, 159–165.

Wright S.W., Jeffrey S.W., Mantoura R.F.C., Llewellyn C.A., Bjørnland T., Repeta D. & Welschmeyer N. (1991) Improved HPLC method for the analysis of chlorophylls and carotenoids from marine phytoplankton. *Marine Ecology Progress Series* **77**, 183–196.

Zhou X. & Mopper K. (1990) Determination of photochemically produced hydroxyl radicals in seawater and freshwater. *Marine Chemistry* **30**, 71–88.

Zhu H., Ming H., Bannenberg G.L., Moldéus P. & Shertzer H.G. (1994) Oxidation pathways for the intracellular probe 2′,7′-dichlorofluorescin. *Archives of Toxicology* **68**, 582–587.

Received 8 December 2000; received in revised form 4 May 2001; accepted for publication 4 May 2001

Journal of Aquatic Ecosystem Stress and Recovery 7: 317–333, 2000.
M.J. Attrill (ed.), Stress in Marine Communities, Part 2.

Impacts of anthropogenic stresses on the early development stages of seaweeds *

Susana M. Coelho[1,2], Jan W. Rijstenbil[2] & Murray T. Brown[1,§]
Marine Biology and Ecotoxicology Group, Department of Biological Sciences and Plymouth Environmental Research Centre, University of Plymouth, Plymouth PL4 8AA, U.K.
Netherlands Institute of Ecology, Centre for Estuarine and Coastal Ecology, P.O. Box 140, NL-4400 AC Yerseke, The Netherlands
Author for correspondence: E-mail: MTBrown@Plymouth.ac.uk

Key words: seaweeds, juvenile stages, stress factors, UV radiation, global warming, eutrophication, trace metal pollution, oil pollution

Abstract

Seaweeds are important primary producers, and as such contribute significantly to nearshore ecosystems. Studies on the effects of anthropogenic stresses on these organisms have largely been concerned with the vegetative adult stages of the life cycle. Here we review the limited information on the sensitivity of early stages in the life cycle of seaweeds to global change (UV increase; global warming; increased storm frequencies) and pollution eutrophication, trace metals and oil). Impacts on fertility, substrate attachment, development, photosynthesis, growth and mortality are highlighted. In their natural habitats, early stages are shade-adapted, as they live shel ered under adult canopies and in pores of the substrata. Although some acclimation under increased moderate rradiance is seen, higher solar irradiance, and especially ultraviolet-B, inhibits early development. Global warming may decrease the fertility and shorten the fertile period of some species. With the increasing likelihood of storms associated with global warming, gamete release may be inhibited while scouring by suspended sediments may detach newly settled stages. Succession and local distribution patterns are likely to be affected. Eutrophication can result in accelerated development of the early stages of some algal species but sewage discharges have a negative impact on sperm motility, fertilisation and can cause increased mortality in germlings. Impacts of other, indirect effects of eutrophication, including increased sediment cover of substrata, scouring caused by wind-induced resuspension of sediments, and grazing, are also expected to be negative. Toxic trace metals affect gamete viability, inhibit fertilisation and development, and reduce growth rates. Gametes are particularly susceptible to oil pollution and interactions between hydrocarbons and the adhesive mucus surrounding the embryonic stages seem to inhibit settlement. Recommendations for future studies are provided that are aimed at gaining greater insight into the effects of anthropogenic stress on the weakest links in the development cycle of seaweeds.

1. Introduction

As a consequence of human activities in the densely populated and industrialised transition zones between land and ocean, macroalgae (or seaweeds) growing in coastal and estuarine waters are exposed to various forms and degrees of anthropogenic stress. Nutrient enrichment, contamination from organic matter and increased cycling of suspended solids, discharges of toxicants such as metals and pesticides have all resulted in alterations to the light climate and chemical environment for these primary producers. Exposure of algal communities to these pollutants is additional to the expected effects of global change resulting from increased ultraviolet radiation, increased carbon

* Communication no. 2677 of NIOO (CEMO).

dioxide levels, global warming, and increased storm frequency. While a few species of seaweed have been used as biomonitors for some of these stress factors, the effects of anthropogenic disturbances on different seaweed species, and their responses to them, have been little studied. For example, the impact of separate stress factors and the tolerance mechanisms of algal species, synergistic and antagonistic effects of cumulated stresses, the impact of these stresses on the physiological state of the vegetative tissue, and their impact as a function of the stage of development of a seaweed, are all poorly understood. This is all the more surprising because seaweeds are the most important primary producers of nearshore waters (Ramus, 1992). Moreover, they provide shelter for other marine organisms, are nursery grounds for fisheries, they buffer against large scale changes in water column nutrient concentrations, and they stabilise sediments (Duarte, 1995). They are also important in terms of biodiversity, and are sources of valuable natural products (Lüning, 1990).

Until recently, studies on the structure of marine benthic communities have focused primarily on the physical, chemical and biological factors that regulate vegetative growth of the adult stages. This is also true of studies on the effects of anthropogenic perturbations on macroalgal assemblages; for example most studies on eutrophication and pollution deal with availability, uptake and storage of nitrogen, phosphorus and metals by adults, and their effects on photosynthesis and growth of vegetative parts of adults. However, the importance of young stages to the structuring and dynamics of intertidal rocky shore and sublittoral communities is now being recognised (Underwood & Fairweather, 1989; Reed, 1990; Bellgrove et al., 1997). Survival of early stages of marine organisms is believed to be critical to the successful establishment of benthic populations (Vadas et al., 1992), and therefore, of great importance to the management of marine habitats. With this recognition has come greater attention to the ecology of early life history phases, including: dispersal, settlement, dislodgement, intra- and inter-specific competition (Norton, 1983; Wright & Reed, 1990; Vadas et al., 1990, 1992; Amsler & Neushul, 1991; Brawley & Johnson, 1991; Fletcher & Callow, 1992; Reed et al., 1992; Andersson et al., 1994; Kendrick & Walker, 1994; Beach et al., 1995; Creed et al., 1997).

The effects of abiotic factors on biological processes in seaweed communities have to a large extent been ignored, except when they are sufficiently severe to produce mortality. However, Davison et al. (1993) have suggested that sub-lethal stress might play an important role in the recruitment success of individuals and the development of seaweed communities on rocky shores. Reductions in fitness, such as decrease in photosynthetic capacity, due to sublethal stresses, may influence the growth of algae and their ability to compete with others. Moreover, their data emphasises the importance of age and stage-related differences in the response to physical factors. Yet, Santelices (1990), Clayton (1992) and Fletcher and Callow (1992) all document the paucity of information on the reactions of early life history stages to environmental stresses.

In light of this, here we deal with some of the consequences of anthropogenic stress for the reproductive cycle as a whole, highlighting the fact that some events in the seaweed life history other than the vegetative growth of adults may be more sensitive to environmental stress. For example, stressors may affect (a) maturation of the reproductive parts, (b) sex ratio, (c) viability of gametes and spores, (d) responses to pheromones and other 'triggers' that regulate the development through gamete release and fertilisation, asexual sporulation, and vegetative growth, (e) mortality rates of gametes, zygotes and germlings. Yet, despite the potential ecological problems arising from such effects, for many of these the impacts are relatively unknown. We provide a summary of the studies that have dealt with the impact of stress on the early stages of the life cycle of seaweeds, and include effects, where known, of global change (ozone depletion, global warming, increased storm frequency) and pollution (eutrophication, metals, and hydrocarbons). We also provide some recommendations for future study in the hope of stimulating further work on these critical stages in the life cycle of macroalgae.

2. Characterisation of transitional stages in the life cycle of macroalgae

The sequence of transitions for benthic macroalgae usually includes four stages: spores or zygotes, germlings, juveniles and adults (Vadas et al., 1992). Macroalgal life histories can follow several patterns, depending on the species and the environment. An alternation between two free-living stages – one a haploid gametophyte, the other a diploid sporophyte – is common, but many variations exist. Sexual reproduction may be isogamous, anisogamous or

ogamous. Syngamy is regulated by cell recognition nechanisms on cell/flagella surfaces. Motile gametes n brown algae, for instance, may be attracted to ach other or to a stationary egg by pheromones Maier, 1993; Lobban & Harrison, 1994). Other eaweed species release propagules into the seawater hat are transported in currents before settling on avail- ble substrata. As there is considerable confusion n the literature about the meaning of early post- ettlement stages (EPS), we will follow the terminol- gy suggested by Vadas et al. (1992). Usually the erm propagule refers to reproductive spore bodies of vhich there are a number of different types (Fletcher ż Callow, 1992).

For the great majority of algae, individual spore odies are released into the pelagic zone, and are ubsequently distributed by water currents over short r long distances. Following release from the adult, : is necessary for a spore to re-enter the benthic oundary layer. In view of the microscopic dimensions f spores compared to the large water volume, there ppears to be very limited reproductive success which ie seaweed tries to balance with an extremely high pore output, as has been reported for genera such s *Laminaria* and *Macrocystis* (Fletcher & Callow, 992). In general, successful colonisation is achieved nder conditions of limited dispersal and/or minimal urrent activity (Fletcher & Callow, 1992). A number f studies report that a high degree of fertilisation uccess can be achieved by fucoid algae (Brawley, 992; Pearson & Brawley, 1996; Serrão et al., 1996a,). *Fucus distichus*, for example, is able to achieve igh levels of fertilisation success in the intertidal zone y releasing gametes synchronously during periods of ery low water motion in tide pools isolated at low de (Pearson & Brawley, 1996). Following release and ertilisation, zygotes remain unattached and are poten- ally subjected to dispersal for a period of at least ne tidal cycle. In the same study, the authors found iat fertilisation success is generally low when high alinity gradients are present in the pools. Both hyper- nd hypo-osmotic conditions can influence gamete elease and fertilisation, since a receptacle of an indi- idual can be positioned near the top or the bottom of ie water column in a rockpool.

Settlement is defined by Vadas et al. (1992) as the iitial post-sinking attachment of propagules to the ubstratum, and recruitment as the process of transi- on into one or more size or developmental stage. he role of recruitment in structuring the adult popula- on is still obscure. Recruitment from propagules is sometimes thought to play a minor role in the structure and growth of adult populations, as e.g. Ang and De Wreede (1990) concluded for *Sargassum* recruits. High recruit mortalities were reported from other experiments (Ang, 1985). In contrast, other researchers concluded that recruitment is important in local persistence of populations, and plays a substantial role in stabilising densities of adults within, for example, *Sargassum* beds (Deysher & Norton, 1982; Kendrick & Walker, 1994).

As regards mortality rates in early developmental stages of seaweeds, there are likely to be size-specific differences (Vadas et al., 1992), as well as age or time-dependent differences (Thélin, 1981), in their susceptibility to disturbance. For example, the mortality rate of young germlings of *Fucus* exposed to pollutants decreases with age. On the other hand, 7-day-old zygotes become more easily detached from their substrata than 2-day-old ones. The probability of survival is not constant throughout life. Creed et al. (1997) found seemingly high mortality rates of *Fucus serratus* in the laboratory (89% in 76 days); however, these were comparable to loss rates of populations on the shore (Creed et al., 1996).

Most studies show that early stages suffer from high mortality and the processes and mechanisms involved are enigmatic (Santelices, 1990). Although substantial progress has been made in the last decades, we still know little about how and why so many thalli die so early in life (Vadas et al., 1992). Early stages are a bottleneck for marine organisms (Underwood & Fairweather, 1989), including the algae. There is a high mortality in early post settlement stages, so the individuals who survive are unique, and represent a gene pool for the subsequent generations. However, there is a high probability that selected genotypes will be determined by chance events, i.e. the propagules that are not washed away by waves and currents will survive. On the other hand, these chance events are not so easily applicable to other environmental triggers, such as temperature, irradiance, desiccation or toxic compounds. The individuals that are best adapted to extreme values of these conditions will be selected on the basis of their genetic constitution. Processes that influence EPS survival not only affects the ecology of species, but also the evolution and the role of communities.

3. Global change effects

3.1. *Ultraviolet increase due to ozone depletion*

The prediction of the effects of global climate change has been one of the most studied topics during the last two decades. A link has been established between the anthropogenic release of certain compounds in the troposphere and the subsequent involvement of these compounds in the destruction of ozone in the stratosphere. A strong relationship exists between measured reductions in total ozone concentration and increased amounts of ultraviolet-B radiation measured at the earth's surface. Reductions in the thickness of the ozone column have increased the amount of UV-B at the earth's surface and shifted the solar spectral distribution to shorter wavelengths.

Despite the importance of macrophytes to coastal ecosystems, most research has focused on the effects of ozone depletion and subsequent UVB increase on phytoplankton and coral reefs. Macroalgae and seagrasses have been less studied, and this applies particularly to their early life history stages (Table 1). The consequences of a changing light climate for the eco-physiology of marine macrophytes have been thoroughly reviewed by Franklin and Forster (1997). We therefore concentrate on the consequences for the early development of macroalgae.

In the marine habitat, especially in the intertidal zone, macrophytes are exposed to diurnal changes of irradiance depending on sun angle, clouds, and tides. Thus, there is a conflict between maximum light harvesting under low light and minimum inhibition and destruction of photosystems under high light periods. Although studies of the effects of light stress on marine macroalgae have largely been restricted to mature stages, several reports indicate that young tissue may be more susceptible to these perturbations (Table 1). The rapid acquisition by spores of basic traits of physiology such as photosynthesis and respiration for growth and development, or of a stress response is of ecological relevance. It ensures their viability *in situ* and, consequently, the recruitment of new individuals or establishment of new populations of the species (Amsler & Neushul, 1991; Beach et al., 1995). Many macroalgae produce large numbers of propagules that are dispersed from the parent population and colonise new sites. These early stages show adaptations that enable survival in shaded environments, under the adult canopy (Kain & Norton, 1990). There is now sufficient evidence to show that high fluences of either photosynthetically active radiation (PAR) alone or PAR+UV radiation can be lethal to algae at certain times in their development (Franklin & Forster, 1997).

The acclimation of early life stages of seaweeds to light, in general, is discussed first. As to the first stage in development (gamete fertility) one example is given. The extent of induction of fertility in *Laminaria* species depends on quantum dose (radiant exposure) and not on photon irradiance (Lüning & Dring, 1975; Lüning, 1980). Female and male gametophytes react in the same way towards blue light inducing their fertility, which is extremely important for successful fertilisation (Lüning, 1980). The period of viability of propagules after release from their parent population is enhanced if these stages are photosynthetically competent upon release, leading to higher success in settlement and recruitment. Reproductive cells capable of fast adaptation to particular light regimes that are common to coastal environments, may be more successful than those without that capacity (Beach et al., 1995). Planktonic propagules have an ephemeral nature (Santelices, 1990), and this is partially attributed to immature chloroplasts in newly released propagules, resulting in reduced photosynthetic rates. Nevertheless, net positive photosynthesis has been reported for algal reproductive unicells (Amsler & Neushul, 1991; McLachlan & Bidwell, 1978; Rodrigo & Robaina, 1997). Reproductive unicells of *Ulva* and *Enteromorpha* species demonstrated substantial rates of photosynthesis in contrast to that observed in kelp zoospores (Amsler & Neushul, 1991). A remarkable difference was found between values of maximum photosynthesis in gametes and zoospores of *Ulva*, with gametes showing values similar to vegetative gametophytes. The photophysiological differences observed between reproductive unicells of (opportunistic) ulvacean algae and kelp (characteristic of late successional communities) are proposed to be representative of exploitive and stress tolerant exploitation strategies, respectively. Spores and young germlings of subtidal algae are very sensitive to light; gametophytes (haploid stages) of *Macrocystis*, *Laminaria* and *Pterigophora* species were killed after exposure to direct sunlight of approximately 1000 μmol m^{-2} s^{-1} for a few minutes (Lüning & Neushul, 1978). Hanelt et al. (1997), who studied photoinhibition and recovery after high light stress in *Laminaria saccharina*, showed that: (a) acclimation to high irradiance is slow in young sporophytes and increases with sporophyte age, but is fastest

Table 1. Key references of studies on the effects of irradiance and ultraviolet radiation on fertility, germination and development of early life history stages of seaweeds

Species	Agent	Indicator	Reference
Ecklonia radiata	PAR/UV radiation	Young gametophytes and sporophytes	Novaczek (1984)
Macrocystis pyrifera	High PAR	Young gametophytes and sporophytes	Graham (1996)
Alaria esculenta *Laminaria digitata* *L. hyperborea* *L. saccharina*	High PAR/Photoperiod	Young sporophytes	Han and Kain (1996)
Pterothamnion plumula *Halarachnion ligulatum* *Ceramium rubrum* *Chondrus crispus* *Ulva pseudocurvata*	High light	Spores and germlings	Leukart and Lüning (1994)
Laminaria digitata *L. hyperborea* *L. saccharina*	UV radiation	Germination, growth and chlorophyll fluorescence of zoospores, gametophytes and young sporophytes	Dring et al. (1996)
Laminaria digitata *L. hyperborea* UV radiation *L. saccharina*	High light/ gametophyes	Fertlity, gametogenesis, young	Lüning (1980)
Laminaria japonica	High light	Zoospores, young sporophytes	Fei et al. (1989)
Laminaria saccharina	High light	Different developmental stages of gametophytes and sporophytes	Hanelt et al. (1997)
Ecklonia radiata	UV radiation	Juvenile plants	Wood (1987)

n gametophytes, (b) photosynthesis in older sporo-hytes and gametophytes is inhibited more rapidly han in young sporophytes, (c) recovery is also faster n gametophytes and older thalli, i.e. there is a faster eversal of the process and hence, a faster restoration f high photon efficiency of photosynthesis occurs. ligh photon irradiances inhibited growth of gameto-hytes and sporophytes of *Ecklonia radiata* less than . mm long, and such a light stress may explain he absence of summer recruits to areas of open ottom in shallow water (Novaczek, 1984). Growth f eulittoral red algae germlings can be reduced by xposure to moderate PAR irradiances. Germlings f strictly subtidal species *Pterothamnion plumula nd Halarachnion ligulatum* showed inhibition of rowth from 30–100 μmol m^{2-} s^{-1}, whereas eulit-oral species *Ceramium rubrum*, *Chondrus crispus* nd *Ulva pseudocurvata* did not show inhibition of rowth until 500 μmol m^{-2} s^{-1} irradiance. Growth f eulittoral germlings of red algae can be reduced by xposure to moderate PAR (Leukart & Lüning, 1994). Post settlement stages (gametophytes, embryonic sporophytes) of the giant kelp *Macrocystis pyrifera*, growing at the upper limit of its zone, survived only under shade but not high irradiances (Graham, 1996). Settlement of shade-adapted *M. pyrifera* zoospores decreased, but was not prohibited under high PAR. This suggests that high irradiances can inhibit recruitment of *M. pyrifera* to shallow water by killing its post settlement stages. The effect of UV was not tested, although it may also potentially affect kelp recruitment in shallow water.

Literature on the additional effect of UV radiation is relatively scarce. According to Dring et al. (1996) the sensitivity of three species of *Laminaria* to UV-radiation was lower in young sporophytes than in gametophytes, and lower in mature sporophytes than in young sporophytes. Germination of zoospores and growth of gametophytes was reduced after exposures to UV longer than 1 h, whereas UV had little effect on the growth of young or mature sporophytes unless exposure was prolonged for more than 48 h. Yabe et

al. (1997) found that gametophyte growth of *Laminaria religiosa* was strongly inhibited by ultraviolet B (320–280 nm) radiation, which indicated that reproduction of this species might be inhibited by sunlight in shallow waters. Exposure of young, shade-adapted sporophytes of the lower intertidal species *Laminaria digitata* to direct solar radiation (UV) showed a higher sunlight tolerance in comparison with the subtidal *Laminaria hyperborea* (Han & Kain, 1996). Sunlight tolerance of the sporophytes of both species could be greatly enhanced following acclimation to higher irradiances (2–5 times the saturation point for growth). This indicates that settlement stages of kelps are capable of "light hardening" (Franklin & Forster, 1997). It demonstrates that juvenile stages of seaweeds are susceptible to UV; however, a gradual acclimation may increase their sunlight tolerance. For example, exposure of shade-adapted juvenile, sub-canopy *Ecklonia radiata* to natural sunlight, after removal of the seaweed canopy, caused tissue damage, bleaching and reduced growth (Wood, 1987). This damage to *E. radiata* germlings did not occur after exclusion of UV, both in field and laboratory experiments.

3.2. *Global warming*

In the atmosphere, certain trace gases both promote global warming and deplete the ozone layer. The primary active trace gases that affect global warming are carbon dioxide, nitrous oxide, chlorofluorocarbons, methane and tropospheric ozone as they trap infrared radiation (Juno et al., 1989). These greenhouse gases and other biogenic trace gases, such as carbon monoxide (CO), nitrogen oxides (NO_x), and a range of volatile organic compounds (VOCs) play a key role in atmospheric chemistry by affecting tropospheric concentrations of ozone, the penetration of photochemically active solar ultraviolet radiation, the production of hydroxyl radicals, and, in the case of dimethyl sulfide (DMS), cloud formation. As a result, it is expected that not only will the average air and water temperature rise, but also that the temperature ranges may become wider, i.e. colder winters and hot summers.

Temperature is the major factor controlling the rate of photosynthesis in all plants (Davison, 1991). In addition to differences between the average temperature of different habitats, algae also experience temperature fluctuations on many different timescales, including rapid fluctuations associated with tidal displacement of the thermocline (Zimmerman & Kremer, 1984) or tidal immersion/emersion, diurnal changes characteristic of many small streams and ponds, seasonal changes and long-term inter-annual variability associated with natural climatic cycles and, possibly, human influence (e.g. "greenhouse effect", Davison, 1991). Various physiological criteria have been used as a measure of the extent of temperature stress on metabolism. Photosynthesis and respiration have been most commonly used, owing to the ease with which they can be measured. The literature contains many descriptions of the short-term response of photosynthesis to a range of incubation temperatures (Oates & Murray, 1983; Zupan & West 1990; reviewed by Davison, 1991). The typical response is an increase in photosynthesis up to an optimum temperature beyond which it declines rapidly. In macroalgae the optimum is typically a range of several degrees rather than a single value (Oates & Murray, 1983; Madsen & Maberly, 1990). As incubation temperature increases, rates of dark respiration (R_d) and light saturated photosynthesis (P_{max}), and the photon irradiance required to achieve net photosynthesis and P_{max} (I_c and I_k respectively) all increase, whereas rates of light limited photosynthesis ($P_{sub\text{-}sat}$) decline (Davison, 1991). Most of these data are derived from work on adult seaweeds. Major and Davison (1998) have studied the effects of temperature (and light) on photosynthesis and growth of *Fucus evanscens* embryos in the laboratory during the first 7–10 days after fertilisation. High-temperature grown embryos had similar lengths but were always larger in biovolume than low-temperature grown. The maximum quantum efficiency Fv/Fm (variable fluorescence) and the photosynthetic capacity (oxygen production) were higher at higher temperatures. However, since only two temperatures were used (5 °, 20 °C) it is not possible to predict the effects of global warming on juvenile stages. Rodrigo and Robaina (1997) reported on the variation in photosynthetic efficiency and capacity of cultivated young sporelings of the red algae *Grateloupia doryphora* under normal conditions and after a short-term incubation at different temperatures (and salinity). The pigment composition of the sporelings (more chlorophyll *a*; less phycoerythrin and phycocyanin than adults) promotes a better photosynthetic performance under chlorophyll *a* excitation. Unexpectedly, they found that sporelings were more tolerant to variations in temperature than older stages.

Data on the effect of global warming on seaweed eproduction are very scarce. As an example, the ercentage of fertile gametophytes of *Laminaria* at a iven quantum dose of photomorphogenically active adiation increases with decreasing temperature. This s in contrast with vegetative growth rates, which ncrease with increasing temperature (Lüning, 1980). n many species, for example fucoids, there is a 'sterile" summer period. Extending periods of high ummer temperatures in coastal waters may result n a further reduction in fertility of certain species hat in turn will bring about changes in competi- ion and composition of seaweed assemblages (e.g. Barry et al., 1995). On a global scale, the expected ise in temperature and their impacts on life history nd growth could significantly influence distribution atterns of certain seaweeds (e.g. Pakker & Breeman, 996). Raven (1992) has suggested that endemic polar pecies may be at particular risk if they fail to adapt eir temperature responses as fast as lower latitudinal pecies adapt to changing photoperiod. Beardall et al. 1998) have recently reviewed the effects of changes in tmospheric CO_2 concentrations on marine plants but ie responses of juvenile stages were not addressed. hey also point out a lack of studies on the combined ffects of increased temperature and CO_2.

.3. *Increases storm frequency*

Vater motion is a major cause of seaweed mortality t all stages of growth, and perhaps especially for ettling spores and zygotes. Storms overturn boulders nd move sand onto and off beaches. These events re disturbances that destroy some organisms and reate space for others (Lobban & Harrison, 1994). In ome areas, storms constitute a seasonal phenomenon, lthough their intensity may vary markedly.

Wave action is generally considered an important ictor in distribution and abundance of intertidal rganisms (Vadas et al., 1990). A certain amount of ater motion is necessary to maintain an effective pply of nutrients; beyond that, the force component f water motion becomes more important. Wave ergy is known to cause indirect mortality to juvenile id adult assemblages through movement of algal onds, logs, rocks and debris. Studies of natural pawning events suggest that higher than average ater velocities or changes in current direction can duce fertilisation success (Oliver & Babcock, 1992; etersen et al., 1992, Pearson et al., 1998). The best iance for organisms to increase external fertilisation success in turbulent environments is to avoid releasing their gametes during periods of high water motion. For example, high water motion inhibits gamete release in fucoid algae (Serrão et al., 1996b) and so if storm frequency increases, there is a decreased likelihood for these species to reproduce successfully.

Vadas et al. (1990) have shown that wave action is a major source of mortality to recently settled spores of *Ascophyllum nodosum* and that water movement was the primary factor controlling recruitment and distributional patterns. In exposed habitats the speed with which algal propagules sink and attach to the substrate is an important factor; this will become even more significant if frequencies of storms increase. Sinking velocity increases with germling size (Norton, 1978) and, while there is occasionally an absence of early adhesion (Hardy & Moss, 1979), adhesive tenacity (attachment strength) usually also increases with germling size (Norton, 1983) and implicitly, with time (Vadas et al., 1992). Norton (1978) found that the number of propagules that settle out from a given inoculum decreases with increasing water velocity, and sinking velocities. Substrate roughness is beneficial in turbulent environments in two ways: it can anchor the germlings and can also "catch" more propagules (Norton, 1983) from turbulent water flows (Norton & Fetter, 1981).

Sand and sediment associated with water movement are major agents of disturbance. As concerns the adult plants, tolerant seaweeds are able to survive scouring and burial. The characteristics of these algae include tough, cylindrical thalli, thick cell walls, great ability to regenerate, asexual reproductive cycle functionally equivalent to regeneration (Norton et al., 1982). The early life stages may be much more sensitive. Whatever water motion conditions are most suitable for algal spore settling, they are also likely to be favourable to sediment settling. Spores that settle on sediment particles are likely to be washed away, especially as they grow into the faster moving water layers. Sand movement on beaches is typically seasonal, building up in spring and being washed into the subtidal in autumn.

Reed and Foster (1984) found that storm disturbance which removes *Macrocystis pyrifera* and *Pterygophora californica* canopies can permit recruitment; inhibition of recruitment due to canopy shading can be overcome by storms. As an example, a major environmental disturbance that took place in May 1982 is described. Irregular winds and positive sea surface temperature anomalies in equatorial central

Pacific marked the onset of perhaps the most extensive El Nino/Southern Oscillation of the past century. From autumn 1982 until summer 1983, warm waters (2–3 °C above mean values) and elevated sea levels (over 20 cm) were recorded (ref. in Gunnill, 1985). Severe winter storms associated with El Nino hit southern California and destroyed many kelp forests along the coast (Dayton & Tegner, 1990). Such storm-related plant removals created an opportunity for recruitment of juvenile plants in the cleared areas. However, recruitment of juveniles into these open spaces was largely unsuccessful during 1983 because the adult plants that survived the winter of 1993 and the newly recruited juveniles were exposed to significantly altered temperatures and patterns of nutrient availability during the remainder of the year (Dayton & Tegner, 1990). Zimmerman and Robertson (1985) studied the effects of El Nino on the growth of *Macrocystis pyrifera* and observed that the canopy was eliminated because growth rates of fronds were so slow that terminal blades were formed before reaching the surface. Moreover, growth rates of juvenile *M. pyrifera*, although abundant in cleared areas during June and July 1983, were also very low with none of them surviving throughout autumn. The authors suggested that these low growth rates are typical of nutrient limited conditions, as the deepening of the isotherms associated with El Nino appeared to reduce the usual input of nutrients during summer and autumn. Gunnill (1985) has reported that both recruits and adult sporophytes of two laminarian brown algae died during a prolonged warm water period associated with El Nino, but net recruitment by other species was relatively high. From this it can be concluded that disturbances caused by strong water motion are important because they can create clear spaces and prevent competitively dominant species from permanently precluding other species.

4. Pollution effects

There is no precise definition of the term "pollution" but one general definition is a stress on the natural environment caused by human activities, resulting in unfavourable alterations of an ecosystem (Lobban & Harrison, 1994). The adverse effects of pollutants on aquatic organisms are in most cases identified in terms of their acute or lethal impacts. However, the term "adverse" may not fully describe these pollution effects, as in the case of eutrophication there is often a stimulation of growth due to increased amounts of nutrients. Three forms of pollutant are discussed: eutrophication i.e. excessive nutrients such as nitrogen and phosphorus (Table 2), trace metals (Table 3) and hydrocarbons (particularly oil). Since the young stages are a sensitive link in a species' life cycle (Andersson et al., 1992), recovery of populations from anthropogenic stress is likely to depend upon recruitment of these early stages. However, very few studies deal with the course of events during the first days and weeks after settlement. Thus, little is known of mortality rates of microscopic stages and the size of the microscopic population.

Table 2. Cited literature on the indirect effects of eutrophication on fertilisation and development of early life history stages of seaweeds

Species	Agent	Indicator	Reference
Laminaria saccharina	Silt	Sporophyte development	Burrows and Pybus (1971)
Macrocystis pyrifera	Sediments	Germling development	Devinny and Volse (1978)
Hormosira banksii *Durvillaea potatorum*	Sewage effluent	Fertilisation, zygote germination, embryo growth and mortality	Doblin and Clayton (1995)

4.1. *Eutrophication*

An increased level of plant growth and biomass production in response to added nutrients is termed "eutrophication" (Lobban & Harrison, 1994). The increased nutrient input may result from land runoff, river inflow, and sewage discharges. A direct response of nearshore vegetation to increased nutrient supply may be a spread of finely branched forms, particularly of epiphytes like *Pilayella litoralis* and *Ectocarpus confervoides*, and some foliose green and red algae. Most of these opportunistic species have high growth rates, high nutrient uptake rates, and often grow at nutrient saturation levels, which gives them a competitive advantage over slow-growing perennials like *Fucus* spp. A deterioration of the light climate due to increased phytoplankton biomass, suspended matter and overgrowing (shading) by epiphytes are the more likely causes for the decline of *Fucus* spp. in Kiel Bay (Vogt & Shramm, 1991), and for a decrease in macrophyte numbers in general (Phillips et al., 1978).

It is not certain whether an increased nutrient supply and nutrient competition can affect the early growth stages of seaweeds. Based on current knowl-

Table 3. Experimental studies on the effects of trace metals and arsenate on fertilisation, germination and development of early life history stages of seaweeeds

Species	Agent	Indicator	Referenc
Laminaria saccharina	Copper	Release of meiospores, settlement of meiospores, development of gametophytes, gametogenesis, germination of meiospores, growth of sporophytes	Chung and Brinkhuis (1986)
Laminaria hyperborea	Copper	Sporophyte development	Hopkin and Kain (1978)
Fucus spp. *Ascophyllum nodosum* *Pelvetia canaliculata*	Cadmium Copper Lead Mercury	Sporophyte growth rate	Stromgren (1980a, b)
Macrocystis pyrifera	Arsenate Copper	Early gametophyte development (germination, germ tube growth and nuclear migration)	Garman et al. 1994
Fucus vesiculosus	Copper	Fertilisation success, zygote germination, apical hair frequency	Andersson and Kautsky (1996)
Fucus serratus	Copper	Spermatozoid motility, fertilisation success, germlings growth rate	Scanlan and Wilkinson (1987)
Fucus spiralis	Copper	Ultrastructure, germling development and growth	Bond et al. (in press)
Macrocystis pyrifera	Zinc	Germination of zoospores, germ tube elongation	Anderson and Hunt (1988)

dge, it is more likely that the direct eutrophication ffect (stimulation by nutrients) is of less importance han the indirect (derived) effects such as reduced ight penetration. In a few cases, it was reported that he nutrients in the sediment benefit the growth of ettled spores. Nutrient concentrations in the water hase are in general lower than those in the sediment ore water, and nutrient availability to germlings is reatly reduced by adult seaweed plants in the water olumn (Dayton, 1984) or indirectly by the effect f adults on water movement (Norton et al., 1982). lthough it was stated by Amsler et al. (1992) that utrient supply in the sediment microclimate inhabted by algal propagules is highly complex and little nderstood, Kennedy (1983) concluded that sedinents have the advantage of providing nutrients for arly development (and protection from disturbance). pores of the kelp *Macrocystis pyrifera* and *Pterygohora californica* are chemotactic to nutrients (Amsler & Neushul, 1989), as they can swim towards a ariety of nutrients that are likely to stimulate gametohytic growth or reproduction. The spores settle more apidly in response to nutrients (Amsler & Neushul, 990), although nutrients do not directly affect settlement rates of newly released spores as settlement stimulation behaviour develops 5–14 h after spores are released. In this sense, in an area that is rich in organic matter there is a probability that spores settle at a higher rate.

Eutrophication effects as a result of sewage discharge on benthic macroalgae have mostly involved surveys of algal abundance, describing effects on established plants and communities (Doblin & Clayton, 1995). Relatively little is known about the responses of individual species of macroalgae, and, in particular, the reasons for the sensitivity of brown macroalgae remain obscure. Recovery from disturbance also depends on the seasonality of propagule production: species that are fertile year-round (e.g. *Ulva* spp.) are probably less affected compared to species that are fertile only in a restricted period. Thus, low levels of recruitment in one or two seasons due to the effects of sewage effluent may be more devastating because there is only one period in which propagules are available for recruitment (Doblin & Clayton, 1995). There have been a few experimental studies to distinguish the effects of sewage effluents on recruitment from the effects on estab-

lished adult seaweeds. For example, Bellgrove et al. (1997) examined the effects of secondarily treated sewage effluent on intertidal macroalgal recruitment processes. They found no evidence for detrimental effects of effluents on these processes for any studied species, as regards either availability of propagules (asexual spores, gametes, zygotes or fragments) or recruitment of artificial or natural substrata, but rather an enhancement of these processes in many of the opportunistic genera like *Ulva* and *Enteromorpha*. These opportunists showed very high recruitment and propagule densities in the water column at polluted sites, apparently benefiting from the increased nutrient availability. There were obvious differences in the species composition of the polluted and unpolluted sites studied, consistent with those described by Brown et al. (1990), but the typical decrease in species number observed in outfall-associated assemblages (Littler & Murray, 1975; Brown et al., 1990) was not recorded in this study. In contrast, Doblin and Clayton (1995) found that secondarily treated sewage effluent had a deleterious effect on the early life-history phases of two species of brown algae, *Hormosira banksii* and *Durvillaea potatorum*. Concentrated sewage effluents inhibited zygote germination (55–95%), retarded embryo development (80–100%) and caused severe embryo mortality. The effect of sewage was found to be not just one of seawater dilution due to large volumes of freshwater input (e.g. Hopkin & Kain, 1978), as zygote germination and embryos growth were considerably more inhibited in sewage compared to freshwater treatments. Nevertheless, an important effect of the lowered salinity is expected in general as a result of wastewater discharges, as for example fucoid sperm motility and fertilisation are severely affected by low salinity (Brawley, 1991). Reduced salinity is also known to inhibit zygote germination (Wright & Reed, 1990), production of fertile tissue (Mathieson, 1982) and release of propagules (Rao & Kaliaperumal, 1983). So, the observed effects of reduced salinity and sewage effluents on zygotes of *H. banksii* and *D. potatorum* have the potential to drastically alter recruitment. The mortality of embryos in high concentrations of sewage effluent would exacerbate the already high rates of mortality experienced by early macroalgal stages in the field (Reed, 1990; Brawley & Johnson, 1991). The absence of any additional adverse effect of low concentrations of sewage apart from reduced salinity suggests that dilution of sewage is important to mitigate its deleterious effects. Several other (derivative) factors related to water waste discharge have been suggested to have adverse effects on early life history stages of seaweeds. These include decreased irradiance due to the presence of suspended solids, increased sedimentation, and poisoning by toxic chemicals as, for example, described for *Macrocystis* by Anderson and Hunt (1988). These authors successfully applied a short-term bioassay protocol using Macrocystis zoospores to monitor the effects of complex effluents. It is unclear, however, what component(s) of the sewage effluent were toxic for the zoospores in this experiment. No data were found concerning eutrophication effects on the fertility of seaweeds, or specific cases in which hormones discharged with sewage interfered with the pheromones that induce the attraction of gametes. However, it is interesting to mention that vegetative thalli of *Ulva* can produce sporulation-inhibiting organics (Nielsen & Nordby, 1975). This might explain the fact that there is hardly any spore production in dense, largely vegetatively growing *Ulva* canopies in eutrophic waters such as the Veerse Meer lagoon (Kamermans et al., 1998).

In addition to the direct effects of eutrophication on macrophytes as a result of sewage discharge (or other diffuse sources of nutrients), there will be an indirect effect of increased suspended solid concentrations on the development of seaweed populations (Table 2). In turbid, eutrophic areas fine sediments cover seaweed thalli, reducing irradiance and inhibiting photosynthesis. For example, Moss et al. (1973) found that *Himanthalia* colonisation was inhibited by silt due to decreased light. The sediment particles also cover the hard substrata making it more difficult for the early stages to attach with the result that fewer spores germinate and survive. Neushul et al. (1976) and Vadas et al. (1992) have shown that algal propagules suffer from silt (sediment) deposition which increases mortality, and Norton (1978) found that even small amounts of silt covering rocks can prevent settlement of (kelp) sporophytes. Devinny and Volse (1978) concluded that the main reason for the loss of young kelp (*Macrocystis*) was that spores attach to sediment grains which are easily washed away by waves and water motion. Although some propagules were substrate-selective, i.e. did not attach to the grains, and this resulted in delayed germination, these propagules became less discriminative with time. Substrate instability can contribute to poor survival, sand accretion and removal is detrimental to the establishment of spores and zygotes and scour, due to sand movement, has been shown to greatly reduce

recruitment (Neushul et al., 1976; Emerson & Zedler, 1978). The loss of hard substrata suitable for *Fucus* spp. as a result of settlement through deposition of eroded cliff material is a contributing factor to the decline and impaired competitive viability of fucoids in the Baltic Kiel Sea (Vogt & Schramm, 1991). In conclusion, seston may adversely affect spores and zygotes, both through siltation and sedimentation, thus smothering them, and through attenuation of light. The combination of water motion (scour) with a sediment cover of the substrata further reduces the survival (synergistic effect). It is a general assumption that the type of substratum is an important factor for successful recruitment, but this seems to apply to hard-substrata seaweeds in particular. Typical soft-bottom species like members of the Ulvales are well adapted to any kind of substrate. Propagules of *Enteromorpha* are able to germinate on any kind of solid substratum, including other plants, shells of *Mytilus* sp. and over sand grains (Schories & Reise, 1993). Occasionally these species can exploit a sediment cover, to complete their life cycle. Kamermans et al. (1998) examined the role of cold resistance and burial for winter survival and spring initiation of *Ulva* spp., and found that burial of vegetative *Ulva* in the sediments of the shallow part of the eutrophic Veerse Meer could explain the rapid increase in *Ulva* biomass in spring. No sporulation of any significance occurred in this lagoon; *Ulva* maintained a vegetative life history.

Of course sedimentation can be a response to both natural and anthropogenic factors; periods of calm weather and turbid water may produce layers of sediment, but this can be exacerbated by human activities through sewage disposal, dredged material disposal, enhancement of erosion, etc. Whatever the cause, it seems that an increase in deposited sediment cover can induce changes in the composition of the macroalgal vegetation by benefiting species releasing their spores during sediment-free periods (Kiiriki & Lehvo, 1996).

Since eutrophication enhances primary production, the number of grazers usually increase too (Garding, 1996), and in shallow waters dense macroalgal canopies provide an additional shelter to grazers which enable them to reproduce more successfully. In turn, this may increase the grazing pressure on the early life stages of seaweeds. Fucoids are thought to be extremely susceptible to grazing when in the juvenile stage. Grazing can drastically reduce the survival of zygotes and early post-settlement stages. However, this is not always found, and seems to depend on the kind of grazer. For example, Chapman (1990) showed that *Fucus distichus* juveniles are more susceptible to grazing than adults, whereas abundance of juvenile *F. spiralis* was not related to the presence of grazers (Chapman, 1989). Snails inhibited *F. vesiculosus* recruitment along the coast of New England (Lubchenco, 1986). Norton (1978) examined the reasons why *Sacchoriza polychides* failed to colonise Lough Ine, a marine inlet in Ireland, in spite of the abundance of spores swept in continuously by the tide. The combined effects of siltation (which prevents attachment of spores), preferential grazing and tissue decay were considered to be the main factors contributing to the absence of this species.

4.2. *Trace metals*

Most studies on the toxic effects of metals focus on the growth and photosynthesis of adult seaweeds, and predominantly deal with zinc, copper and cadmium (Andersson & Kautsky, 1996; Gledhill et al., 1997; Anderson et al., 1990; Anderson & Hunt, 1988; Chung & Brinkhuis, 1986; Bond et al., 1999). Copper, although an essential micronutrient, is considered to be the second most toxic metal (after mercury) to algae. The mechanisms of copper toxicity have been extensively described for microalgae (Lobban & Harrison, 1994) but the information on macroalgae is still scarce. Although copper has been studied more than any other metal, precise information on the mechanistic basis of cellular toxicity and its physiological effects are still lacking (Brown & Depledge, 1998).

Little is known about the effects of elevated metal concentrations on the reproductive processes of macrophytes, although it has been suggested that metals may inhibit reproduction in brown algae by interfering with the ability of sperm to find eggs, perhaps via interference of the pheromone attractant (Maier, 1995). It is becoming apparent that different stages in the life histories of seaweeds have different degrees of tolerance to metal exposure (Table, 3), and several studies have shown that younger stages are more sensitive than adults (Hopkin & Kain 1978; Chung & Brinkhuis 1986; Anderson et al., 1990; Garman et al., 1994; Andersson & Kautsky, 1996).

Most of these studies have dealt with brown algae, both fucoids and kelps. From a study on different developmental stages of *Fucus serratus*, Scanlan and Wilkinson (1987) concluded that spermatozoa and newly fertilised eggs were the most sensitive to toxicants, and they proposed the use of these stages for toxicity tests. Andersson and Kautsky (1996) studied

the response to copper on different reproductive stages (at different salinities) of Baltic Sea *Fucus vesiculosus*. Their results suggest that the most important factor for the response to copper stress is the pre-existing stress level of the zygotes rather than the influence of salinity on metal availability. Cell walls of fucoid algae, composed of the polysaccharides alginate and fucoidan, can bind cations and have a high affinity for copper (Lignell et al., 1982). The effect of copper and other metals is therefore expected to be more detrimental to zygotes that are exposed to metals prior to the development of a protective cell wall. However, it is also possible that the mucus layer surrounding embryos may adsorb metals in different ways, resulting in a shortage of, for example, iron, manganese or zinc all of which are essential for metabolic processes.

In kelps the microscopic gametophyte phase is more susceptible to elevated trace metal concentrations than macroscopic sporophytes (e.g. Hopkin & Kain, 1978). It has also been shown that long-term effects (of cadmium) are more serious than is immediately evident and that exposure time is important in determining the extent of the effects of toxic substances, for example reductions in photosynthesis and dark carbon assimilation (Markham, 1980). In *Laminaria saccharina* each stage of development had a quite different response to copper (Chung & Brinkhuis, 1986). There was no effect on the first stage (meiospore settlement and germ tube development) below a copper concentration of 500 $\mu g\ L^{-1}$. In the early phase of gametophyte development, growth was inhibited at 50 $\mu g\ L^{-1}$ copper and above. In mature gametophytes, development into sporophytes occurred at concentrations below 50 $\mu g\ L^{-1}$, but growth rates at all copper treatments were significantly lower than controls. Garman et al. (1994) studied the effects of two metals (arsenate and copper) on the development of gametophytes of *Macrocystis pyrifera*. Nuclear migration, a critical event in gametophyte development, was inhibited by ca. 40–90% upon exposure to environmentally relevant levels of copper, i.e. within the range of values given for effluent (Anderson et al., 1990; 58 $\mu g\ Cu\ L^{-1}$) and sediment interstitial water (Burgess et al., 1993; 100 $\mu g\ Cu\ L^{-1}$). They also found a 70% inhibition in nuclear events after exposure to environmentally relevant levels of arsenic (120 $\mu g\ L^{-1}$). This work showed that nuclear migration could be a good biomarker of the response of *M. pyrifera* gametophytes to sublethal concentrations of toxic compounds. A developmental delay due to inhibition of nuclear events would affect gametophyte viability in that it would increase the time-span in which gametophytes would be susceptible to grazing, abrasion (scour) and burial in sediments (Devinny & Volse, 1978). Thus, failure to recruit, delayed development, decreased growth rates, reductions in chlorophyll content and changes in the fine structure of the microscopic gametophyte phase can all potentially impact on kelp primary production, which in turn could have deleterious effects on higher trophic levels.

There have been few studies on recovery from metal toxicity. Garman et al. (1994) found that nuclear migration, germ tube growth and germination of *Macrocystis pyrifera* remain inhibited by arsenic for at least 24 h after replacement of the toxicant with clean seawater. These data suggest that arsenic toxicity is not readily reversed. However, Bond et al. (1999) have shown that retarded development of fucoid germlings exposed to copper could be reversed upon transfer to clean seawater.

The physiological effects of copper and other metals on seaweeds are poorly studied. Copper (II) ions cause leakage of K^+, and changes in cell volume; however this type of response was not detected by Andersson and Kautsky (1996) in young stages of *Fucus vesiculosus*. When transported to the chloroplasts, Cu^{2+} inhibits electron transport to $NADP^+$. Chung and Brinkhuis (1986) have suggested that copper affects iron transport into plastids or incorporation of iron into iron-binding enzymes, and Cu^{2+} may also be responsible for peroxidative degradation of chloroplast membrane lipids. Garman et al. (1994) suggested that toxicants that primarily inhibit cellular events in *Macrocystis pyrifera* gametophytes may act via effects on intracellular pH regulation but no details were provided.

As for less toxic metals, there are few reports on either adult or younger stages. Anderson and Hunt (1988) have studied the effects of zinc on microscopic stages of the kelp *Macrocystis pyrifera*. A short-term exposure to zinc initially stimulated the germination of kelp zoospores before declining at higher concentrations. However, neither the short-term or long-term experiments could clarify what toxic effects high concentrations of zinc were having. It was suggested that inhibition of reproduction could have been caused by a zinc-induced disruption of the photosynthetic apparatus by changes in the thylakoid membrane structure or the distribution of photosystem biomolecules within it (Anderson & Hunt, 1988).

4.3. *Hydrocarbons*

Petroleum (crude oil) is a complex mixture of hydrocarbons including alkanes, cycloalkanes and aromatics with some additional compounds containing oxygen, sulphur, nitrogen and metals (Lobban & Harrison, 1994). If an oil spill occurs nearshore, and if the wind is in the right direction, beaching of the oil may occur. The oil may adhere to rocks, seaweeds and animals or may be worked into the sediment if a dispersant has been used. Penetration into the interstitial space of sand and smaller sediment grains results in very slow degradation rates (Lobban & Harrison, 1994). With a few exceptions, the studies of effects of oil in macroalgal metabolism are restricted to adults (Thélin, 1981). Schramm (1982) observed reduction in photosynthesis of three species of brown algae associated with the coating of the thallus and subsequent reduction in CO_2 diffusion and light penetration. Reductions in photosynthetic rates correlated with the thickness of the oil layer. Studies of the effects of petroleum on early stages have been neglected, although it is known that the sensitivity to pollutants varies as a function of age and developmental stage (ref. in Thélin, 1981). For example, Thélin (1981) found that the resistance of *Fucus serratus* to oil increases with age, and that in the stage before fertilisation, gametes were extremely sensitive to hydrocarbons. Johnston (1977) has also shown that water soluble extracts containing 0.1 μg mL^{-1} crude North Sea oil prevented further development of unfertilised eggs; 0.5 μg mL^{-1} greatly reduced the percentage of fertilisation. Extracts with more than 1 μg mL^{-1} of crude oil did not kill developing *F. serratus* embryos even after a 96-h exposure. However, a significant growth reduction was observed, and as a result of a marked decrease in secretion of the polysaccharide mucilage at these high oil contents the adhesion of settling spores was inhibited. The latter is of great ecological significance. It can be concluded that the susceptibility of fertilisation and settlement to low levels of aromatic hydrocarbon pollution could have a significant impact on the growth of fucoids in areas with chronic oil pollution, as for example ports.

5. Conclusions and recommendations

5.1. *Global change*

Ultraviolet radiation. The sensitivity of early developmental stages to irradiance is species-dependent, in that some eulittoral (intertidal) species are less sensitive to moderate light than subtidal species. Direct sunlight is harmful to most species, inhibiting growth or even killing them in a time-span of minutes, although some acclimation after a gradual increase of irradiance is possible. The ultraviolet component (especially UVB) has a significant impact on the viability of gametophytes and sporophytes. In some cases young sporophytes are the most vulnerable stage, but UV sensitivity diminishes with age. As literature on UV effects is scarce, more experimental work is required on the early development of various algal groups and species, in relation to their position in the tidal zone and within the canopy of the adult seaweeds. As UVB levels increase further, longer term field experiments using early stages on test substrata (glass slides, tiles) are recommended. The combination of stress caused by sunlight, emersion and extreme temperatures might show results that enable predictions to the effects of global change on species competition, succession and geographic distribution.

Global warming. Stress by increased average temperatures and wider temperature ranges (extremes) has received little attention as regards possible effects on the early life stages. It was mentioned that the fertility of the gametophytes may decrease, that sporophyte growth will increase with temperature, and that early sporophytes may even be more tolerant to temperature variations than older stages. Effects of global warming on the life cycle and on succession etc. are poorly documented and therefore laboratory and field experiments that mimic the effects of increasing average and range of temperature, on the mechanisms of early development, specific growth rates and species competition need to be undertaken. The combined responses of elevated temperature and CO_2 concentration also require investigation.

Increased storm frequencies. The stress caused by excessive wave forces, and scour by resuspension of sediment particles (e.g. sand) on early life stages has been studied during storm events. Increased average current speeds may inhibit gamete release, wash spores away from the shore where they are produced, and hamper the settlement on suitable substrata. Some species may be successful because they release gametes only in calm weather, or because they are able to prolong their existence as a spore in turbulent environments. The earliest stages often

have less adhesive tenacity, but both adhesion and sinking rate increase with the age/size of a spore, germling or propagule. Storms may clear part of the old canopies, which enables new, colonising species to attach. Increased storm frequencies may thus contribute to the speed of succession. Experiments in which extreme wave forces and (sand) scour can be mimicked should be performed to measure adhesive strengths as a function of the species and the stage of development.

5.2. *Pollution*

Eutrophication. As regards the influence of increased nutrient levels on early development of seaweeds, it has been reported that spores are chemotactic to nutrients that stimulate gametophytic growth or reproduction, and that spores settled on sediment-covered substrata may benefit from the higher nutrient levels in the interstitial water. However, as a rule eutrophication effects are indirect, and have a negative impact on development. In most seaweeds so far studied, sewage discharge impacts on early stages, inhibiting sperm motility, fertilisation, and embryo development, which often results in increased mortality. Opportunistic species (green foliose algae), however, show a higher recruitment as a result of elevated nutrient levels. Lack of sporulation in dense green algal blooms in eutrophic waters may be due to sporulation inhibiting hormone-like molecules. In such cases, opportunistic species such as *Ulva* and *Enteromorpha* have an annual cycle that is completely vegetative. Increased sedimentation rates in eutrophic waters inhibit settlement and growth of early stages, reduce the substratum availability and prevent a firm attachment (adhesion) of the spores. Apart from attenuating the sunlight required for photosynthesis, the increased amounts of suspended matter cause a high mortality due to scour. Grazing pressure is usually higher in eutrophic waters, which can result in a considerable loss of recruits in seaweed populations. In general, more experimental work is required to explain the impact of the indirect (derivative) eutrophication effects on early stages. We consider that these stress factors play an important role in colonisation, competition for space, succession and success of development. Although many of these factors have been suggested to contribute to a decline in growth of many hard-substratum species in coastal waters, in many cases real evidence is lacking.

Trace metals. It is not clear whether metals influence the early stages of the life cycle under natural environmental conditions. Most of the literature describes laboratory experiments exposing the algae to relatively high metal levels with little insight into metal speciation and availability. Furthermore, the polysaccharide layer surrounding the cell walls of early stages of many species may scavenge metals, resulting in decreased metal availability and toxicity. Perhaps because of the lack of this polysaccharide mucus in the first stages, gametes seem to be most sensitive to metal (in particular copper) toxicity. Metals (copper) can strongly inhibit fertilisation; however the sensitivity after fertilisation decreases with age. Studies on metal stress on early development should be extended using environmentally relevant concentrations of metals. It is also important to know the conditions at the sites where adults have been collected, as parent plants acclimated to high metal levels may be genetically adapted, and the gametes would thus inherit these tolerance traits. Furthermore, it is important to study responses at relatively lower concentrations during the first few days after fertilisation and settlement. Speciation of the metals in the aquatic environment has to be taken into consideration, as well as the metal-binding capacity of the outer layer of the early stages, and the transfer of metals from there to the cytosol. This requires high-precision equipment suitable for microscopic life stages. Methods used in the analysis of metal stress biomarkers should be adapted for use on these small early stages. It is evident that moderate metal stress affects the life cycles of seaweeds, particularly at the stage of fertilisation and very early embryonic development. As sensitivity to metals is highly species-dependent, effects on various genera and taxa should be examined. Metal stress may have a greater influence on species competition than assumed thus far, and should be tested on artificial test substrata under experimental and field conditions.

Oil. Relatively little has been documented on the effects of hydrocarbons on early development. Laboratory experiments conducted on *Fucus*, exposing early stages to water extracts of crude oil, have shown that the stage before fertilisation is the most sensitive, and that resistance increases with age. Oil may also affect the polysaccharide mucus layer around the zygotes, and thus inhibit adhesion to the substrata (settlement). It is recommended that further studies should be carried out on the effects caused by

chronic oil pollution on a larger number of species, not only to assess the effects of spills (and beaching) of oil but also the impact of hydrocarbons discharged in ports.

Other organic pollutants. The effects of synthetic organic chemicals, including herbicides, insecticides, industrial chemicals and antifouling compounds on all life history stages have, to date, largely been ignored (Lobban & Harrison, 1994; Scarlett et al, 1997). However, with increasing concern about their possible effects on non-target algal species, it is evident that further studies are needed, including assessment of the possible reduction in reproductive success and impairment of development in such species.

References

Amsler, C. & M. Neushul, 1989. Chemostatic effects of nutrients on spores of the kelps *Macrocystis pyrifera* and *Pterygophora californica*. Mar. Biol. 102: 557–564.

Amsler, C. & M. Neushul, 1990. Nutrient stimulation of spore settlement in the kelps *Pterygophora californica* and *Macrocystis pyrifera*. Mar. Biol. 107: 297–304.

Amsler, C. & M. Neushul, 1991. Photosynthetic physiology and chemical composition of spores of the kelps *Macrocystis pyrifera*, *Nereocystis luetkeana*, *Laminaria farlowii* and *Pterigophora californica* (Phaeophyceae). J. Phycol. 27: 26–34.

Amsler, C., D. Reed & M. Neushul, 1992. The microclimate inhabited by macroalgal propagules. Br. Phycol. J. 27: 253–270.

Anderson, B. S. & J. W. Hunt, 1988. Bioassay methods for evaluating the toxicity of heavy metals, biocides and sewage effluent using microscopic stages of giant kelp *Macrocystis pyrifera* (Agardh.): A preliminary report. Mar. Environ. Res. 26: 113–134.

Anderson, B. S., J. W. Hunt, S. L. Turpen, A. R. Coulon & M. Martin, 1990. Copper toxicity to microscopic stages of giant kelp *Macrocystis pyrifera*: Interpopulation comparisons and temporal variability. Mar. Ecol. Prog. Ser. 68: 147–156.

Andersson, S. & L. Kautsky, 1996. Copper effects on reproductive stages of Baltic Sea *Fucus vesiculosus*. Mar. Biol. 125: 171–176.

Andersson, S., L. Kautsky & N. Kautsky, 1992. Effects of salinity and bromine on zygotes and embryos of *Fucus vesiculosus* from the Baltic Sea. Mar. Biol. 114: 661–665.

Andersson, S., L. Kautsky & A. Kalvas, 1994. Circadian and lunar gamete release in *Fucus vesiculosus* L. in the atidal Baltic Sea. Mar. Ecol. Prog. Ser. 110: 195–201.

Ang, P., 1985. Studies on the recruitment of *Sargassum* spp. (Fucales, Phaeophyta) in Balibago, Calatagan, Philippines. J. Exp. Mar. Biol. Ecol. 91: 293–301.

Ang, P. & R. De Wreede, 1990. Matrix models for algal life history stages. Mar. Ecol. Prog. Ser. 59: 171–181.

Barry, J. P., C. M. Baxter, R.D. Sagarin & S. E. Gilman, 1995. Climate-related, long-term faunal changes in a Californian rocky intertidal community. Science 267: 672–675.

Beach, K. S., C. M. Smith, T. Michael & H. W. Shin, 1995. Photosynthesis in reproductive unicells of *Ulva fasciata* and *Enteromorpha flexuosa*: Implications for ecological success. Mar. Ecol. Prog. Ser. 125: 229–237.

Beardall, J., S. Beer & J. A. Raven, 1998. Biodiversity of marine plnats in an era of climate change: Some predictions based on physiological performance. Bot. Mar. 41: 113–123.

Bellgrove, A., M. Clayton & G. Quinn, 1997. Effects of secondarily treated sewage effluent on intertidal macroalgal recruitment processes. Mar. Freshwatr. Res. 48: 137–146.

Bond, P., M. T. Brown, R. M. Moate, M. Gledhill, S. J. Hill & M. Nimmo, 1999. Arrested development in *Fucus spiralis* germlings exposed to copper. Eur. J. Phycol. 39: 513–521.

Brawley S., 1991. The fast block against polyspermy in fucoid algae is an electrical block. Dev. Biol. 144: 94–106.

Brawley S., 1992 Fertilization in natural popluations of the dioecious brown algae *Fucus ceranoides* L. and the importance of the polyspermy block. Mar. Biol. 113: 145–157.

Brawley, S. & L. E. Johnson, 1991. Survival of fucoid embryos in the intertidal zone depends upon developmental stage and microhabitat. J. Phycol. 27: 179–186.

Brown, M. T. & M. H. Depledge, 1998. Determinants of trace metal concentrations in marine organisms. In: Langston, W. J. & M. J. Bebiano (eds), *Metal Metabolism in Aquatic Environments*. Chapman & Hall, London: 185–217.

Brown, V. B., S. Davies & R. Synnot, 1990. Long-term monitoring of the effects of treated sewage effluent on the intertidal macroalgal community near Cape Schanck, Victoria, Australia. Bot. Mar. 33: 85–98.

Burgess, R. M., K. A. Schweitzer, R. A. McKinney & D. K. Phelps, 1993. Contaminated marine sediments: Water column and interstitial toxic effects. Environ. Tox. Chem. 12: 127–138.

Burrows, E. M. & C. Pybus, 1971. *Laminaria saccharina* and marine pollution in north-east England. Mar. Poll. Bull. 2: 53–56.

Chapman, A. R. O., 1989. Abundance of *Fucus spiralis* and ephemeral seaweeds in a high eulittoral zone: Effects of grazers, canopy and substratum type. Mar. Biol. 102: 565–572.

Chapman, A. R. O., 1990. Effects of grazing, canopy cover and substratum type on the abundance of common species of seaweeds inhabiting littoral fringe tide pools. Bot. Mar. 33: 319–326.

Chung, I. K. & B. H. Brinkhuis, 1986. Copper effects in early stages of the kelp *Laminaria saccharina*. Mar. Poll. Bull. 17: 213–218.

Clayton, M., 1992. Propagules of marine macroalgae: structure and development. Br. Phycol. J. 27: 219–232.

Creed, J. C., T. A. Norton & S. P. Harding, 1996. The development of size structure in a young *Fucus serratus* population. Eur. J. Phycol. 31: 203–209.

Creed, J. C., T. A. Norton & J. M. Kain, 1997. Intraspecific competition in *Fucus serratus* germlings: The interaction of light, nutrients and density. J. Exp. Mar. Biol. Ecol. 212: 211–223.

Davison, I. R., 1991. Environmental effects on algal photosynthesis: Temperature. J. Phycol. 27: 2–8.

Davison, I. R., L. Johnson & S. Brawley, 1993. Sublethal stress in the intertidal zone: Tidal emersion inhibits photosynthesis and retards development in embryos of the brown alga *Pelvetia fastigiata*. Oecologia 96: 483–492.

Dayton, P. K., 1984. Processes structuring some marine communities: Are they general? In: Strong, D. R., D. Simberloff, L. Abele & A. Thisle (eds), *Ecological Communities: Conceptual Issues and the Evidence*. Princetown Univ. Press, Princetown, New Jersey: 181–197.

Dayton, P. & M. Tegner, 1990. Bottoms beneath troubled waters: Benthic impacts of the 1982–1984 El Niño in the temperate zone. In: Glynn, P. (ed.), *Global Ecological Consequences of the 1982–1983 El Niño/Southern Oscillation*. Elsevier, Amsterdam: 433–465.

Devinny, J. & L. Volse, 1978. Effects of sediments on the development of *Macrocystis pyrifera* gametophytes. Mar. Biol. 48: 343–348.

Deysher, L. & T. Norton, 1992. Dispersal and colonization in *Sargassum muticum* (Yendo) Fensholt. J. Exp. Mar. Biol. Ecol. 56: 179–195.

Doblin, M. A. & M. N. Clayton, 1995. Effects of secondarily-treated sewage effluent on the early life-history stages of two species of brown macroalgae: *Hormosira banksii* and *Durvillaea potatorum*. Mar. Biol. 122: 689–698.

Dring, M. J., V. Makarov, E. Schoschina, M. Lorenz & K. Lüning, 1996. Influence of ultraviolet radiation on chlorophyll fluorescence and growth in different life-history stages of three species of *Laminaria* (Phaeophyta). Mar. Biol. 126: 183–191.

Duarte, C., 1995. Submerged aquatic vegetation in relation to different nutrient regimes. Ophelia 41: 87–112.

Emerson, S. & J. Zedler, 1978. Recolonization of intertidal algae: An experimental study. Mar. Biol. 44: 315–324.

Fei, X., B. Jiang, M. Ding, Y. Wu, R. Huang & H. Li, 1989. Light demends of juvenile *Laminaria japonica*. Chin. J. Oceanol. Limnol. 7: 1–9.

Fletcher, R. & M. Callow, 1992. The settlement, attachment and establishment of marine algal spores. Br. Phycol. J. 27: 303–329.

Franklin, L. & R. Forster, 1997. The changing irradiance environment: Consequences for marine macrophyte physiology, productivity and ecology. Eur. J. Phycol. 32: 207–232.

Garding E., 1996. Effects of eutrophication and *Cladophora* on the survival of *Fucus vesiculosus* zygotes in the Baltic Sea. M.SC thesis, Univeristy of Stockholm, 24 pp.

Garman, G. D., M. Pillai & G. N. Cherr, 1994. Inhibition of cellular events during early algal gametophyte development: Effects of select metals and an aqueous petroleum waste. Aquatic Toxicol. 28: 127–144.

Gledhill, M., M. Nimmo, S. J. Hill & M. T. Brown, 1997. The toxicity of copper (II) species to marine algae, with particular reference to macroalgae. J. Phycol. 33: 2–11.

Graham M., 1996. Effect of high irradiance on recruitment of the giant kelp *Macrocystis* (Phaeophyta) in shallow water. J. Phycol. 32: 903–906.

Gunnill F., 1985. Population fluctuations of seven macroalgae in Southern California during 1981–1983 including effects of severe storms and an El Niño. J. Exp. Mar. Biol. Ecol. 85: 149–164.

Han, T. & J. Kain, 1996. Effects of photon irradiance and photoperiod on young sporophytes of four species of the Laminariales. Eur. J. Phycol. 31: 233–240.

Hanelt, D., C. Wiencke & U. Karsten, 1997. Photoinhibition and recovery after high light stress in different developmental and life-history stages of *Laminaria saccharina* (Phaeophyta). J. Phycol. 33: 387–395.

Hardy, F. & B. Moss, 1979. Attachment and development of the zygotes of *Pelvetia canaliculata* (L.) Dcne. et Thur. (Phaeophyceae, Fucales). Phycologia, 18: 203–212.

Hopkin, R. & J. M. Kain, 1978. The effects of some pollutants on the survival, growth and respiration of *Laminaria hyperborea*. Estuar. Coast. Mar. Sci. 7: 531–553.

Johnson, C. S., 1977. The sub-lethal effects of water soluble extracts of crude oil on the fertilization and development of Fucus serratus L. (serrated wrack). Rapp. P. Réun. Int. Explor. Mer. 171: 184–185.

Juno, P., P. Worest & C. Janetos, 1989. Scientific linkages in global change. Ecol. Res. Ser. U.S. Environm. Prot. Agency, 18 pp.

Kain, J. M. & T. A. Norton, 1990. Marine ecology. In: Cole, K. M. & R. G. Sheath (eds). *Biology of the Red Algae*. Cambridge University Press: 377–422.

Kamermans, P., E. J. Malta, J. M. Verschuure, L. F. Lentz & L. Schrijvers, 1998. Role of cold resistance and burial for winter survival and spring initiation of an *Ulva* spp. (Chlorophyta) bloom in a eutrophic lagoon (Verse Meer lagoon, The Netherlands). Mar. Biol. 131: 45–51.

Kendrick, G. & D. Walker, 1994. Role of recruitment in structuring beds of *Sargassum* spp. (Phaeophyta) at Rottnest Island, Wetern Australia. J. Phycol. 30: 200–208.

Kiiriki, M & A. Lehvo, 1997. Life strategies of filamentous algae in the northern Baltic Proper. Sarsia 82: 259–267.

Leukart, P. & K. Lüning 1994, Minimal spectral light requirements and maximum light levels for long term germling growth of several red algae from different water depths and a green algae. Eur. J. Phycol. 29: 103–112.

Littler, M. & S. Murray, 1975. Impact of sewage on the distribution, abundance and community structure of rocky intertidal macro-organisms. Mar. Biol. 30: 277–291.

Lignell, A., G. M. Roomans & M Pedersen, 1982. Localization of absorbed cadmium in *Fucus vesiculosus* by X-ray microanalysis. Z. Pflanzenphysiol. 105: 103–109.

Lobban, C. S. & P. J. Harrison, 1994. *Seaweed Ecology and Physiology*. Cambridge University Press, pp. 366.

Lubchenco J., 1986. Relative importance of competition and predation: Early colonization by seaweeds in New England. In: Diamond, J. (ed.), *Community Ecology*. Harper & Row, New York: 537–555.

Lüning, K. & M. Neushul, 1978. Light and temperature demands for growth and reproduction of laminarian gametophytes in Southern and Central California. Mar. Biol. 45: 297–309.

Lüning, K. & M. Dring, 1975. Reproduction, growth and photosynthesis of gametophytes of *Laminaria saccharina* grown in blue and red light. Mar. Biol. 29: 195–200.

Lüning, K., 1980. Critical levels of light and temperature regulating the gametogenesis of three *Laminaria species* (Phaeophyceae). J. Phycol. 16: 1–15.

McLachlan, J. & R. Bidwell, 1978. Photosynthesis of eggs, sperm, zygotes and embryos of *Fucus serratus*. Can. J. Bot. 56: 371–373.

Madsen, T. V. & S. C. Maberly, 1990. A comparison of air and water as environments for photosynthesis by the intertidal algae *Fucus spiralis* (Phaeophyta). J. Phycol. 26: 24–30.

Maier, I., 1993. Gamete orientation and induction of gametogenesis by pheromones in algae and plants. Plant, Cell Environ. 16: 891–907.

Maier, I., 1995. Brown algal pheromones, In: Chapman, R. (ed.), *Progress in Phycological*. Research, Biopress Ltd.: 51–102.

Major, K. M. & I. Davison, 1998. Influence of temperature and light on growth and photosynthetic physiology of *Fucus evanescens* (Phaeophyta) embryos. Eur. J. Phycol. 33: 129–138.

Markham, J. W., B. P. Kremer & K. R. Sperling, 1980. Effects of cadmium on *Laminaria saccharina* in culture. Mar. Ecol. Prog. Ser. 3: 31–39.

Mathieson, A., 1982. Physiological ecology of the brown algae Phaeostrophion irregulare Setchell et Gardner: I. Juvenile plants. Bot. Mar. 25: 87–91.

Moss, B., S. Mercer & A. Sheader, 1973. Factors affecting the distribution of Himanthalia elongata (L.) S. F. Gray on the North-east Coast of England. Estuar. Coast. Mar. Sci. 1: 233–243.

Neushul, M., M. S. Foster, D. A. Coon, J. W. Woessner & B. W. W. Harger, 1976. An in situ study of recruitment, growth and

survival of subtidal marine algae: Techniques and preliminary results. J. Phycol. 12: 397–408.

Norton, T., 1978. The factors influencing the distribution of *Saccorhiza polyschides* in the region of Lough Ine. J. Mar. Biol. Ass. U.K. 58: 527–536.

Norton, T., 1983. The resistance to dislodgement of *Sargassum muticum* germlings under defined hydrodynamic conditions. J. Mar. Biol. Ass. U.K. 63: 181–193.

Norton, T. & R. Fetter, 1981. The settlement of *Sargassum muticum* propagules in stationary and flowing water. J. Mar. Biol. Ass. U.K. 61: 929–940.

Norton, T., A. Mathieson & M. Neushul, 1982. A review of some aspects of form and function in seaweeds. Bot. Mar. 25: 501–510.

Novaczek I., 1984. Response of *Ecklonia radiata* (Laminariales) to light at 15 °C with reference to the field light budget at Goat island Bay, New Zealand. Mar. Biol. 80: 263–272.

Oates, B. & S. Murray, 1983. Photosynthesis, dark respiration and desiccation resistance of the intertidal seaweeds *Hesperophycus harveyanus* and *Pelvetia fastigiata f. gracilaris*. J. Phycol. 19: 371–380.

Oliver, J. & R. Babcock, 1992. Aspects of the fertilization ecology of broadcast spawning corals: Sperm dilution effects and in situ measurements of fertilization. Biol. Bull. 183: 409–417.

Pakker, H. & A. M. Breeman, 1994. Temperature ecotypes in seaweeds-adative significance and biogeographic implications. Bot. Mar. 37: 171–180.

Pearson, G. & S. Brawley, 1996. Reproductive ecology of *Fucus distichus* (Phaeophyceae): an intertidal algae with successful external fertilization. Mar. Ecol. Prog. Ser. 143: 211–223.

Pearson, G., E. Serrão & S. Brawley, 1998. Control of gamete release in fucoid algae: Sensing hydrodynamic conditions via carbon acquisition. Ecology 79(5).

Petersen, C., Warner, R., Cohen, S., Hess, H. & Sewell, A., 1992. Variable pelagic fertilization success: Implications for mate choice and spacial patterns of mating. Ecology 73: 391–401.

Phillips, G., D. Eminson & B. Moss, 1978. A mechanism to account for macrophyte decline in progressively eutrophicated freshwaters. Aquat. Bot. 4: 103–126.

Rao, M. U. & N. Kaliaperumal, 1983. Effects of environmental factors on the liberation of spores from some red algae of Visakhapatnam coast. J. Exp. Mar. Biol. Ecol. 70: 45–53.

Ramus J., 1992. Productivity of seaweeds. In: Falkowski, P. G. & A. D. Woodhead (eds), *Primary Productivity and Biogeochemical Cycles in the Sea*. Plenum Press, New York: 239–255.

Raven, J. A., 1992. The coastal fringe: Habitats threatened through global warming. Trans. Bot. Soc. Edin. 45: 437–462.

Reed D., 1990. The effects of variable settlement and early competition on patterns of kelp recruitment. Ecology 71: 776–787.

Reed, D. & M. Foster, 1994. The effects of canopy shading on algal recruitment and growth in a giant kelp forest. Ecology 65: 937–948.

Reed, D., C. Amsler & A. Ebeling, 1992. Dispersal in kelps: Factors affecting spore swimming and competency. Ecology 73: 1577–1585.

Rodrigo, M. & R. R. Robaina, 1997. Stress tolerance of photosynthesis in sporelings of the red alga *Grateloupia doryphora* compared to that of stage III thalli. Mar. Biol. 128: 689–694.

Santelices, B., 1990. Patterns of reproduction, dispersal and recruitment in seaweeds. Ocean. Mar. Biol. Ann. Rev. 28: 177–276.

Scanlan, C. M. & M. Wilkinson, 1987. The use of seaweeds in biocide toxicity testing. Part 1: The sensitivity of different stages in the life-history of *Fucus* and of other algae, to certain biocides. Marine Environ. Res. 21: 11–29.

Scarlett, A., M.E. Donkin, T. W. Fileman & P. Donkin, 1997. Occurrence of the marine antifouling agent Irgarol 1051 within the Plymouth Sound locality: Implications for the green macroalga *Enteromorpha intestinalis*. Mar. Pollut. Bull. 34: 645–651.

Schories, D. & K. Reise, 1993. Germination and anchorage of *Enteromorpha* spp. in sediments of the Wadden Sea. Helgolander Meeresunters 47: 275–285.

Serrão, E., L. Kautsky & S. H. Brawley, 1996a. Distributional success of the marine seaweed *Fucus vesiculosus* in the brackish Baltic Sea correlates with osmotic capabilities of Baltic gametes. Oecologia 107: 1–12.

Serrão, E., G. Pearson, L. Kautsky & S. H. Brawley, 1996b. Successful external fertilization in turbulent environments. Proc. Natl. Acad. Sci. USA, 93: 5286–5290.

Stromgren, T., 1980a. The effect of dissolved copper on the increase in length of four species of intertidal brown algae. Mar. Environ. Res. 3: 5–13.

Stromgren, T., 1980b. The effect of lead, cadmium and mercury on the increase in length of five intertidal Fucales. J. exp. Mar. Biol. Ecol. 43: 107–119.

Thélin, I., 1981. Effets, en culture, de deux pétroles bruts et dún dispersant pétrolier sur les zygotes et des plantules de *Fucus serratus* Linneaus (Fucales, Phaeophyceae). Bot. Mar. 24: 515–519.

Underwood, A. J. & P. G. Fairweather, 1989. Supply-side ecology and benthic marine assemblages. Trends Ecol. Evol. 4: 16–20.

Vadas, R. L., W. A. Wright & S. L. Miller, 1990. Recruitment of *Ascophyllum nodosum*: Wave action as a source of mortality. Mar. Ecol. Prog. Ser. 61: 263–272.

Vadas, S., S. Johnson & T. A. Norton, 1992. Recruitment and mortality of early post-settlement stages of benthic algae. Br. Phycol. J. 27: 331–335.

Vogt, H. & W. Schramm, 1991. Conspicuous decline of *Fucus* in Kiel Bay (Western Baltic): What are the causes? Mar. Ecol. Prog. Ser. 69: 189–194.

Wood, W., 1987. Effect of solar ultraviolet radiation on the kelp *Ecklonia radiata*. Mar. Biol. 96: 143–150.

Wright, P. J. & R. H. Reed, 1990. Effects of osmotic stress on gamete size, rhizoid initiation and germling growth in fucoid algae. Br. Phycol. J. 25: 149–155.

Yabe, K., M. Makino & M. Suzuki, 1997. Growth inhibition on gametophytes of *Laminaria religiosa* induced by UV-B irradiation. Fisheries Science 63: 668–670.

Zimmerman, R. & J. Kremer, 1984. Episodic nutrient supply to a kelp forest ecosystem in Southern California. J. Mar. Res., 1984. 42: 591–604.

Zimmerman, R. & D. Robertson, 1985. Effects of El Niño on local hydrography and growth of the giant kelp, *Macrocystis pyrifera*, at Santa Catalina Island, California. Limnol. Oceanogr. 30: 1298–1302.

Zupan, J. & J. West, 1990. Photosynthetic responses to light and temperature of the heteromorphic marine alga *Mastocarpus papillatus* (Rhodophyta). J. Phycol. 26: 232–239.